Modelling and Evaluation of SWER Channel for PLC-based Protection Scheme Applications

by

Md Mahamudul Hasan

A Dissertation Submitted in Fulfilment of the
Requirements for the Degree of
DOCTOR OF PHILOSOPHY

Institute for Sustainable Industries and Liveable Cities (ISILC)

College of Engineering and Science
Victoria University, Melbourne, Australia

Abstract

After the disastrous “Black Saturday" bushfires of 2009, bushfire mitigation efforts for preventing power line faults has become one of the most intriguing research topics for the Australian industry. This thesis presents narrowband channel modelling efforts supported by experimental analysis of key fundamental concepts in developing a novel Power Line Communication (PLC)-based protection scheme for rural Single Wire Earth Return (SWER) networks. A SWER line often breaks and makes contact with vegetation when hit by a falling tree, starting fires. The proposed protection scheme relies on transmitters at various ends of the network continually transmitting to a receiver at the substation end. If the line breaks, then there will be a loss of transmission indicating a potential line breakage.

Irrespective of the application, accurate channel modelling is critical in studying how the SWER channel would perform as a potential communication channel for PLC signal transmission and assessment of the channel’s performance with regards to key questions on the attenuation, signal-to-noise ratio, and reliability. This thesis therefore presents narrowband modelling procedure and analysis of an exemplary SWER distribution network as a potential PLC communication channel. The protection scheme is to be implemented over this channel. The research presented focuses on the channel modelling and network coupling aspects of the work, rather than the design of the protection scheme itself.

Narrowband network modelling includes High-Frequency (HF) modelling of overhead conductors, transformers, and a capacitive coupling circuit. Three different types of SWER conductors have been tested and modelled to justify the model. Line modelling was undertaken based on the mathematical modelling of overhead conductors using a lossy line model with frequency-dependent characteristic such as the characteristic impedance, line resistance and radiation. Another key contribution is the introduction of a modelling method that relied on s-parameter measurements of network elements such as transformers and coupling circuits and their integration into the narrowband model. This was used particularly in the modelling of transformers by measuring, recording, and integrating real data from these network elements. One-port winding impedance measurements and two-port s-parameter data have been integrated into the model significantly reducing the effort required in the modelling of transformers evading a time-intensive discrete modelling process.

High Frequency (HF) modelling of an entire end-to-end network has enabled simulation of the overhead network to predict PLC signal tone strengths for a number of cases including the de-energised and grid connected network scenarios. The technique has been used for an evaluation of the profile of transmitted and received signals under different conditions. The proposed narrowband model has been verified by comparing with measurements from field injection tests. PLC propagation field tests were successfully undertaken with the logistic support from the industrial partner, which included network access, site acquisition and other in-house support during the test dates. Results show high accuracy between the actual measurements and the model predicted signal strengths with a mean error rate of 2.27 dB and 3.10 dB across the frequency band for the de-energised and grid connected cases respectively. The network model has also been used to analyse the impacts of parameters such as network size, pole height, and loading effect on the PLC propagation with findings expected to inform the development of the proposed protection scheme.

Development of a High Voltage (HV) coupling circuit is one of the biggest challenges in HV-PLC applications. In this work, a HV coupling capacitor based L-C impedance matching circuit has been designed, built and tailored for the proposed SWER PLC protection application. Impedance characterization of the power line integrated HV-coupling capacitor was a real challenge, which has been addressed in this thesis and a simplified method demonstrated for its modelling. This frequency dependent impedance measurement technique could be used to categorize the impedance characteristics of other HV-coupling capacitor-based PLC applications. The designed coupling circuit shows promising performance, with only around -4 dB insertion loss for evaluated 50 kHz to 150 kHz band.

The thesis has been divided into seven chapters. Chapter 1 introduces the motivation behind the work, key objectives and the methodology employed. Chapter 2 covers an up-to-date literature review. Chapter 3 comprises the design, evaluation and performance analysis of the proposed HV capacitive coupling matching circuit. Chapter 4 presents impedance modelling of a various SWER conductors with mathematical detailing. Chapter 5 discusses a novel hardware in loop approach for modelling HF SWER transformers. Chapter 6 represents the entire end-to-end network model, its simulation studies, and comparison of simulation results against measurements from field propagation tests. Chapter 7 includes the conclusion by summarizing all significant key findings with hints on potential future works.

Student Declaration

I, Md Mahamudul Hasan, declare that the PhD thesis titled “Modelling and Evaluation of SWER Channel for PLC-based Protection Scheme Applications" is no more than 100000 words excluding tables, figures, appendix, footnotes and references. The contents of this thesis, in whole or part, have not been submitted previously for the award of any other academic degree or diploma. Except otherwise mentioned, this thesis is my own work.

Md Mahamudul Hasan Date: 08-12-2020

Acknowledgements

I would like to thank my supervisor Dr. Cagil Ozansoy for his immense support during my doctoral studies in terms of technical advices, constructive feedbacks and suggestions on this thesis and publications which helped me not only to complete the PhD degree but also to become a good researcher. Special thanks to Professor Mike Faulkner and Dr. Mohd Noor Islam for their technical feedback throughout the PhD journey.

I delightedly acknowledge the continuous financial assistance of Victoria University Research Training Program during my doctoral studies. I would also like to thank the Graduate Research Office and the Institute of Sustainable Industries and Liveable Cities (ISILC) for processing and supporting me financially to attend conferences, seminars and paying article processing charges. I would also like to thank United Energy Ltd, the industry partner, especially for access to an HV coupling capacitor, SWER and isolation transformer and various technical data to carry out various parts of this research work.

I would like to dedicate this thesis to all the members of my beloved family for their boundless love and support throughout this epic journey.

List of Publications

List of Articles (Published)

1. H. Mahamudul and C. Ozansoy, "L-C band pass impedance matching coupling circuit for high voltage PLC applications," International Journal of Electrical Power & Energy Systems, vol. 117, p. 105639, 2020/05/01/ 2020. (**Q1-Ranked Journal**).
2. H. Mahamudul, C. Ozansoy and E. Haque, "Evaluation of Butterworth coupling arrangement and line trap circuit for PLC integrated power system," 2017 IEEE, International Conference on Telecommunications and Photonics (ICTP), Dhaka, 2017, pp. 43-47. (Peer-reviewed conferences)

List of Articles (Under Review)

1. Mahamudul, H., & Ozansoy, C., M. N. Islam, and M. Faulkner, "Performance Evaluation of SWER Distribution Network Communication Channel Modelling," IEEE Transactions on Power Delivery **(Q1).** (Under review, 2nd Revision)
2. H. Mahamudul, C. Ozansoy (2019) High-Frequency Characterisation of a High Voltage Coupling Capacitor for Broadband PLC Application," (Under review in journal of electrical system **(Q3)**)

List of Articles (Under Preparation)

1. H. Mahamudul, C. Ozansoy (2019), A Comprehensive Review on Technical Aspects, Applications and Implementation Challenges of Power Line Communication Systems" (Ready to be submitted in Engineering Science and Technology, an International Journal. **(Q1)**)
2. H. Mahamudul, C. Ozansoy (2019), A Novel Technique to Model High Voltage Transformer for PLC Applications Using Hardware in Loop Approach"(Under Preparation for IEEE Transactions on Communications)

List of Symbols and Acronyms

Symbols and Acronym	**Symbol and Acronym Definitions**
ACSR	Aluminium Conductor Steel Reinforced
AWR	Microwave Office
a	Radius of the conductor
C	Capacitor
CC	Coupling Capacitor
CENELEC	European Committee for Electrotechnical Standardization
D	Carson's depth
f_R	Frequency of Resonance
L	Line inductance
Z	The line impedance
ρ (rho)	Resistivity of conductor
ρ_s	Resistivity of the soil
ε_r	Relative permittivity of the conductor
δ	Skin depth
μ	Permeability
HF	High Frequency
HV	High voltage
MV	Medium Voltage
LV	Low Voltage
HIF	High Impedance Fault
HV_a	High Voltage Active
MV_a	Medium Voltage Active
LV_a	Low Voltage Active
HV_e	High Voltage Earth
MV_e	Medium Voltage Earth
LV_e	Low Voltage Earth
OFDM	Orthogonal Frequency Division Multiplexing
F.D.I	Frequency Dependent Impedance
Touchstone File	S-parameter measurements data file
S_{len}	Section length
SCAC	Aluminium Clad Steel conductors
SCGZ	Galvanised steel conductors
SWER	Single Wire Earth Return
VNA	Vector Network Analyzer

Table of Contents

List of Figures

List of Tables

Chapter 1

Introduction

1.1 Introduction

Single Wire Earth Return (SWER) is a popular power distribution medium in rural Australia. A total length of about 200,000 km of SWER lines, at 19.1 kV and 12.7 kV voltage levels, is still in operation in this country [1]. SWER has a lot of advantages such as being inexpensive, easy to install and requiring only one pole. It may therefore be the best possible solution to supply electricity to the sparsely populated areas. SWER has some prolonged critical weaknesses such as exposure to vegetative High Impedance Faults (HIFs). This is primarily because of the fact that the SWER conductor is very thin and runs through forests and other vegetation under very high tension [2]. Due to wind, lighting or other likely causes, this SWER conductor often breaks and makes contact with vegetation creating HIFs, which may produce embers that could start bush fires.

Arching as a result of contact by a falling tree branch is also likely to lead in to a bushfire. The research on the history and reason of the disastrous “Black Saturday” of 2009, reveals the fact that HIFs of the SWER line was one of the main cause behind the catastrophic event [2, 3]. After this incident research on the detection of HIFs on a power line get accelerated exponentially in Australia. The current technology is not sensitive enough to detect such vegetation faults. This research is expected to evaluate a SWER Channel to implement a highly sensitive PLC-based Protection Scheme to reduce powerline ignited bushfires in rural networks. The main focus of this work is to develop a complete SWER system in microwave office platform to observe its behaviour and analyze the reflection from other network elements such as coupling circuit, transformer on the SWER channel at high frequency PLC signal.

1.2 SWER Networks

The SWER network, depicted in Fig 1.1, is a cost-effective solution in rural electrification. The distinguishing feature of a SWER network is that the earth is used as the

return path for the current, to avoid the need for a second wire (or neutral wire) to act as a return path. For these networks, the normal load current is therefore simply designed to flow to earth. Power is supplied to the SWER line by an isolating transformer, which isolates the grid from ground or earth, and changes the grid voltage from 22 kV to the SWER voltage (12.7 kV). The SWER network consists of a single conductor that may stretch for tens or even hundreds of kilometres, with a number of distribution transformers along its length. Current flows from the line, through the primary coil of a step-down local transformer, to earth through an earth stake. The secondary winding of the step-down local transformer supplies the customer with the 0V line connected to the safety earth that does not normally carry any current.

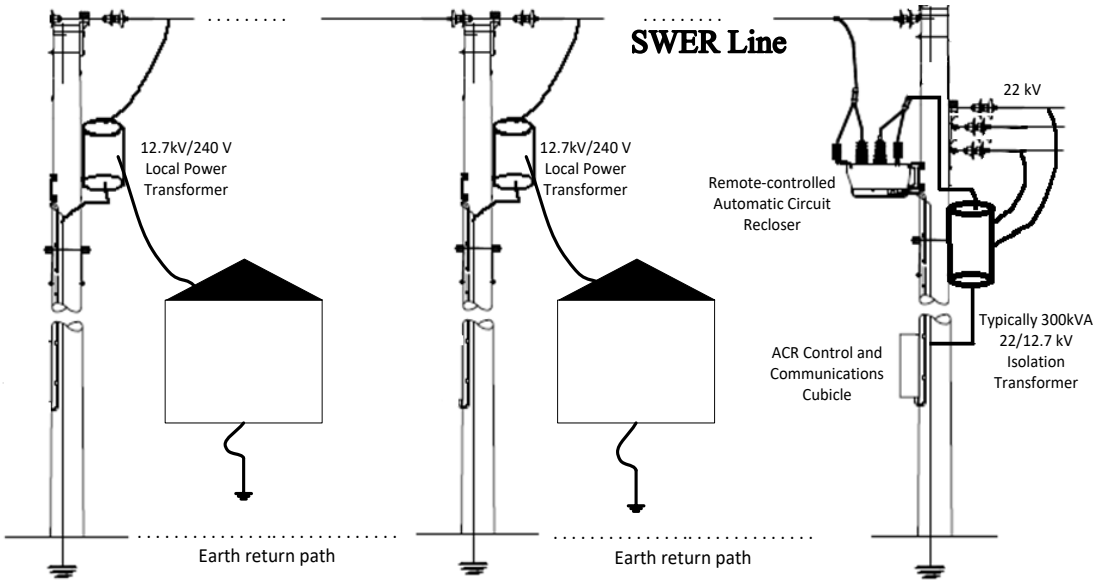

Fig 1.1: Schematic arrangement of a complete PLC system

The SWER design simplicity offers some bushfire mitigation features because the single line cannot simply clash with other lines. However, SWER networks consist of thin and typically long conductors under high tension and the conductor is prone to breaking when a fault occurs. A broken SWER conductor can short to ground across a high-impedance structure such as a tree. On SWER networks, the only type of short circuit fault is a phase to earth fault. It is often a challenge to detect such high impedance phase to earth faults because a small additional current due to vegetation contact cannot be always be distinguished from the current caused by a small amount of additional customer load. Hence, low current faults in SWER networks such as a dry tree branch contacting a live wire may not be immediately

detected by over-current protection systems and the line remains energised. The line could remain 'live' for long periods increasing the likelihood of a fire starting. The SWER conductor could fail for several reasons including failure due to age, corrosion or impact from a tree. Most impacts will cause the conductor to fail thus initial contact and, in most cases, the fire will not start until the conductor has been in contact with the ground for some time. If the SWER protection operates to trip the conductor before it hits the ground, then the fire can be prevented. The undertaken PhD project has been part of a larger industry funded project that aimed to develop a novel protection system for Single Wire Earth Return (SWER) networks utilizing the Powerline Communication technology.

1.3 Current SWER Protection Schemes

Automatic Circuit Reclosers (ACRs) are usually used for protection in SWER systems. The ACR control and communications cabinet often includes protection relays incorporating directional overcurrent, negative phase sequence and earth fault protection elements. The main problem is that the relay incorporating the overcurrent element fails to detect the high-impedance fault conditions and fails to trip the ACR. An alternative to the scheme depicted in Fig 1.2 is required for more effective fault detection in SWER networks [4]. The ACR is used as a circuit breaker that trips when a fault is detected.

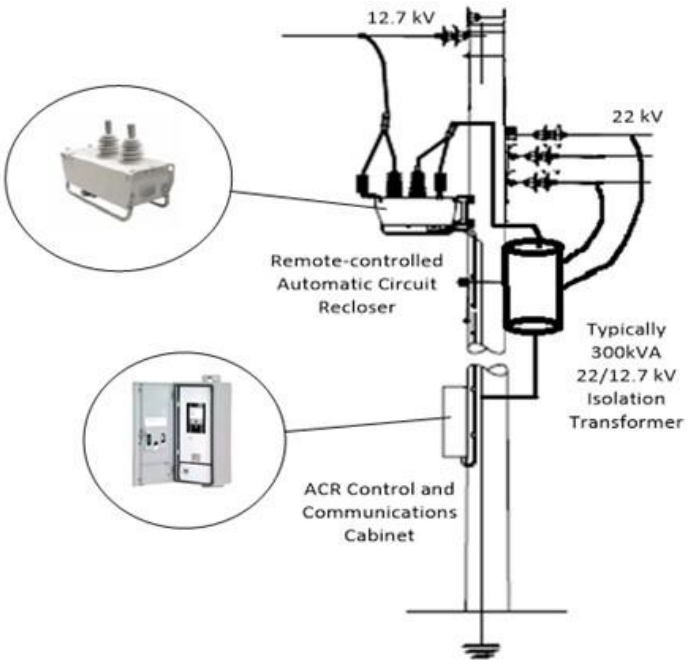

Fig 1.2: Existing SWER protection systems

The ACR control cubicle provides all the protection, data logging and communications functionalities in a single device. The basis of fault detection should be to detect the broken conductor, not the current flow to earth or the increase in the line current. Ideally, the desired scheme should operate to trip the ACR before the conductor hits the ground for maximised fire prevention. High fault detection sensitivity and low risk of false positives and very high protection operating speed are amongst the desired performance criteria.

1.4 Proposed PLC-Based Protection Schemes

Fig 1.3 shows the proposed PLC-communications based SWER protection scheme and one available connection options, i.e. coupling onto the MV line. The concept relies on detecting broken conductors by placing PLC transmitters at certain positions at the end of SWER lines with a receiver at each ACR. If the signal is lost, then the ACR is instantaneously tripped.

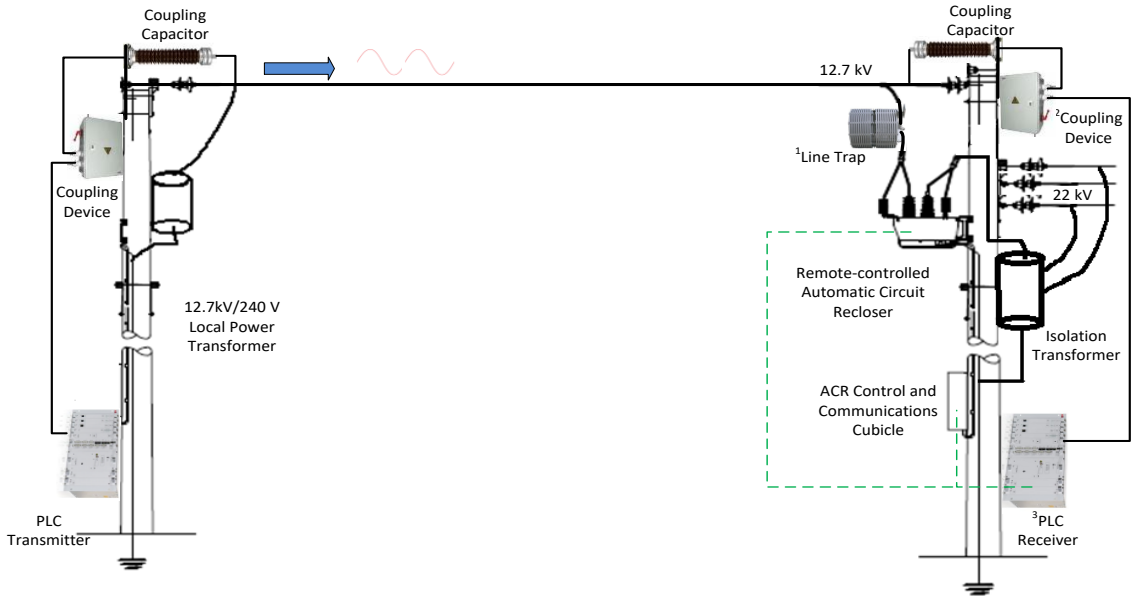

Fig 1.3: PLC-Based SWER Protection Concept

A line trap prevents the transmission of high frequency carrier signals unwanted destinations by presenting high impedance to carrier frequencies and low impedance to the 50 Hz power frequency. Powerline Communication (PLC) is a communication method that uses the existing overhead electrical conductor for data communications. In contrast with the

electric power frequency, PLC utilizes high-frequency signals with components beginning from a couple of hundred Hz up to a couple of hundred MHz [5, 6].

Frequency separation and safe isolation of the 50 Hz power frequency and over voltage transients occurs in the coupling device (line tuner). PLC signals are often transmitted in the CENELEC-A frequency band from 9 kHz to 95 kHz, which is the band set aside for use by Power Supply Companies. The main challenges with PLC communications are high noise, and high attenuation. These challenges and an analysis of their impacts on the application of PLC communications in the protection of SWER systems are at the core of this research.

Individual transmitters shall be used at the end of each branch (i.e. the spur) to allow uniquely coded PLC signals to be transmitted from the end of each branch. The individual transmitters should be configured in such a way to allow the transmission of unique PLC signals from each end and their identification at the receiver, which will be placed as close to the ACR as possible. Any combination of the loss of signals should initiate the tripping of the ACR. An analysis of the uniquely coded PLC signals received at the receiver should also allow the approximate location (at least the spur fault has taken place) of the fault to be automatically identified.

1.5 Research Aims

This PhD thesis will critically analyze Single Wire Earth Return (SWER) networks, as the communication channel, for the implementation of the PLC technology based protection scheme to avert bushfires. The key focus will be on channel modelling of an exemplar SWER network to understand how the SWER communication channel would perform for transmission over in the designated PLC signal frequency band.

A low loss coupling circuit is critical for the implementation of any PLC based application over power system networks. Low insertion loss coupling circuit is the pre-requisite for an efficient PLC integrated power network. In this thesis, the design and implementation procedure of a novel L-C band pass impedance matching coupling circuit for SWER network is presented. A low loss L-C impedance matching coupling circuit for the SWER line has also been tailor designed, built and experimentally tested as part of this PhD thesis. It must be clearly noted that this PhD thesis formed a part of an industry-funded project on the design

and development of a PLC communications based SWER protection scheme to evaluate the efficacy and reliability of such a scheme in the detection of conductor breaks in SWER networks. Works undertaken as part of this PhD composed parts of the overall objective but did not encompass all tasks.

Wide band modelling of an exemplar SWER network is critical in understanding how the SWER communication channel will perform. Wide band modelling of the Myers Road SWER network, as an exemplar communication channel, was carried out using discrete models for the transmission lines, SWER transformers, and the isolation transformer. This thesis presents the development of each discrete model as well as system studies. These models will provide answers to some key questions on the reliability and effectiveness of the proposed scheme. These include:

- Impacts of line construction, conductor size and materials used in the SWER network,
- PLC performance in networks with different segments of varying conductor size/material,
- Impact of the SWER transformer loading on signal attenuation and the carrier performance and the impact of network size on the received signal strengths,
- Required transmitter output power considering attenuation.

This research thesis presents wide-band modelling and analysis of an exemplary Single-Wire Earth Return (SWER) distribution network as a potential Power Line Carrier (PLC) communication channel. This includes high-frequency modelling of overhead conductors, transformers, and a capacitive coupling circuit. A key contribution is the introduction of a modelling methodology that relies on s-parameter data measurements and their integration into the modelling software. High Frequency (HF) modelling of the entire network has enabled simulation of the overhead network to predict PLC signal tone strengths for a number of cases including the de-energised and grid connected network scenarios. Model predictions were then compared with actual measurements in the field.

A SWER transformer is a crucial element of SWER network. An accurate SWER transformer model at PLC frequency is very important to get the exact impact of PLC

propagation on the overall network. In this thesis, an exclusive hardware in loop transformer model for PLC application has been demonstrated, which can be used to represent any transformer connected to a PLC integrated power network. Hence, the specific objectives of this work can be summarised as follows:

- Channel modelling of an exemplary SWER network using the Microwave Office (AWR) platform inclusive of overhead conductors, transformers, and a capacitive coupling circuit,
- Design and development of a low-loss HV coupling capacitor based matching circuit and its evaluation in terms of insertion loss and attenuation,
- Wide band modelling of SWER transformer equivalent circuit models to analyse the impact of reflections from transformer on the PLC signal strength and attenuation with respect to various loading conditions,
- Evaluation of the efficacy of the SWER network as the communication channel for digital transmission within the designated frequency band.

1.6 Research Methodologies and Techniques

This thesis has been broken into seven chapters. For each chapter, a specific methodology detailed by a flowchart below has been developed and followed. Comprehensively, the workflow in these chapters can be referred to as the research methodology of the thesis. Figs 1.4 -1.8 show these flow charts demonstrating the overall methodology of this thesis.

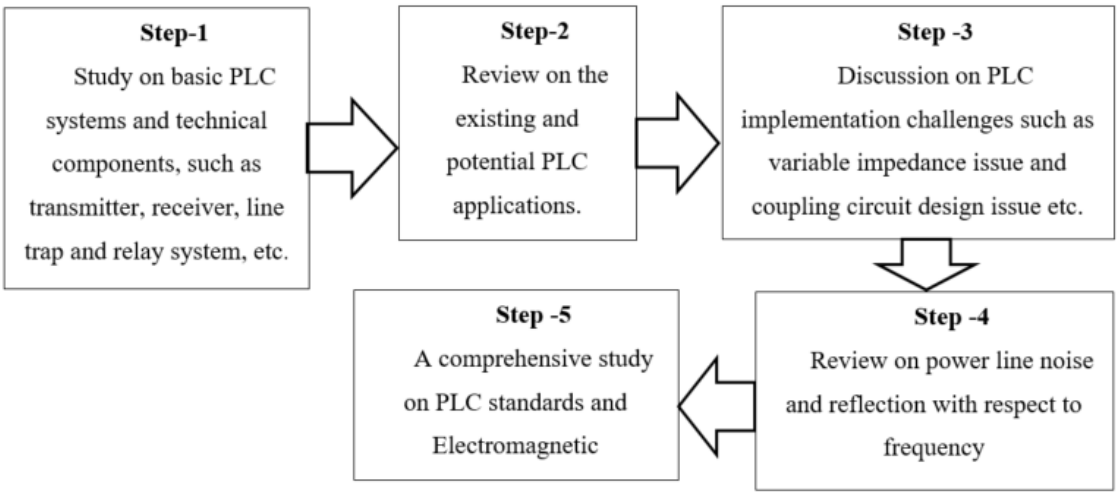

Fig 1.4: Research Methodology for Chapter-2: Literature Review

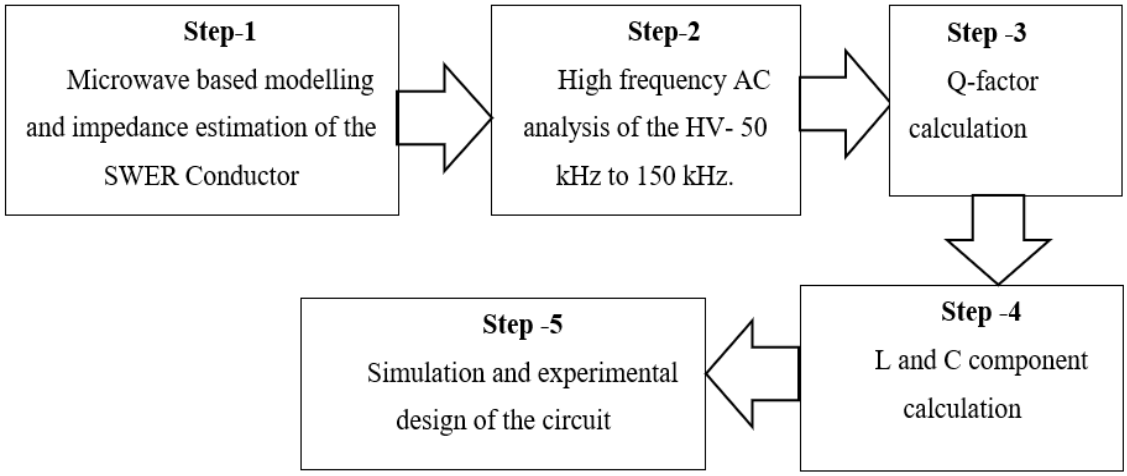

Fig 1.5: Research Methodology for Chapter-3: Coupling Circuit Design

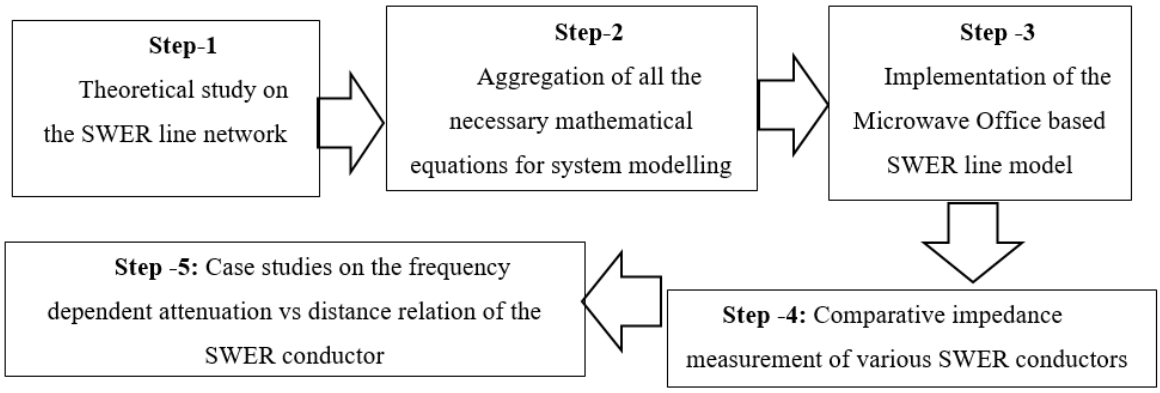

Fig 1.6: Research Methodology for Chapter-4: SWER Line Modelling

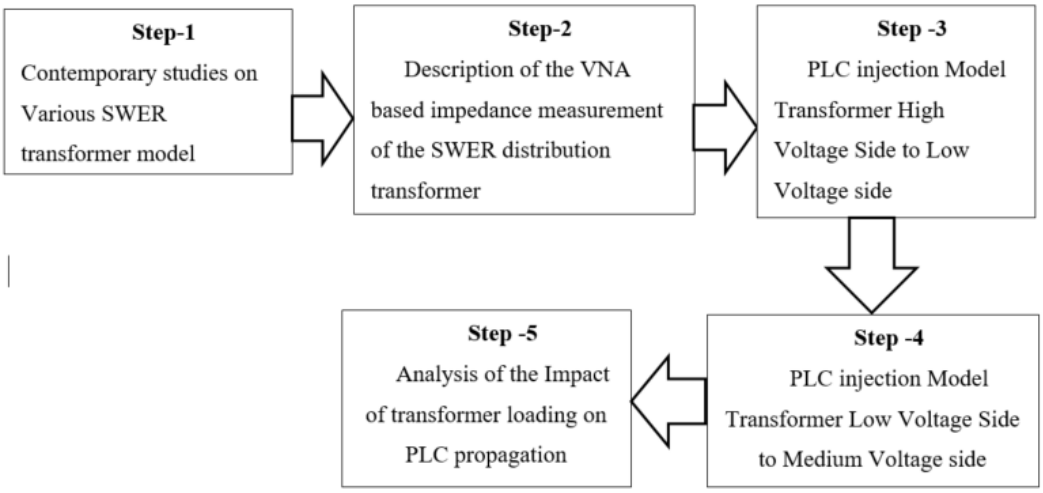

Fig 1.7: Research Methodology for Chapter-5: HF SWER Transformer Modelling

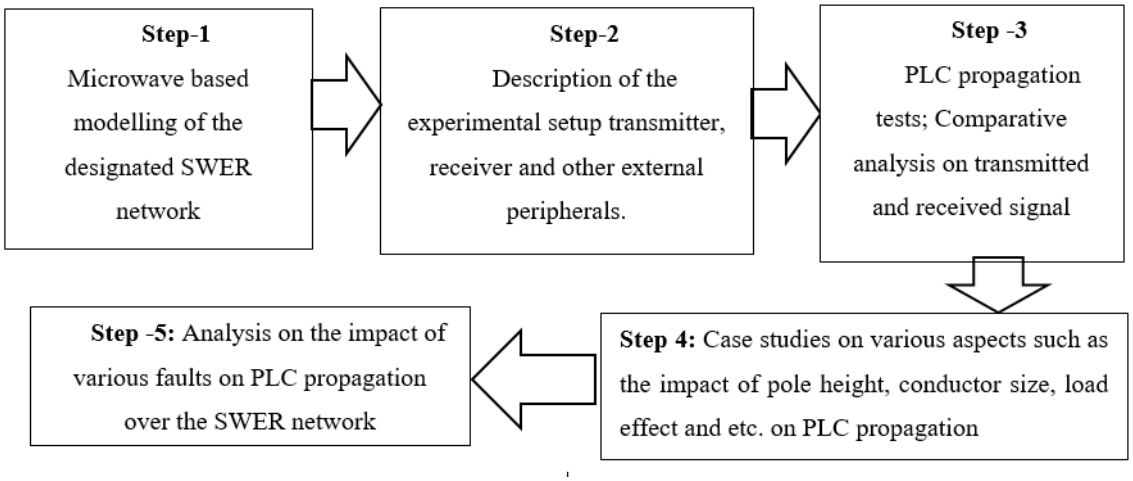

Fig 1.8: Methodology for Chapter-6: HF SWER Communication Channel Evaluation

1.7 Significance and Contributions to Knowledge

Installation of an efficient SWER protection technology is not only a national demand, but also, a global necessity. In developed countries like the United States of America, Australia, New Zealand, the SWER line has been popular during the last few decades. Because of the feeble protection scheme, particularly Australia has been bearing a considerable measure since the last couple of years. Since Australia has an incredible vegetation-based skyline and any sort of vegetation faults in SWER lines may create a threat of bushfires. It has been confirmed that if power line protection systems can detect high impedance low current earth faults, then fire risks from vegetation faults might be reduced by a significant percentage. This means that highly sensitive protection schemes are required to achieve substantial reductions in fire risk. The results of the decreased fire hazard will be exceptionally helpful in various aspects, for example, fewer individuals will pass on, domesticated animals' ranches and industrial facilities will be insignificantly influenced and general conservative harmed will be brought down.

The primary focus of the PhD thesis is on investigating the Single Wire Earth Return (SWER) network, as a communication channel to apply PLC based protection scheme to reduce bushfires. A number of significant scientific contributions have been made in this thesis and as part of the undertaken works, which can be encapsulated as follows:

- A simplified SWER line modelling technique including ungrounded coaxial cables. Significant analysis on impedance estimation, distance dependent path loss analysis of various SWER conductors, and effect of spurs.
- A low loss L-C impedance matching circuit design based on the HV coupling capacitor based coupling to the SWER network.
- Modelling of each injection and coupling method as a frequency dependent 2-port network represented by s-parameter measurements (Touchstone file)
- A novel hardware in-loop s-parameter based High-Frequency (HF) SWER transformer model, which can serve as a good building block for other research works in transformer winding fault detection and transformer overvoltage studies.
- System studies to evaluate the impact of network size, SWER transformer loading, impact of conductor height
- A complete PLC propagation test procedure over the SWER network, and system studies on various aspects such as impact of network size, impact of conductor height, and response PLC signals with various faults situations.

1.8 Thesis Outline

The organisation of this Thesis is as follows:

Chapter 2: In this chapter, a technical overview of the PLC technology is given. This has been pursued with an evaluation of different PLC applications and key challenges in implementing a PLC system. The PLC basics are introduced with a detailed discussion of various key components. Major application domains of this technology are discussed and the review of the use of this application specifically in transmission and distribution networks have been highlighted. This chapter also provides an assessment of key technical challenges inhibiting PLC applications. Finally, a discussion on different PLC standards and electromagnetic compatibility regulations have been included in this chapter.

Chapter 3: The aim of this chapter is to give an understanding of the coupling circuits needed for PLC applications. An efficient coupling arrangement is important for a reliable PLC system. There are a number of coupling circuit designs in existence in the literature each having particular pros and cons. As part of this research, a novel HV L-C resonant

based coupling circuit has been designed for coupling to the SWER line through a coupling capacitor. Simulation, modelling and experimental validation of the proposed coupling circuit are the focus of this chapter. The justification of the performance of the designed circuit with respect to its contemporary coupling design has also been given.

Chapter 4: Wideband modelling of an exemplary SWER network at PLC frequencies is one of the major contributions in this thesis. This chapter presents the modelling of SWER conductors based on detailed mathematical modelling in the Microwave office platform. The focus of this chapter is to estimate the impedance of the SWER line at PLC frequencies. The impedance of three different conductors (SCAC 3/2.75, SCGZ 3/2.75, and SCGZ 3/12) have been estimated using Microwave Office. The experimental procedure to validate the impedance model has also been included in this chapter.

Chapter 5: This chapter highlights the impedance modeling of SWER and isolation transformers at PLC frequencies. The SWER transformer is one of the most important elements of SWER networks and has a significant impact on PLC signal propagation over the network. In this chapter, a novel high-frequency transformer modelling technique has been proposed with experimental validation. System-level performance analysis at different conditions such as load variation of the transformer has been carried out in this chapter.

Chapter 6: In this chapter, a real-time SWER network from rural Victoria, operated by the United Energy, has been modeled using the Microwave Office platform. The overall hardware setup for PLC transceiver system has been explained in this section of this thesis. This chapter includes the holistic discussion from the generation of the transmitted signal to received signal measurements at the load end. Various case studies on the impact of network size, conductor height, and response of the PLC-integrated SWER network with various fault scenarios have also been featured in this chapter.

Chapter 7: The final chapter of this work includes the gist of all the contributions of the thesis. This chapter also represents the advances of this work in the related field from the present state of knowledge. Significant findings of this work are also emphasized in this section to justify the work. This chapter identifies future points of improvement and makes suggestions on potential future extensions. The chapter concludes by highlighting the significance of this research in terms of Australian and global perspectives.

Chapter 2

Literature Review

2.1 Introduction

Power Line Communications (PLC) is a communication innovation that has been primarily utilized in power networks to control remote loads. The availability of the power line and the simplicity of implementation makes it extremely appealing for the stakeholders to invest in this technology. Over the last two decades, it has been vigorously investigated. Institutionalization and standardization have impelled a ton of enthusiasm to implement cutting-edge technology on this exciting system [7-9].

However, the research on PLC systems intensified after the revolution of the smart grid concept. Undoubtedly, the smart grid concept is going to evolve the next generation distribution network due to its multidimensional capabilities. Reliable two-way communication is often necessary for a reliable smart grid technology establishment[10]. PLC offers this capability with a convenient cost and availability. As a result, many smart grid research efforts are focused on PLC integrated smart distribution networks.

PLC signals are often transmitted in the CENELEC-A frequency band from 9 kHz to 95 kHz, which is the band set aside for use by Power Supply Companies. CENELEC B, C, and D frequency bands from 95 kHz to 148.5 kHz can still be used by utilities [11], but can also be used for analog/digital applications within homes/industrial premises. Key components of a PLC system include the coupling capacitor, line tuner, line traps, and PLC transmitters and receivers. Different application domains of PLC systems exist in in-house, last-mile, and industrial processes. Published literature covers applications in automatic meter reading, distributed energy generation monitoring as well as automation and demand-side management. Numerous research and development works are going on throughout the world on PLC systems, but the progress on the field is still not visible in large-scale applications. Researchers are mainly focusing on various technical aspects of a PLC system, evaluating new PLC standards, and exploring new domains of potential PLC application [12].

The selection of the appropriate frequency range for the application of PLC signals on a power network is important. Background noise/signal analysis over the communication channel should be performed before the selection of the appropriate frequency. Carrier frequency, line construction, phase conductor size & material, shield wire size and material, type and location of transpositions, weather conditions, earth conductivity, and insulator leakage are key primary factors affecting signal losses on an overhead line. A transformer tapped, to a PLC channel, may also attenuate the carrier signal. Maximum out-of-phase reflections of the PLC signal will occur when a tapped line is not terminated into any tuned carrier equipment. Reflections of one-quarter or odd multiples of the carrier frequency wavelength can be experienced in the case of power transformer terminations. The type of modulation and error correction will have significant impact on the signal-to-noise ratio and accurate transfer of key information on a carrier signal. The selection of the appropriate PLC standard is therefore critical in designing an effective PLC system.

The signal-to-noise ratio plays a key role in the reliability of a PLC scheme, as communication over power lines is prone to electrical noise. The continuous noise is present at all times with varying amplitudes. Impulse noise is a sequence of short rises in the noise amplitudes. Large impulses of noise can have an adverse effect on the carrier receiver operation making it impossible to detect the carrier signal under certain conditions. The goal should be to get a signal level to the receiver above the sensitivity of the receiver, with a signal-to-noise ratio well above the minimum enabling the receiver to take correct decisions. When the PLC signal is injected into the power line, an impedance mismatch may occur between the coupling arrangement and network conductor. Because of this impedance mismatch, the PLC signal will be reflected and added as an extra voltage to the output magnitude of the transmitter. This extra-high voltage will then be fed into the communication devices, potentially damaging these devices. Coupling circuits are the hearts of PLC systems as the PLC signal is injected into the power line through the coupling circuit. The design of a suitable coupling circuit is significant and requires impedance matching.

However, research on the challenges towards the PLC system implementation is overlooked previously. Considering the gaps, this literature review chapter mainly focuses on summarizing the key technical aspects and implementation challenges, which must be addressed to establish an efficient PLC system over the electricity network.

2.2 PLC Basics

Power Line Communication (PLC) systems use existing overhead electrical conductors or underground insulated cables for data communication with High-Frequency (HF) carrier signals from a couple of hundred Hz up to a couple of hundred MHz [13]. Power Line Digital Subscriber Line (PDSL), mains communication, Power Line Telecom (PLT), Power Line Networking (PLN), or Broadband over Power Lines (BPL) or such systems that use electrical conductors in power transmission and distribution systems for carrying data can be referred to as Power Line Communication or Power Line Carrier System.

PLC is a primitive idea that started at the beginning of the 20th Century, nearly that period of time a 500 Hz signal on the power line was used to control streetlights in New York City [14]. After this innovation, power distribution companies in different parts of the world have started to use this technology for different applications such as Automatic Meter Reading (AMR), remote load control, or similar. Earlier PLC systems were operated with single carrier Narrow-Band PLC (NB-PLC). NB-PLC had a very low-frequency band and low data rates. As time passed, the technology matured, and the area of application has expanded. Currently, the NB-PLC type multi-carrier transmission protocol is being widely used. However, standards of PLC communication protocols are still in the phase of improvement. Fig 2.1 represents a schematic arrangement of a complete PLC system with various associated components such as the line trap, coupling capacitor, line tuner, transmitter, and receivers units.

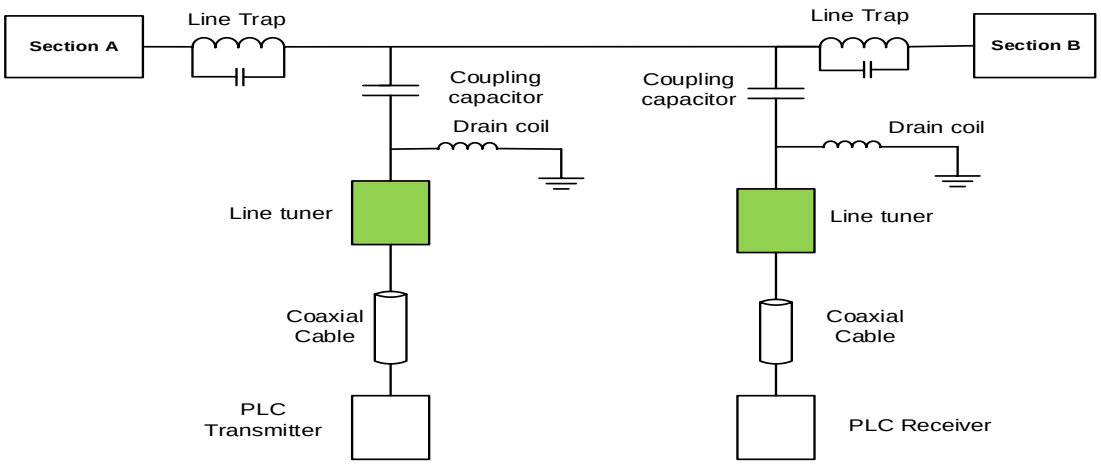

Fig 2.1: Schematic arrangement of a complete PLC system

The PLC transmitter transmits the HF carrier signal. The HF signal will often be injected into the power line via the Coupling Capacitor (CC) and Line Tuner circuit [15]. The carrier signal travels along the overhead line and will be received at the receiver. The line trap blocks the HF carrier signal from penetrating into any undesirable areas of the network. This section reviews the key components of a PLC system including the coupling capacitor, line tuner, line traps, and PLC transmitters and receivers.

2.3 PLC Transceiver

PLC transceivers are also known as PLC modems, which generate the HF carrier signal that later gets injected into the power line using some additional mechanism. Practically, PLC transceivers are mounted in racks and kept in a safe place such as in a cabinet. The device is then connected with a coaxial cable, followed by the line tuner, and the end of the line tuner is connected to a Coupling Capacitor (CC). Finally, the PLC signal is injected into the power line through the CC. Many companies are manufacturing different PLC modems. These include Texas Instruments, GridComm, STM Electronics, CODICO, and Microchip. Fig 2.2 shows the GridComm LV PLC modem. The GridComm GC9200 is claimed to "automatically configure and self-adapt to the varying conditions on power lines, resulting in extremely reliable and robust communications in an LV power network" [16].

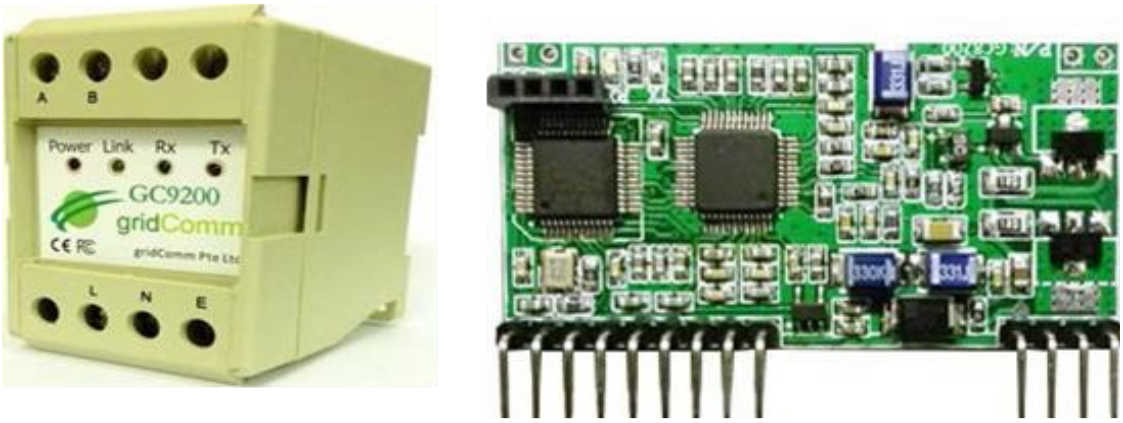

Physical View Internal electronic circuitry

Fig 2.2: GC9200 LV PLC Modem [16].

It is configurable with up to 54 carrier frequencies out of 100 pre-installed frequencies,

between 5 kHz to 500 kHz over 18 channels. It supports different modulation schemes such as 3QPSK, 3BPSK or 1BPSK with up to 18 levels of redundancy [17] . The power network consists of several branches with connected loads, and there should be at least one PLC modem placed on each branch if all branches need to be monitored.

2.4 Coupling Capacitor (CC)

The CC provides a low impedance path for the HF signal to the power line, but a high impedance path to the power frequency. It drops the line voltage across its capacitance with its LV end grounded through an inductor, called the drain coil. The drain coil provides a low impedance path for the power frequency, and a high impedance path to ground for the carrier signal. This arrangement for the Omicron MCC 124 CC is shown in Fig 2.3. The 1 nF MCC 124 CC provides 3.184 kΩ impedance to the 50 kHz signal and 3.184 kΩ impedance to the power frequency. MCC 124 has the drain coil labelled as L1 in the diagram.

$$Z_{C-50Hz} = \frac{1}{2 \times \pi \times f \times C} = \frac{1}{2 \times \pi \times 50 \times 1nF} \approx 3{,}184\ k\Omega \qquad (2.1)$$

$$Z_{C-50\ kHz} = \frac{1}{2 \times \pi \times f \times C} = \frac{1}{2 \times \pi \times 50k \times 1nF} \approx 3.184\ k\Omega \qquad (2.2)$$

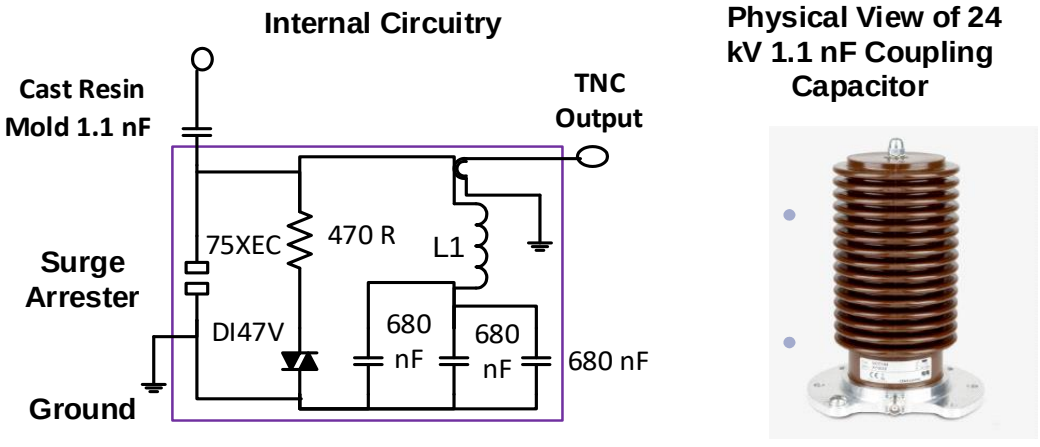

Fig 2.3: Omicron MCC124 CC equivalent circuit and drain coil arrangement[18].

2.5 Line Tuner

The line tuner is a supporting device that is connected with the CC. The purpose of line tuner is to provide a low loss path to the HF PLC signal, so that the PLC signal can be injected into the line. The combination of the line tuner, CC, and the drain coil is used to couple the PLC signal to the conductor and block the power signal from entering the PLC modem. Two basic types of line tuners exist, resonant and broadband [17]. The lead between the CC and tuner should be as short as possible.

The line tuner also helps to match the impedance between the PLC transmitter and the power line. The resonant type tuners can be categorized as single- frequency and double-frequency tuners and used for single-channel or double-channel systems with narrow bandwidth requirements. There will be a protection unit in line tuners, connected from the output lead to ground to limit voltage on the output. It consists of a grounding switch and a protective gap.

The resonant single-frequency and double-frequency line turner diagrams are shown in Fig 2.4. The single-frequency tuner has a single inductor arranged to form a series resonant circuit with the coupling capacitor. The resonant circuit provides a low impedance path for the carrier signal to the power line when tuned to the carrier frequency. The matching transformer provides the impedance match between the 50 Ω coaxial cable and the characteristic impedance of the power line (usually between 150 to 500 Ω).

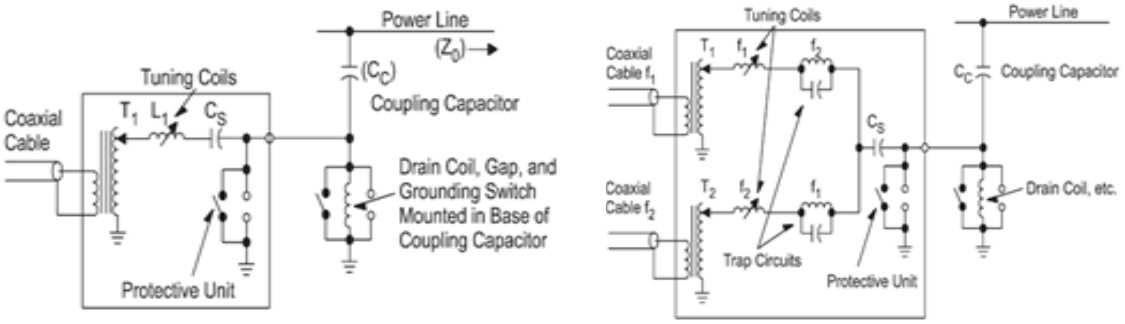

Single resonant circuit Double resonant circuit

Fig 2.4: Types of resonant circuitry: single and double frequency line tuners [17].

The double-frequency tuner has two sets of resonant circuits (each with its own matching transformer and series inductor) tuned to pass two frequencies by providing a low loss path. Each path is tuned to series resonance with the CC at its given frequency. The two-frequency tuner also isolates the two sets of carrier equipment from each other with a parallel LC circuit used for blocking the carrier signal from the other path. The parallel LC circuits resonate at the frequency passed by the other path. Broadband coupling must be used if more than two narrow band frequency groups must be placed on the line [17]. The high-pass tuner is one example of broadband coupling. The high-pass tuner circuit schematic and its equivalent circuit are shown in Fig 2.5. The CC is used as one of the series branches of the high-pass circuit. The low-frequency cut-off depends on the size of the CC and the terminating impedance of the power line.

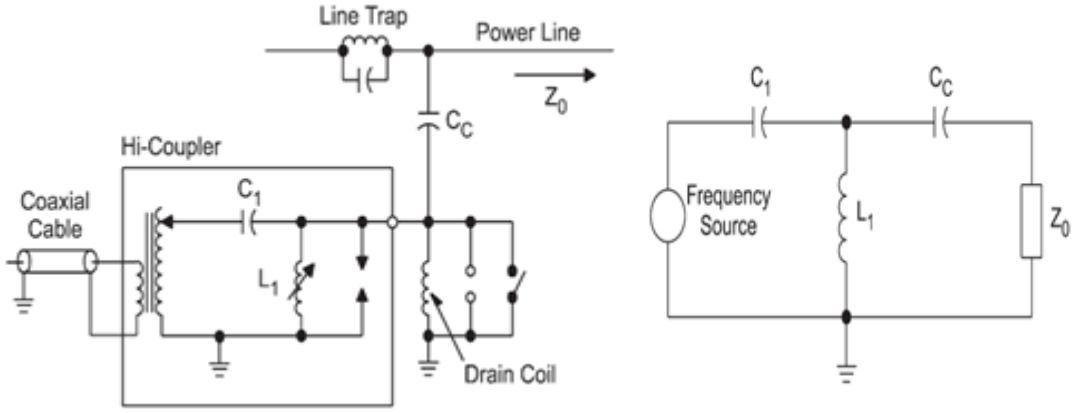

High-pass tuner with power line

High-pass tuner equivalent simplified circuit

Fig 2.5: High-pass tuner and its equivalent circuit [17]

The characteristic curves for the high-pass tuner are shown in Fig 2.6. The circuit does not have a stable characteristic impedance around the cut-off frequency so carrier frequencies close to the cut-off frequency should be avoided. Currently, tuning devices are being manufactured that can simultaneously serve as the coupling circuit and line tuner, such as the MCD 80 [19] from ABB Electronics, which is a popular coupling device for high voltage PLC applications. Fig 2.7 shows the circuit schematic of the ABB MCD 80 [19] coupling device and its setting table. This coupling device is custom designed for application in transmission lines and is programmable for the following line impedances: 240 Ω and 320 Ω.

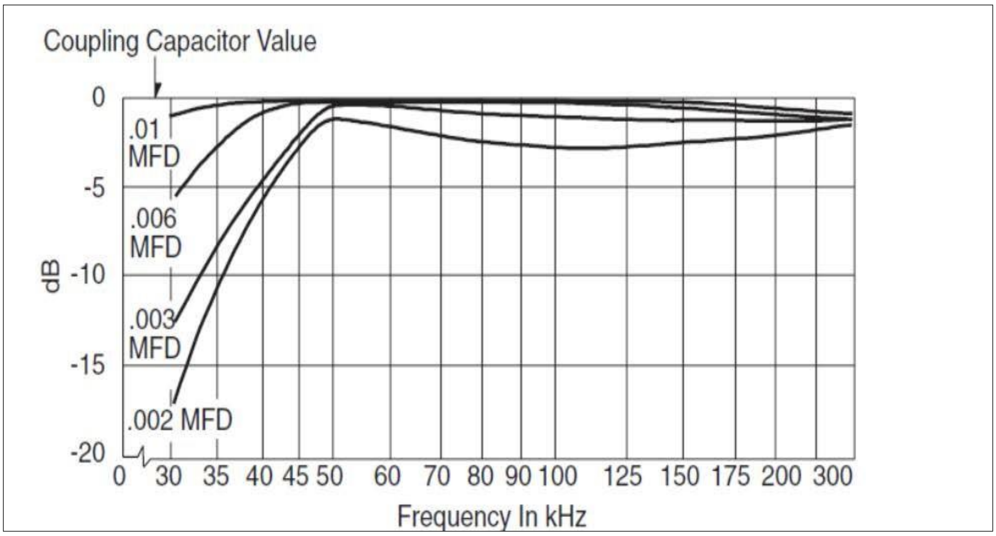

Fig 2.6: High-pass tuner typical characteristic in the 0.01µF to 0.02µF range

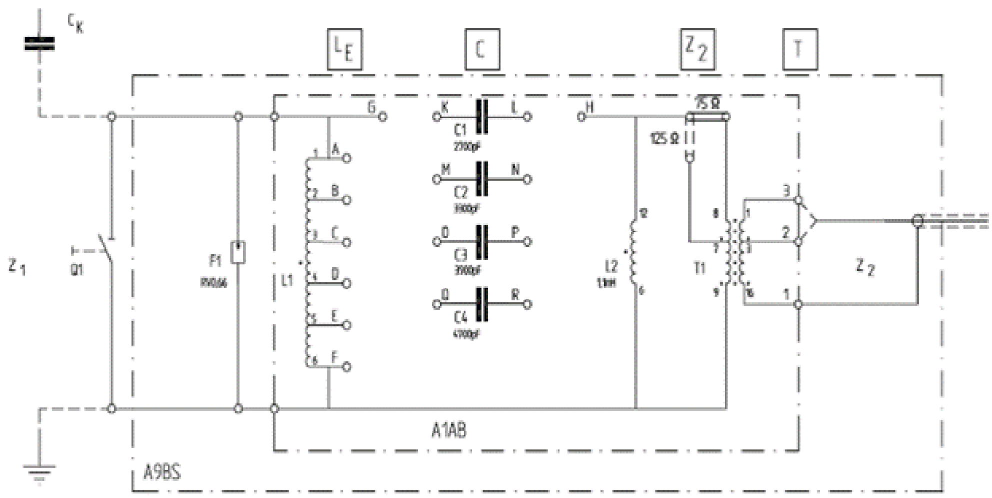

Standard-Einstelltabelle						Tabelle de programmation standard										Standard setting guide								
	Z_2 nom = 75 Ω / 125 Ω f_2 = 500kHz																							
C_K (nF)	f1 (kHz)	Z_1 nom = 240 Ω											f1 (kHz)	Z_1 nom = 320 Ω										
		Verbindungen/Straps/Liaisons										T		Verbindungen/Straps/Liaisons										T
		L_E				C								L_E			C							
1500 .. 2.199	232	AB	DE	EF		HK	LP	GO				3	180	BC	EF		HL	LP	KN	NO	MR	GQ		2
2.200 .. 2.699	158	AB	EF			HK	LN	NR	GM	MQ		3	128	EF			HM	NR	GQ					2
2.700 .. 3.299	132	BC	EF			HM	NP	PR	GO	OQ		3	102	CD	DE		GM	LN	NR	HK	KQ			2
3.300 .. 3.899	115	AB	BC	CD	DE	GQ	LP	PR	HK	KO		3	90	AB	BC	DE	GO	NP	PR	HM	MQ			2
3.900 .. 4.699	96	AB	BC	CD		GM	HN					3	78	AB	DE		GO	LN	NP	PR	HK	KM	MQ	2
4.700 .. 5.599	80	CD	DE			HK	KO	LN	PR	GM	MQ	3	76	BC	CD		GK	KM	NO	PQ	HL	LR		3
5.600 .. 6.799	70	AB	BC	DE		GK	KM	NO	PQ	LR	RH	3	70	AB	BC	DE	GK	KM	NQ	HL	LR			3
6.800 .. 7.499	60	AB	DE			GK	KO	PQ	HL	LR		3	58	AB	DE		GM	MO	PQ	HN	NR			3
7.500 ..	52	BC	DE			GK	KM	HL	LN			3	52	AB	BC		GQ	QN	KM	HL	LR			3

Fig 2.7: MCD80 type A9BS filter circuit schematic and equivalent circuit [19].

The CC ranges specified in the settings table of Fig 2.7 are greater than 1.5 nF. The RFL 9512 [20] line tuning unit from RFL Electronics is an alternative tuning device for turning in the 40-500 kHz range. The product can be connected to CC having a capacitance between 2 to 10 nF. It consists of a drain coil, inductors, and capacitors as shown in Fig 2.8. The optional drain coil drains the power frequency current from the coupling capacitor to ground. The matching transformer enables to match the power line impedance with that of the PLC terminal. The IEEE Standard for 'Power-Line Carrier Line-Tuning Equipment (30 kHz to 500 kHz) Associated with Power Transmission Lines [21] covers the protective devices that facilitate the safe operation and maintenance of the line-tuning components under normal and usual operating conditions.

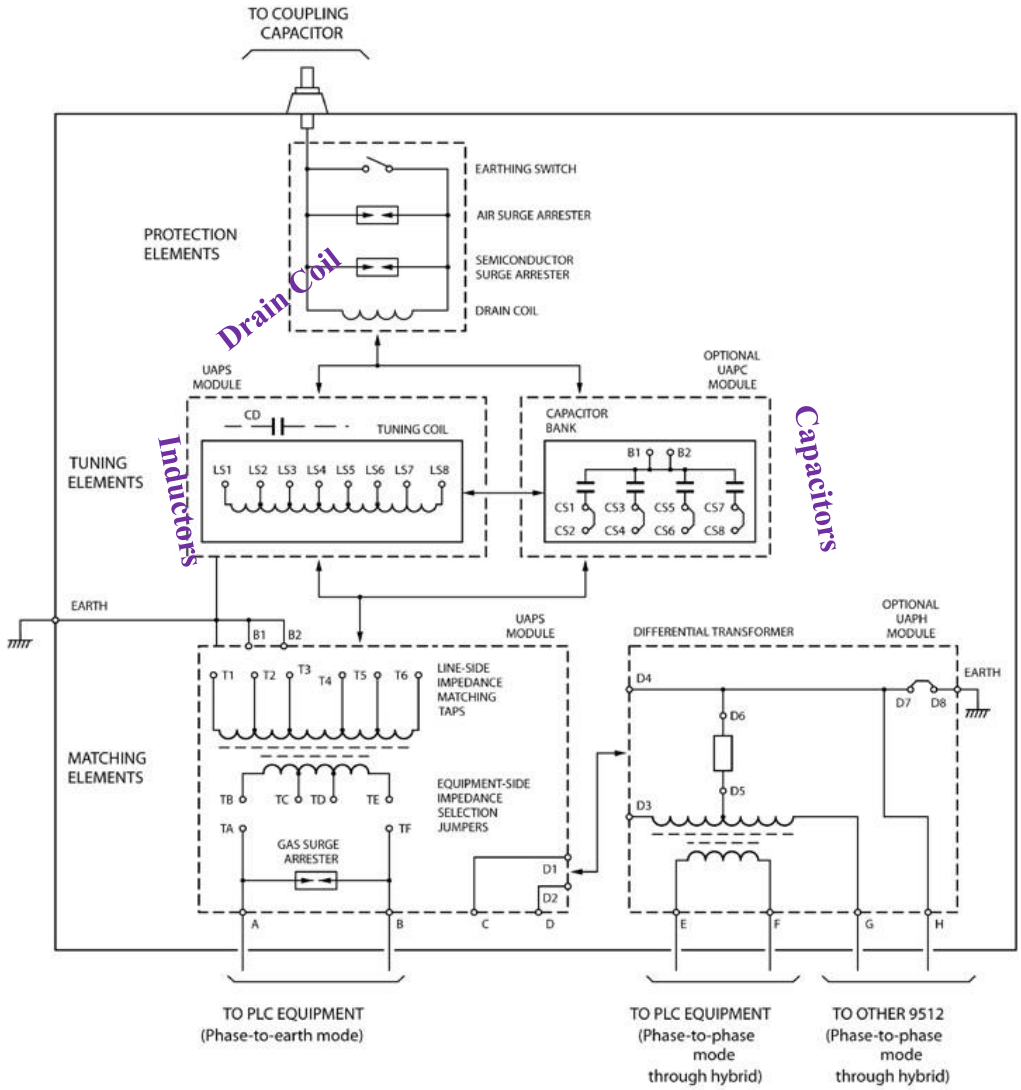

Fig 2.8: Internal circuit schematic of the RFL line-tuning unit [20]

2.6 Line Trap

When the carrier signal is coupled to the power line, it can propagate to the remote line terminal or into the station bus and onto other lines. If the signal is transmitted to a large portion of the system, then some of the energy of the carrier signal will propagate out to other lines, which is undesirable. A line trap is needed to block the energy from going back into the station bus and direct it towards sections of the network where communications is required. A line trap would ensure that the PLC signal is kept within the desirable section of the network. A line trap consists of a parallel LC-resonant circuit in series with the line.

A line trap presents a high impedance to the carrier signal at its resonant frequency stopping the carrier signal from flowing through. On the other hand, the coil of the line trap gives a very low impedance to the power frequency, enabling it to flow through the coil. The physical size of the line trap coil may be very large, because transmission or distribution lines handle large amounts of power. A wide-band trap will block a large bandwidth of frequencies, but it has a low blocking impedance. Bandwidth requirements and the value of the blocking impedance is critical in designing a wide- band line trap. Fig 2.9 shows the typical tuning curve characteristic for a wide-band line trap.

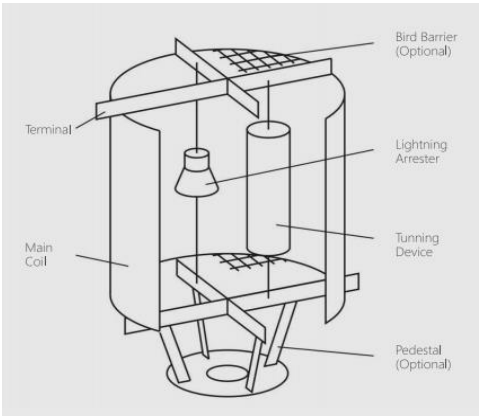

The **main coil** is an air-core dry-type power inductor. The **tuning device**, connected across the main coil, forms a blocking circuit providing high impedance over a specified PLC-frequency range.

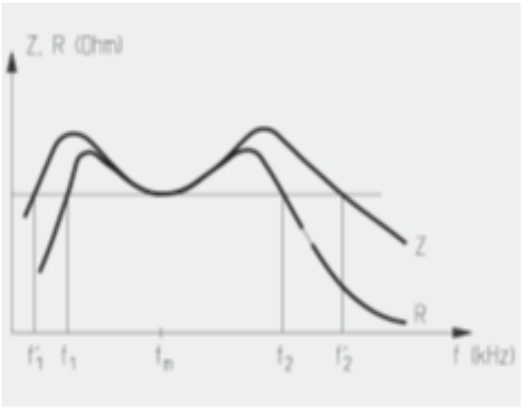

Z= Blocking impedance
R=Resistive component
f= Carrier Frequency
f_m=Resonant Frequency (Geometric Mean Frequency)
f_1f_2= Frequency limits of blocking impedance
$f_1'f_2'$= Frequency limits of resistive blocking impedance

Fig 2.9: Characteristics of a wide-band line trap tuning curve [22]

The tuning device consists of inductors, capacitors and resistors. The tuning device, together with the inductance of the main coil, adjusts the circuit to a resonant frequency (fm) with the minimum blocking impedance/resistance within a band of frequencies. The blocking requirement of a line trap depends on the characteristic impedance of the line where the PLC system is applied.

The line trap blocking characteristics can be specified in terms of Blocking Impedance (**Z**), Blocking Resistance (**R**), Tapping Loss (**At**), and Blocking Attenuation (**Ab**).

Z: is the complex impedance of the complete Line Trap within a specified PLC frequency range.

R: is the value of the resistive component of the blocking impedance within a specified frequency range.

At: also known as the "Insertion Loss", A_t is a measure of the loss of power sustained by a carrier frequency signal due to the finite blocking ability of the Line Trap. The tapping loss should be very low.

A_b: is a measure of the relative transmitted carrier frequency signal, which enters the trapped circuit section of network. The blocking attenuation should be high.

A_t and **A_b** can be calculated using the characteristic impedance of the line (Z_1), Z, and R_b as in Eq. (2.3) and Eq. (2.4). A minimum blocking impedance of 400 ohms is often used. R_b often substitutes Z_b in **At** and **Ab** calculations. The characteristic impedance of the line Z_1 is assumed to be between 300 Ω and 600 Ω.

$$A_t\,(\mathrm{db}) = 20 \times \log_{10}\left(1 + \frac{Z_1}{2 \times Z}\right) \qquad (2.3)$$

$$A_b\,(\mathrm{db}) = 20 \times \log_{10}\left(1 + \frac{Z}{Z_1}\right) \qquad (2.4)$$

2.7 Different Application Domains of PLC Systems

The application of the PLC technique has a long history. The first ever business operation of communication over electrical cables was in Japan in the year 1918 [23]. In that same year, the Imperial Japanese Electro- Technical Laboratory of Tokyo effectively established

a wave communication over a ninety-mile long power line. Some other companies like Fuji Hydroelectric co. installed a PLC system over their 22 kV 3-phase power line by the end of 1918 [24]. However, the most successful PLC system was introduced by AGE, which was reported as the most effective and cheapest mode of communication between its load centers and interconnected generators [23]. The company tested the communication system over an 11 kV, 60-cycle over a 12-mile long distribution power line [24]. However, the primary application of a PLC system in the primitive times was to establish a telephone communication over the power transmission line. Nowadays PLC is considered as one of the innovative technologies for the next generation smart grid. This section reviews different applications of PLC systems in power system networks.

2.7.1 In-House Applications

The in-house application of PLC systems started with the automation of domestic appliances enabling household utilities to be operated with PLC signals. All common utilities can be synchronized with the PLC signal through an Ethernet port, and the PLC signal can be generated using a reliable communication modem to be injected into the AC transmission line. In this context, the PLC system refers to on-line remote operation of different household devices such as computers, printers, or others including coffee makers, hot shower arrangement, water heater, etc. [25].

In [26], the authors focused on the characterization of Brazilian in-home power line channels for data communication based on measurements carried out in seven Brazilian residences. A statistical characterization of the frequency response magnitude, coherence bandwidth, root mean squared delay spread, average channel gain, coherence time, achievable data rate, additive noise and access impedance were presented, in frequency bands from 1.7 up to 30, 50 and 100 MHz . The results show that average channel gain in Brazil is higher than those other countries. The coherence bandwidth was found to be wider than those that were reported in Europe. Root mean squared delay spread was determined to be shorter than those that were reported in United States and Europe. The measured coherence time was shorter than what is previously reported in the literature.

Whiffen *et al.*[27] published a review paper on the applicability of PLC systems in developing a Building Energy Management System (BEMS) for non-commercial or

medium-scale non-domestic buildings. As a survey of accessible technologies, the work examined a novel PLC system for BEMS control. The authors predict that such PLC applications will dominate the automation of small-to-medium size non-domestic premises in the future.

2.7.2 Last-Mile Applications

This kind of application refers to data communication over the power line, which can be used by the broadband Internet Service Providers (ISP) to give internet services to the community. The service might be included with voice (IP telephony), video (VHS video quality), surveillance systems, entertainment (gaming) and utilities metering (electricity/water/gas) services [25, 28]. The cost related to the connection set up for each individual user, in each building, is very high and instalment of this system is difficult because of the different building infrastructure. It might be more efficient to place the PLC device out of the apartment on an electric pole, and then use a wireless trans-receiver to transmit the PLC signals, where the user can access internet from their location within the range of the transmitter. Biao *et al.* [29] investigated the impact of cumulative interference in Broadband Power Line (BPL) communication systems, and developed a 2-D model for describing the BPL transmission activity. The focus was on investigating the interference of electromagnetic field radiating from the power line with other radio systems. The model was based on transmission characteristics of the network and considered the coexistence effect of the BPL devices. The maximum acceptable density of BPL devices and the radiation field were determined.

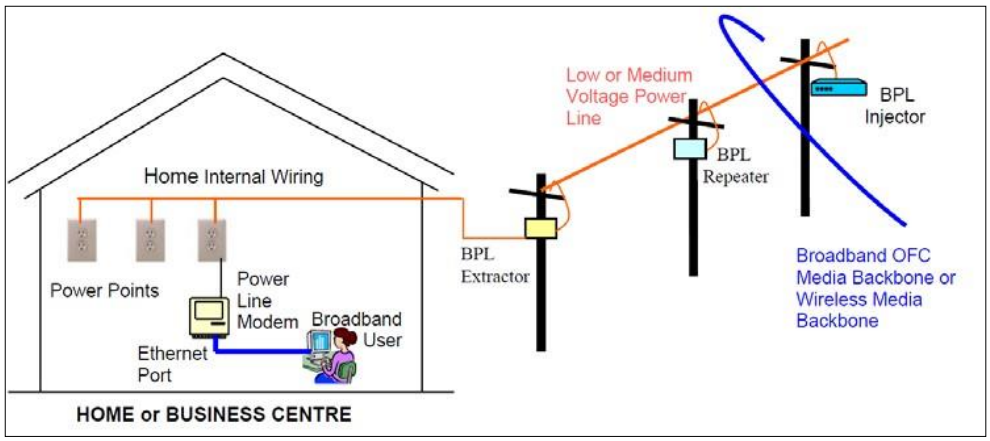

Fig 2.10: Schematic arrangement of PLC based web access networking [30].

Currently, one of the major focus in PLC based research is to establish reliable data communication for internet connectivity over distribution networks. The fundamental idea of this innovation is that it offers fast web access to remote homes through the usually available overhead power lines and house internal wiring. Such a scheme would remove the need of transmission of information over the last mile through the copper link, short pull satellite frameworks, optical fiber links, or through remote innovations, e.g. Wi-Max. Fig 2.10 shows the schematic arrangement of the overall concept of the PLC based WEB access network.

Specially, in rural areas of developing countries, no access to internet is commonly available. Therefore, PLC could become a desirable option for the provision of internet services over an existing electrical power network. A number of researchers from different parts of the world have worked in this field. For example, Krishna *et al.* [31] have been working on BPL-PLC based internet access connectivity over the conventional power lines in India. In [31], the authors highlighted the BPL access technology in terms of features, working principles, drawbacks, deployment & future challenges, and advantages. BPL is now a growing communication network technology, which is penetrating into the competitive markets of broadband internet services in the international telecom field.

Kikkert *et al.* [32-35] have also worked on establishing PLC based data communication over the Single Wire Earth Return (SWER) network in the Australian rural outback. In some papers, the authors discussed the modelling procedures of some individual components of the SWER system such as the transformer and coupling circuit. Then, Kikkert and collaborating authors have published on different loss calculations such as the radiation, attenuation, and return losses in SWER networks [36-38]. Overall, this group has studied the feasibility of data communication over the Australian SWER line.

2.7.3 PLC Technology in Industrial Networks

PLC-based systems could be an option for information transmission in industrial applications, similar to systems used to control machines and gathering sensor readings at the field level. The introduction of PLC systems in industrial environments reduces the effort of ground worker, increasing reliability and efficiency of the machines. Modern industrial applications require interminable trustworthy exchanges for multipoint frameworks, which

will be capable of large node operation with quick response times. As a committed communication medium, wireless and fiber-optic based systems may not be the most feasible choices for controlling and monitoring a large distributed industrial network. In these cases, PLC could be a reliable solution through the existing electricity distribution network. The noisy communication channel in an industrial environment may compromise the reliability of PLC technologies and cause interference.

Rinaldi *et al.*[39] investigated a multi-protocol instrument for PLC performance in industrial applications. A solution was proposed to characterize and decode several PLC systems with different physical modulations using a software-defined architecture. A working prototype was built and used in a real industrial plant to study potential issues affecting PLC. Fig 2.11 shows the architecture of the developed prototype and its implementation using USRP boxes from Analog Instruments. The results of the study showed that PLC technology could be reliably used in an industrial environment to provide non-critical information over a distance longer than 100 m. A careful selection of transmission frequency band was however shown to be critical, in limiting the influence of distorting electric loads.

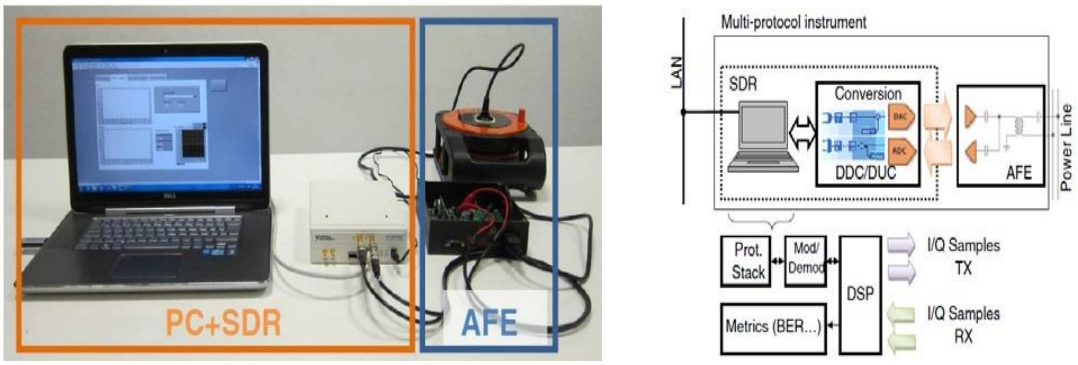

Fig 2.11: Prototype developed for PLC based monitoring in industrial networks.[39]

2.7.4 Other Potential Applications

Another very common application of PLC system is broadcasting radio programs over the power network, similar to providing internet connectivity to rural communities. Some rural areas might still be out of radio network coverage due to low population but have access to an overhead electricity distribution system. The radio companies can easily use this power

network to broadcast their programs through PLC facilities [40, 41]. They can also use the PLC system as a redundant channel to operate emergency programs, if any emergency occurs and normal radio channel may be out of service. The PLC system might also be used for some other specialized purposes such as in remote EEG and ECG monitoring [13]. Many rural areas have poor health facilities and the tele health industry is a very rapidly growing technology, limited to giving suggestions and prescribed medicine to the patient. This technology can easily go one-step ahead with some extra accessories to make it possible to monitor the EEG and ECG signal of a patient, transmitted to a doctor through the electrical network. This will help the doctor in taking the right decisions about a patient living in a rural community and quality of tele health care will definitely informed by adopting this technology.

Ding *et al.* [40] proposed a hybrid PLC and visible light communication-based utility control system for a modern hospital. PLC can utilize the pervasive electrical cable system to control the light-emanating diode lights while filling in as the main network arrangement for the indoor visible light communication frameworks. In [41], a hybrid broadband electrical cable and visible light communication framework, with orthogonal recurrence division multiplexing adjustment, was proposed for the indoor healing facility applications. The proposed scheme is a brand-new solution to supersede the traditional remote communication frameworks in a hospital, offering a brand-new solution to replace the conventional wireless communication systems in hospitals.

2.7.5 PLC Applications in Transmission and Distribution Systems

This section reviews the use of PLC concept for various applications in transmission and distribution networks. Applications such as automatic meter reading, remote monitoring of distributed generation, protective relaying, demand side management, and voltage regulation in smart grid networks are discussed.

2.7.5.1 Automatic Meter Reading

Theodore George introduced the first automatic meter-reading framework in 1974 [11]. It is a very common consumer complaint that the retailer issues their electricity bill in prediction not by real checking. In this regard, PLC integrated automated meter information from the

consumer can be consequently gathered and exchanged to a main database for billing. At the end of each month, the retailer can produce the billing information inclusive of a load curve, which could help the customer to identify hidden energy waste and manage their use in an effective manner.

In [41] the authors presented an analysis of narrowband PLC modems, and implemented a hybrid PLC-wireless module for smart metering applications. The experimental measurement focused on investigating the reliability of the PLC solution, using vacant wiring between a transmitter and receiver for a distance of 500 meters in the absence of noise. The results showed stability of communication for all types of modulations. In undertaking the measurements, 1000 packets were transmitted with maximum packet size according to modulation method. This included a maximum transmitter gain of 6 dB, and communication without acknowledgment of transfer. The hybrid PLC-wireless solution was based on HDR NB-PLC and **G3-PLC** standard and a chip from MAXIM (MAX2992 and AFE MAX2991). Fig 2.12 shows the XBee PRO 868 development kit was used for the wireless modem.

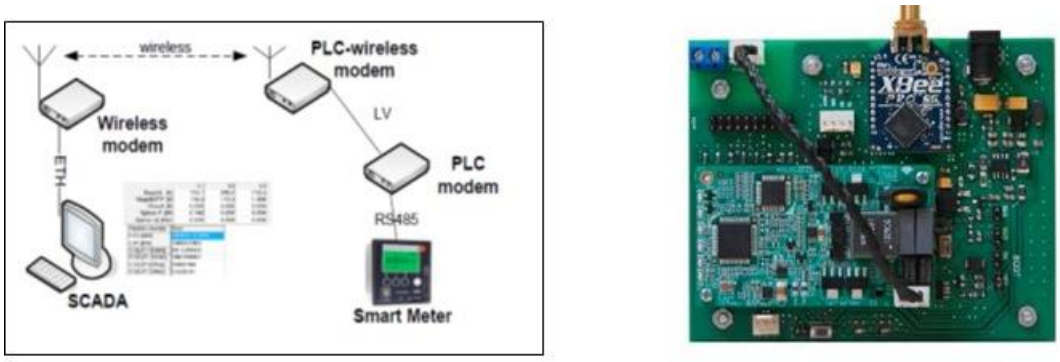

Fig 2.12: Prototype of the hybrid PLC-wireless module [41].

2.7.5.2 Monitoring Distributed Energy Generation

With increased demand for green energy, renewable sources such as small hydropower, wind turbines, and PV systems are growing day by day. It is a challenge to connect and coordinate these micro generating stations within a conventional distribution network. To ensure efficient power transmission and monitor the operation of these Small Electricity Generating Plants (SEGPs) within a distribution grid, a reliable two-way transmitting media is often needed. PLC systems can offer this service. In such a system, there will be an

Operation and Control Centre (OCC), which will be linked with all the SEGPs through PLC communications. From OCCs, operators will get necessary information to monitor the status of the power flow between the grid and SEGPs [42, 43]. Fig 2.13 illustrates the schematic of the PLC based SEGPs monitoring for transmitting data on MV (13.8 kV) networks. The project was only evaluated in the laboratory through modems connected to the LV network. The authors are yet to install any equipment in the field, to assess the quality of services parameters and performance of the PLC technology under real conditions of use.

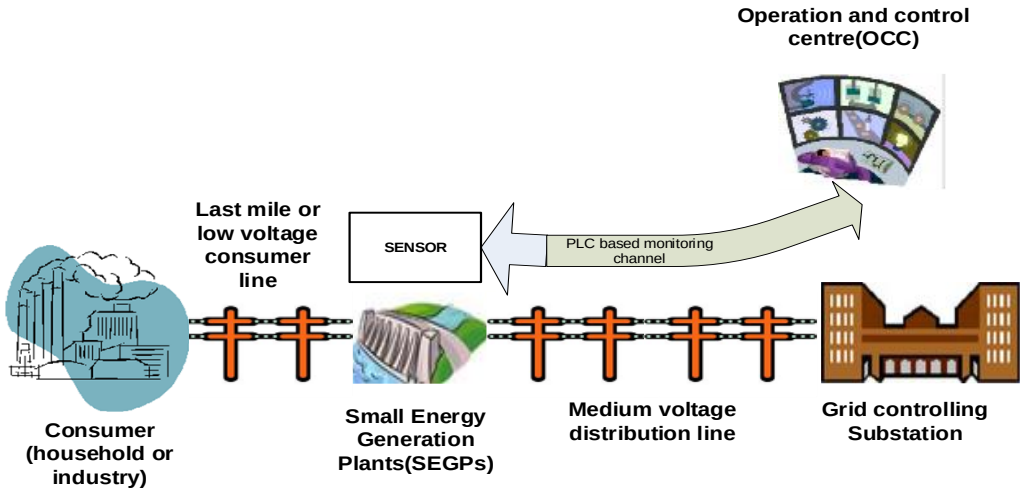

Fig 2.13: PLC based SEGPs monitoring project [43]

Petit *et al.* [44] have also published work with a similar concept, where they developed a PLC based monitoring system for distributed renewable energy sources connected with the HVDC bus. The authors analysed the working modes of communication interfaces based on PLC using the Amplitude-Shift-Keying (ASK) modulation. The conclusion was that basic solutions offer poor quality of signal and generate many harmonics of the fundamental carrier inducing important electromagnetic perturbations. An original solution was thus developed and implemented in a PLC interface. This was based on a narrow spectrum carrier, on a resonant HVDC bus, working at a low frequency allowing to minimize the generation of harmonics and thus to increase the quality of the transmitted information.

2.7.5.3 Automation and Demand Side Management

Remote Energy Management and automation of the distribution devices using PLC is one recent evaluation in the PLC sector. Execution of Distribution Automation (DA) and

Demand Side Management (DSM) is expected to serve both utilities and an extensive number of clients, spread over a vast region and requiring a wide-zone two-way correspondence framework. DA and DSM devices (e.g. meters, switches) enabled with PLC capability can utilize the power line as the channel in developing a financially perceptive and fast transmission correspondence arrangement. PLC capability in such devices would enable an economic, secure and reliable communication system [45, 46].

The communication system for DA/DSM applications requires multi-tasking as automatic remote meter reading, load management, on-request meter reads, and other distribution control and monitoring functions must be simultaneously implemented. Lu *et al.* [47] proposed remote energy management over power lines using PLC technology to maintain a hierarchy. The distribution voltage levels were divided into two levels as master and slave. The MV master is connected with the ISP through TCP/IP link, and a PLC link connects the MV-master with the MV-slave. Similarly, the LV- master is connected with the LV-slave thorough PLC links. At the final stage, the LV-slave will be connected with an application software such SCADA. The authors analysed and simulated the proposed system to evaluate the communication performance. A new scheduling policy was proposed to provide differentiated QoS in a multitasking environment. The conclusion was that the proposed PLC system would meet the demands of DA/DSM application. However, no real-life implementation was carried out to prove the concept further.

2.7.5.4 Protection of Electrical Networks

Sanders and Ray [17] were the first engineers to introduce the PLC idea for transmission line protection options and discuss the details of a typical relaying schemes using power line carrier signal. They introduced a blocking system, where the channel is used to indicate an external fault, sending a signal to prevent tripping (blocking). On the other hand, a permissive overreaching transfer trip system was outlined as one that uses the channel to indicate an internal fault, giving permission to a trip. They raised a concern regarding that a fault may result in attenuation of the signal. This was likely to prevent the arrival of the signal at the remote end, when the receiver logic should allow tripping on loss of channel for some predetermined time, usually about 150 ms. The basic elements of the directional-comparison blocking system are shown in Fig 2.14.

At each terminal, directional phase and ground trip units (P1 and P2) are located and set to operate for all internal faults. The start units (S1 and S2) are set more sensitively than the remote trip units. P units are directional overcurrent relays, where S units are non-directional overcurrent relays. The key idea is to transmit blocking signals to the protected line such that breakers do not trip not interrupting the power supply. Besides the conceptual discussion of this protection framework, Sanders and Ray presented no real life implementation or test results. That is a significant shortcoming of the comprehensive guide given in [17].

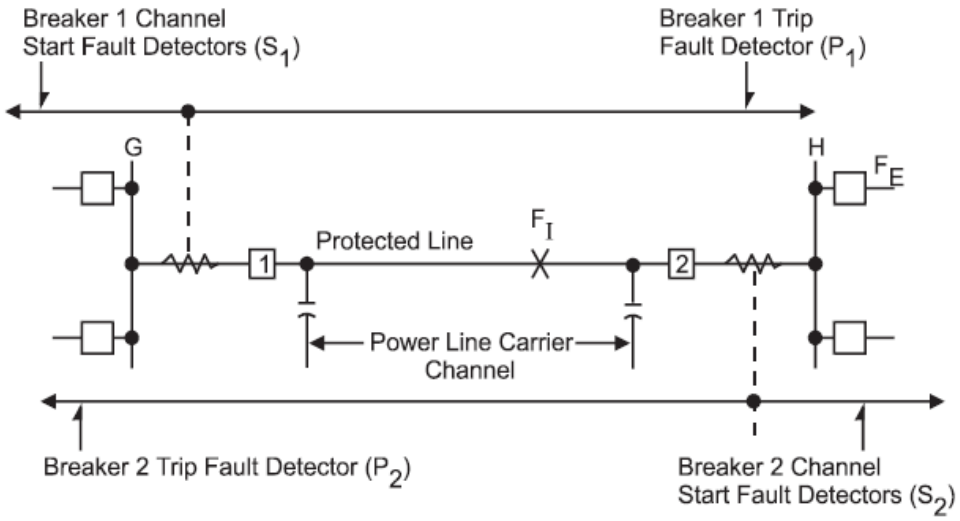

Fig 2.14: Directional comparison blocking scheme [17]

Benato *et al.* [48] proposed a PLC based MV distribution network protection and control scheme. The basic concept of the scheme was that the PLC signal would be superimposed over the MV distribution network through a suitable coupling device. The signal will be generated by the transmitter (Tx) located at the MV substation bus and transmitted through the network until received in the receiver (Rx) located at the common coupling of dispersed generators. The main schematic arrangement of the proposed protection and control scheme is shown in Fig 2.15. The PLC system is used for islanding detection such that any line- tripping event at the substation will be immediately detected by each dispersed generator at the point of common coupling, independently of the actual power flow in the feeder before the loss of main supply. The scheme is recommended as a solution to prevent DG islanding. No real-life implementation was discussed and no results besides a conceptual discussion was presented.

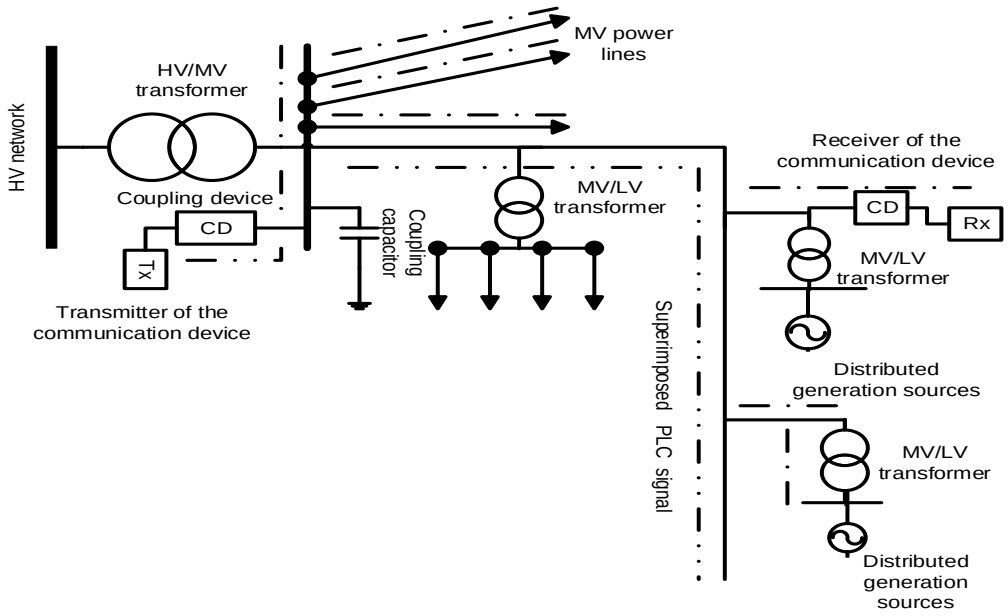

Fig 2.15: PLC based islanding prevention scheme [48]

Milioudis *et al.* [49-53] have also done significant work on a PLC based protection scheme using high frequency impedance measurements. The main theme of these works is to use an algorithm to measure the input impedance of the distribution network at faulty and steady state conditions. Finally, they compared the impedance values to differentiate the faults on the lines. The key objective was to detect occurrence of High Impedance Faults (HIFs) in rural overhead power distribution networks [50, 53].The works were conceptual and numerical, and only presented simulation results. Moreover, the structure of the distribution network was very complex and the line distances were very long. As a result, implementation of PLC of this structure would be associated with lots of challenges such as noise and high attenuation. None of these challenges were discussed by Milioudis et. al. [49-53]. Hence, the implementation challenges of PLC system such as background noise levels and carrier signal attenuation were not really considered.

In their works, Milioudis *et al.* [50, 53].mainly implemented a simulation-based GIS-PLC oriented enhanced protection scheme for the conventional single phase and 3-phase power lines. Their studies mainly present simulated results, and the authors have implemented an algorithm, which compares the impedance value of the power line in healthy and faulty conditions to detect abnormalities. A serious shortcoming of the studies in [50, 53] is that authors failed to validate their design on a real network and failed to consider the impact of network noise on the viability of their proposal. At high frequencies,

the behavior of network equipment such as transformers, coupling circuits, and line traps change rapidly. Specially, the insertion loss of the PLC signal would increase while passing through this equipment and if reduced to a certain level, then the PLC modem may not able to receive the signal due to a high signal-to-noise ratio. Assuming a threshold insertion loss of 40 dB for a G3-PLC modem, any signal with an insertion loss beyond this will not be received by the modem.

2.8 PLC Implementation Challenges

Power lines are designed to operate on the 50 Hz power frequency. For this reason, various unfavorable conditions may occur when HF PLC signals are injected onto power lines. For example, the impedance of line varies with frequency. Different communication signals such as radio or mobile communication signals will cause interference and the designated PLC signal will be attenuated. Typical electrical equipment, for example line transformers, create reflections and attenuation. Power electronics devices and different loads may add noise to the channel. However, such challenges can be alleviated by adopting technical measures such as adding subsidiary communication devices, using high profile signal repeaters, correct coupling and matching, and using the appropriate modulation technique. Adoption of these measures in a PLC system will help in making such systems more reliable in applications including remote internet access, smart network management, and monitoring. In this section, we discuss different challenges that should be seriously considered in designing and implementing a PLC system

2.8.1 Frequency Spectrum Selection

Selection of the frequency range for PLC signal application on a power network is a very important task aligned with the selection of the appropriate PLC standard. There may be other communication systems operating over the same frequency range. Different FM and AM radios, signals from different mobile operators may also exist over the same frequency range. This implies that before the selection of the appropriate frequency, background noise/signal analysis over the communication channel should be performed. Herewith, a cross check of the PLC standard must be done on the compatibility of the frequency range with the specific application. Future growth of the existing electricity network must also be

considered before implementing the PLC system. Some other issues must also be considered such as the range of the PLC frequency band and expected levels of noise and attenuation at different frequencies within the band.

2.8.2 Line Attenuation

The primary factors for losses on a line are the carrier frequency, line construction, phase conductor size & material, shield wire size and material, type and location of transpositions, weather conditions, earth conductivity, and insulator leakage. As shown in Fig 2.16, line losses increase as frequency increases due to shunt capacitance becoming lower at higher frequencies. It is important to note in Fig 2.16 that there is close to a linear relationship between the carrier frequency and attenuation for network voltage levels ranging from 34.5 kV to 765 kV. This close to a linear relationship is more obvious for lower system voltages such as 34.5 kV and 69 kV.

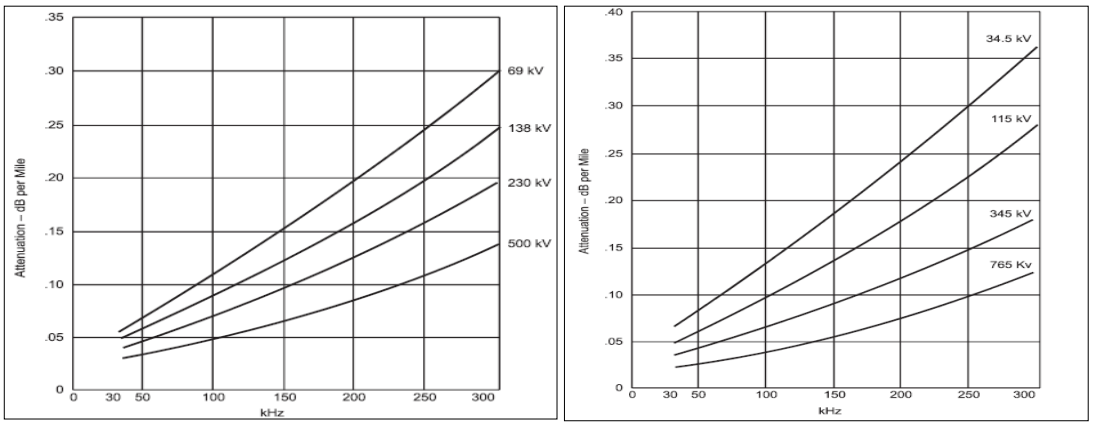

Fig 2.16: Attenuation with respect to frequency [17].

A secondary reason for the attenuation is conductor losses due to the increased skin effect decreasing the conductor area available to the higher frequency current. Weather conditions, such as heavy frost, play a large role in the changing of the line attenuation and increased losses. In the case of frost, due to skin effect, the carrier signal propagates on the ice instead of the conductor leading to significant changes in the attenuation as much as 4 or 5:1, depending on the frequency [17]. Changes in earth conductivity (due to extreme changes in soil moisture) would also affect line losses especially when the coupling method relies on modes of propagation requiring the earth as a return path.

2.8.3 Power Line Noise

This section reviews noise considerations in two sub-sections. First, general background on sources of noise are discussed followed by a detailed review of the real-time noise measurements undertaken during the 'Vegetation Conduction Ignition Testing' project undertaken as part of the Power Line Bushfire Safety Program (PBSP) in Australia [54].

2.8.3.1 Continuous and Impulsive Noise in Power Networks

The received signal-to-noise ratio will be instrumental in predicting the reliability of the proposed scheme as communication over power lines is prone to electrical noise. During the process of travelling to the other end, the PLC signal will not only be attenuated, but noise will also be added to the signal. Power line noise can be categorized as either continuous noise or impulsive noise. Continuous noise is always present with varying amplitude as per the frequency considered. AM radio noise will be picked up on the network as continuous noise. Lightning, the operation of machinery, electrical arc or faults within customer installations can also cause impulsive noise with amplitudes much greater than the average level of the continuous noise. Impulse noise is sequences of short rises in the noise amplitudes. The sources of impulse noise are emissions from devices connected to the power grid. On the other hand, impulsive noise will only exist for short periods, e.g. during the start-up of a farm motor. Large impulses of noise can have an adverse effect on the carrier receiver operation making it impossible to detect the carrier signal under certain conditions. The work by Sanders *et al.*[17] has analyzed noise levels for a 230 kV power line at frequency ranges from 30 kHz to 300 kHz.

The results show that weather has a huge effect on the power line noise. The goal should be to get a signal level to the receiver that is above the sensitivity of the receiver, with a signal-to-noise ratio well above the minimum enabling the receiver to take correct decisions based on the information received. The type of modulation and application of the channel will have an impact on the signal- to-noise ratio. Carrier frequency is also significant as noise on the power line decreases as the frequency increases. This is depicted in Fig 2.17. On the other hand, attenuation increases as the frequency increases so the carrier frequency should be selected within the CENELEC range taking both noise and attenuation into consideration.

It is necessary to determine how noise levels would affect decision making in the receiver and whether the signal-to-noise ratio is going to present an issue.

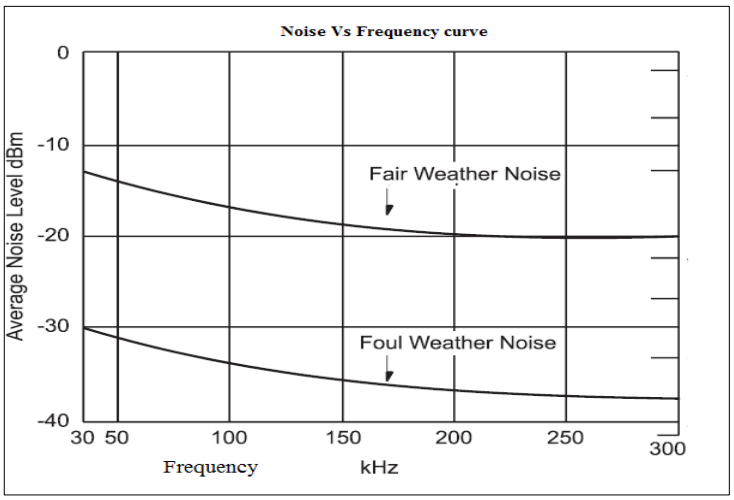

Fig 2.17: Noise variations with respect to frequency [17].

2.8.3.2 Noise Measurements at the Springvale (VIC, Australia) Test Facility

The 'Vegetation Conduction Ignition Testing' [54], one of the funded research projects of the Power Line Bushfire Safety Program (PBSP), tested a variety of vegetation species on a real 22 kV feeder under various fault scenarios including phase to phase and phase to earth faults. These tests produced a large database of High Impedance Fault (HIF) signatures with high sampling resolution, low-noise, and wide-band recordings. During the tests, background noise levels were also recorded for a conductor with a peak voltage of 18 kV. Noise measurements were recorded with no fault present in the network. Most recordings were taken for the 12.7 kV RMS phase-to-earth voltage at the test rig.

Low-Frequency Network Voltage Background Noise: This subsection provides a review of LF background noise levels up to 50 kHz. In the LF channel, a low-pass anti-aliasing filter with a cut-off frequency of 50 kHz was used and a Digitiser sampling rate of 100 kS/s was adopted. Fig 2.18, Fig 2.19, and Fig 2.20 show the frequency spectrum analysis of the measured voltage. In the 0 to 1 kHz range, the power frequency and its harmonics were dominant. The 5th, 7th, 11th, and 13th harmonics dominated the harmonic distortion with harmonic pairs visible in the spectrum well beyond 1,000 Hz [54]. The noise floor clearly reduced as the frequency increased as shown in Fig 3.20.

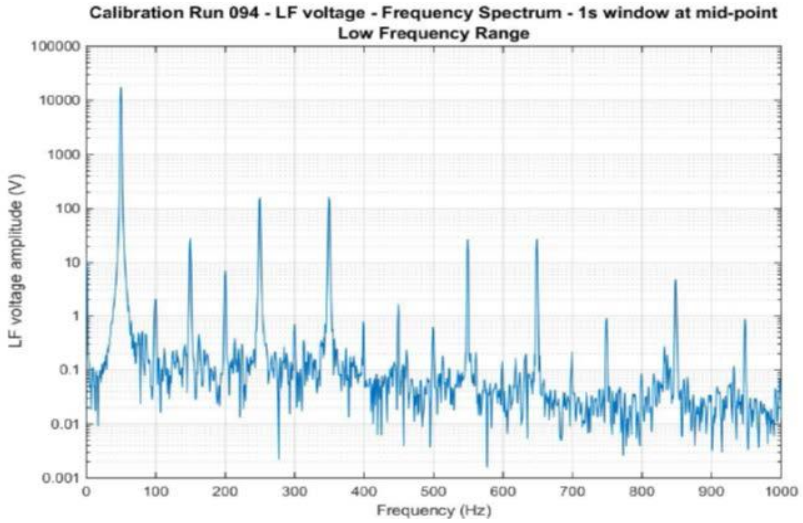

Fig 2.18: Noise in the range 0 to 1 kHz [54].

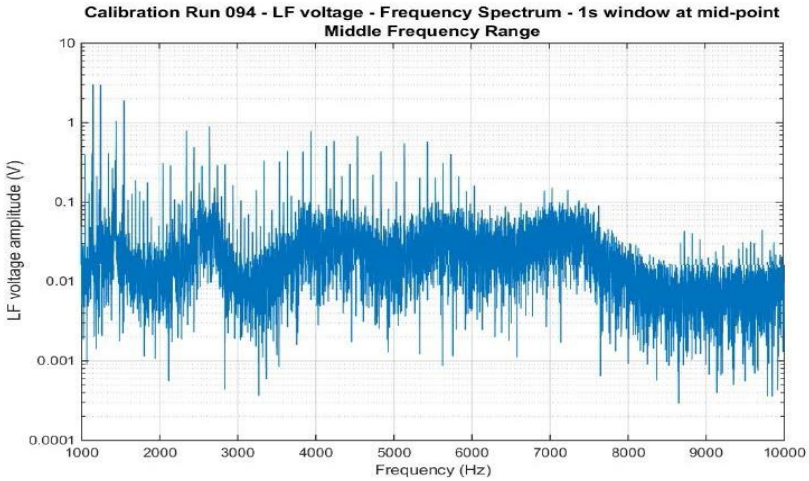

Fig 2.19: Noise in the range 1 kHz to 10 kHz [54].

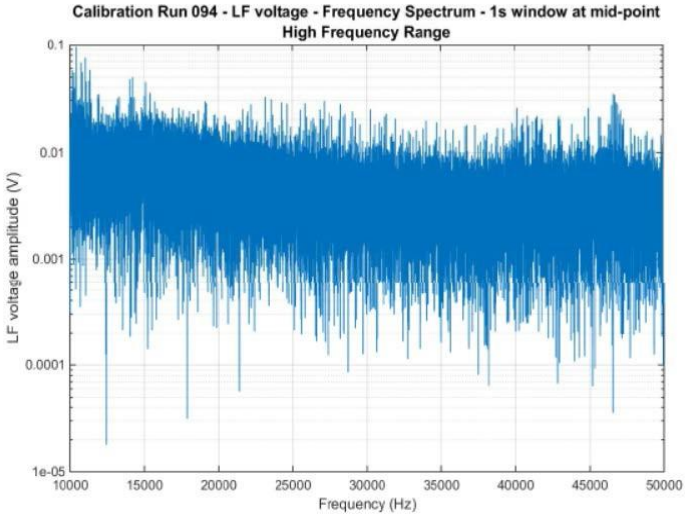

Fig 2.20: Noise in the range 10 kHz to 50 kHz [54].

High-Frequency Network Voltage Background Noise: For the same Calibration, the HF phase-to-earth HF voltage spectrum was obtained as shown in Fig 2.21 and Fig 2.22 for frequencies up to 200 kHz. Typically, the high-frequency voltage noise varied between 0.3-0.8 volts according to Marxsen [54]. The high-frequency voltage noise has broad amplitude peaks around 7 kHz, 11 kHz, 15 kHz and 100 kHz before decreasing to less than 0.5 mV beyond 500 kHz [54].

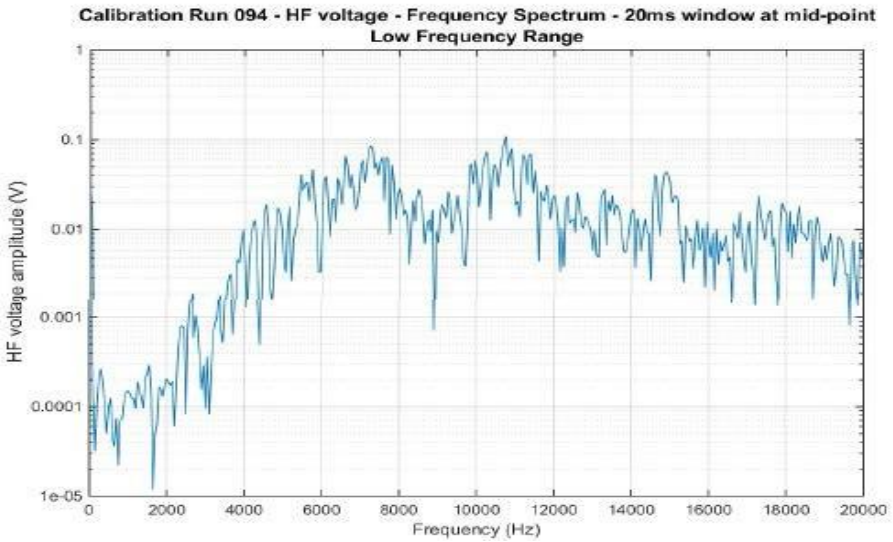

Fig 2.21: HF Noise in the range 10 kHz to 50 kHz [54].

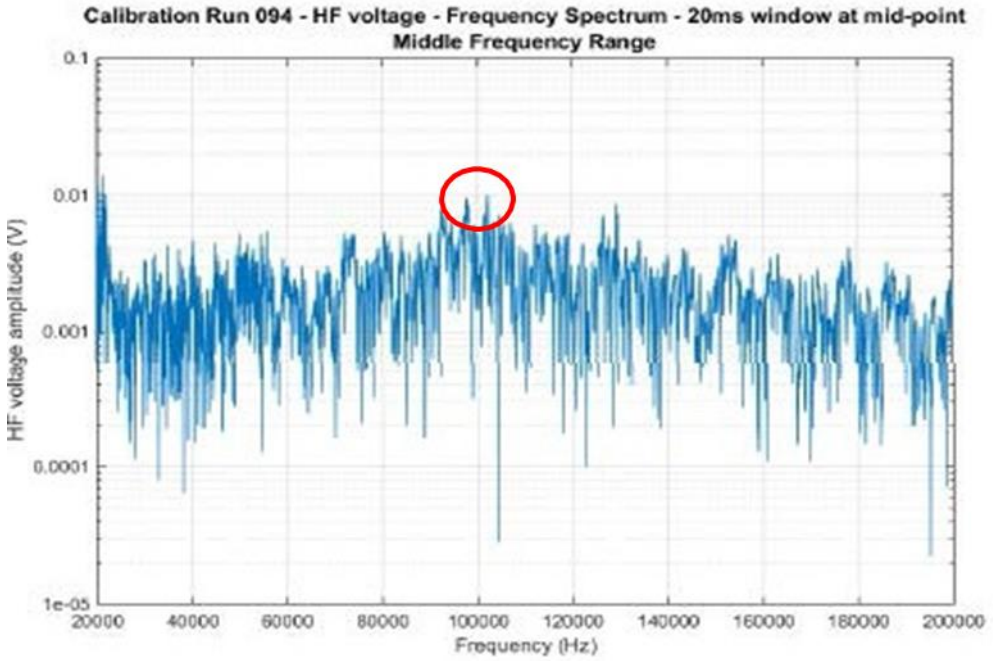

Fig 2.22: HF Noise in the range 20 kHz to 200 kHz [54].

2.8.4 Impedance Variation

One of the major troublesome features of implementing a PLC system on power lines is the variation of the impedance at high frequencies. From literature, it was determined that the net characteristic impedances of a power line are in the range of 100 Ω [55, 56]. However, the network topology, conductor size, connected loads etc. influence the characteristic impedance. Due to variations of the characteristics impedance with frequency, when PLC signal is injected into the power line, an impedance mismatch may occur between the coupling arrangement and network conductor. Because of this impedance mismatch, the PLC signal will be reflected and added as an extra voltage to the output magnitude of the transmitter. This extra-high voltage will then be fed into the communication devices, potentially causing damage to the devices. Calculation of the characteristic impedance at high frequencies is very important for the effective integration of a PLC system into the network. Several researchers have worked to estimate the impedance of the power line at high frequencies.

Research approaches for frequency dependent impedance (FDI) measurement has a long history, J.R. Carson from the USA and F. Pollaczek from Germany are the pioneers on this field, both of them published two bench-mark papers on (FDI) measurement method in 1926 and 1931 [57, 58] . Until now, those have been considered as the standard method for (FDI) measurement. However, the Carson's technique has an inadequacy; it represents the impedance by means of complex integral. Subsequently, if this complex integral does not calculate properly, Carson's technique may cause impressive truncation errors at high frequencies. After a half century of Carson's publication, C. Gray, a research engineer of French Electricity Board has proposed a modified approach [59] which could minimize the truncation error of the Carson's method by replacing complex integral into a solvable equation. Unfortunately, the new approach did not receive much attention due to lack of enough theoretical proof.

However, five years later after Gray's publication, A. Deri, a Professor from the Budapest University, Hungary established a relation between the Carson's method and Gray's approach [60]. In his paper, Deri rigorously proved Gray's modified approach was more accurate for high frequency impedance estimation, which is valid for a large frequency

range. This was a milestone in the development of high frequency impedance measurement technique evaluation. Since then, this method has been widely used in different applications of electric power engineering.

Amongst researchers, Cavdar *et al.* [61] developed interpolation-based equations to estimate the impedance of different types of power lines in a frequency range from 10 kHz to 170 kHz. These equations can be used to estimate the impedance value of a specific power line in the designated frequency range. In recent time, Kikkert *et al.*[33, 62, 63] have published works on developing on-line high frequency impedance measurement techniques. Besides the above, a few other researchers have also done some good work on high frequency impedance prediction of a power line those are given in [63-66]. Hence, it is very important to analyze the impedance value of the distribution network before implementing PLC system over it.

2.8.5 Coupling Circuit Design

One of the major problems in practical implementation of a PLC system is the use of an appropriate coupling device. Coupling circuits are the hearts of PLC systems as the PLC signal is injected to the power line through the coupling circuit. However, design of a suitable coupling circuit for any PLC network is a great challenge. Specially, in terms of high voltage lines, the coupling capacitor price is very high, which in some cases demotivate utilities in applying PLC system on their networks. A number of research on demonstration and lab-based application of various coupling circuits have been directed in [67-72] which focus on displaying the coupling circuit from a hypothetical perspective, without thinking about the proposed explicit application in real-network. The authors likewise did not consider the execution possibility of their proposed circuits utilizing economically accessible components. Some researchers like Rensburg *et al.*[67-69] have represented some efficient coupling arrangements, such as transformer integrated LC- coupling circuit, power line-integrated impedance matching coupling circuits, etc.. All these works are related to the low voltage (230 V) PLC base home automation system applications. Hence, they have not focused on high voltage coupling arrangements as well as on HV-CCs and the methods are not suitable for high voltage PLC applications.

Beyond this, few prominent researchers in the field of PLC, have been done a notable amount of work on high voltage coupling systems. For example, in [73-75], Kikkert modelled various coupling arrangements using 12 nF and 6 nF high voltage capacitors for 19.1 kV SWER line. Artale *et al.* [76] proposed a capacitor voltage divider circuit arrangement for PLC application for a 52 kV medium voltage power line. All the above coupling circuits are tailored for a limited frequency range of around 10 kHz to 150 kHz and for all the above coupling design high voltage capacitor is the main element but none of these research works shade lights on the actual behavior of an HV-CC. Especially, the behavior of HV-CC has a significant impact on the coupling circuit behavior at the higher broadband range of above 500 kHz. Few others investigated coupling circuit designs, but often not considered the feasibility of real-word implementations demonstrated by the choice of simulation-based random component values only available at LV ratings [71, 72, 77].

2.8.6 Reflections from Transformers

A transformer tapped, to a PLC channel, may attenuate the carrier signal for several different reasons. The length of the tapped line may be near the quarter-wavelength of the carrier, and the transformer may present either a low or a high impedance to the signal, creating reflections that will interfere with the main signal. The transformer may even present a short circuit to the carrier signal [78]. Maximum out-of-phase reflected signal occurs when a tapped line is not terminated into tuned carrier equipment, or terminated into a power transformer, and is one-quarter wavelength of the carrier frequency in length or odd multiples thereof. This reflected out of phase signal causes cancelation of the transmitted signal. To minimize this, line traps can be placed as close to the line as possible to attenuate the signal traveling into the tapped line and the reflected energy returning from the tap section. The amount of isolation will depend on the trap impedance with respect to the impedance of the main line. The higher the trap impedance, the greater the signal attenuation.

2.9 PLC Standards and Electromagnetic Compatibility

The term ‘PLC standard’ refers to some guidelines and rules required for the development of any kind of product, process, or services related to PLC applications. PLC standards are very important for the establishment of a transparent communication over the power line

network [79-83]. The International Telecommunication Union (ITU), International Organization for Standardization (ISO), International Electrotechnical Commission (IEC), Institute of Electrical and Electronics Engineers (IEEE), Federal Communication Commission (FCC), and the European Committee for Electrotechnical Standardization (CENELEC) are the main Standardization Organizations (SDOs) that develop and propose standards in the communication sector. On the other hand, G3-PLC, Power Line Intelligent Metering Evolution (PRIME), the American National Standards Institute (ANSI), KNX and HOMEPLUG are some groups and alliances that deploy these standards and technologies in the PLC sector.

Based on the overall frequency allocations, the PLC system can be divided into two types: Narrowband Power Line Communications (NBPLC) and Broadband Power Line Communications (BBPLC). BBPLC deals with frequencies above 1 MHz, while NBPLC deals with frequencies less than 500 kHz. Different SDOs work in different frequency ranges. For example, CENELEC works within the NB-PLC range, while ITU and IEEE work within both NB-PLC and BB-PLC ranges. Different Standardization Organizations (SDOs) propose different PLC standards, which are being followed by different PLC application providers to establish this standard in real time. However, among SDOs, the IEEE, ITU, IEC and CENELEC are the most widely recognized standard provider in the world. Table 1 on the next shows most SDOs categorized according to their frequency allocation ranges.

Table 1: PLC frequency ranges in different standards.

Name of the SDOs & PLC standards		Range of Frequency	PLC system
CENELEC	A	3 kHz –95 kHz	NB-PLC
	B	95 kHz –125 kHz	
	C	125 kHz –140 kHz	
	D	140 kHz – 148.5 kHz	
FCC		145.3 kHz - 478.125 kHz	NB-PLC
IEEE	IEEE 1901.1	9 kHz - 500 kHz	NB-PLC

	IEEE 1901.2	2 MHz -50 MHz	BB-PLC
ITU	ITU-T. G.-9955/96	9 kHz - 475 kHz	NB-PLC
	ITU.T.G. (ISO)	3 kHz -1610 kHz	NB+BB PLC
	ITU-T. G.-9960/61 50M	2 MHz - 50 MHz	BB-PLC
	ITU-T. G.-9960/61 100M	2 MHz - 100 MHz	BB-PLC
	ITU-T. G.-9960/61 SGP	2 MHz -30 MHz	BB-PLC
IEC	NBPLC	3 kHz - 76 kHz	NB-PLC
	IEC12139 (SGFG)	2 MHz - 100 MHz	BB-PLC
HomePlug	HomePlug Green PHY (HPGH NB)	120 kHz - 400 kHz	NB-PLC
	HomePlug Green PHY (HPGP BB)	1.8 MHz -30 MHz	BB-PLC
	HomePlug AV (HPAV)	1.8 MHz - 30 MHz	BB-PLC
	HomePlug AV2	30 MHz - 86 MHz	BB-PLC
Electric Power Research Institute (EPRI)		3 kHz - 90 kHz	NB-PLC
Association of Radio Industries and Businesses (ARIB)		10 kHz- 450 kHz	NB-PLC
Special International Committee on Radio Interference (CISPR)		3 kHz -76 kHz	NB-PLC
Interference Causing Equipment Standard (ICES)		0 - 535 kHz	NB-PLC
Other companies (Intel, Lantiq, Panasonic)		2 MHz - 100 MHz	BB-PLC

2.10 Conclusion

This chapter has provided a survey of relevant background information and advancements in PLC communication technology with a review on technical details of different components of the system including the transmitter and receiver platforms, coupling

capacitor, line tuner, and line traps. This chapter strongly focuses on the knowledge gaps, potential applications, and major challenges on the various aspects of the PLC technology. The main highlights of the chapter can be included as follows:

- A review on key technical components of PLC systems such as various line traps, line tuner, drain coils, coupling capacitor. This information could be an important document to re-design that hardware for future improvement of the PLC technology.
- Discussion on major challenges towards the implementation of PLC technology such as frequency-based impedance variation and coupling circuit issues. Impedance of a power line changes significantly with the high frequency. Matching this varying impedance to the coupling arrangement is one of the major challenges to inject PLC signal over the power line. Various impedance matching techniques have been covered with hints on developing a new matching technique for PLC applications.
- Coupling circuits are the main components of the PLC system. A brief review on existing coupling methods have been presented and shortcomings of existing coupling circuits for High Voltage (HV) and Medium Voltage (MV) applications were intensively focused on.
- Noise is an important issue on PLC implementation as it can impact the PLC propagation significantly. A specific noise measurement technique with practical demonstration results have been reviewed. This discussion on noise analysis could be very useful for all the other potential application especially for PLC based fault detection application, on-line metering, and remote network monitoring purposes.
- Some other important findings from the literature such as voltage versus attenuation, distance versus attenuation, and EMC compatibility are also discussed.

Overall, this chapter has provided a technical discussion on the peripherals, reliability, attenuation, noise, and distortion considerations in using PLC systems over power lines. Line impedance matching problems and the effect of transformer reflections on the attenuation of the carrier signal have been noted. Various PLC standards and electromagnetic interference regulations have been summarized with insights into technical details and critical challenges of PLC systems. Irrespective of application, accurate channel modelling is critical in studying how the SWER channel would perform with regards to key questions on reliability

and quality of the proposed scheme. A key weakness in previous work is that network modelling included large lumped segments up to 10.5 km. Presented results were limited to comparison of measured attenuation results against those predicted by software models. One significant knowledge gap addressed in this thesis will be the development of an exemplary fine-detailed segment-by-segment modelling of a SWER overhead network including spurs with short segment line lengths as short as 22 m. System level simulations will also be targeted enabling a direct comparison between actual measured carrier tone voltages and those predicted by the modeling. Modelling of the SWER transformer and the capacitive coupling circuit will be based on a novel methodology that involves taking Touchstone file (containing s-parameter measurements) of the same. These s-parameter based models will be incorporated into the overall model and efficacy of this approach assessed.

Chapter 3

Coupling Circuit Design

3.1 Introduction

In a PLC integrated power network, the coupling circuit plays an important role. A decent volume of research has been conducted on the development of PLC applications on SWER networks by Kikkert *et al.* [35, 73-75]. Their works mainly concentrated on establishing a communication system over SWER powerlines, which influenced authors to observe the individual high-frequency behavior of various equipment. The coupling circuit by Kikkert are mostly transfer integrated impedance matching unit coupled to the 12.7 kV SWER powerline through a High Voltage (HV) Coupling Capacitor (HV-CC).

The coupling circuits by Kikkert and associates were always designed as per the rated capacitance without considering the internal circuitry of HV capacitor units. Off-the shelf CCs always include protective circuitry, which influence the overall capacitance of the unit. In this regard, a 1 nF/24 kV capacitor has been tested over a range of frequencies to characterize the exact value and electrical behavior of the capacitor, which helps to design the appropriate coupling circuit for the SWER network.

Cost and size of the HV-CC increase with the increase of the capacitive value. Most previous works related to high voltage coupling system relied on higher valued CCs. For example, in [73, 75], 12 nF and 6 nF high voltage capacitors were used possibly rated 19.1 kV or higher. In this thesis, only a 1nF/HV-CC has been used for 12.7 kV network coupling. Hence, the featured coupling circuit is certainly a good choice for PLC-implementation in SWER network in terms of economic viability. Research on modelling and lab-based implementation of different types of coupling circuits have also been conducted in [70, 71, 77], which concentrate on modelling the coupling circuit from a theoretical point of view, without considering the intended specific application in real world. The authors also did not consider the implementation feasibility of their proposed circuits using commercially available components.

Few researchers have worked intensively on coupling circuit design, such as Rensburg *et al.* [67-69], who modified coupling arrangements with different circuit schemes such as the LC matching technique [68], and adopted impedance matching transformer in his coupling arrangements [67, 68]. However, the circuits they developed are well applicable for Low Voltage (230 V) PLC-based home automation systems. Typical SWER powerline voltages are (12.7 kV) and (19.1 kV). Hence, the coupling circuit designs by Rensburg are not suitable for SWER network. There is a clear need to develop low attenuation coupling circuit designs that can be applied in SWER networks and other mediums including high voltage powerlines. Considering the aforementioned issues and knowledge gaps, this work focuses on the modelling, design and evaluation of PLC coupling onto SWER networks using available off-the-shelf products.

This thesis proposes a novel L-C band pass impedance matching circuit for PLC applications coupled to a Single Wire Earth Return (SWER) network via a 1.1 nF High Voltage (HV) Coupling Capacitor (CC). The work begins with characteristic impedance prediction of various SWER conductors followed by an analysis of the theoretical LC-resonant based coupling arrangements. A key finding is that high inductance and capacitance values are required for such LC-resonant based arrangements increasing the cost of solutions. An HV CC is then analyzed and its effective capacitance is demonstrated, to be impacted by its internal protection circuitry. An L-C band pass matching circuit is then designed, built and tested as per the derived capacitance of the chosen HV-CC. The proposed coupling circuit produces only -4 dB insertion loss over the targeted 50 kHz to 150 kHz band and includes off-the-self components for a commercially viable solution. The design is based on the capacitance of an HV-CC and uses of off-the-shelf components setting this work aside from comparative works, which only considered hypothetical designs using unviable component values.

This chapter discusses the comprehensive research methods and flow chart of the work. It presents the modelling of SWER powerline for impedance prediction. Highlights the evaluation of a transformer integrated coupling circuit considering SWER powerline impedance. This chapter characterizes the electrical equivalent circuit of the 1 nF/HV-CC integrated with SWER powerline in the PLC frequency range. The theoretical modelling and simulation of the proposed coupling circuit is also presented. Finally, hardware

implementation of the proposed is discussed along with a comparative performance analysis.

3.2 Overview of a PLC System

A PLC coupling circuit can behave like a high pass or band pass filter, which rejects the low-frequency power signal from entering the modem and allows the PLC signal to penetrate onto the SWER powerline. In this work, the CENELEC band 50 kHz to 150 kHz has been chosen as the range of analysis signal because this band complies with EN 50065. The application of the Coupling Circuit in SWER powerlines is sophisticated because the impedance of the SWER powerline varies at different PLC transmit frequencies, which is a key factor that must be considered in the design of a coupling circuit. The comprehensive methodology of the system can be described as follows: the PLC modem generates signals in the 1-500 kHz frequency range, the band pass circuit extracts the designated band and feeds into the SWER powerline after adjusting the impedance issue through the HV-CC. Fig 3.1 shows the schematic arrangement of a PLC integrated SWER network.

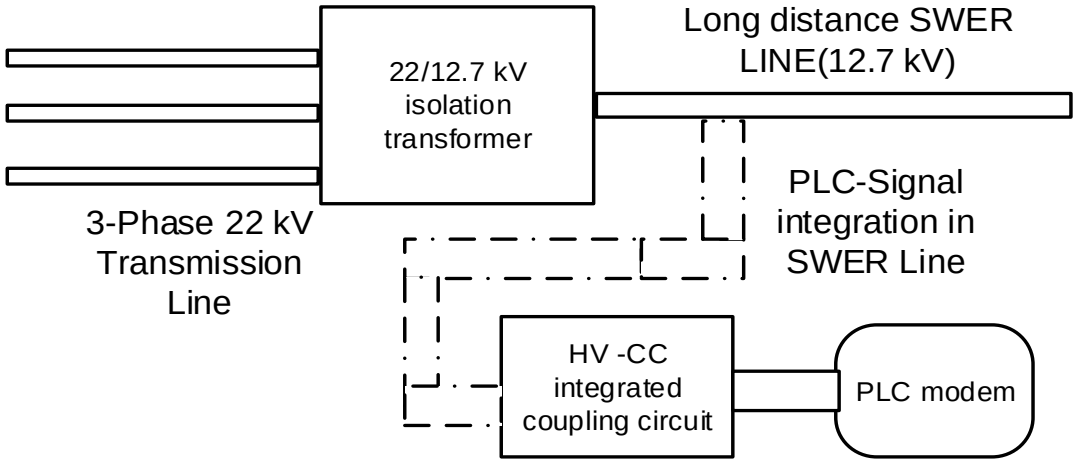

Fig 3.1: Schematic arrangement of PLC-integrated SWER powerline

3.3 Conventional Component Based Coupling Circuit

In this section, conventional component-based coupling circuits such as the LC resonant type coupling circuit and a modified transformer integrated LC-resonant type coupling circuit have been modelled and evaluated considering the SWER powerline properties. Fig

3.2 shows a very simple, series LC resonant circuit and Fig 3.3 shows an impedance matching transformer integrated LC resonant circuit. In these circuits, Port-1 has been taken as the SWER powerline side (receiving side) and Port-2 has been taken as the PLC modem side (the transmitting side). The impedance combination has been considered as 260 Ω/50 Ω, which are the standard SWER powerline and modem impedances respectively. Eqs. (3.1) to (3.3) were used for the parametric calculation of the LC-resonant circuit.

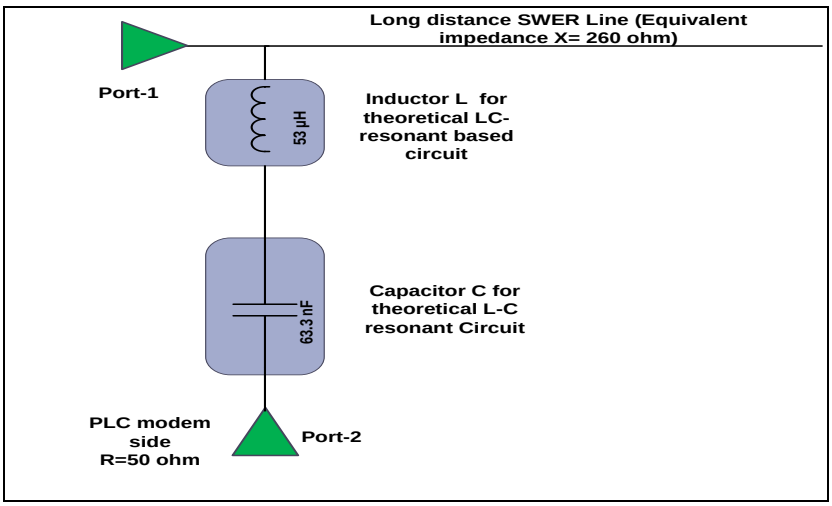

Fig 3.2: A simple series LC resonant circuit

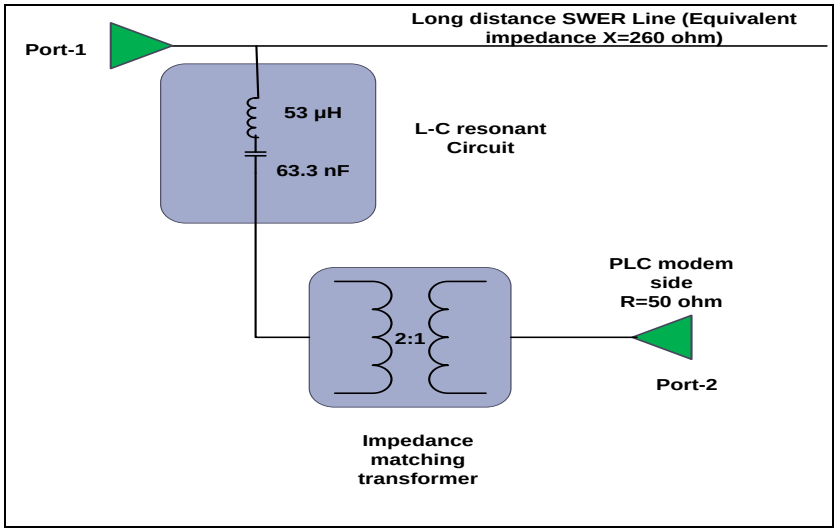

Fig 3.3: An impedance matching transformer integrated LC-resonant circuit

Eqs. (3.1, 3.2, and 3.3) can be used to calculate the capacitance, inductance and the frequency of resonance respectively.

$$C = \frac{1}{2\pi X f_{Low}} \quad (3.1)$$

$$L = \frac{X}{2\pi f_{High}} \quad (3.2)$$

$$f_R = \frac{1}{2\pi\sqrt{LC}} \quad (3.3)$$

Where,

L is used for inductor.

C is for capacitor,

$\mathbf{f_R}$ is for the resonance frequency and

X is the impedance of the SWER powerline side.

R is the impedance of the PLC modem port

A 100 kHz bandwidth in the 50 kHz to 150 kHz band is targeted. For this reason, 50 kHz has been chosen as the lower cut-off frequency and 150 kHz has been chosen as the upper cut-off frequency. Using Eqs. (3.1) to (3.3), the key parameters of the resonant circuit have been obtained as C = 63.63 nF; L = 53 μH and the frequency of resonance f_R as 86.662 kHz. Table 2 shows the parameters used for the theoretical calculation.

Table 2: Components values of LC-resonant circuit

Parameters	Values
Receiving (SWER powerline) side impedance, X	260 Ω
Transmitting (PLC Modem) side impedance(R)	50 Ω
Lower cut-off frequency, f_{low}	50 kHz
Higher cut-off frequency, f_{high}	150 kHz
Resonance frequency, f_R	86.66 kHz

The insertion loss profile of the above LC-resonant circuit can be further improved by using an impedance-transforming unit, such as a transformer as shown in Fig 3.3, a transformer enables impedance matching using its turn's ratio. Different types of transformers (normal two winding, center tapped, and auto tap changing) can serve for this purpose. For example, in Fig 3.3, an LC-coupling circuit with an integrated transformer (2:1) connected to the SWER powerline and PLC modem has been shown.

The turn's ratio of a transformer is given by Eq. (3.4),

$$N = \frac{N_s}{N_p} = \text{turns ratio} \qquad (3.4)$$

Where **N** is the turn's ratio,

$\mathbf{N_s}$ is the number of turns on the secondary and $\mathbf{N_p}$ is the number of turns on the primary.

The relationship between the turns ratio and impedance of the transformer's primary and secondary windings is given by Eqs. (3.5) and (3.6)

$$\frac{Z_s}{Z_p} = \left(\frac{N_s}{N_p}\right)^2 \qquad (3.5)$$

$$\frac{N_s}{N_s} = \sqrt{\frac{Z_s}{Z_s}} \qquad (3.6)$$

Where

$\mathbf{Z_s}$ is the impedance of the secondary winding and

$\mathbf{Z_p}$ is the impedance of the primary side.

Using Eqs. (3.5) and (3.6) the turn's ratio of the transformer required to match the impedance on both sides can be calculated as in Eq. (3.7).

$$\frac{N_s}{N_p} = \sqrt{\frac{Z_s}{Z_p}} = \sqrt{\frac{260}{50}} = 2.25 = \sim 2{:}1 \qquad (3.7)$$

As shown, a transformer with a turn's ratio of (2:1) needs to be connected between the SWER powerline and PLC modem for 260 Ω to 50Ω impedance matching. Fig 3.4 shows the two-insertion loss curves: one for the simple LC-resonant type coupling and another for the transformer integrated LC-resonant coupling respectively. The curve with circular marking shows the insertion loss graph of the simple LC-resonant type coupling circuit when connected to the SWER powerline and PLC modem. As shown, the insertion loss is -2.717 dB at both the upper and lower cut-off frequencies. At the centre frequency, the insertion loss reduces to -2.667 dB.

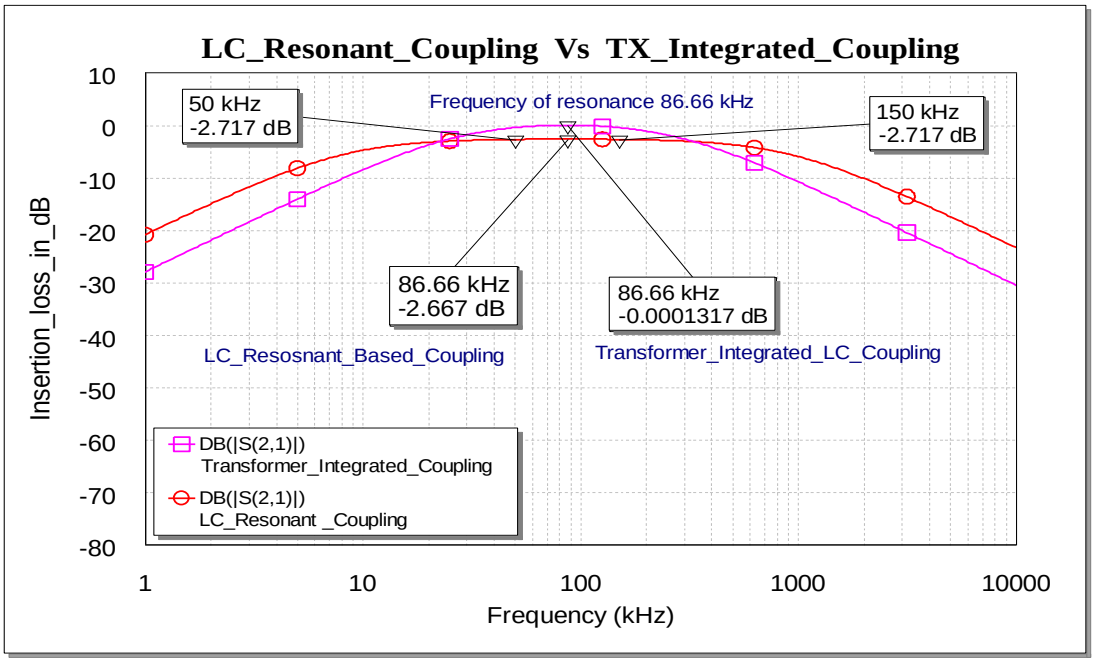

Fig 3.4: Insertion loss graph of LC-resonant vs transformer integrated coupling circuit

On the other hand, the inclusion of the transformer improves the matching criteria between Ports 1 and 2. The curve with circular marking presents the improved loss profile, after adding the transformer. As shown, the insertion loss has gone down to nearly zero (~0 dB) at the centre frequency of 86.66 kHz. For the whole 50 kHz to 150 kHz band, this modified circuit exhibits less than -0.5 dB insertion loss, which is significantly lower compared to the previous LC resonant only coupling.

Though these circuits produce very low insertion loss, unfortunately the inductive (L) and capacitive (C) values needed for these design are not practical or commercially available

[12, 37, 56, 84]. The design of this highly optimistic coupling circuit would require a 63.3 nF HV capacitor. Capacitors with much lower capacitance values such as the 1 nF/24 kV demonstration capacitor [18] already cost several thousand dollars and weight around few kilograms . Moreover, the design of the custom 63.3 nF capacitor would require 63 single capacitor units connected in parallel, which is not feasible in terms of cost, size, weight and effort. A number of works have used extensive higher capacitance to design coupling circuits for high voltage (HV) or medium voltage (HV) lines, adopting T or Pi-matching network theories such as [72, 73, 85]. Due to the impracticability of such theoretical designs, next section investigates the feasibility of a commercially available off-the-shelf HV-CC integrated band-pass impedance matching coupling circuit for SWER network.

3.4 Characterization of SWER Powerline Integrated HV-CC

Previous sections have explored the theoretical design of LC resonant circuit based coupling circuits and identified that capacitive and inductive units required for such coupling circuits may be impractical to procure. To address these challenges, a relatively low-cost 1 nF/24 kV, HV-CC has been chosen and the impedance matching circuit accordingly redesigned. Two main points are highlighted such as characterization of the HV-CC and impedance predictions of SWER line-integrated HV-CC at the required PLC frequency band. Finally, an equivalent circuit for the combined SWER powerline and HV-CC for the desired PLC frequency band has been derived and presented in this section of the paper. The reason behind the selection of the 1nF/24 kV CC is its suitability for use in SWER networks with its nominal voltage rating. Besides, most commercial HV-CC are minimum 8800 pF/72 kV rated [86], which is not suitable for SWER applications because of large size, higher cost and over-rating. Typically, a CC provides a low impedance path for the HF signal to the HV line, but a high impedance path to the power frequency. It drops the line voltage across its capacitance with its LV end grounded through an inductor, called the drain coil. The drain coil provides a low impedance path for the power frequency and a high impedance path to ground for the carrier signal. Using Eqs. (3.8) and (3.9), it is verified that the 1 nF commercial CC provides 3.184 kΩ impedance to the 50 kHz PLC signal and 3,184 kΩ impedance to the power frequency.

$$Z_{C-50Hz} = \frac{1}{2 \times \pi \times f \times C} = \frac{1}{2 \times \pi \times 50 \times 1nF} \approx 3{,}184\ k\Omega \qquad (3.8)$$

$$Z_{C-50\ kHz} = \frac{1}{2 \times \pi \times f \times C} = \frac{1}{2 \times \pi \times 50k \times 1nF} \approx 3.184\ k\Omega \qquad (3.9)$$

All manufactures provide HV-CCs with nominal values excluding the internal protection circuit, which normally consists of a drain coil, diodes and surge arresters. To design an efficient coupling arrangement for a HV-CC, the electrical equivalent circuit including the protection circuit must be decoded. Fig 3.5 shows visual graphic and internal equivalent circuit of the commercial 1.1 nF/24 kV CC[18], where the 1.1 nF capacitor is connected in series with the internal protection circuit and the output is taken from the top end TNC output port of the CC. The protection circuit includes the surge arrester, freewheeling diode pair, drain coil, and few capacitors all these components affect the overall capacitance of the HV CC at high frequency.

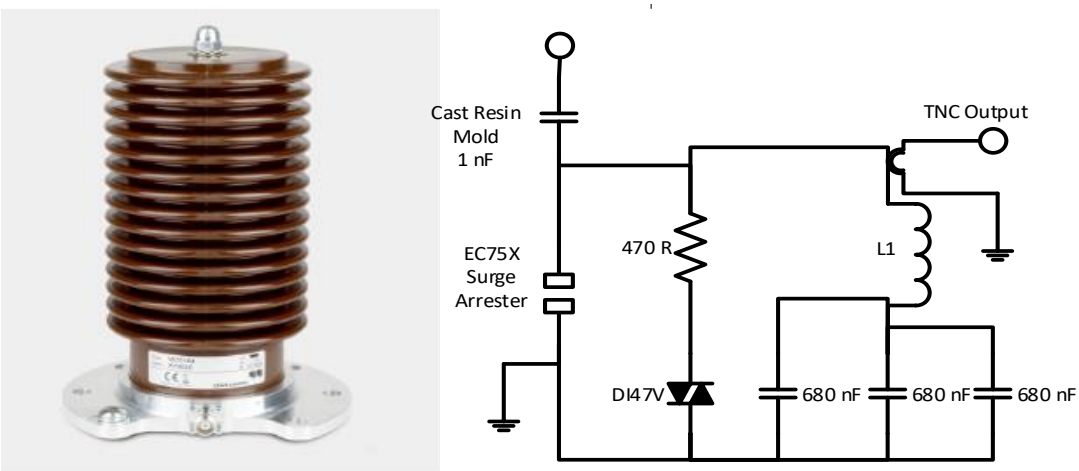

Fig 3.5: Commercial HV-CC and internal protection circuit arrangement [18]

The experimental setup shown in Fig 3.6 has been connected for testing the HV-CC to test and understand its HF response. Procedure can be described as follows: a known voltage is applied to the input port from a function generator in the PLC frequency range and output is taken from the TNC port. To visualize the input and output waveforms, both the input and output have been measured with the two channels of the oscilloscope. To demonstrate the accurate behavior of the CC, input signals have been given at three different frequencies such as 50 kHz, 100 kHz and 150 kHz. For all the cases, similar input and output values

have been measured at the oscilloscope. The curve obtained from the oscilloscope for the 100 kHz input and output case is shown in Fig 3.7.

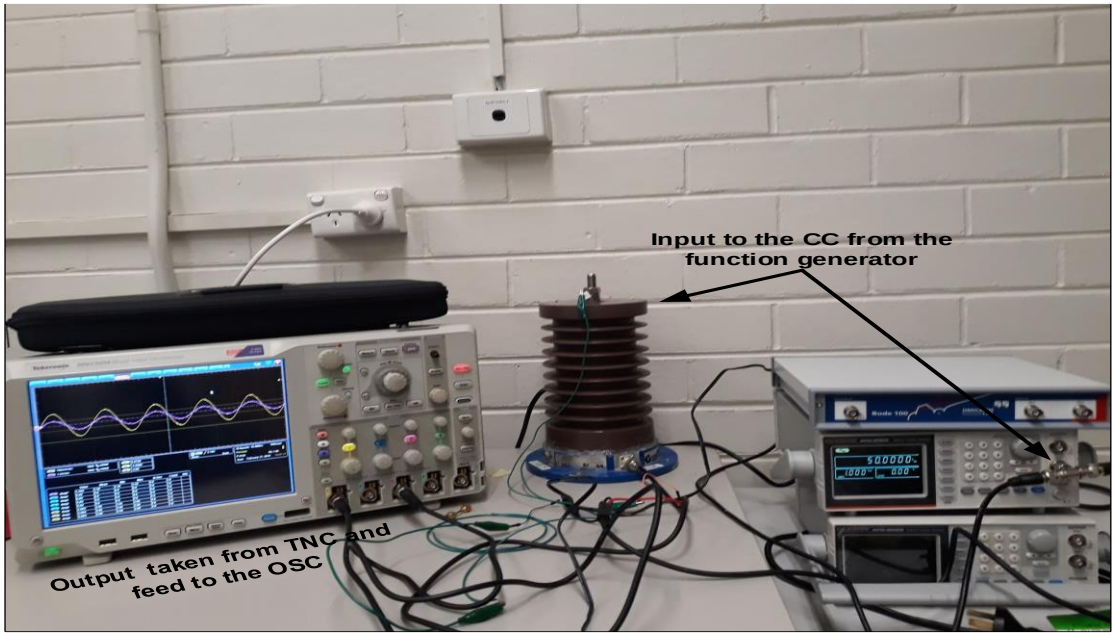

Fig 3.6: Experimental setup for HV-CC characterization at high frequency

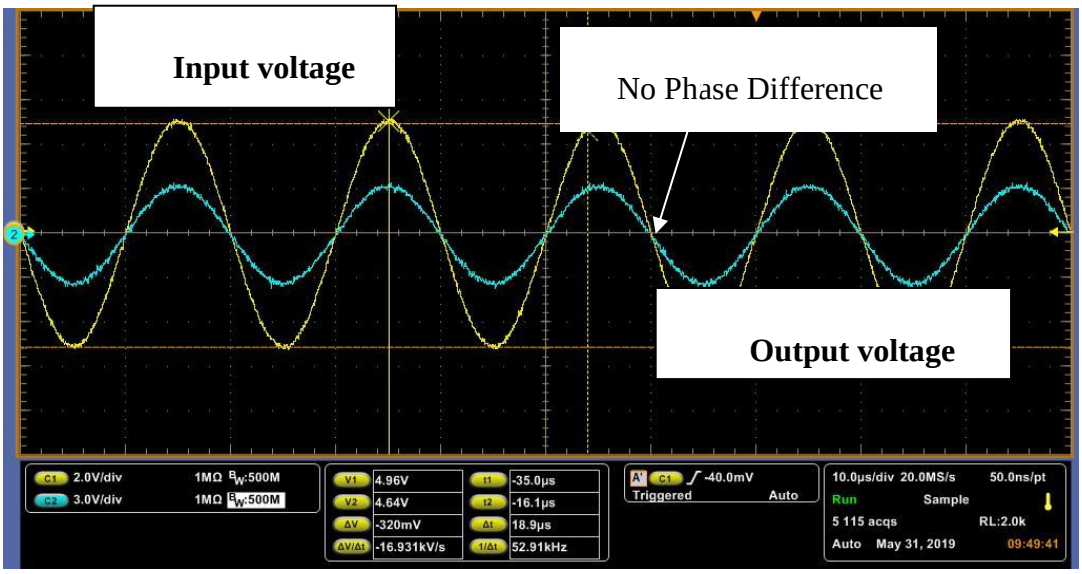

Fig 3.7: Input and output voltage curve of HV- CC at 100 kHz.

As shown, there is no phase difference between the input and output curves, which demonstrates that the behavior of the protection circuitry of the CC is similar to a capacitor. Hence, the revised electrical equivalent circuit for the 1.1 nF/HV-CC can be re-drawn as shown in Fig 3.8.

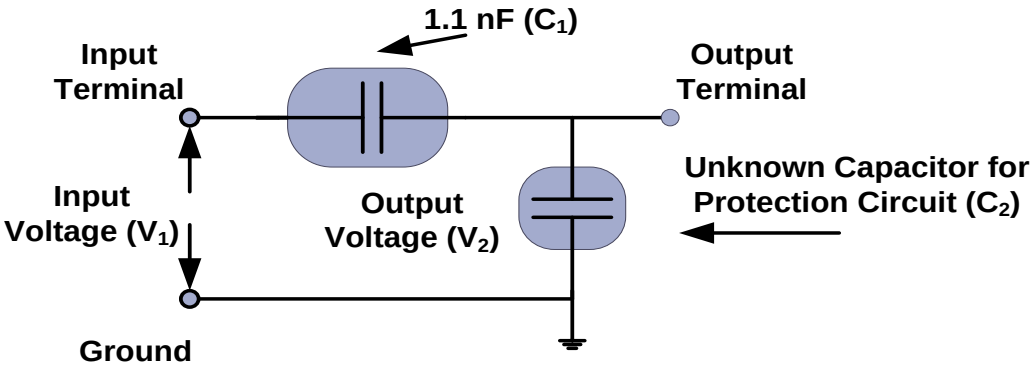

Fig 3.8: Simplified electrical equivalent circuit of the HV- CC

The unknown capacitance can be easily calculated using the voltage divider equation of Eq. (3.10). In Eq. (3.10), setting the value of measured input voltage (V_1) to 2.01 V, output voltage (V2) to 1.17 V and C_1 as 1.1 nF; the unknown capacitance for protection circuit can be obtained as 0.79 nF. Hence, the equivalent circuit of the SWER powerline integrated high voltage 1.1 nF/ HV-CC can be redrawn with it's the internal capacitance value as shown in Fig 3.9.

$$V_2 = \frac{C_1 \times V_1}{C_1 + C_2} \quad \Rightarrow C_2 = \frac{C_1 \times V_1 - V_2 \times C_1}{V_2} \tag{3.10}$$

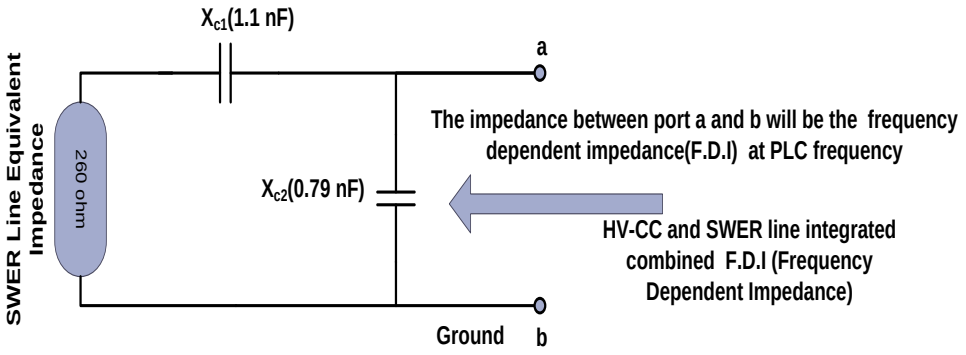

Fig 3.9: Equivalent circuit of the SWER Line-integrated HV-Coupling Capacitor.

Considering the HV-Equivalent circuit (HV-CDC), a comparative magnitude and phase analysis have been carried out to show the difference between the HV-CDC and ideal HV-Capacitor with respect to the commercial 1.1 nF/24 kV coupling capacitor. Fig 3.10 shows the magnitude and Fig 3.11 shows the phase difference between these circuits. Both figures show that the difference for the CDC and the commercial capacitor is lower than the ideal

capacitor. This deviation becomes more visible at higher frequencies. For example at 30 MHz, in terms of magnitude, the HV-CDC and actual capacitor show a deviation of only 2 dB, whereas the ideal capacitor and commercial capacitor show a deviation of 8 dB at the same frequency. Similarly, in terms of phase, the HV-CDC and the actual capacitor exhibits lower differences, whereas the difference between actual capacitor and the 1.1 nF ideal capacitor is quite high.

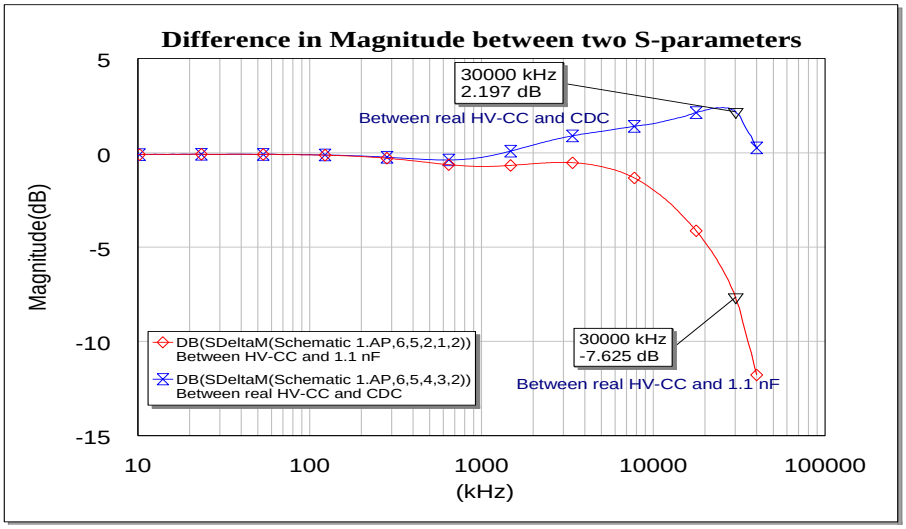

Fig 3.10: Magnitude difference of insertion loss (S21)

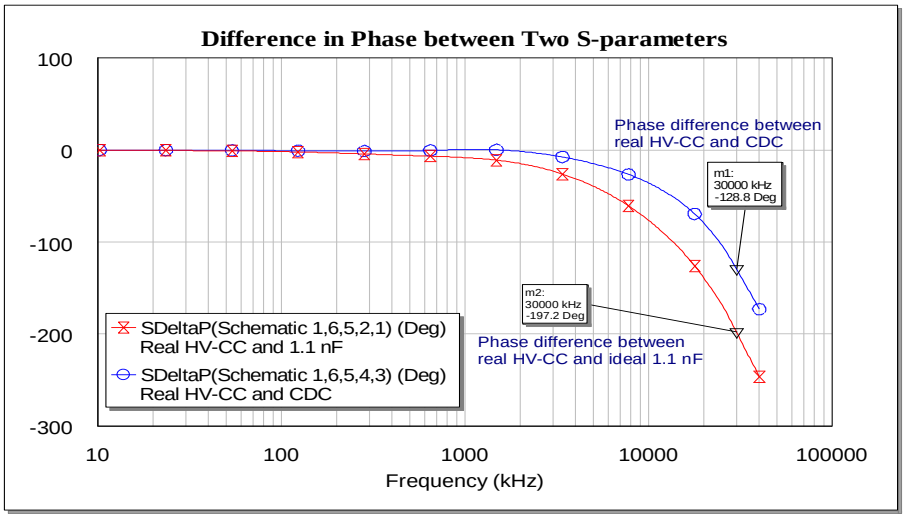

Fig 3.11: Phase difference of insertion loss (S21)

Due to this internal capacitance, the traditional matching methods such as the T-network or Pi-network do not apply to this configuration [70, 87, 88] since traditional matching circuits develops their equations considering a simple series or parallel capacitor connected

with the load. In this case, due to the internal capacitance, the HV-CC cannot be represented as linear as the previous theoretical circuits. Hence, in this paper, the band-pass impedance matching coupling circuit will be proposed considering the internal capacitance of the HV-CC due to its protection circuitry. The Frequency Dependent Impedance (F.D.I) of the SWER powerline with the integrated CC (F.D.I $_{\text{SWER line-integrated\_CC}}$) can be represented by Eq.(3.11), which has been extracted using the two-port network theorem and voltage divider rule.

$$\text{F. D. I}_{\text{swer line}-\text{integrated\_CC}} = \frac{(260+X_{c1})\times X_{c2}}{260+X_{c1}+X_{c2}} \qquad (3.11)$$

The $\text{F. D. I}_{\text{swer line}-\text{integrated\_(CC)}}$ was also simulated with the sophisticated RF design suite the Microwave Office and the impedance curve plotted as shown in Fig 3.12.

$$\text{C} = \frac{1}{2\pi \text{fX}_\text{c}} = \frac{1}{2\pi\times 100\times 10^3\times 805.89} = \tilde{}2 \text{ nF} \qquad (3.12)$$

The frequency component 100 kHz has been considered as the center frequency, hence, the F.D.I for the HV-CC integrated SWER powerline at center frequency was extracted as R = 78.14 Ω and X_c=-805.89 Ω. From the negative X_c value, the equivalent capacitive component of the circuit can be calculated as in Eq. (3.12). The overall equivalent circuit of SWER powerline HV-CC integrated band-pass matching circuit and PLC modem can then be redrawn as shown in Fig 3.13.

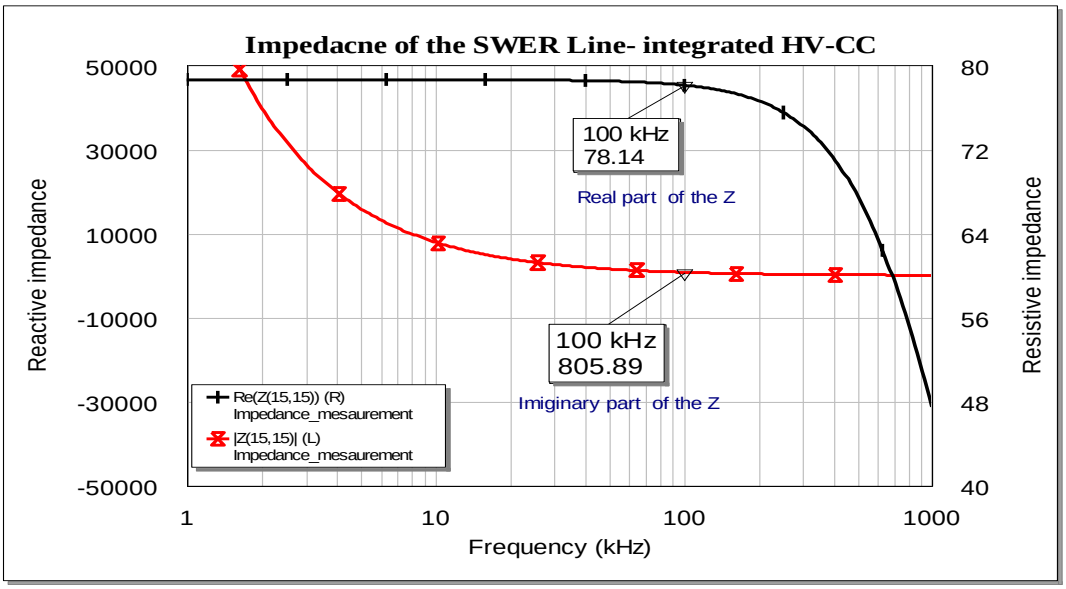

Fig 3.12: F.D.I curve of the SWER line- integrated HV-CC

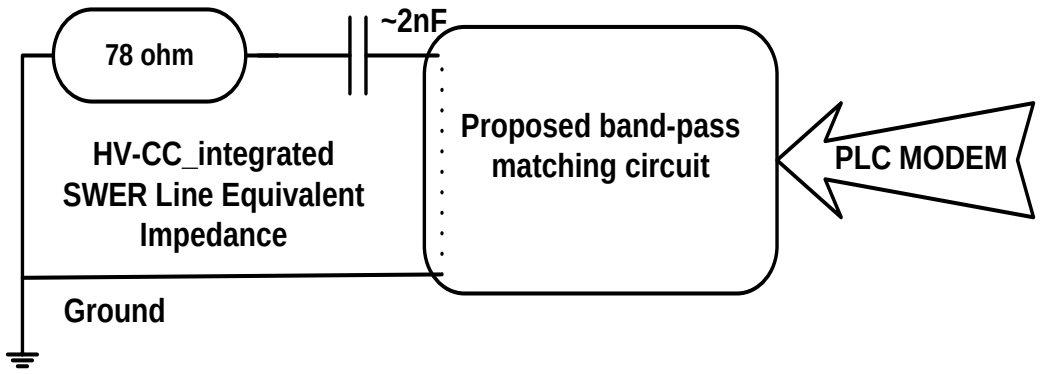

Fig 3.13: Overall equivalent circuit of the complete system

3.5 Theoretical Background of the Coupling circuit

This section presents the design of the proposed L-C band pass matching circuit considering the equivalent HV-CC integrated-SWER powerline impedance. The concept and background theory of virtual resistor matching technique has been documented in [88-91]. The impedance matching circuit can be of high-pass, low pass or band pass nature depending on the application of PLC system and frequency requirements. The authors have chosen the band-pass circuit because of the frequency of interest being within 50 kHz to 150 kHz range. Therefore, the L-C section connected with the source needs to behaves like low-pass and the section connected with the SWER powerline as of high-pass. Cascading of these two sections will produce the required band pass response.

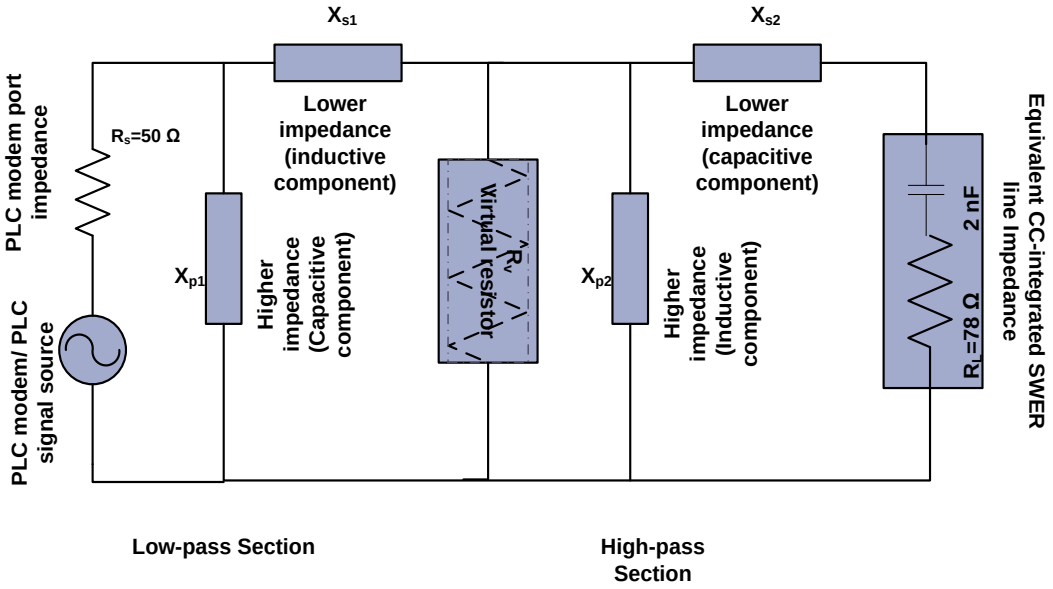

Fig 3.14: Circuit diagram of the virtual resistor based matching arrangement

Herewith, the low-pass L-C section will be connected with the 50-Ω standard PLC modem impedance and high pass L-C section will be connected to the 78-Ω (resistor) and 2 nF (capacitor) based equivalent impedance of the SWER powerline HV CC. According to the virtual resistor concept, a shunt resistor will be placed between the two sections and both the sections will be matched with this conceptual impedance. To implement the matching circuit, the resistive element will be first considered followed by the addition of the capacitor. The schematic diagram of the method has been shown in Fig 3.14.

In this schematic X_{s2}, X_{p1}, X_{p2} and R_v are the unknown impedances. The properties of these impedances have been given in Table 3. X_{s1} and X_{s2} are the smaller impedances for both sections and will be connected in series. For the low-pass section, X_{s1} will be inductive and X_{s2} capacitive. On the other hand, with the X_{p1} and X_{p2} will be vice versa.

Table 3: Impedance properties of the virtual resistor based matching circuit

Impedance Name	Low pass section			Impedance Name	High-pass section		
	Value	Properties	Connection		Value	Properties	Connection
X_{s1}	Low	Inductive	Series	X_{s2}	low	Capacitive	Series
X_{p1}	High	Capacitive	Parallel	X_{p2}	high	Inductive	Parallel

The calculation of the parameters start with the calculation of the virtual resistor (R_v) which can be done by Eq. (3.13) [88, 92].

$$R_v = \sqrt{R_s \times R_L} = R_v = \sqrt{R_s \times R_L} = \sqrt{50 \times 78} = 62.5\ \Omega \qquad (3.13)$$

Here, the PLC modem port impedance is R_S=50 Ω and equivalent SWER powerline impedance is R_L=78 Ω. The virtual impedance R_v is 62.5 Ω. Q-factor defines the steepness of the cut-off frequency slope of a filter. A higher Q-factor gives a sharper cut-off frequency band. The value of Q-factor can be readjusted according to requirement by changing the source impedance. However, the Q-factor and the other unknown parameters of the circuit of Fig 3.12 (e.g. L and C component values for the high pass and low pass sections) can be determined as follows.

The calculation of Q followed by X_{s1}, X_{p1}, L and C for low-pass section:

$$\mathrm{Q_{Lp}} = \sqrt{\frac{\mathrm{R_v}}{\mathrm{R_s}} - 1} = \sqrt{\frac{62.5}{50} - 1} = \sqrt{\frac{5}{4} - 1} = \sqrt{\frac{1}{4}} = 0.5 \quad (3.14)$$

$$\mathrm{X_{s1-LP}} = \mathrm{Q_{low-pass}} \times \mathrm{R_v} = 0.5 \times 62.5 = 31.25\ \Omega \quad (3.15)$$

$$\mathrm{X_{p1-LP}} = \frac{\mathrm{R_s}}{\mathrm{Q_{low-pass}}} = \frac{50}{0.5} = 100\ \Omega \quad (3.16)$$

Calculation of inductive (L) and capacitive (C) components consider the center frequency as 100 kHz and these have been determined as 50 µH and 15 µH as in Eqs. (3.17-3.18)

$$\text{Hence, } \mathrm{L_{low-pass}} = \frac{\mathrm{X_{s1}}}{2\pi \mathrm{f}} = \frac{31.25}{2\pi \times 100 \times 10^3} = 50\ \mu\mathrm{H} \quad \text{and} \quad (3.17)$$

$$\mathrm{C_{low-pass}} = \frac{1}{\mathrm{X_{p1}} \times 2\pi \mathrm{f}} = \frac{1}{100 \times 100 \times 100^3} = 15\ \mathrm{nF} \quad (3.18)$$

Q_{HP} X_{s2}, X_{p2} have been determined as 0.5, 39 Ω and 125 Ω as shown in Eqs. (3.19-3.21)

$$\mathrm{Q_{HP}} = \sqrt{\frac{\mathrm{R_L}}{\mathrm{R_v}} - 1} = \sqrt{\frac{78}{62.5} - 1} = \sqrt{1.248 - 1} = \sqrt{0.248} = \sim 0.5 \quad (3.19)$$

$$\mathrm{X_{s2-HP}} = \mathrm{Q_{high-pass}} \times \mathrm{R_L} = 0.5 \times 78 = 39\ \Omega \quad (3.20)$$

$$\mathrm{X_{p2-HP}} = \frac{\mathrm{R_v}}{\mathrm{Q_{high-pass}}} = \frac{62.5}{0.5} = 125\ \Omega \quad (3.21)$$

For the above, Q_{HP} the (L_{HP}) and (C_{HP}) calculated as follows at 100 kHz

$$\text{Hence, } \mathrm{C_{high-pass}} = \frac{1}{2\pi \mathrm{f} X_{p2}} = \frac{1}{2\pi \times 100 \times 10^3 \times 39} = 40\ \mathrm{nF} \quad \text{and} \quad (3.22)$$

$$\mathrm{L_{high-pass}} = \frac{\mathrm{X_{s2}}}{2\pi \mathrm{f}} = \frac{125}{2\pi \times 100 \times 10^3} = 200\ \mu\mathrm{H} \quad (3.23)$$

After obtaining these L and C values, the complete electrical equivalent circuit of the proposed band-pass impedance matching coupling circuit can be drawn as in Fig 3.15. On the high pass section, the overall capacitor can be calculated from the sum of the 38 nF coupling circuit and 2 nF internal HV CC integrated SWER powerline capacitance.

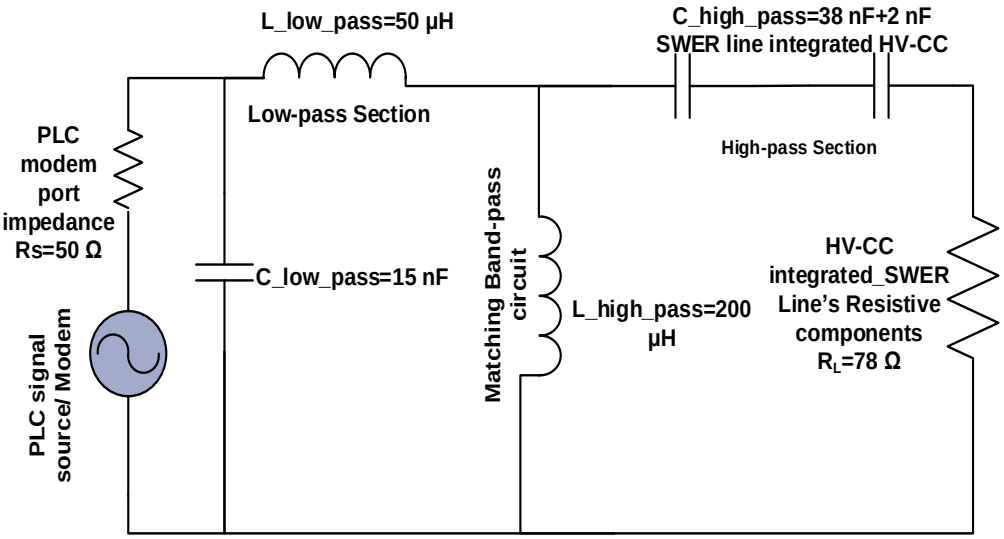

Fig 3.15: Final coupling circuit with L and C values

The insertion loss profile of the above coupling circuit was obtained using the Microwave Office platform. Fig 3.16 shows this insertion loss profile to be around -2 dB within the target frequency band of 50 kHz to 150 kHz. This low insertion loss certifies that this designed circuit will minimize PLC signal attenuation in signal injection to a SWER network via a 1.1 nF CC.

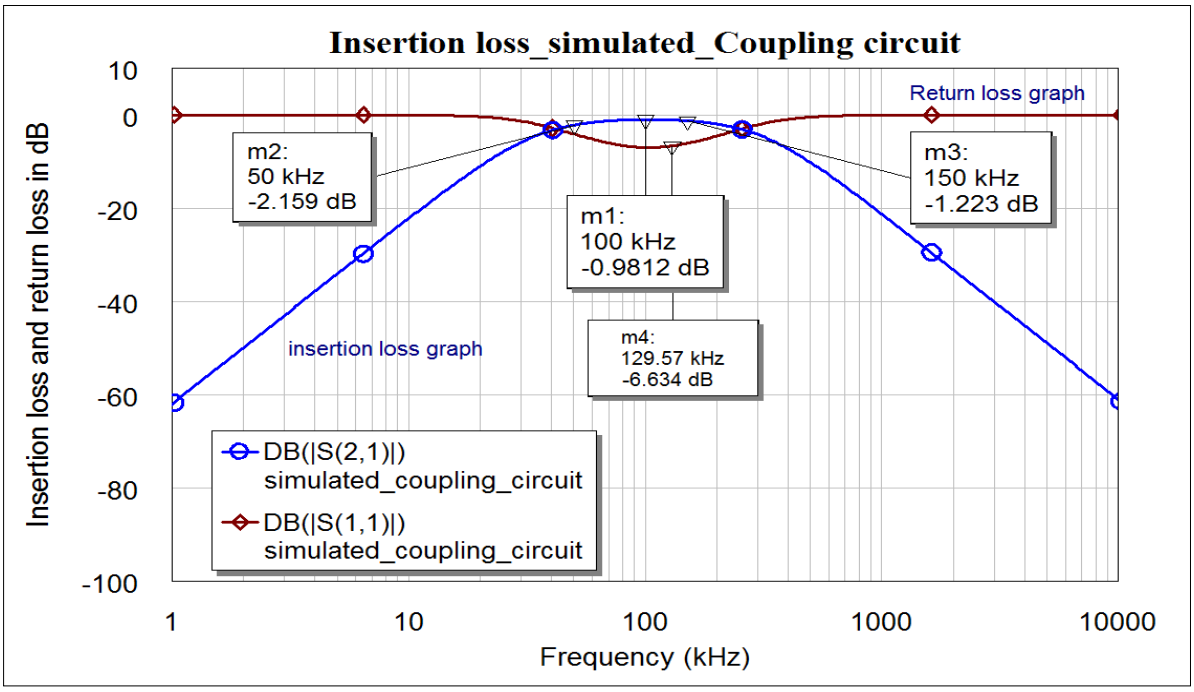

Fig 3.16: Insertion loss profile of the coupling circuit

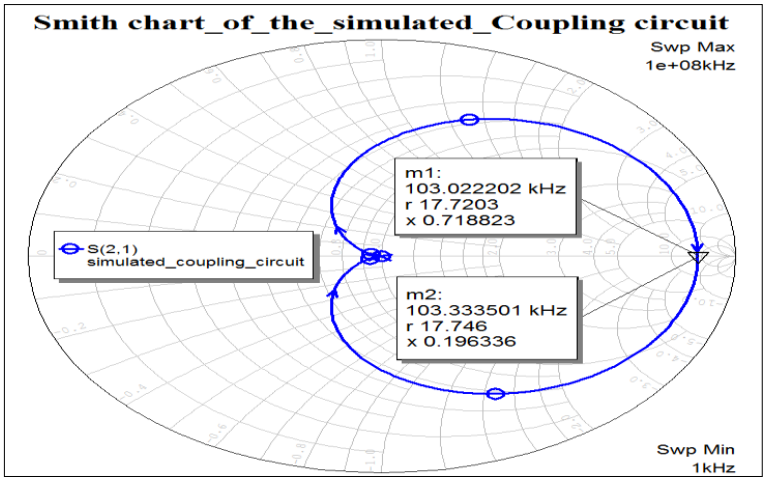

Fig 3.17: Smith chart-based impedance graph of the coupling circuit

The impedance behavior of the overall coupling circuit can be explained using a Smith Chart. The Smith Chart of Fig 3.17 shows that from 0.01 kHz (10 Hz) to 103 kHz, this circuit is inductive and after 103 kHz to the maximum 5000 kHz, this circuit behaves like a capacitor dominated circuit. Another important task of a coupling circuit is to block the high voltage power frequency. In this respect, an AC analysis has been done considering a 12.7 kV input from the SWER powerline and the voltage and current at the PLC modem port has been determined. Fig 3.18 shows the electrical equivalent circuit for the AC analysis.

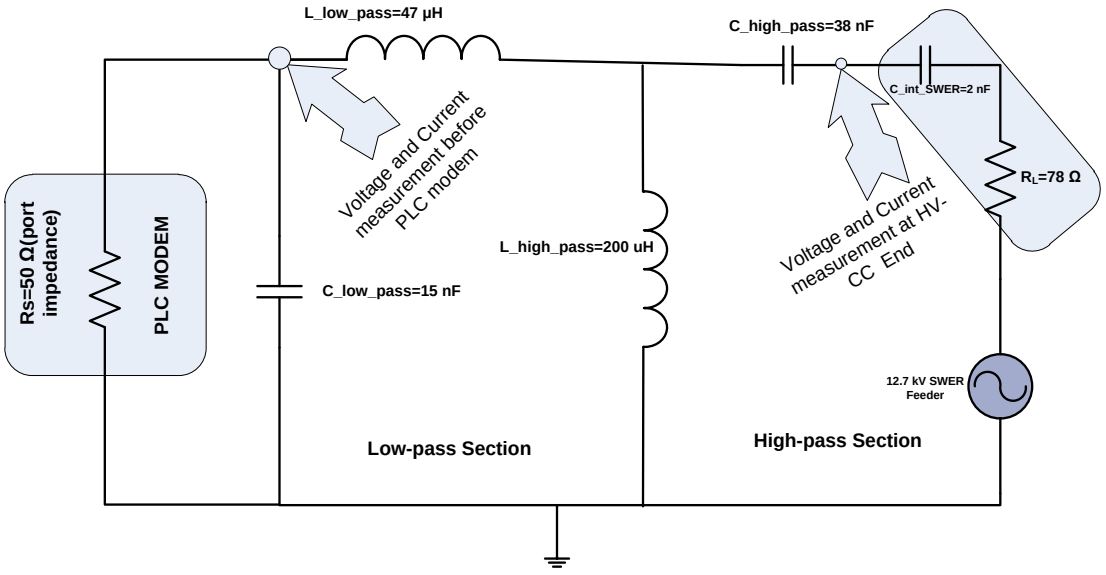

Fig 3.18: Revere AC (12.7 kV) analysis of the coupling circuit.

From the simulation, it has been determined that the voltage at the input of the PLC modem is (0.476 mV) and current will be only 0.00943 mA. Hence, this small amount of

50 Hz reverse power towards the PLC modem will not create any harm to the modem circuitry. Fig 3.19 presents the 50 Hz voltage and current curves at the PLC modem end with a 12.7 kV input voltage applied at the SWER powerline end.

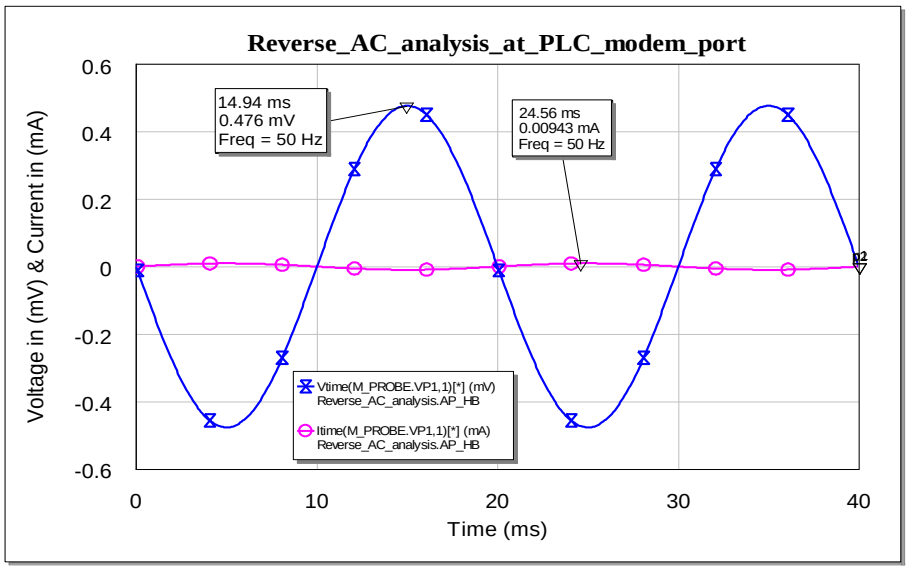

Fig 3.19: PLC modem end voltage and current curve

Similarly, the voltage at the HV-CC end is 632.5 V as depicted in Fig 3.20. Hence, the rating of the capacitor of the high pass section must be higher than 632.5 V. In addition, the proposed design can also be developed for higher frequency by selecting the operating frequency followed by the adjustment of Q-factor and L, C parameter calculations.

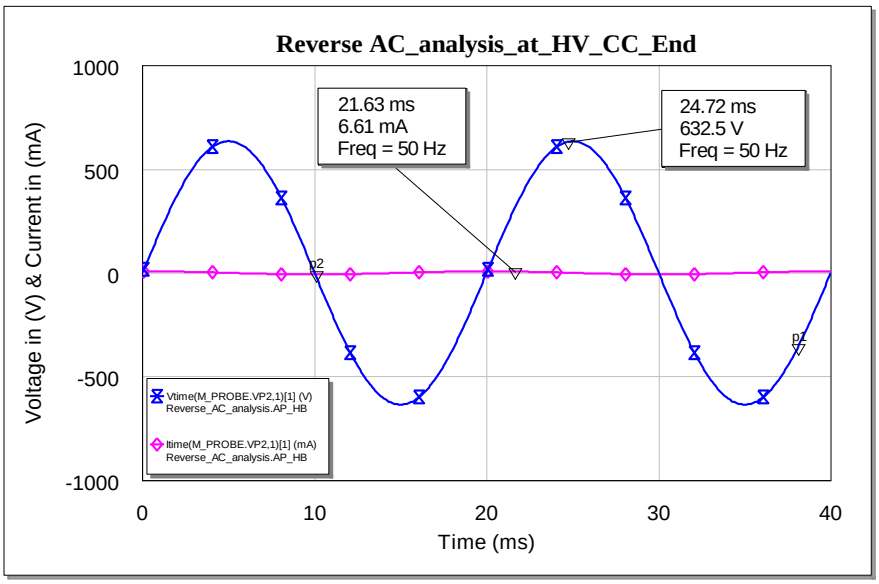

Fig 3.20: HV-capacitor end voltage and current curve

3.6 Experimental Evaluation of the developed coupling circuit

The simulation results have been verified with a lab based hardware implementation of the circuit. First step of the experimental work was the selection of inductor and capacitor units. One of the major focus of this work was to build the CC with commercially available components. Hence, the closest inductor and capacitor units compatible with the modeled circuit were used for building the circuit. These include a 220 µH commercially available inductor in place of the 200-µH inductor. Similarly, two 22 nF capacitors were connected in parallel instead of the 40 nF capacitor. However, while selecting any L or C units, self-resonance must also be checked. This is because if the component resonates (with self) before the frequency of interest, the circuit will not give the expected response. The self-resonance was verified for both the components with the BODE-100 analyzer.

Fig 3.21 presents the self-resonance curve for the components and it shows that the self-resonance frequency for both the capacitor and inductor is around 350 kHz to 400 kHz, which is way beyond the designated frequency.

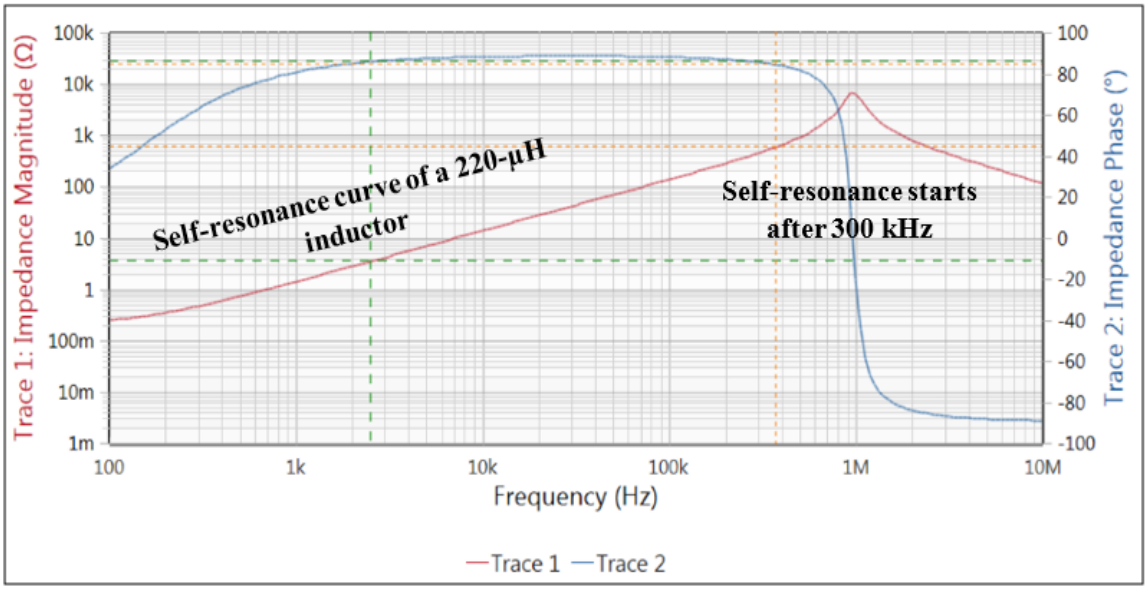

Fig 3.21: Self-resonance curve of the 220-µH inductor unit

Therefore, the selected components are suitable for coupling within the target band. After selecting the suitable L and C units, the circuit has been prototyped with a breadboard. The RF frequency swept input from the signal range of 100 Hz to 10 MHz has been given at the

PLC modem input and output has been taken from the equivalent SWER powerline and HV capacitor end. All the L and C components were connected according to the circuit of Fig 3.22. The 78-Ω SWER powerline impedance was achieved by connecting the 50-Ω vector network port with a series 27-Ω external impedance, which gave the nearest value. RF input functionality and response of the circuit has been recorded with the PC-Based Vector network analyzer (PC-VNA). Fig 3.22 shows the experimental setup of the circuit in lab environment with equivalent resistor.

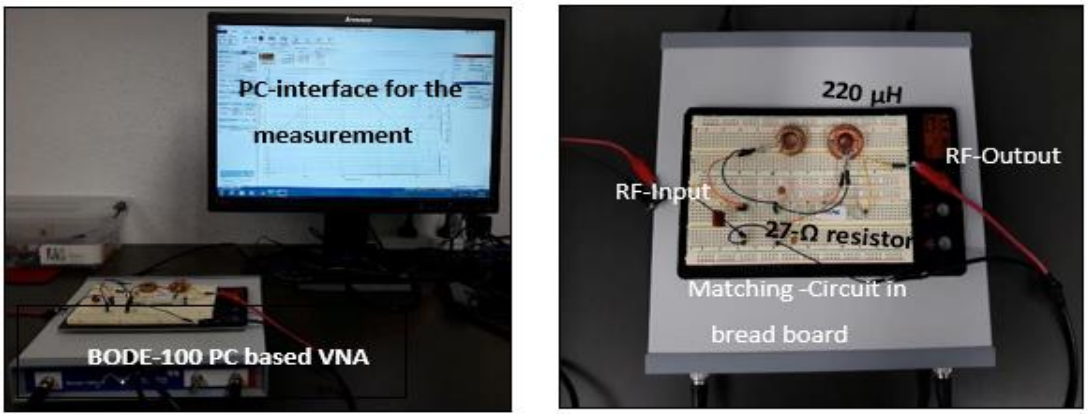

Fig 3.22: The experimental setup of the circuit in lab environment.

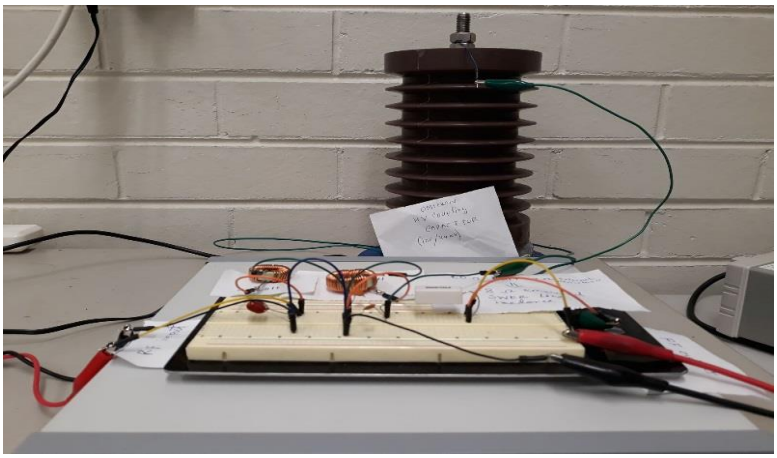

Fig 3.23: The experimental setup of the circuit in lab environment

Along with the equivalent resistor, the coupling circuit has been tested with the coupling capacitor itself. Fig 3.23 shows the experimental setup of coupling circuit connect with the (1 nF/24 kV) CC. The insertion loss profile for both the configuration was similar. The experimental gain or insertion loss S21 and reflection or S11 graphs have been plotted as shown in Fig 3.24. The real time insertion losses in the designated frequencies are -4 dB at

50 kHz, -3.5 dB at 100 kHz, and finally -4 dB at 150 kHz. This experimental result has also been compared with simulated result in Fig 3.25.

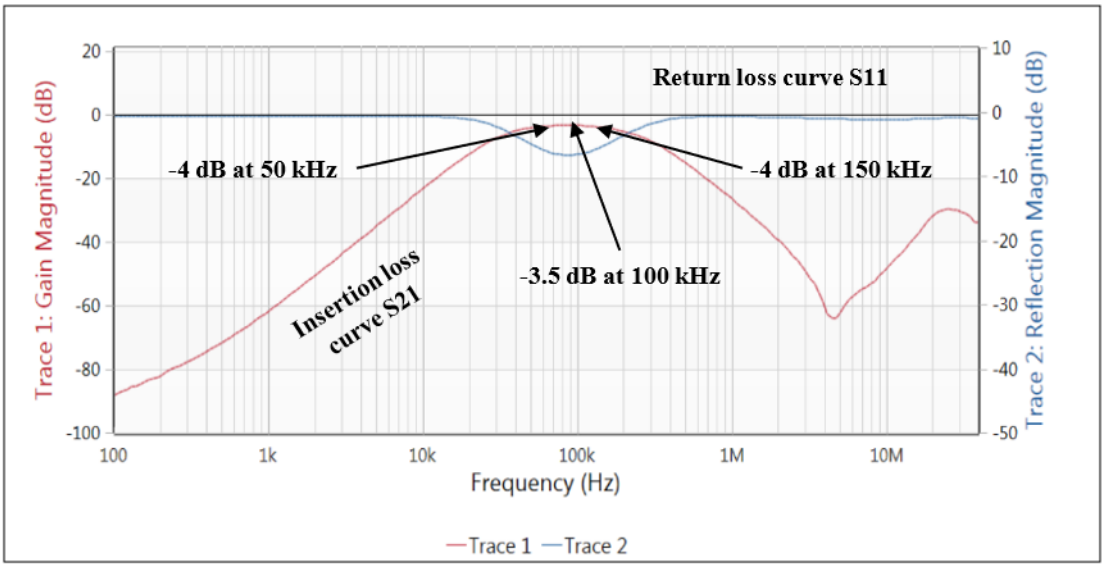

Fig 3.24: Experimental insertion loss and reflection loss graph of the circuit.

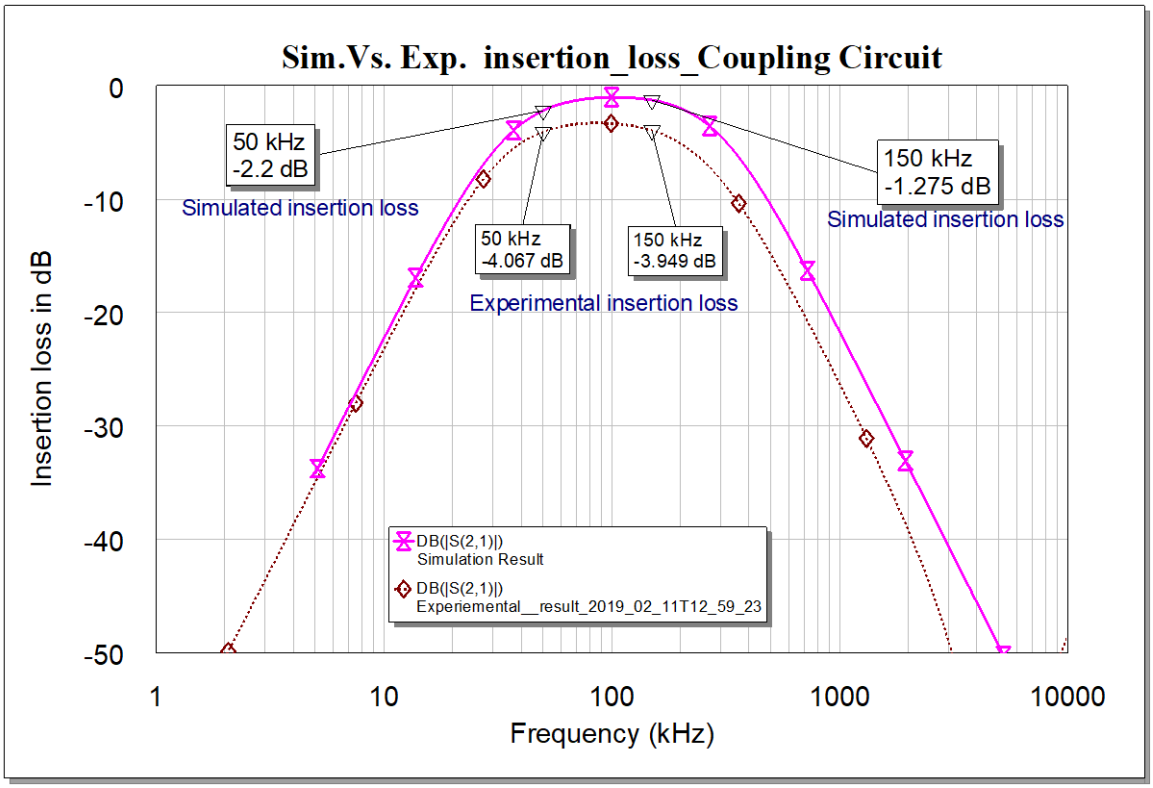

Fig 3.25: Comparison of the experimental and simulated insertion loss

From the graph, it can be shown that the simulation-based insertion loss for this circuit was higher than -3 dB, whereas the experimental result is around -4 dB. To analyze the error in detail, the deviation between the attenuation of simulated circuit and the experimentally designed circuit have been studied for different frequency components from 50 kHz to 500 kHz. These are included in Table 4, which the covers the designated PLC frequency band.

Table 4: Deviations in attenuation between simulated and experimental Coupling arrangement

Frequency in kHz	Attenuation in dB (Experimental)	Attenuation in dB (Simulation)	Error or deviation in attenuation (dB)
50	-2.2	-4.066	1.866
100	-1.014	-3.327	2.313
150	-1.275	-3.95	2.675
200	-1.994	-5.083	3.089
250	-3.081	-6.573	3.492
300	-4.442	-8.251	3.809
350	-10	-5.957	4.043
400	-11.71	-7.521	4.189
450	-13.36	-9.066	4.294
500	-14.91	-10.56	4.35

Following the table, a functional graph of frequency vs error of attenuation of the simulated and designed circuit is shown in Fig 3.26. The error curve shows that the deviation tends to increase beyond the designated frequency range. Such as, till 150 kHz, the error is less 3 dB, but on the other hand, at higher frequencies above 450 kHz, the curves get stable around 4 dB deviation in attenuation. The difference is possibly due to not using the exact component values and the effect of the internal DC resistance of the inductors.

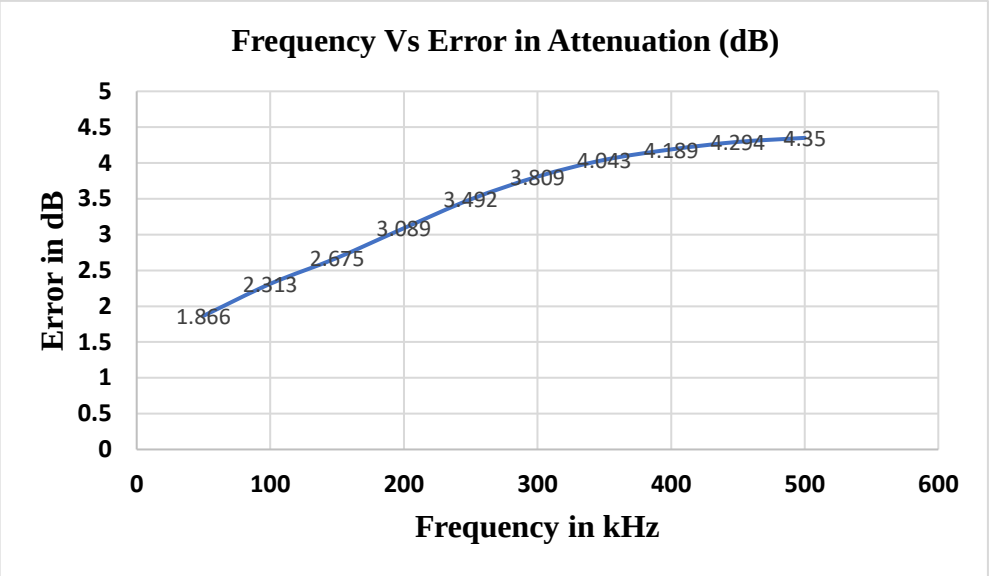

Fig 3.26. Frequency Vs Error in Attenuation for simulated and designed circuit

Above findings like the overall insertion loss of designed circuit, reasonable error between the simulation and experiment results reinstates the feasibility of the circuit to be used in a real-time PLC coupling. However, in other coupling circuits for low-voltage PLC applications such as in [87, 88], authors were not able to reduce the insertion loss less than -10 dB making this particular circuit very promising to use in real-time PLC applications over SWER networks. Photos of CC injection and reciver setup shown in Appendix E and F.

3.7 Comparative Performance Analysis

A list of comparative parameters of the proposed model with its contemporary coupling circuits in terms of voltage range, bandwidth, insertion loss, approximate cost etc. have been provided in Table 5 and Table 6. From the analysis, it is clear that most previous works in this field are related to the low voltage PLC applications [67-69, 87, 88]. These are not applicable to SWER powerlines and have higher insertion losses than the proposed circuit.

The previously designed coupling circuits from [73, 75] and [93, 94] (see Table. 5) could be used in SWER network PLC applications. Works by Artale *et al.* [93, 94] did not specify the capacitive value of the utilized CCs in their works, which is a major shortcoming. In [73, 75] 6-12 nF CCs were used. The cost of these solutions [73, 75] are likely to be much higher

and not commercially viable for large scale applications, considering that higher value CCs cost more. Herewith, these circuits [73, 75, 93, 94] also did not consider the internal circuitry of the utilized CCs, and relied their designs on the rated capacitance. However, as presented herein, the internal protection circuitry of a HV-CC creates impedance mismatch, which must be considered in designing a good coupling circuit.

Table 5 : Comparison with conventional low voltage coupling arrangements

Type of Coupling	**Application Voltage**	**Bandwidth**	**Insertion Loss**	**Applicability and approximate cost comparison**
T-type coupling circuit for broad band PLC applications [87]	120 V (Low Voltage PLC)	1.8-30 MHz	-10 dB	Not applicable in SWER networks.
Coupling unit for narrow-band power line communication channel measurements [95]	220 V (Low Voltage PLC)	9 kHz to 500 kHz	-6 dB	Not applicable in SWER networks.
Dual impedance adopting power line communications coupler [68]	220-240 V (Low Voltage PLC)	50-500 kHz	-7 dB	Not applicable in SWER networks.
Impedance matching L-shaped passive components for narrow band PLC coupling arrangement [88]	220 V (Low Voltage PLC)	10 kHz -210 kHz	-10 dB	Not applicable in SWER networks.
Transformer capacitive coupling for narrowband power line communication applications [70]	220 V (Low Voltage PLC)	60 kHz to 200 kHz	-10 dB	Not applicable in SWER networks.
Proposed: L-C Band pass Impedance Matching Coupling Circuit for High Voltage PLC Applications	PLC Applications over Medium Voltage 12.7 kV SWER powerlines	50-150 kHz	-2 dB to -4 dB	Specially proposed for the SWER powerline and cost is minimum among the existing HV coupling arrangements

Table 6: Comparison with the high voltage coupling arrangements

Type of Coupling	**Application Voltage**	**Bandwidth**	**Insertion Loss**	**SWER Applicability. Cost.**	**HV-CC Spec.**	**Internal Circuitry.**
Capacitor voltage divider coupling arrangement [93, 94]	52 kV (MV PLC)	100 kHz - 115 kHz	-9 dB	Yes. Higher.	Not specified	Not considered
MV to LV Transformer PLC Bypass Coupling Networks for a Low Cost Smart Grid Rollout [73, 75]	19.1 kV (MV PLC)	9-95 kHz	-2 dB to -5 dB (Simulated only)	Yes. Higher.	6-12 nF	Not considered
Proposed: L-C Band pass Impedance Matching Coupling Circuit for HV PLC Applications	PLC Applications over 12.7 kV SWER	50-150 kHz	-2 dB to -4 dB	Specially proposed for SWER powerline. Cost minimum among the existing HV coupling arrangements	1.1 nF/ HV-CC	Circuit designed considering the internal circuitry of the HV-CC

Furthermore, the bandwidth and insertion loss properties of the proposed circuit are still superior to the works in [73, 75, 93, 94]. The proposed circuit offers the widest range with a 100 kHz bandwidth and its insertion loss is 5 dB better than the only other circuit experimentally validated [93, 94]. Whilst the works in [73, 75] discuss network application, there is no evidence that these coupling circuits were individually analyzed and experimentally validated.

3.9 Conclusion

A 12.7 kV SWER network dedicated coupling circuit has been proposed in this chapter. The key motivation behind this work has been the need to design a low cost, and high-performance coupling circuit enabling PLC applications over rural SWER networks. The chapter highlights that conventional LC-based coupling circuits are unviable for HV or MV powerlines such as SWER networks. A key finding is that high inductance and capacitance values are required for such LC-resonant based arrangements increasing the cost of solutions. This work has also shown that theoretically modelled ideal component-based

coupling circuits are not feasible for real word PLC implementation in SWER networks. These would require very large CCs, which are difficult and expensive to procure making such solutions commercially unviable. In this work, coupling to the 12.7 kV network was achieved through a relatively low-cost 1nF HV-CC.

One key contribution in this chapter is the design of a LC band-pass coupling circuit using a relatively low capacitance 1nF HV-CC. In designing, a revised electrical equivalent circuit (inclusive of a capacitive divider) has been developed for the HV-CC in consideration of the impacts of its internal protection circuitry on the terminal behavior. The internal HV-CC protection circuity includes the surge arrester, freewheeling diode pair, drain coil, and few capacitors all having an impact of the equivalent capacitance of the HV CC at high frequencies. This in return enabled a more accurate design of the band-pass circuit by applying the virtual resistor matching technique. The relatively low insertion loss achieved from the final design when used in conjunction with the HV-CC is one evidence of the superiority of this novel approach.

The built band-pass circuit, when experimentally validated with the HV-CC, produced an insertion loss of around -3.5 dB to – 4 dB; a characteristic superior to any other comparative design. This was around 2 dB higher than the simulation performance. Experimental validation, low capacitance HV-CC specific design and consideration of the impacts of the HV-CC protection circuitry on its terminal behavior are factors that set this work aside from comparable work. The design offers the widest range with a 100 kHz bandwidth and its insertion loss is 5 dB better than the only other circuit experimentally validated

Chapter 4

Modelling of SWER Line at PLC Frequency

4.1 Introduction

SWER is one of the popular electricity distribution systems throughout the world. The advantages feature such as low installation cost, remote electricity access easy up-gradation facilities keep SWER network still strongly exist. A number of researchers are working on various aspects of the SWER network but still the results are not convincing to use in large scale commercial platforms. However, Australia is among one of the SWER dominated regions where SWER line is being in use for more than 28000 km over the country [96, 97]. Rather than this SWER is in extension in Subsharian-Africa region because of low installation cost and it will be increasing in the coming years because access to the electricity in the underdeveloped countries is very low, for example, Somalia (19.1), South Sudan(4.5), Mali(27.3), Kenya (36.4) Myanmar(52.7), Bangladesh(62.5) and India(79.2) [96, 98].

SWER could be a very good option for these countries to be used as a compatible and low-cost electricity distribution medium. Consequently, it can also be predicted that the rural areas of these countries might not have access to the internet. As SWER lines are being used as the electricity distribution medium around the rural areas, hence, this could be one of the potential options for PLC-based wired data communications. Similarly, PLC techniques can also be used on an existing SWER line for other purposes as well, such as- fault detection on SWER line, remote metering, online load monitoring etc.

To implement PLC system over the SWER network, impedance prediction of the SWER conductor's is a prerequisite. Exact impedance estimation of the line helps to select the coupling arrangements, transformer systems and other communication devices for the efficient PLC integration over the SWER distribution network. This chapter focuses on the prediction of the impedance of various SWER conductors, attenuation analysis of the conductors with frequency and other related aspects.

4.2 Equations for High Frequency SWER Line Modelling

This section presents modelling details of the SWER overhead lines including the impedance estimation of various SWER conductors. There few types of SWER conductors are currently in use around the world but in Australia mainly the SCAC and SCGZ are the popular choices. These conductors typically have three strands, with SCAC, each stand has a diameter of 2.75 mm (SCAC 3/2.75). SCGZ has the 2.75 mm (SCGZ 3/2.75) and 2.06 mm (SCGZ 3/12) options. SCGZ 3/12 is the imperial sized conductor with a diameter of 12 Gauge, around 2.06 mm. Among the SCGZ conductors, SCGZ 3/2.75 and SCGZ 3/12 type's conductors are widely used in the SWER networks, due to its lower cost. However, the impedance of a SWER conductor associated with various resistance, capacitance, and inductance properties altogether, which have been discussed sequentially with necessary mathematical equations.

The resistance of a conductor increases with frequency due to the skin depth. The resistance of a conductor made up of several strands with a steel core can be approximated by Eq. (4.1) [37]. A correction was required for the DC resistance calculation presented in(R). In(R), Eq. (4.1) was given with the skin depth (δ) not being square, which is incorrect. Even though the DC resistance formulae were incorrectly given in [37], the Microwave Office modelling included the correct representation of the following formulae.

$$R = \sqrt{\frac{R_{Cdc}^2 \times a_s^2}{4 \times \delta^2} + R_{Wdc}^2} \quad \Omega/km \qquad (4.1)$$

Where,

$\mathbf{R_{Cdc}}$ is the DC line resistance of the conductor strands (assuming all Aluminium or all steel) (Ω/km)

$\mathbf{R_{Wdc}}$ is the actual DC resistance of the whole conductor in (Ω/km), as is the radius of each strand in meters, and δ is the skin depth in meters.

Eq. (4.2) gives the calculation for the DC line resistance of an n strand conductor [75]. For SCAC, R_{Cdc} is calculated using the properties of Aluminium, whereas, for SCGZ, the properties of steel are used.

$$R_{Cdc} = \frac{\rho}{n \times \pi \times a_s^2} \qquad (4.2)$$

Where

R_{Cdc} is the DC resistance of the conductor strands in **Ω**/m,

ρ is the resistivity of the conductor in ohm-meters,

$\boldsymbol{a_s}$ is the radius of each strand in meters, and n is the number of conductors.

Eq. (4.3) gives the calculation for the skin depth [75].

$$\delta = \sqrt{\frac{2 \times \rho}{2 \times \pi \times f \times \mu_o \times \mu_R}} \qquad (4.3)$$

Where

δ is the skin depth in meters, ρ is the resistivity of the strand material in ohm. meters,

f is the frequency, μo is the permeability constant = 4π×10-7=1.257×10-6

μ_R is the relative permeability of either Aluminium or Steel.

The radiation resistance (RR) of the SCAC and SCGZ conductors was approximated by Kikkert as (1.35×10-16) ×Freq (Hz) 2.77 Ω/km. This approximation was used without any alterations. The total segment resistance can be calculated from Eq. (4.4).

$$R_{seg} = 0.001 \times (R + R_R) = 0.001 \times \left[\sqrt{\frac{R_{Cdc}^2 \times a_s^2}{4 \times \delta^2} + R_{Wdc}^2} + (1.35 \times 10^{-16}) \times \text{Freq (Hz)}^{2.77} \right] \quad \Omega/m \qquad (4.4)$$

In calculating the characteristic impedance, the line inductance and capacitance needs to be calculated. The line inductance can be approximated from Eqs. (4.5-4.6).

$$L_i = \frac{\mu_o \times \mu_R}{\sqrt{\frac{a^2}{4 \times \delta^2} + 1}} \qquad (4.5)$$

$$L = \frac{4}{10 \times K} \text{Log}_e \left(\frac{D}{a} + L_i \right) \quad \frac{mH}{km} \qquad (4.6)$$

Where

L is the inductance of the line and Li is the internal inductance,

μ_o is the permeability constant = 4π×10-7=1.257×10-6,

μ_R is the relative permeability of aluminium or steel,

a is the overall conductor radius in meters (i.e. not the radius of each strand),

K = 2 if the conductor is above the ground plane, δ is the skin depth in meters,

D is the distance between the conductor and one carrying return path,

h is the height of the SWER line above ground.

D is given by the Carson's Equation as in Eq. (4.7).

$$D = 2 \times \left(h + \sqrt{\frac{\rho_s}{2 \times \pi \times f \times \mu_0}}\right) \qquad (4.7)$$

Where

D is the distance between the conductor and one carrying return path,

h is the height of the SWER line above ground taken as 6.7 metres,

ρ_s is the soil resistivity taken as 30 Ω.m,

f is the frequency,

μ_o is the permeability constant = 4π×10-7=1.257×10-6

The line capacitance (line-to-neutral) can be calculated from Eq. (4.8). Eq. (4.8) differs from that given in [75], as the equivalent formulae provided in [75] included a factor of 36 in the denominator, which is an oversight and only applicable when calculating the line-to-line capacitance.

$$C = \frac{2 \times K \times \epsilon_r}{18 \times \mathrm{Log_e}\left(\frac{D}{a}\right)} \quad \mu F/km \qquad (4.8)$$

Where

C is the capacitance of the line, K = 2 if the conductor is above the ground plane,

ϵ_r is the dielectric constant taken as 4.5 referring to [36],

D is the distance between the conductor and return path given by Carson's equation,

a is the overall conductor radius in meters (i.e. not the radius of each strand).

The well-established equation of the characteristic impedance Z_c is given by Eq. (4.9). The characteristic impedance Z_c and the propagation constant γ are related to per-unit length

parameters of the transmission line. For a lossless line, the characteristic impedance in ohms can be approximated as in Eq. (4.9).

$$Z_c = \sqrt{\frac{L}{C}} \quad (4.9) \qquad (4.9)$$

Where

Z_c is the characteristic impedance in Ohms,

L inductance (mH/m),

C is the capacitance (mF/m).

4.3 SCAC 3/2.75 Conductor

For the SCAC conductor, the R_{Cdc} (DC line resistance of the 3/2.75 mm SCAC conductor) can be calculated from Eq. (4.10) assuming that the strands are pure aluminium. The conductor has three strands and each standard has a diameter of 2.75 mm. The resistivity of aluminium has been taken as 2.82 × 10−8 Ω.m. The skin depth (in terms of the frequency) for the SCAC conductor can be calculated from Eq. (4.11). Fig 4.1 shows the variation of the skip depth for the 3/2.75 mm SCAC conductor. As shown in Fig 4.1 the skin depth at 100 kHz frequency is 0.0002673 meters.

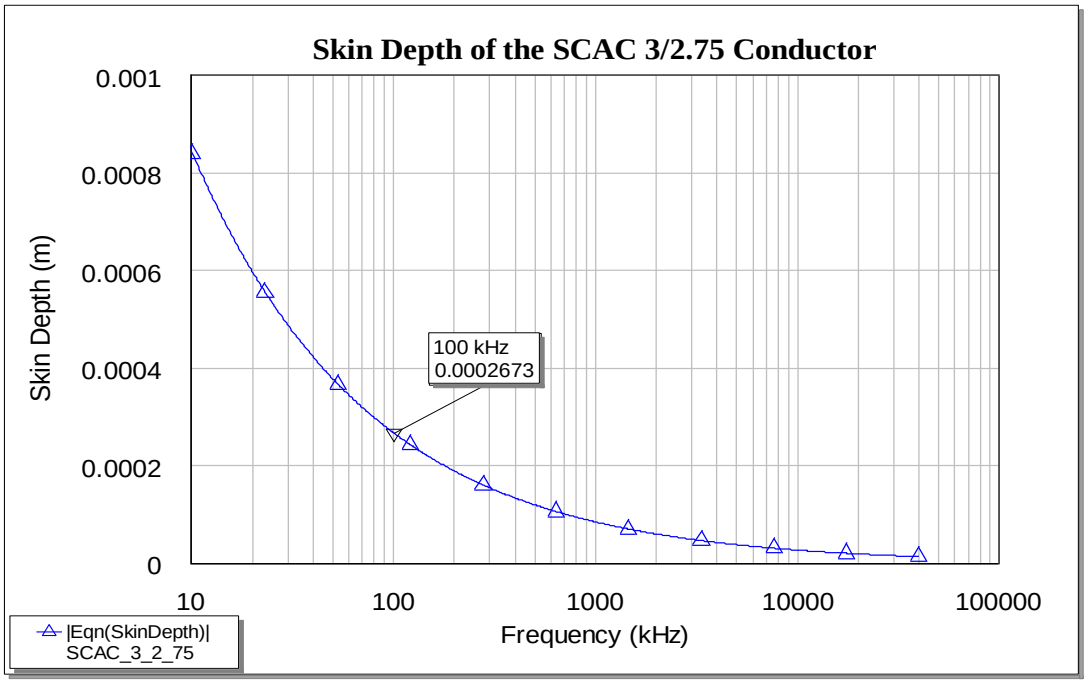

Fig 4.1: SCAC Conductor skip depth variation with frequency

$$R_{\mathrm{Cdc}} = \frac{\rho}{n \times \pi \times a_s{}^2} = \frac{2.82 \times 10^{-8}}{3 \times \pi \times (1.375 \times 10^{-3})^2} = 0.001583\ \Omega/\mathrm{m} = 1.583\ \Omega/\mathrm{km} \quad (4.10)$$

$$\delta = \sqrt{\frac{2 \times 2.82 \times 10^{-8}\ \Omega.\mathrm{m}}{2 \times \pi \times f \times 1.257 \times 10^{-6} \times 1}} \quad (4.11)$$

The resistance (R) of the SCAC 3/2.75 conductor can then be approximated using Eq. (4.12). The radiation resistance (RR) of the SCAC conductor was approximated by Kikkert as (1.35×10-16) ×Freq (Hz) 2.77 Ω/km.

$$\mathrm{R} = \sqrt{\frac{1.583^2 \times 1.375 \times 10^{-3}{}^2}{4 \times \delta^2} + 4.8^2} \quad \Omega/\mathrm{km} \quad (4.12)$$

The overall section (per meter) resistance of the SCAC conductor can be calculated from Eq. (4.13).

$$\mathrm{R}_{sec}(\mathrm{f}) = 0.001 * (R + (1.35 \times 10^{-16}) \times \mathrm{Freq\ (Hz)}^{2.77}) \quad \Omega/\mathrm{m} \quad (4.13)$$

The characteristic impedance plot for any conductor can be computed using Eqs. (4.5-4.9) and the DC resistance calculation using Eqs. (4.12-13). Table 7 shows the parameters used in calculating the resistance and impedance of the 3/2.75 SCAC conductors. Fig 4.2 shows the characteristic impedance plot for the SCAC 3.2/75 mm conductor with respect to the frequency variations. At 100 kHz, the characteristic impedance for SCAC/3/2.75 conductor is 256.6 Ω and the DC resistance is 6.294 Ω/km.

Table 7 : 3/2.75 mm SCAC Conductor Parameters

Feature	Value
Resistivity of Aluminium	2.82 × 10−8 Ω.m
Soil Resistivity	30 Ω.m
Dielectric Constant (relative permittivity)	4.5
Relative Permeability of Aluminium (μR-aluminium)	1 H/m
No of Strands	3
DC Resistance in Ω/km (RWdc)	4.8 Ω/km
SCAC Conductor Diameter in m	5.9 ×10-3 m
SCAC Conductor Radius in m	2.95×10-3 m
Strand Diameter in m	2.75 ×10-3 m
Strand Radius in m	1.375×10-3 m
Height of conductor above ground	6.7 meters

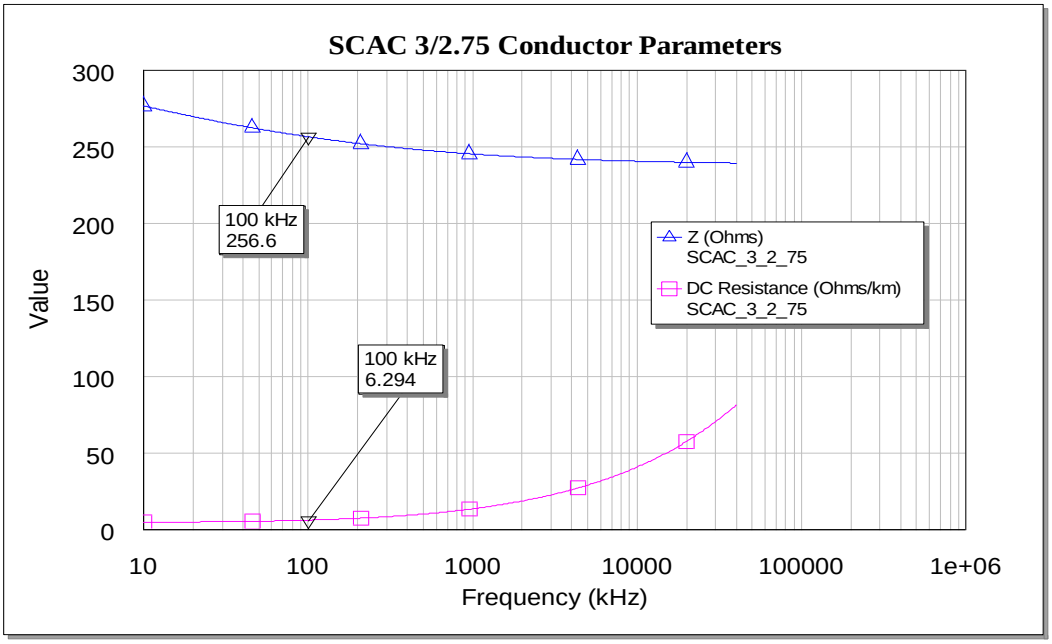

Fig 4.2: SCAC 3/2.75 Conductor Characteristic Impedance and DC Resistance.

Fig 4.3 shows the DC, radiation, and total segment resistances of the SCAC 3/2.75 mm conductor per segment (per km). As shown, the radiation resistance is dominant after 1000 kHz and rises at a corner frequency of 1000 kHz. The total segment resistance is the sum of the radiation and DC resistances. The line DC resistance is dominant in the total segment resistance for frequencies below 1000 kHz.

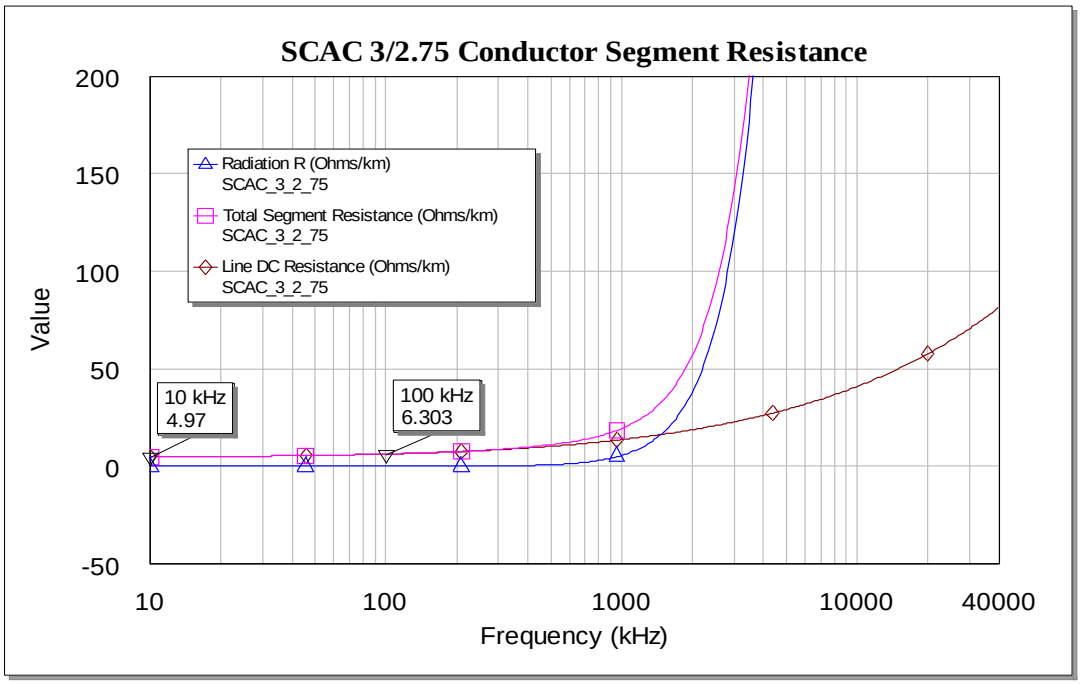

Fig 4.3: SCAC 3/2.75 Conductor Radiation, Segment and DC Resistances.

Fig 4.4 shows the S21 parameter (attenuation) characteristic and Fig 4.5 shows the S11 (reflection) characteristic of the developed SCAC 3/2.75 mm conductor based. The S21 and S11 analysis were carried out for a segment length of 2 metres with a height of 6.7 meters above the ground. The attenuation at 100 kHz was -0.01563 dB for the 50 Ω terminated line model.

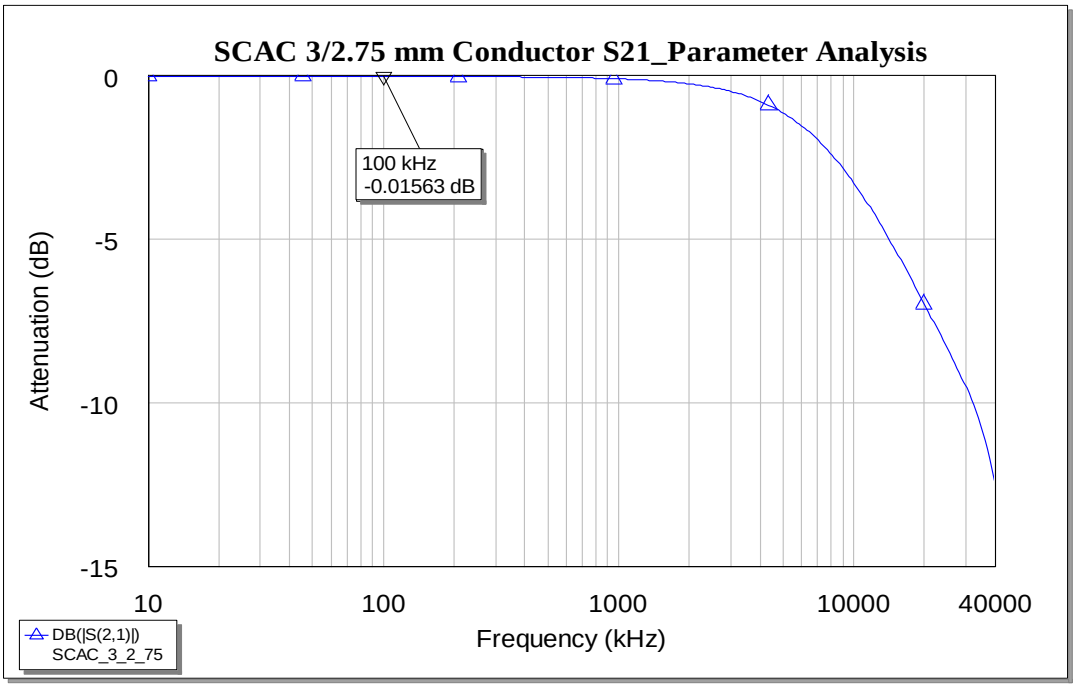

Fig 4.4: S21 Characteristic of the 2-meter SCAC 3/2.75 mm conductor.

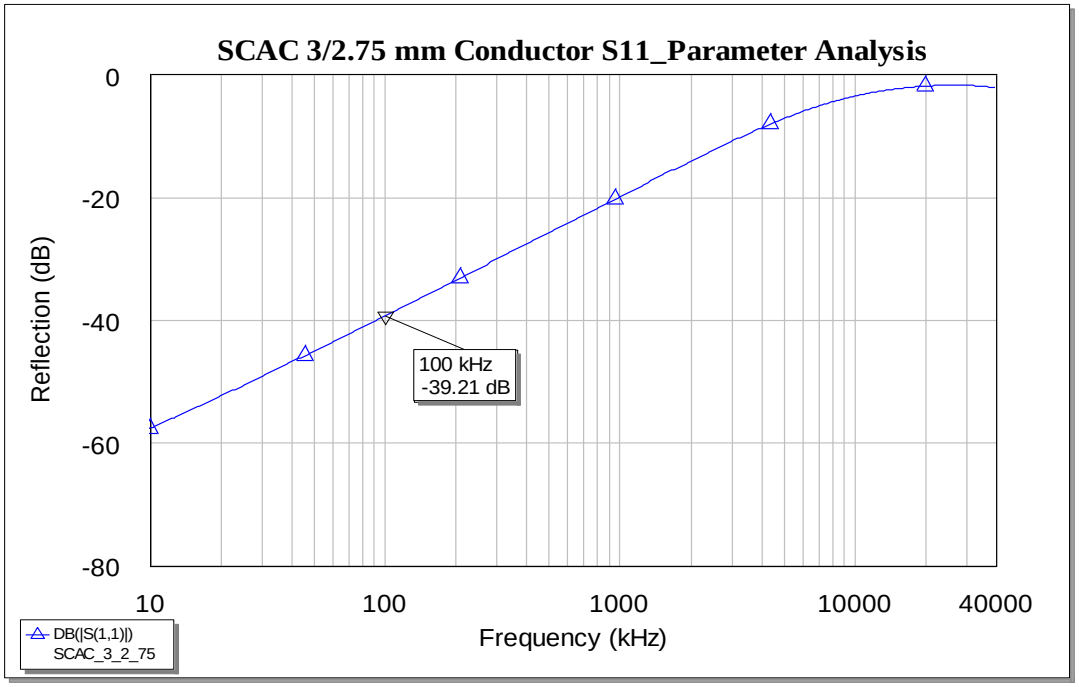

Fig 4.5: S11 Characteristic of the 2-meter SCAC 3/2.75 mm conductor

Fig 4.6 shows the Sub-circuit segment model of the SCAC 3/2.75 conductor. Fig 4.7 show the mathematical equations and values of all parameters associated with SWER line modelling in the Microwave Office schematic window. In developing the segment model, all the constants such as dielectric constant and relative permeability of aluminium are first recorded after which frequency-dependent line resistance, radiation, and characteristic impedance formulations are formed. These frequency-dependent forms variables of the impedance and coaxial elements from the AWR library. As shown, the segment model is formed by adding each half of the total segment resistance to each end of the AWR library coaxial model. Ground resistance was assumed zero.

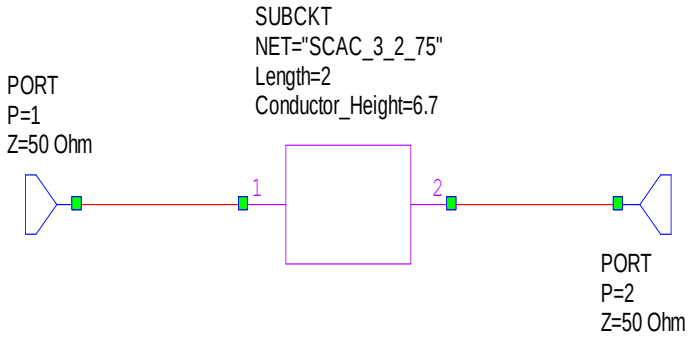

Fig 4.6: Microwave conductor model and sub-circuit

4.4 SCGZ 3/2.75 Conductor

Table 8 shows the parameters used in calculating the DC resistance, overall resistance, and characteristic impedance of the SCGZ 3/2.75 mm conductor. Eqs. (1-9) were used in computing these with resistivity and relative permeability of steel used in place of those of aluminium. Fig 4.8 shows the DC resistance and characteristic impedance calculations for the SCGZ 3/2.75 mm conductor. At 100 kHz, characteristic impedance (Z) is 256.5 Ω and the DC resistance (R) is 85.32 Ω/km. As shown, the resistance of the SCGZ 3/2.75 mm conductor is much larger rising at a much lower corner frequency compared to the SCAC conductor. The value of the calculated characteristic impedance (256.5 Ω) differs from that (270.26 Ω) given in despite using Eqs. (4.5-4.9) in all calculations as recommended in [75]. A characteristic impedance of 270.26 Ω is not achievable as long as soil resistivity is not increased well beyond 100 Ω.m. The total segment resistance of the SCGZ 3/2.75 mm conductor is dominated by the DC resistance up to 1000 kHz and by the radiation resistance from that point onwards.

Mathematical equations and values of all parameters associated with modelling of the SWER line/conductor segment model in the Microwave Office Platform

Constants

Soil resistivity	Rhos = 30	SCAC Specific	
Dielectric constant	Ers = 4.5	Conductor DC Resistance/km	RWdc = 4.8
Relative Permeability of Aluminium	Mur = 1	Conductor Diameter	DiaL=5.9e-3
Length per section km	Slen = 0.001	Radius of the SCAC Conductor	RadL = DiaL/2.0
Permeability Constant	Muo = 4*_PI*1e-7	Strand Diameter in meters	DiaC = 2.75e-3
K = 2 when the conductor above a ground plane	K = 2	Strand Radius in meters	RadC = DiaC/2.0
Height of the conductor above ground	h = Conductor_Height		

Equations

Equivalent Aluminium DC Resistance Calculation		Angular frequency	Wf = 2*_PI*_FREQ
Resistivity of Aluminium	Rho = 2.82e-8	Skin Depth	SkinDepth = sqrt((2*Rho)/(Wf*Mur*Muo))
Number of Strands	n = 3	Ground resistance in Km	Zgndkm = 1
Resistance/km if all Al line	RCdc =1000*(Rho/(n*_PI*RadC*RadC))	Ground Resistance	ZgndS = Zgndkm*Slen

Line Resistance Calculation

Line DC Resistance ohms/km	RLineSeckm = (sqrt(((RCdc*RCdc*RadC*RadC)/(4*SkinDepth*SkinDepth))+RWdc*RWdc))
Alternative Line DC Resistance Calculation ohms/km	TotalDC_R = RCdc*(RadC/2*SkinDepth)
Line DC Resistance ohms/m	RLineSec = (sqrt(((RCdc*RCdc*RadC*RadC)/(4*SkinDepth*SkinDepth))+RWdc*RWdc))*Slen
Radiation Resistance ohms/km	RR = 1.35e-16*pow(_FREQ,2.77)
Radiation Resistance ohms/m	Rr = 1.35e-16*pow(_FREQ,2.77)*Slen
Total Segment Resistance ohms/m	RLS = Rr+RLineSec

Line Impedance Calculation

Distance between conductor and earth	D = 2*(h+sqrt(Rhos/(Wf*Muo)))
Internal Impedance Constant	qi = (RadL*RadL)/(4*SkinDepth*SkinDepth)
Internal Inductance	Li = (Mur*Muo)/(sqrt(qi+1))
Line Inductance in H per km	L = (4/10*K)*log((D/RadL)+Li)/1000
Line Capacitance Constant	Ci=18*log(D/RadL)
Line Capacitcane in F per m	C=((2*K*Ers)/(Ci))/1000000
Charcateristic Line Impedance in Ohms per meter	Z=sqrt(L/C)
Alternative Line Impedance Calculation	Zv2=120*log(D/RadL)/(K*sqrt(Ers))

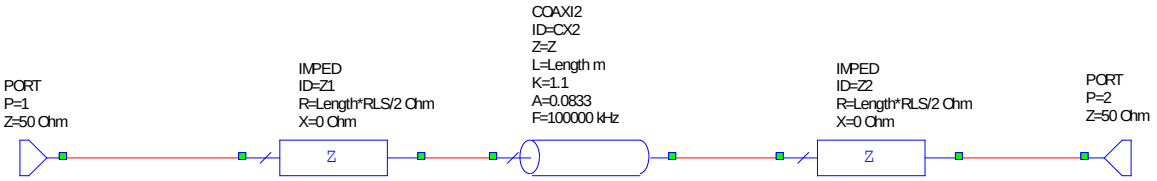

Fig 4.7: SCAC 3/2.75 mm Conductor Segment Model (per meter).

Table. 8: 3/2.75 mm SCGZ Conductor Parameters

Feature	Value
Resistivity of steel	1.74×10^{-7} Ω.m
Soil resistivity	30 Ω.m
Dielectric constant (relative permittivity)	4.5
Relative permeability of steel ($\mu_{R\text{-aluminium}}$)	70 H/m
No of Strands	3
DC Resistance in Ω/km (R_{Wdc})	11 Ω/km
SCGZ Conductor Diameter in m	5.93×10^{-3} m
SCGZ Conductor Radius in m	2.965×10^{-3} m
Strand Diameter in m	2.75×10^{-3} m
Strand Radius in m	1.375×10^{-3} m
Height of conductor above ground	6.7 meters

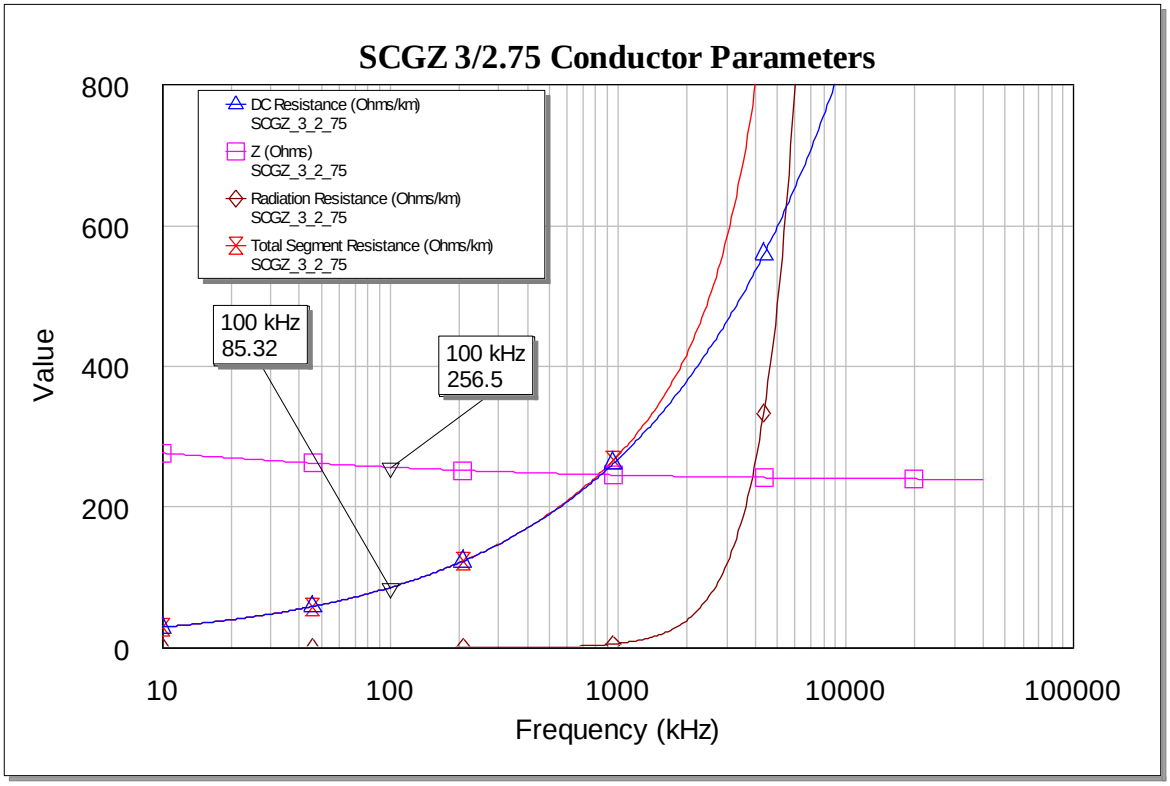

Fig 4.8: SCGZ 3/2.75 Conductor Characteristic Impedance and DC Resistance.

Fig 4.9 and Fig 4.10 shows the attenuation and reflection analysis of the SCGZ 3/2.75 conductor. As shown, the 100-kHz attenuation is -0.02931 dB for the 50 Ω terminated line model. As expected, the attenuation is higher compared to the SCAC line model due to the higher DC resistance of the SCGZ 3/2.75 conductor.

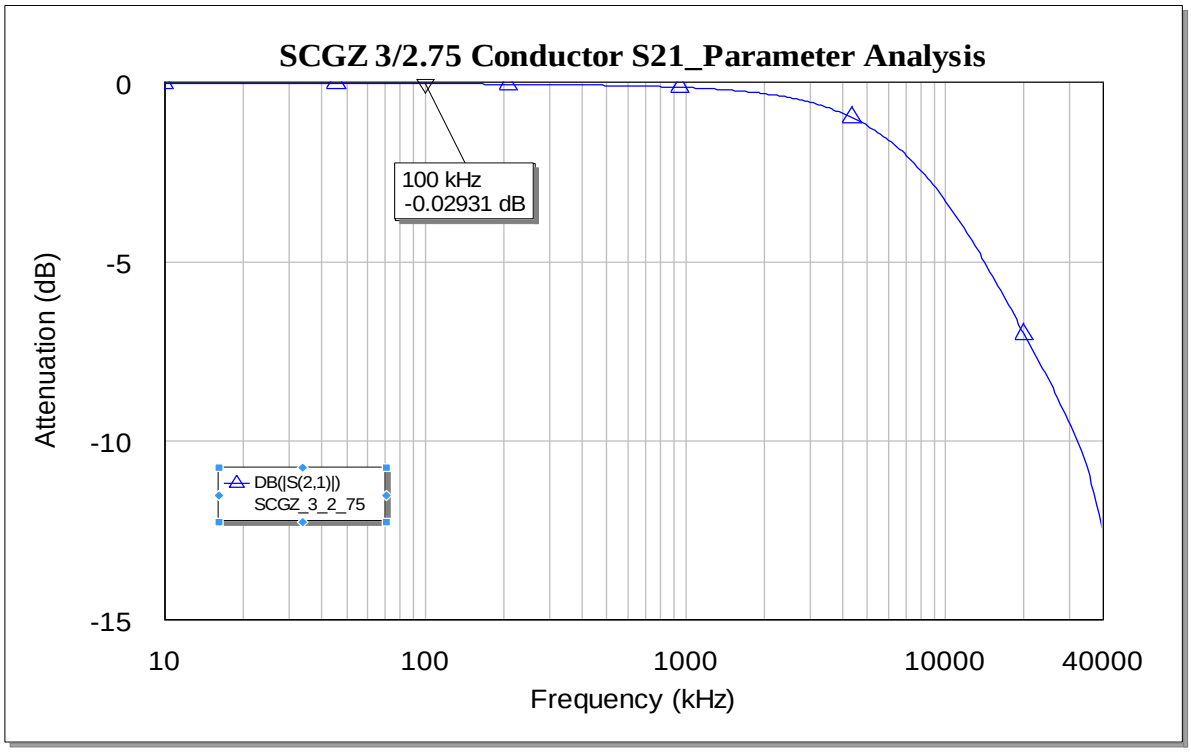

Fig 4.9: S21 Characteristic of the SCGZ 3/2.75 Conductor

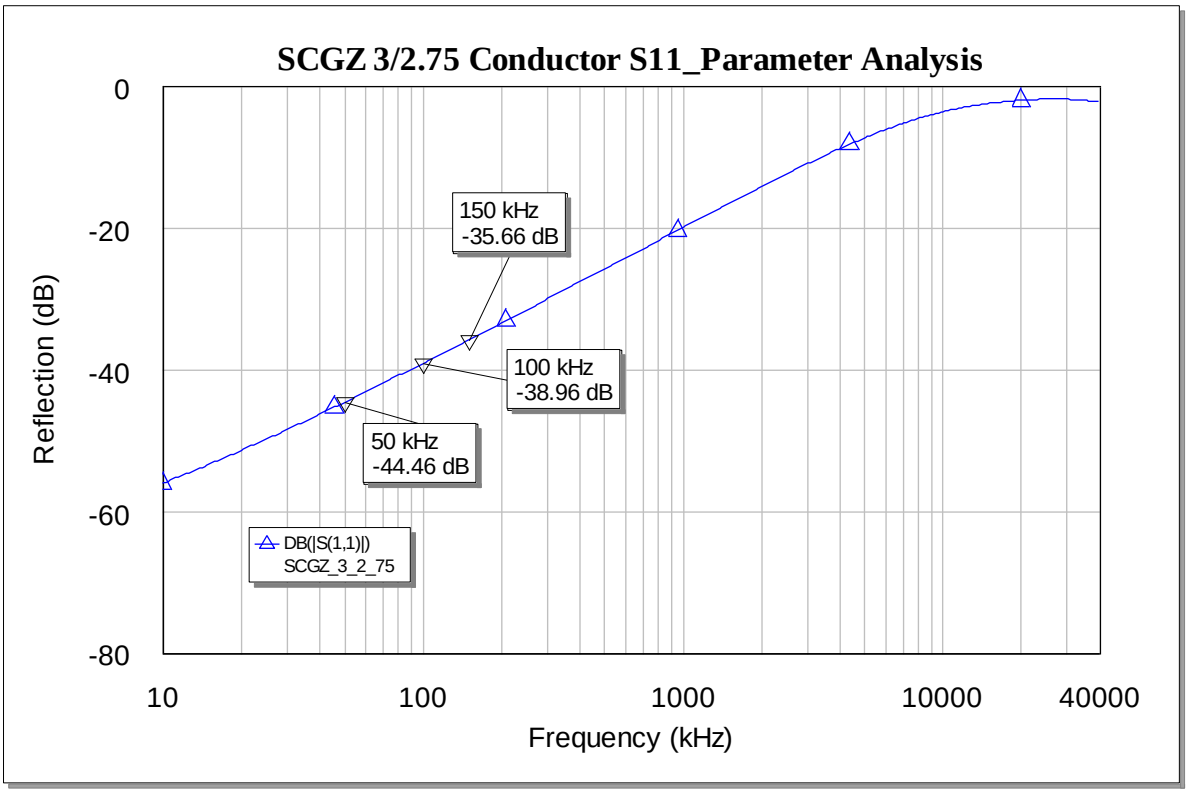

Fig 4.10: S11 Characteristic of the SCGZ 3/2.75 Conductor.

4.5 SCGZ 3/12 Conductor (Imperial Measurement; 12 gauge)

Table 9 shows the parameters in calculating the DC resistance, overall resistance, and characteristic impedance of the SCGZ 3/12 conductor. The strand diameter is 12 Gauge (2.06 mm). The DC resistance (RWdc) of the SCGZ 3/12 conductor is also higher and is given as 11.93 Ω/km. SCGZ 3/12 is also commonly referred to as the 3/2.06 mm conductor in this report. Fig 4.11 shows the DC resistance and characteristic impedance (Z) variation of the SCGZ 3/12 conductor with frequency. At 100 kHz, Z is 260.8 Ω and the DC resistance is 113.6 Ω/km. As shown, the resistance (113.6 Ω/km) of the SCGZ 3/12 conductor is larger than that of the SCGZ 3/2.75 conductor (85.32 Ω/km). The radiation resistance and total segment resistance of the conductor are also shown Fig 4.11.

Table 9: 3/12 SCGZ Conductor Parameters (Height = 6.7 metres above ground)

Feature	Value	Feature	Value
Resistivity of steel	1.74×10^{-7} Ω.m	Dielectric constant	4.5
Soil resistivity	30 Ω.m	Relative permeability of steel	70 H/m
No of Strands	3	DC Resistance in Ω/km (R_{Wdc})	11.93 Ω/km
SCGZ Conductor Diameter in m	5.1×10^{-3} m	SCGZ Conductor Radius in m	2.55×10^{-3} m
Strand Diameter	2.06×10^{-3} m (12 Gauge)	Strand Radius in m	1.03×10^{-3} m

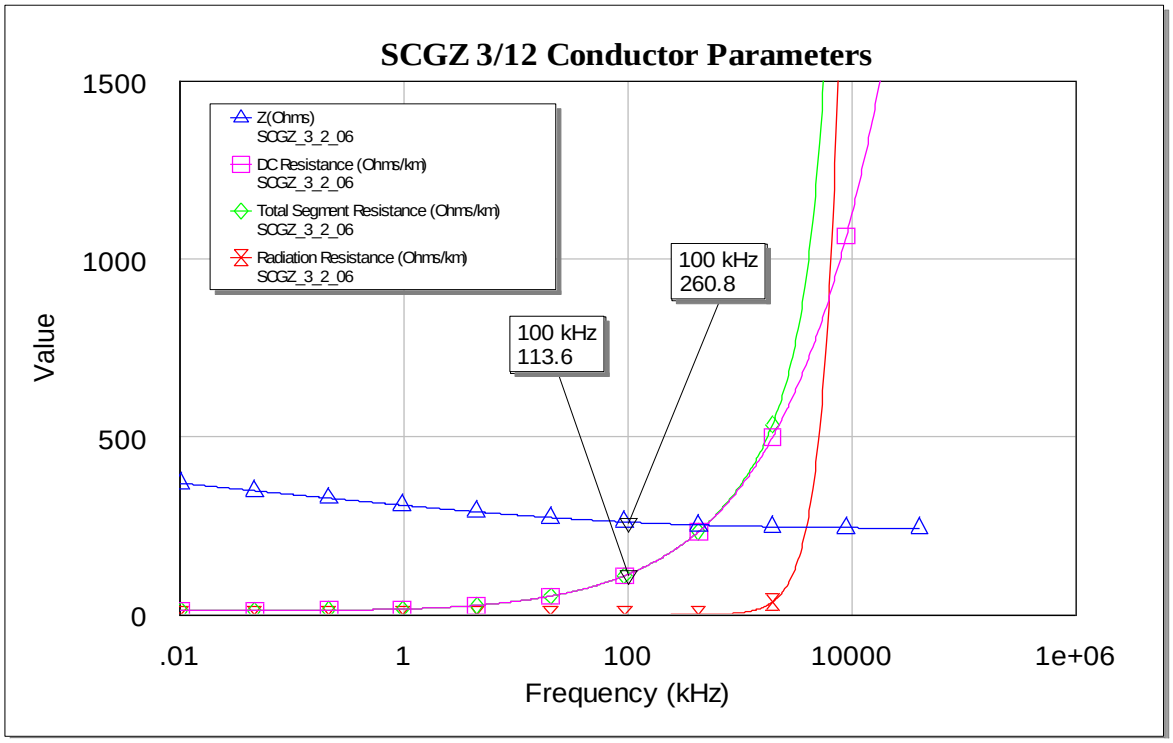

Fig 4.11: SCGZ 3/12 Conductor Characteristic Impedance and DC Resistance.

Fig. 4.12 shows the gain analysis of the 2-metre SCGZ 3/2.06 conductor with 6.7 metres in height. The attenuation at 100 kHz was -0.034 dB for the 50 Ω terminated line model. As expected, the attenuation is higher compared to the SCGZ 3/2.75 model due to the higher DC resistance of the SCGZ 3/2.06 conductor. Regulations allow utilities to go down to about 5.7 metres for the height of the conductor above ground. Fig 4.13 shows the attenuation analysis of the 2 metre SCGZ 3/12 conductor of 5.7 metres in height. The attenuation at 100 kHz is slightly lower than the 6.7-metre case.

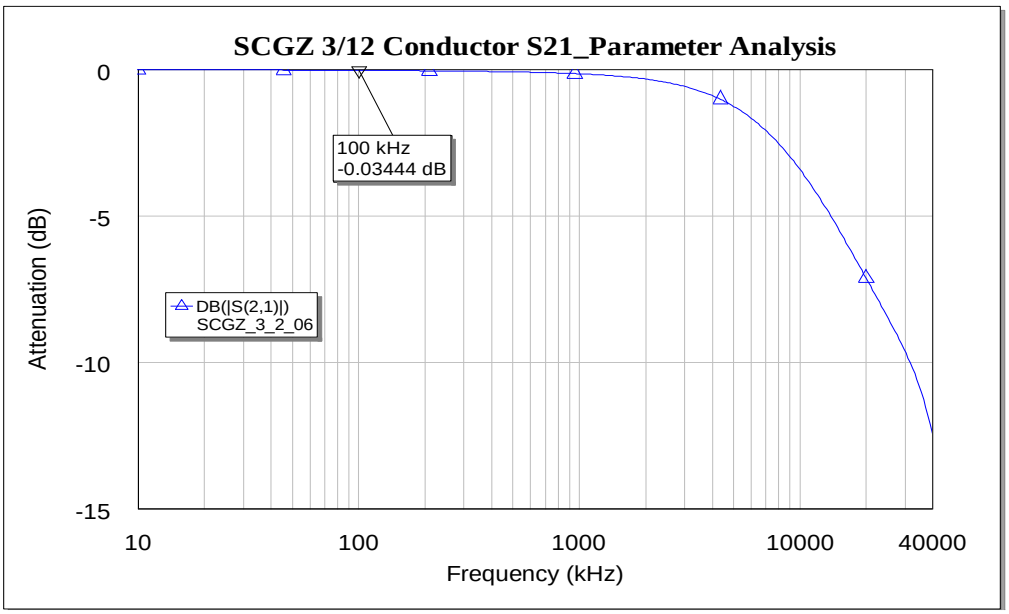

Fig 4.12: SCGZ 3/12 conductor attenuation analysis (2 meter; height = 6.7 meters)

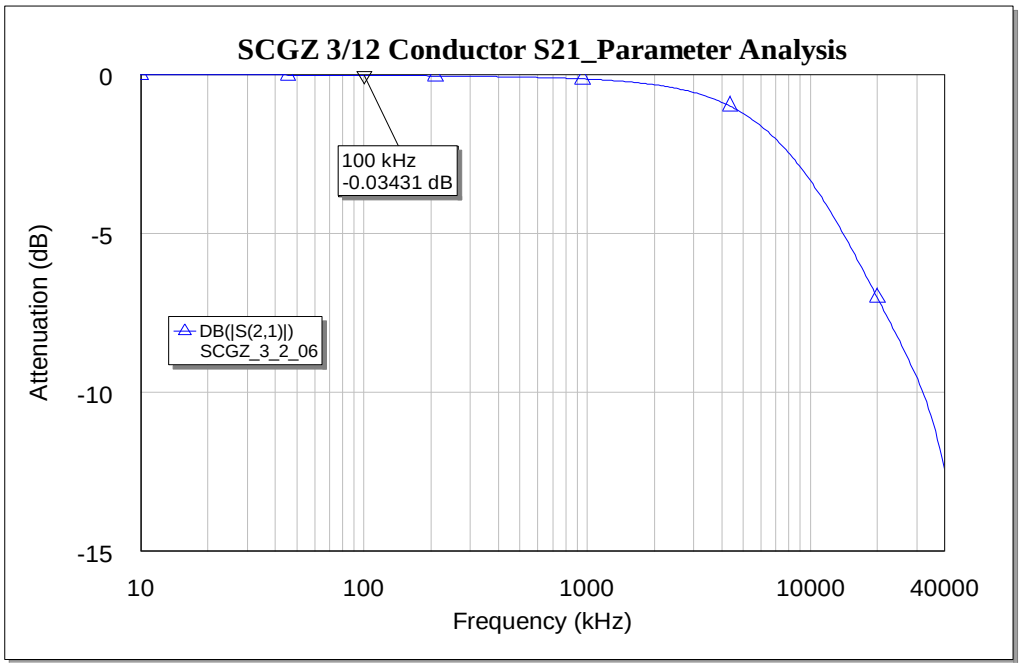

Fig 4.13: SCGZ 3/12 conductor attenuation analysis (2 meter; height = 5.7 meters)

4.6 Attenuation Analysis Comparison (2-metre lines; 50Ω termination)

Fig 4.15 shows the S21 parameter analysis comparison of the three conductor types for the 50-1000 kHz range with the 2-metre conductors terminated with 50 Ω ports as shown in Fig 4.14. As shown in Fig 4.15, there is no significant difference between the attenuation characteristics of the conductors.

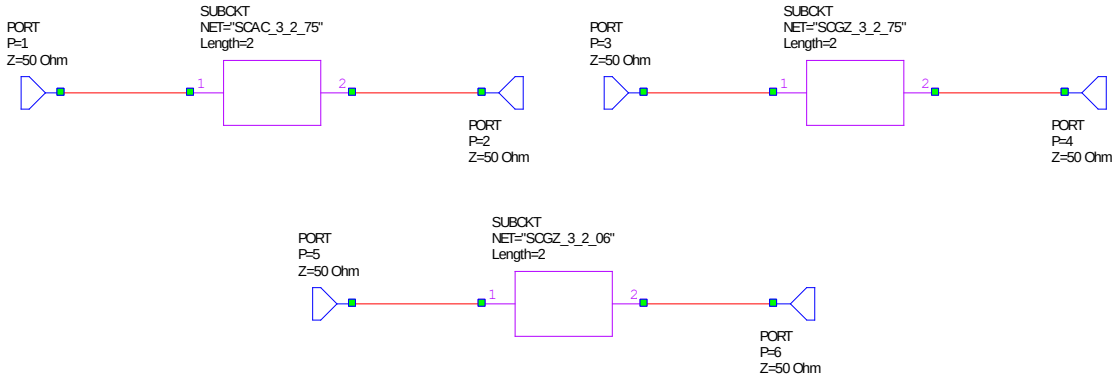

Fig 4.14: Attenuation Analysis Schematic.

The 50-Ω port termination was chosen to match the port impedance setting of the Vector Network Analyser (VNA) and the standard output impedance of most RF equipment. SCAC conductor has the minimum attenuation loss and SCGZ 3/12 conductor has the poorest attenuation (S21) characteristic. When the conductor lengths are increased, significant attenuation is observed, as the Sub circuits are not matched.

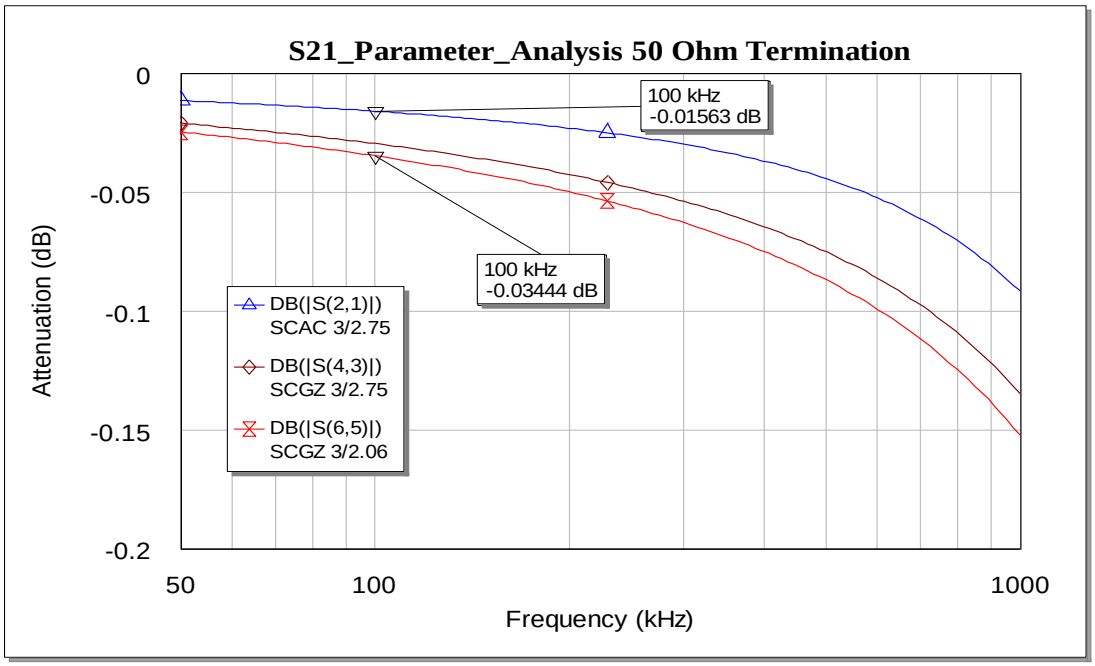

Fig 4.15: Attenuation Analysis Comparison of the 2-meter SCAC 3/2.75 conductor.

4.7 Attenuation Analysis Comparison (2-metre lines; 260Ω termination)

Fig 4.17 shows the S21 parameter (gain) analysis comparison of the three conductor types for the 50-1000 kHz range with the 50-metre conductors terminated with 260 Ω ports as shown in Fig 4.16. The 260-Ω port termination was chosen to match the characteristic impedance of the lines. As shown in Fig 4.16, the attenuation of the SCAC conductor is the minimum with -0.137 dB loss at 100 kHz. The SCGZ 3/12 conductor has the poorest attenuation (S21) characteristic with an attenuation of -0.2261 dB at 100 kHz. No significant attenuation difference is observed when the height (above ground) is changed to 5.7 metres.

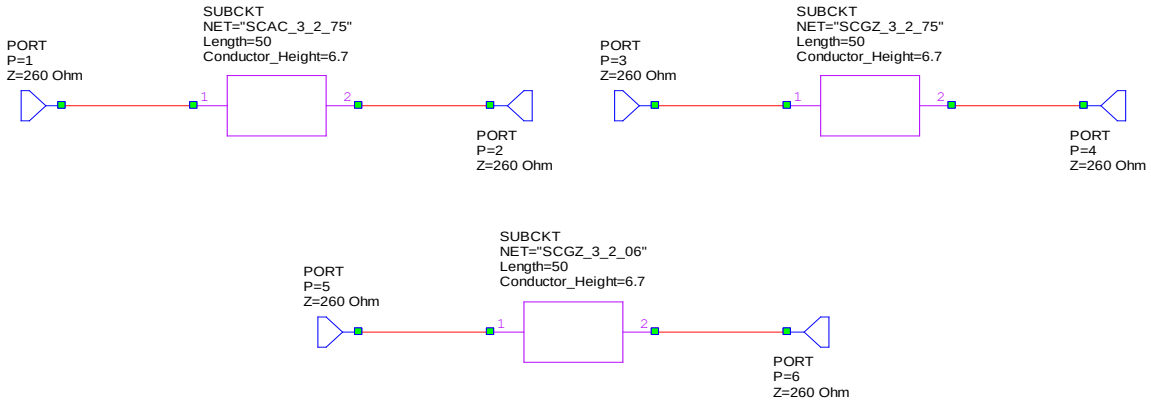

Fig 4.16: 50-metre Conductor Sub circuits Terminated by 260-Ω Termination Ports.

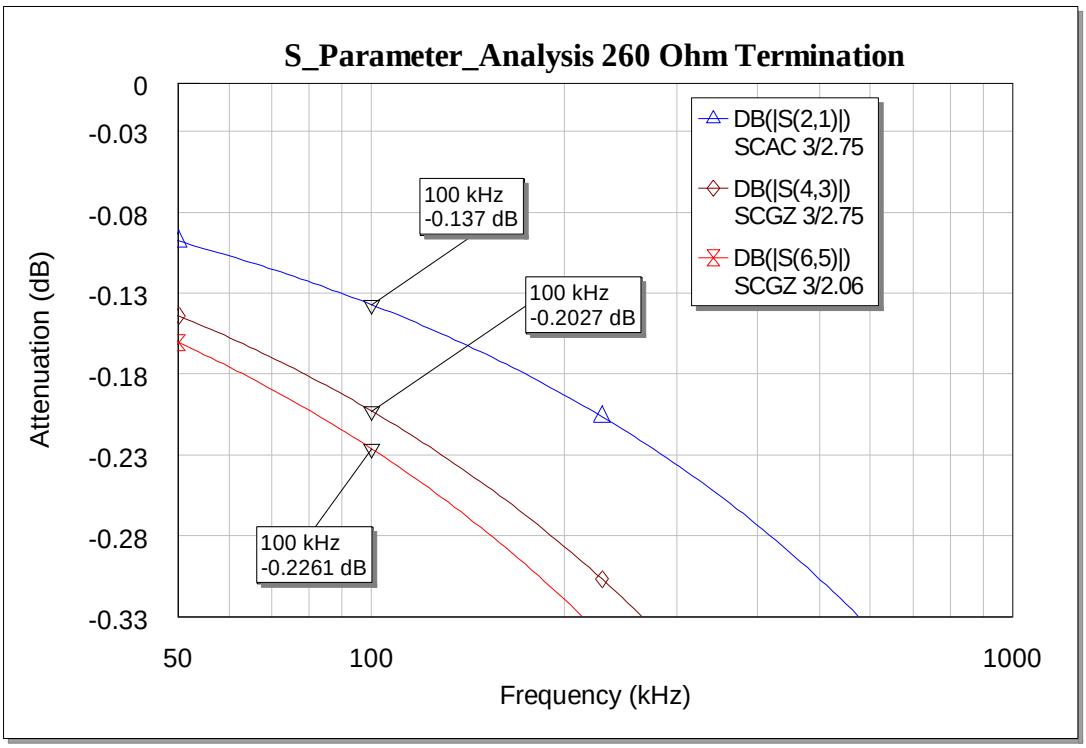

Fig 4.17: Attenuation analysis Comparison of the 50-metre Conductors.

4.8 Length Based Attenuation Analysis

Fig 4.18, Fig 4.19 and Fig 4.20 show the attenuation analysis of the SCAC 3/2.75, SCGZ 3/2.75 and SCGZ 3/12 conductors for different segment lengths. Same system configuration shown in Fig 4.16, with a change of distance and conductor type have been used to get the value of attenuation vs frequency with a specific conductor length.

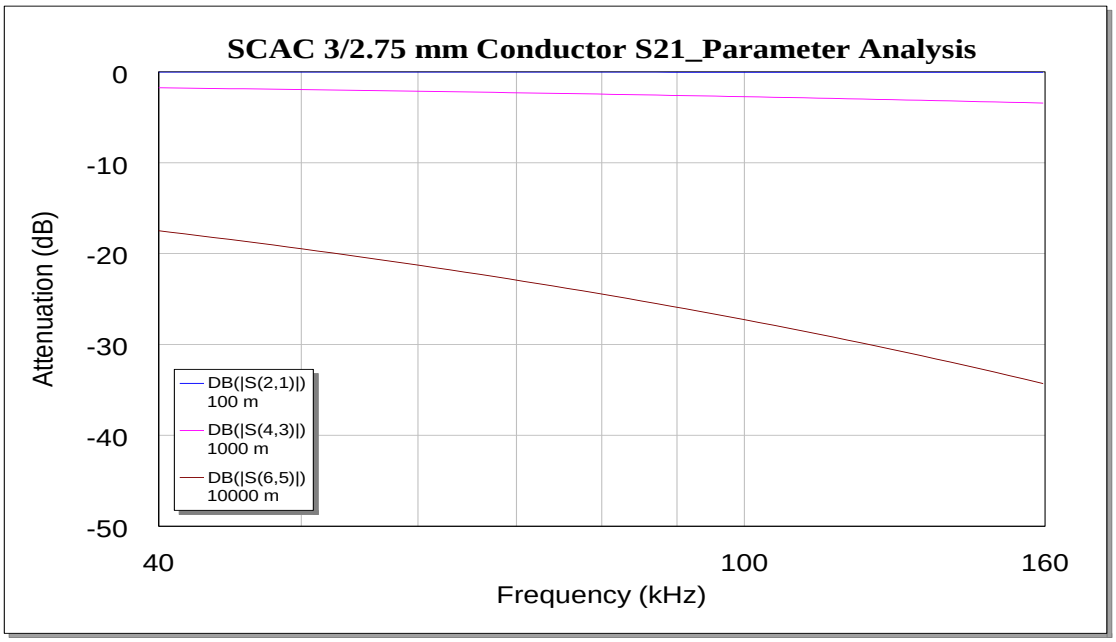

Fig 4.18: Distance-Based Attenuation Analysis of the SCAC 3/2.75 Conductor.

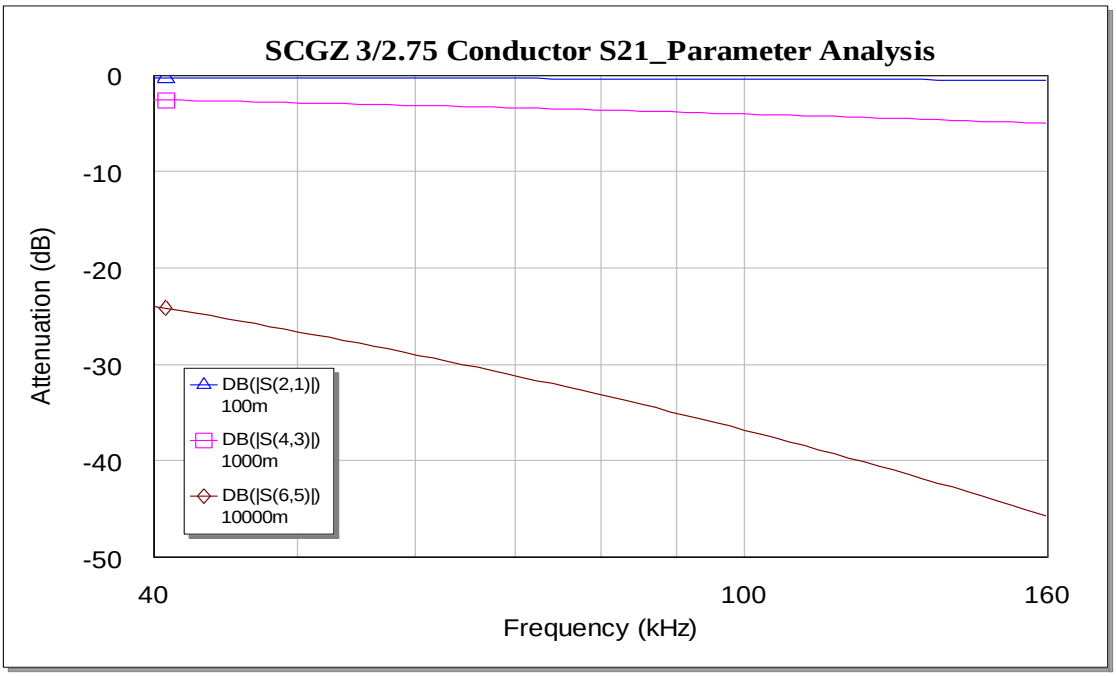

Fig 4.19: Distance-Based Attenuation Analysis of the SCGZ 3/2.75 Conductor.

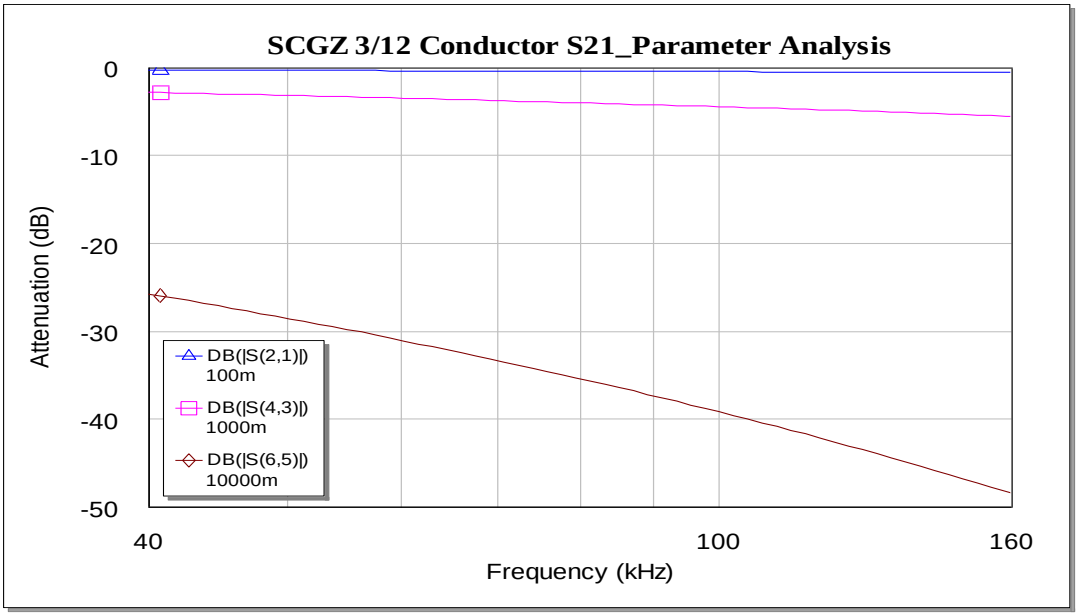

Fig 4.20: Distance-Based Attenuation Analysis of the SCGZ 3/12 Conductor.

Table 10, Table 11 and Table 12 tabulate the attenuation characteristics of all the conductors at different frequencies and for various segment lengths including 100 m, 1 km, and 10 km.

Table 10 : SCAC 2/2.75 Conductor Attenuation for Different Segment Lengths.

Frequency (kHz)	Length (m)	Attenuation (dB)
50	**100**	**-0.19571**
	1000	**-1.9512**
	10000	**-19.489**
100	**100**	**-0.27302**
	1000	**-2.7071**
	10000	**-27.276**

Table 11 : SCGZ 2/2.75 Conductor Attenuation for Different Segment Lengths.

Frequency (kHz)	Length (m)	Attenuation (dB)
50	**100**	**-0.2873**
	1,000	**-2.856**
	10,000	**-26.62**
75	**100**	**-0.3511**
	1,000	**-3.504**
	10,000	**-32.18**
100	**100**	**-0.405**
	1,000	**-4.023**
	10,000	**-36.8**

125	**100**	**-0.4528**
	1,000	**-4.455**
	10,000	**-40.83**
150	**100**	**-0.4961**
	1,000	**-4.864**
	10,000	**-44.43**

Table 12 :SCGZ 3/12 Conductor Attenuation for Different Segment Lengths

Frequency (kHz)	**Length (m)**	**Attenuation (dB)**
50	**100**	**-0.3201**
	1,000	**-3.161**
	10,000	**-28.55**
75	**100**	**-0.3912**
	1,000	**-3.879**
	10,000	**-34.35**
100	**100**	**-0.4512**
	1,000	**-4.45**
	10,000	**-39.15**
150	**100**	**-0.552**
	1,000	**-5.353**
	10,000	**-47.03**

4.9 Mathematical Relation Development for Length vs Attenuation

In this section, an intensive simulation has been carried out using the SCAC conductor to establish a relation between length vs path loss of a SWER conductor. Measured attenuation values at ten different frequency components, for three different segment lengths, has been set out in the Table 12.

Table 13 shows the attenuation characteristics for six different segment length (100 m, 200 m, 500 m, 1000 m, 5000 m, 10,000 m) for three different carrier frequencies including the 50 kHz, 100 kHz and 150 kHz.

Table 13: SCAC 3/2.75 Conductor attenuation for ten different frequency components

Lengths	Frequency Variations in kHz										
	50.119	60.256	70.795	81.283	91.201	100	109.65	120.23	131.83	141.25	151.36
	Attenuation Variations in dB										
100 m	-0.1952	-0.213	-0.2307	-0.246	-0.261	-0.273	-0.2856	-0.2988	-0.3127	-0.3235	-0.3467
1000 m	-1.9512	-2.1332	-2.3071	-2.4678	-2.6103	-2.7304	-2.8561	-2.9879	-3.1264	-3.2348	-3.3475
10000 m	-19.489	-21.308	-23.044	-24.649	-26.074	-27.279	-28.534	-29.853	-31.234	-32.313	-33.431

Table 14 : SCAC 3/2.75 Conductor attenuation for six different lengths segment at 50 kHz, 100 kHz and 150 kHz frequency components.

Frequency (kHz)	Length (m)	Attenuation (dB)	Frequency (kHz)	Length (m)	Attenuation (dB)
50	100	-0.19571	100	100	-0.27302
	200	-0.39032		200	-0.54624
	500	-0.97571		500	-1.3661
	1000	-1.9512		1000	-2.7071
	5000	-9.7502		5000	-13.645
	10000	-19.489		10000	-27.276
150	100	-0.33489			
	200	-0.67051			
	500	-1.6755			
	1000	-3.3475			
	5000	-16.725			
	10000	-33.431			

For establishing a mathematical relation, two graphs have been plotted as in Fig 4.21 and Fig 4.22 making use of the data available in Tables 13 and Table 14, these include:

- Frequency vs attenuation graph with constant conductor length, and
- Length vs attenuation at constant carrier frequencies

The trend-line in Microsoft Excel platform has been used to determine the approximate mathematical relations. Fig 4.21 shows the frequency vs attenuation curves for the SCAC conductor at three different lengths including 100 m, 1,000 m (1 km) and 10,000 m (10 km).

As shown, the impact of conductor length is critical and the increase in attenuation at higher frequencies is more severe when the conductor length is longer. This potentially

shows that in large networks where the direct distance between the transmitter and receiver is very long, lower carrier frequencies should perhaps be favoured.

Using the trend line tool from the Microsoft Excel, it has been identified that the length vs attenuation curves of a SWER conductor share a linear mathematical relation at any specific length. The properties of the equation change linearly with the multiplier of the length. With an increase in length, the slopes of the attenuation change get steeper. The value of the **correlation coefficient (R^2=0.99)** also reveals the same fact that for all the cases, the change of attenuation is nearly 100% dependent on the change of frequency.

The coefficient of determination, R-squared (or R^2) is a measure of the relationship between two data sets used in a mathematical model. It represents the proportion of fluctuation in the reliant variable that can be anticipated from the free factor in the model.

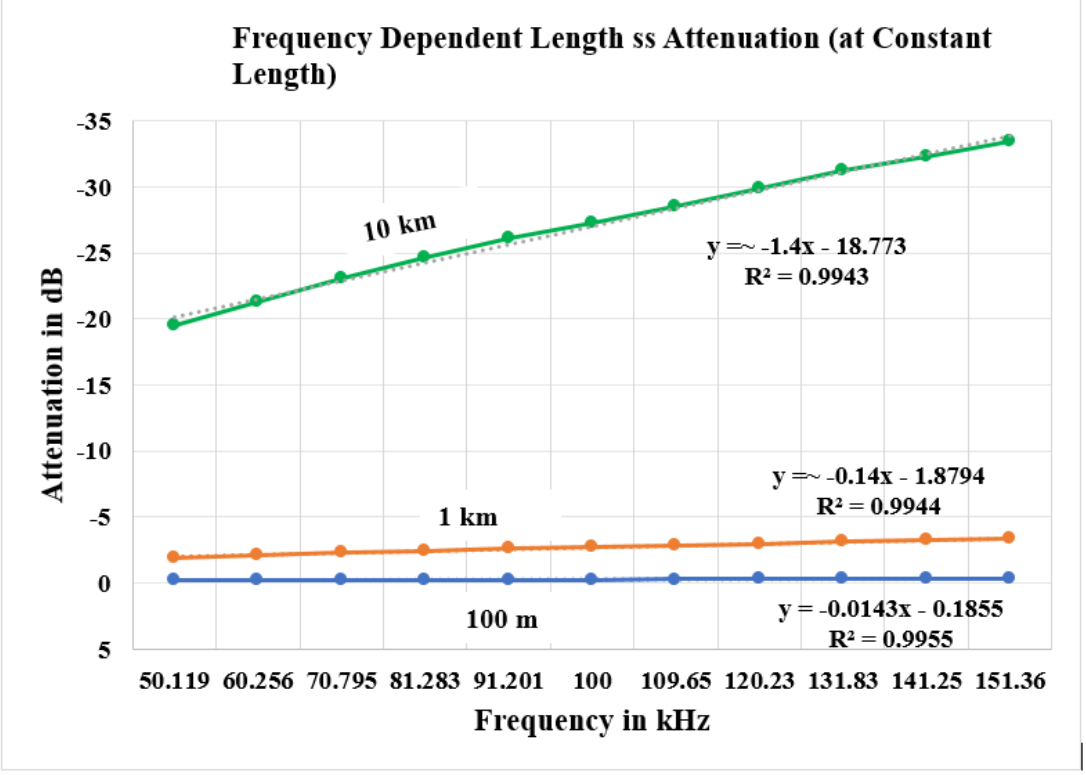

Fig 4.21: Analysis of relation between frequency and attenuation (SCAC 3/2.75).

The mathematical relation between the attenuation and conductor length can be represented more specifically using the following derivation. As in the Fig 4.21, the equation for 100 m SCAC 3/2.75 can be written as:

$$Y_{100\,m} = -ax - c \tag{4.14}$$

Where, a= ~0.014 and c=~0.18

Similarly, the equation for a 10×100 m =1000 m (1 km) will be

$$Y_{1\,km} = -(10 \times a)x - 10 \times c \tag{4.15}$$

Finally, the equation for a 10×10×100 m=10000 m (10 km) will be

$$Y_{10\,km} = -(10 \times 10 \times a)x - (10 \times 10) \times c \tag{4.16}$$

All of the above Eqs. (4.14-4.16) have two constants *a* and c. Most interestingly, both constants share the nearly same value for a specific conductor. For example, for the case of the SCAC conductor, the value of ***a*** is approximately (0.014) and ***c*** is approximately (~ 0.18). This analysis also shows that the other conductors are expected to follow the similar mathematical trends with length-based frequency-dependent attenuation. This finding can be used as a benchmark in future extension or up-gradation of a SWER network. In the following section, a similar analysis has been carried out to establish the relation between length vs attenuation at a constant frequency.

Fig. 4.22 shows the analysis carried out for establishing the relation between length vs attenuation at constant frequencies. From the analysis of Fig 4.22, it can be observed that the attenuation vs length curve at a constant frequency shares a linear mathematical relation. Attenuation increases with the increase of the frequency. Please note that the negative sign indicates a loss (attenuation) with the magnitude of the loss giving the dB difference. Similar to the curve of Fig 4.21, the value of the **correlation coefficient (R^2=1)** in Fig 4.22, also shows that at a constant frequency, attenuation is 100% dependent on the change of length.

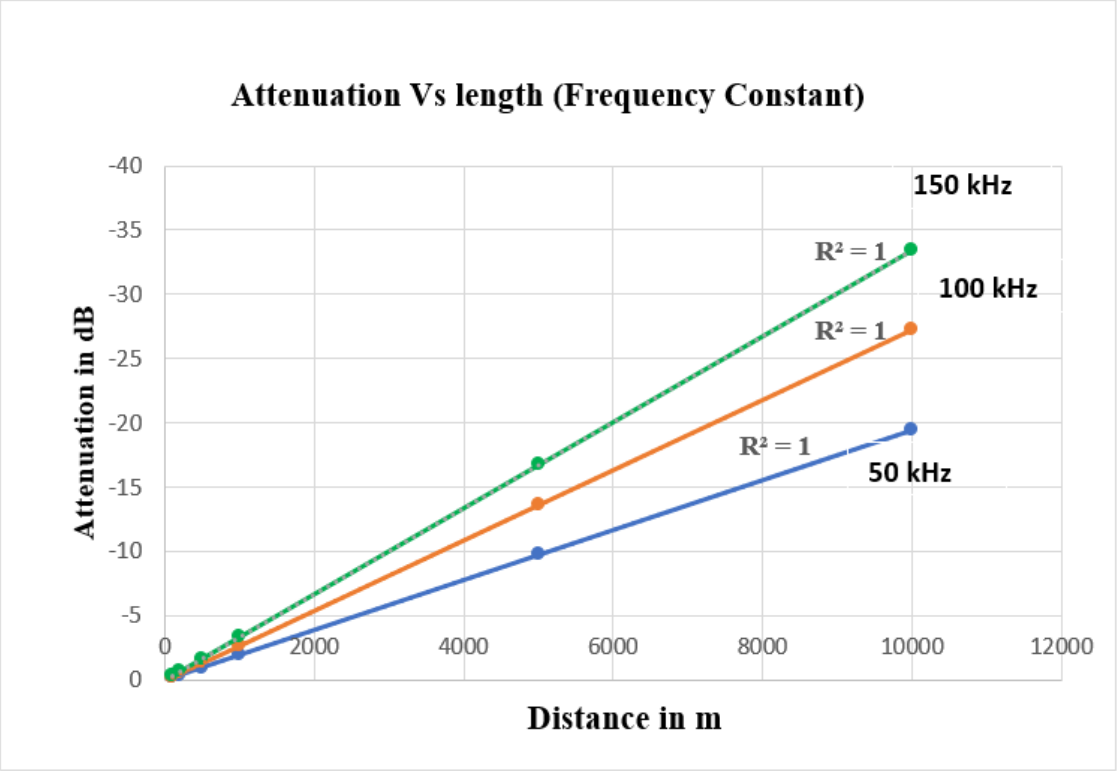

Fig 4.22: Attenuation vs Length with constant frequency.

4.10 ACSR/GZ Conductor

The 22 kV OH line is the ACSR/GZ 6/1/2.50 mm (Almond) conductor. ACSR/GZ is a composite conductor with a single stranded galvanised steel core surrounded by layers of stranded aluminium wires. These are economical conductors for high-tension overhead lines combining the lightweight and good conductivity of aluminium and high tensile strength of steel. The Myers Road network has the 6/1 stranding pattern shown in Appendix C and GMR calculation data sheet is shown in Appendix D. The overall diameter of the conductor is 7.5 mm and its radius (R_c) is 3.75 mm. The 'SWER Distribution Manual' [99] by the now obsolete State Electricity Commission of Victoria shows the typical configuration of a SWER isolation transformer as in fig $.23

As shown in Fig 4.23, the ACSR/GZ 6/1/2.50 mm (Almond) conductor forms a two-wire single-phase line at the Active and Neutral terminals of the SWER ISO Transformer. In calculating the inductance and capacitance of the two-wire single-phase line, the formulations given in [100] have been used.

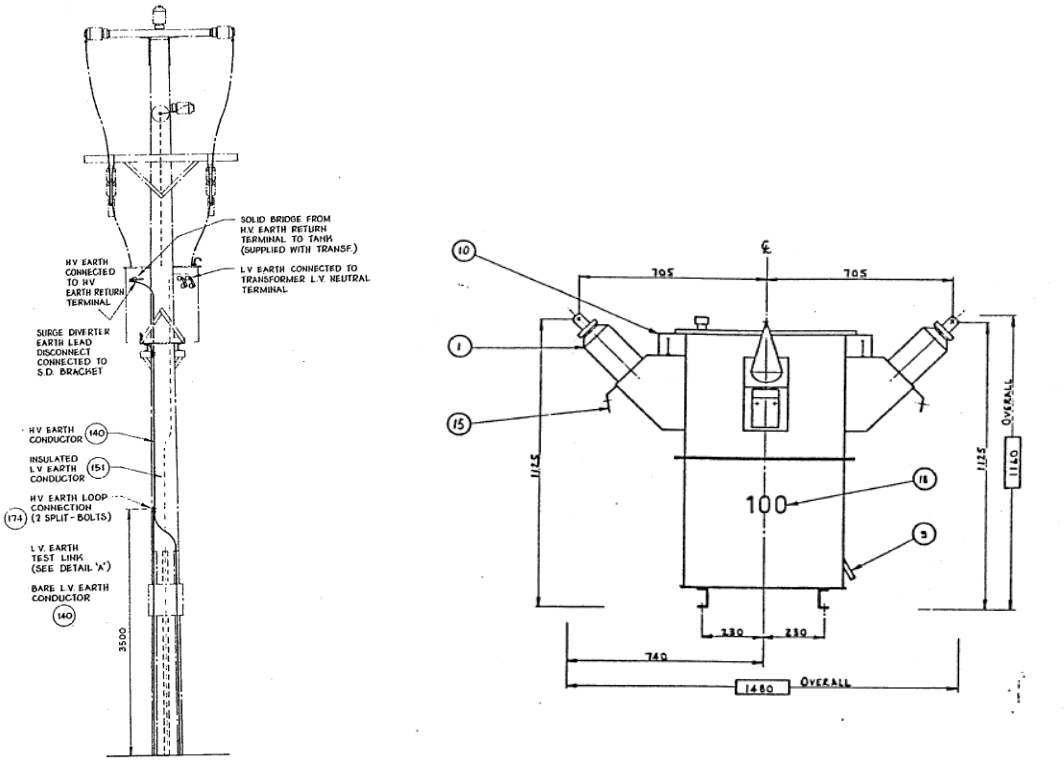

Fig 4.23: SWER Isolation Transformer and Overhead Connections.

As per [101], for a two-wire single-phase line with solid cylindrical conductors A and B with the same radius and same length separated by a distance D, the total inductance per unit length is given by (4.17). The Geometric Mean Radius (GMR) is given by (4.20) as per the coefficients (refer to Appendix D for the set of coefficients) given in [100] and AS 3851.

$$\mathrm{L}_{1-phase-system} = \frac{\mu_o}{\pi}\ln\left(\frac{D}{GMR}\right) = \frac{4\pi\times10^{-7}}{\pi}\ln\left(\frac{D}{GMR}\right) = 4\times10^{-7}\times\ln\left(\frac{D}{GMR}\right)\ \frac{\mathrm{H}}{\mathrm{m}} \quad (4.17)$$

$$\mathrm{GMR} = 0.8255 \times R_c = 0.8255 \times 0.00375 = 0.0031 \quad (4.18)$$

The total inductance per unit length of the ACSR/GZ 6/1/2.50 mm (Almond) conductor can then be calculated from Eq. (4.19) as 2.45 micro Henry per meter.

$$\mathrm{L}_{1-phase} = 4\times10^{-7}\times\ln\left(\frac{1.480}{0.0031}\right) : 40^{-7}\times\ln(454.2) = 2.447\ \times10^{-6}\ \mathrm{H/m} \quad (4.19)$$

According to [101], for a two-wire single-phase line with solid cylindrical conductors A and B with the same radius and same length separated by a distance D, the total capacitance

between conductors (CAB) per unit length is given by (4.20). The capacitance from either line to ground (CAG) is twice the capacitance between the lines as given in (4.21).

$$C_{AB} = \frac{\pi \times \varepsilon_o}{\ln\left(\frac{D}{r}\right)} = \frac{\pi \times \frac{10^{-9}}{36\times\pi}}{\ln\left(\frac{D}{r}\right)} = \frac{\frac{10^{-9}}{36}}{\ln\left(\frac{D}{r}\right)} \text{ F/m} \quad (4.20)$$

$$C_{AG} = 2 \times \frac{\frac{10^{-9}}{36}}{\ln\left(\frac{D}{r}\right)} \text{ F/m} \quad (4.21)$$

The actual capacitance values (CAB and CAG) for the two-wire ACSR/GZ 6/1/2.50 mm (Almond) single-phase system can be calculated as in (4.22-4.22).

$$C_{AB} = \frac{\frac{10^{-9}}{36}}{\ln\left(\frac{1.408}{0.00375}\right)} = \frac{\frac{10^{-9}}{36}}{\ln(375.5)} = 4.67 \times 10^{-12} \frac{\text{F}}{\text{m}} \quad (4.22)$$

$$C_{AG} = 2 \times C_{AB} = 9.34 \times 10^{-12} \text{ F/m} \quad (20) \quad (4.23)$$

The characteristic impedance of the two-wire ACSR/GZ 6/1/2.50 mm single-phase system can be calculated from (4.24) using the capacitance between conductors.

$$\text{Z}_\text{c} = \sqrt{\frac{\text{L}}{\text{C}}} = \sqrt{\frac{2.447 \times 10^{-6}}{4.67 \times 10^{-12}}} = \sqrt{0.524 \times 10^{+6}} = 723.87\ \Omega \quad (4.24)$$

The characteristic impedance of the two-wire ACSR/GZ 6/1/2.50 mm single-phase system can be calculated as in (4.25) using the capacitance from either line to ground.

$$\text{Z}_\text{c} = \sqrt{\frac{\text{L}}{\text{C}}} = \sqrt{\frac{2.447 \times 10^{-6}}{9.34 \times 10^{-12}}} = \sqrt{0.262 \times 10^{+6}} = 512\ \Omega \quad (4.25)$$

The characteristic impedance calculated in (4.25) using the capacitance between conductors will be used in this study as the ACSR/GZ 6/1/2.50 mm (Almond) conductor forms a two-wire single-phase line at the Active and Neutral terminals of the SWER ISO Transformer with the capacitance between the conductors.

4.11 Experimental Test set-up SWER conductor

To validate the performance of the conductor model, an experimental s-parameter test has been conducted on a 2-meter SCGZ 3/2.75 SWER segment. The schematic arrangements and experimental setup have been shown in Fig 4.24 (a) and (b).

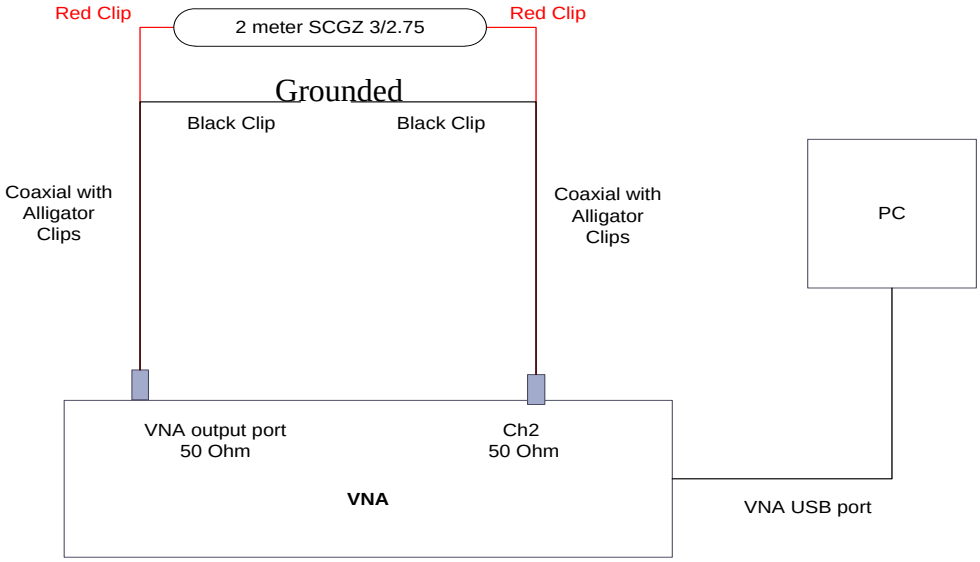

Fig 4.24 (a): Schematic arrangement of the SWER conductor's s-parameter extractions.

Experimental set-up of the S-parameter extraction of the SWER conductor:

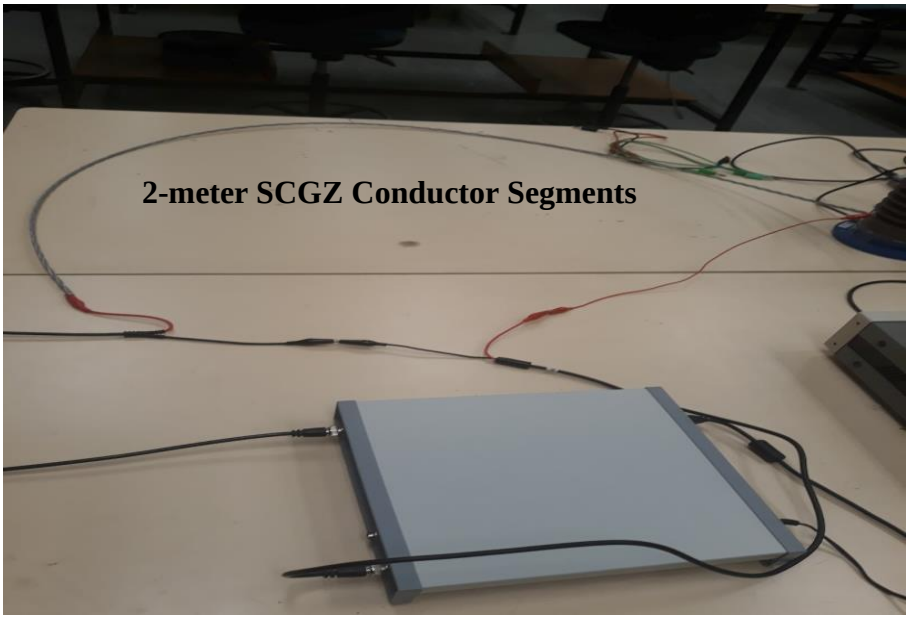

Fig 4.24 (b): Experimental set-up of the SWER conductor's s-parameter extractions

Comparative s-parameter graphs of the SWER conductor have been shown in Fig 4.25

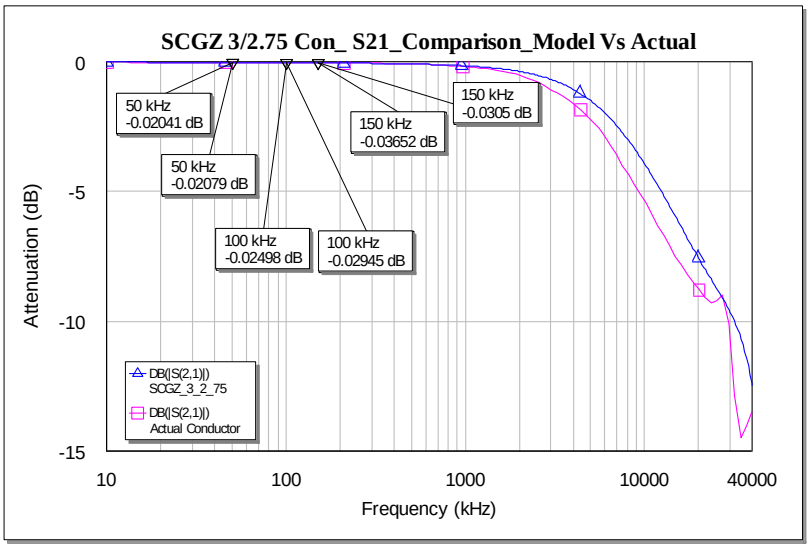

Fig 4.25: Comparative S-parameter graphs of the modeled and actual SWER conductor

The comparison shows a good agreement between the S_{21} parameters of experimental and modelled SWER conductor. Difference between the attenuation at the designated frequency band of 50 kHz to 150 kHz is marginal. For example, the attenuation of modeled SWER conductor at 100 kHz is -0.024 dB and the actual SWER conductor is -0.029 dB. In Table 15, attenuation differences have been summarized with respect to the frequency component.

Table 15: Variation in attenuation of an experimental and modelled SWER conductor

Frequency Band	S21 or Attenuation of Modelled SWER conductor (dB)	S21 or Attenuation of Actual SWER conductor (dB)	Difference of Attenuation (dB)
50	-0.020	-0.020	~0
100	-0.024	-0.029	0.005
150	-0.030	-0.036	0.006

Similar results have been obtained for the other SWER conductor's like SCGZ 3/2.06 and SCAC 3/2.75 as well. Hence, this comparative analysis intensifies the feasibility of the aforementioned SWER conductor's modelling method for PLC applications.

4.12 Conclusion

This chapter discussed SWER line modelling considering various aspects such as the conductor size, conductor type, soil properties, and pole height. Three different conductor types have been investigated. Generic mathematical equations related to the modelling of the SWER lines have been introduced. These include those associated with the calculation of the inductance, capacitance and impedance of the SWER conductor. As the fundamental modelling technique, one unit length of the SWER conductor has first been mathematically modelled as a building block, and then used to demonstrate the performance of the three different types of SWER conductors with different segment lengths. In Chapter 6, the developed SWER line segment model is used as a key building block to build a large 10.2 km end-to-end SWER distribution network. All major frequency dependent characteristics of the SWER conductors such as the skin depth, capacitance, inductance, impedance, and attenuation have been assessed and graphically demonstrated. Beyond this analysis, focus has also been given to derive mathematical correlation relationship for two specific cases including (i) the relation between the conductor length and attenuation at a constant frequency (ii) the relation between attenuation and frequency for constant conductor length. This chapter has also highlighted the construction and mathematical modelling of the 22 kV ACSR overhead conductor as an integral element of the SWER network. This approach of line modelling can be used to model other power networks for PLC applications.

Chapter 5

SWER Transformer High Frequency Modelling

5.1 Introduction

Application of powerline communication systems over remote electricity networks such as Single Wire Earth Return (SWER) networks has tremendous appeal. Many countries such as Australia, New Zealand, South Africa, Brazil, and India supply power to many of their remote communities through SWER power lines. Many remote areas are often out of mobile coverage. Power line based internet services could as well be a potential solution for access to broadband internet services. PLC systems could be potentially used for smart metering in these areas. Beyond the traditional communication or metering services, the PLC technique can also be applied to protect the electrical transmission or distribution lines as discussed in Chapter 1. Application of the PLC technology within electricity distribution networks requires an understanding of the electrical behaviour of the network elements at high frequencies including that of the SWER and isolation transformers. Without knowledge of the narrowband nature of the network elements, the application of PLC system over a power network could be very challenging and unpromising.

There are several network elements that are existence in power networks such as the conductors, feeders, boosters, insulators, surge arresters, and transformers. Among the elements, the transformer plays the most important role in PLC signal transmission. A key reason is the fact that PLC signals can potentially be injected through a SWER transformer. Transformer loading can also influence signal strengths on the network, and therefore must be investigated. Especially, the impact of the Low Voltage (LV) side loading on the reflections from the transformers is a key area of concern.

For this reason, characterisation of transformers at high frequencies gets special attention from researchers. For example, Kikkert *et al.* [34, 35, 74] presented various approaches to model SWER and Power Transformers at high frequencies. Abu-Siada *et al.* [102] also proposed a prominent High-Frequency (HF) transformer model that was used extensively in

transformer winding fault analysis by investigating the high-frequency response. Besides, Zhao *et al.*[103] worked on finding various winding deformation faults of the transformer using a frequency response approach. All the above applications require an accurate high-frequency transformer model. However, the existing transformer models cannot fully explain the behaviour of the transformer accurately. Jurisic *et. al.* [104] summarised some of the key challenges in developing a HF transformer model. To match the simulated models to the real-time transformer performance, most researchers [105-107] introduced various error adjustment equations in the modelling of transformers. This complicates the use of their techniques for all kinds of transformers.

One of the key parameters for modelling the HF response of a transformer is the measurement of the transformer winding impedances, which are not sufficient for accurate modelling because most of the transformers have similar impedance characteristics at high frequencies [108, 109]. Considering the aforementioned constraints of the previous HF transformer models, this work focuses on utilizing the experimental s-parameter data to model the HF transformer. Modelling of the SWER distribution and isolation transformers, using the touchstone s-parameter measurement method, has been descried in this chapter. Those models will be later incorporated as sub-circuits into the overall SWER system communication channel model described in the preceding chapter. This method of modelling has not previously been reported elsewhere and is a novel aspect of this work.

This chapter discusses the shortcomings and flaws of conventional high-frequency transformer modelling techniques with technical highlights. Novel hardware in the loop s-parameter based transformer modelling technique is then proposed as a simple and accurate means of modelling a transformer in HF applications. This approach was applied to the HF modelling of a 25-kVA SWER transformer and a 100-kVA isolation transformer with different loading conditions. This was achieved by recording the S11 and S21 data using a PC-Based Vector Network Analyser (Bode 100) for both the Medium Voltage (MV) to Low Voltage (LV) path and then for the LV to MV path. A system-level analysis of PLC propagation test over the transformer windings was also undertaken with various load conditions. In Chapter 6, the developed models will be integrated into a system-level overall network model and results compared with those measured on the real network test. The developed SWER transformer models will be used in Section 6 for the fine-detailed segment-

by-segment modelling of an exemplary SWER overhead network including spurs with short segment line lengths as short as 22 m.

5.2 Contemporary Research on High-Frequency Transformer

All previous works related to high frequency transformer modelling are based on high-frequency winding impedance measurements and software based evaluation. None of them considered the s-parameter based modelling of transformers acquired by Touchstone file measurements. The conventional modelling approaches can be classified into three different types such as the black-box, white-box, and gray-box models.

Black-box models are linear time-invariant multiple network models. With this kind of modelling technique, the network impedances are excited with individual voltage sources at different terminals, which produces a current response for each terminal. Relating the voltage and current of all the ports through an admittance matrix, the value of the transformer winding is calculated. Eq. (5.1) was given in [109, 110] to express the voltage current relationship of an N-port high-frequency transformer model.

$$\begin{bmatrix} I_1 \\ \vdots \\ I_N \end{bmatrix} = \begin{bmatrix} Y_{11} & \dots & Y_{1N} \\ \vdots & \dots & \vdots \\ Y_{N1} & \cdots & Y_{NN} \end{bmatrix} \begin{bmatrix} V_1 \\ \vdots \\ V_N \end{bmatrix} \tag{5.1}$$

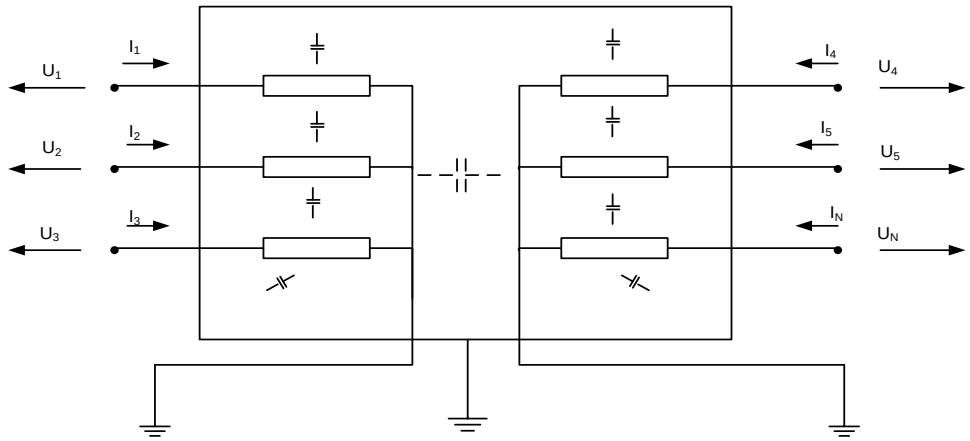

Fig 5.1: Circuit diagram of the black-box model of transformer [111]

Eq. (5.1) relates an N-terminal transformer's voltage-current relation with the admittance matrix, Y. The basic of the black-box model is the measurement of the admittance matrix, which can be calculated, using the voltage and current relation of a transformer. The black box model does not care about the lumped element of the transformer's winding. The black-box impedance model for the transformer is shown as Fig 5.1.

The white box modelling is associated with the geometric configuration of the transformer. This technique considers the entire active parts of the transformer such as the transformer core, windings, stray electric field, and magnetic field. The HF parasitic and ground capacitances are also considered in this modelling procedure. Abu-Siada *et al.*[102] developed a well-established transformer model based on the white-box modelling technique, as shown in Fig 5.2.

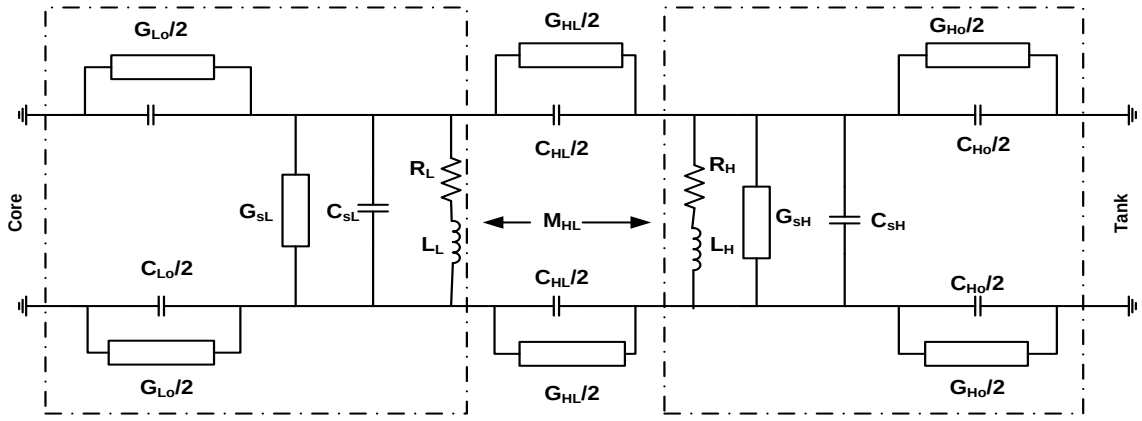

Fig 5.2: Circuit diagram of the white-box high-frequency transformer model [102]

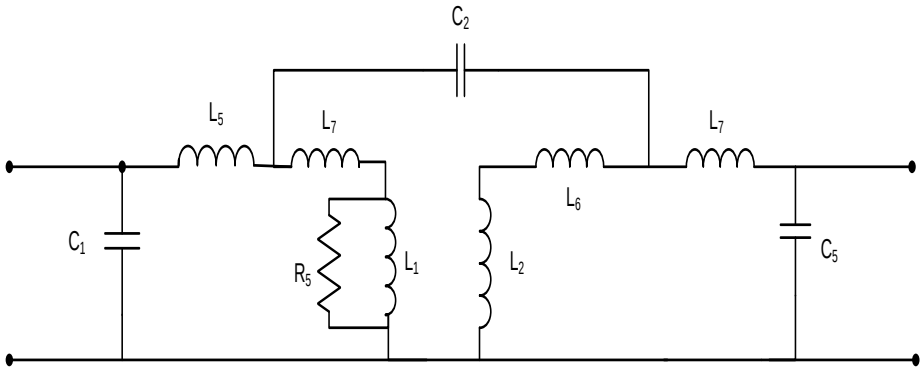

Fig 5.3: A simple Gray-box high-frequency transformer model [112]

Gray-box modelling refers to the simplified lumped element-based modelling. This technique can represent the transformer characteristics at low frequencies. At high frequencies, the winding structure and inter-winding coupling create a parasitic capacitance in the transformer and the gray-box model cannot represent such parasitic capacitance responses. However, gray-box modelling can predict approximately the accurate admittance matrix applicable in few applications such as, power transformer winding modelling, transformer transient studies [112, 113] etc. Fig 5.3 shows a simple single-phase high-frequency gray-box transformer model.

Due to these shortcomings, a number of modern researchers are following the gray box model, but they incorporate their own contributions to modify the model accurately for extended applications. For example, Kikkert [35] has developed a pioneering model of a SWER transformer, which is given below in Fig 5.4. In the model, to represent the magnetic coupling, internal resonance and matching of the winding impedances with the measured value, Kikkert introduced the following components: RL1, RL2, R12, L1, L2, L3, C1, C2 and C12 with the transformer internal circuit configurations.

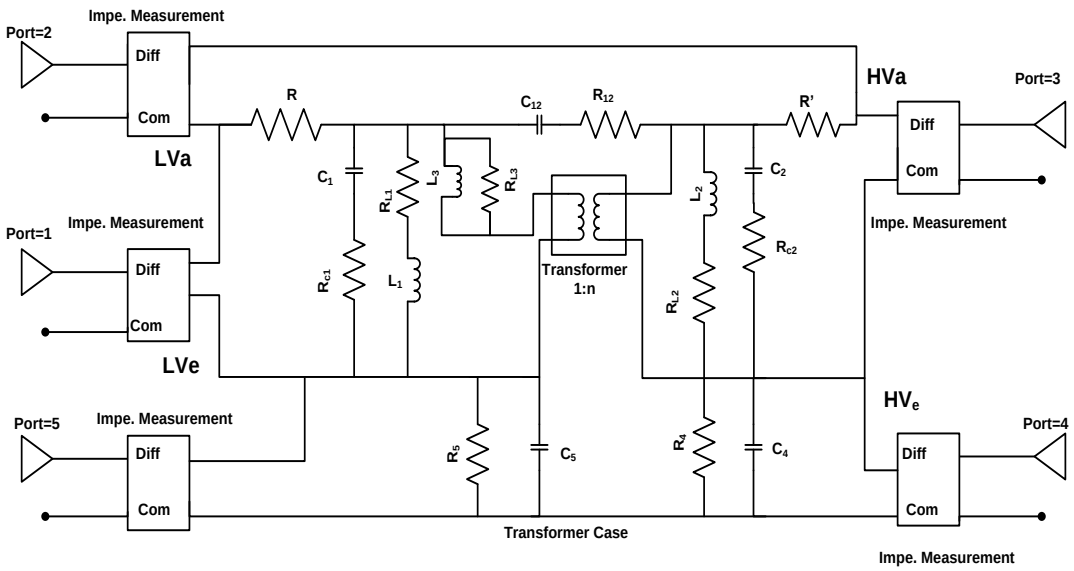

Fig. 5.4: Modified gray-box transformer or Kikkert model [35]

Likewise the Kikkert model, most other models [110, 114-116] also require a large number of unknown R, L, C components to represent various resistive, magnetic and

parasitic components of transformer windings at high frequencies. The values used for those components are experimentally measured and optimized with various mathematical procedures using different software tools such as the Microwave Office, ATP, and MATLAB.

The well-known experimental set up for the impedance measurement has been shown in Fig 5.5. The measurement procedure is based on the basic voltage divider principle. Signals in the PLC frequency range is generated from the signal generator. An oscilloscope is used to display the input and output voltage waveforms. By analysing the recorded input and output voltage waveforms and adjusting the value of the precision resistor, the unknown impedance can be predicted. After comparing the measured and modelled impedance values, the error between these need to be optimized, which is analytically computed.

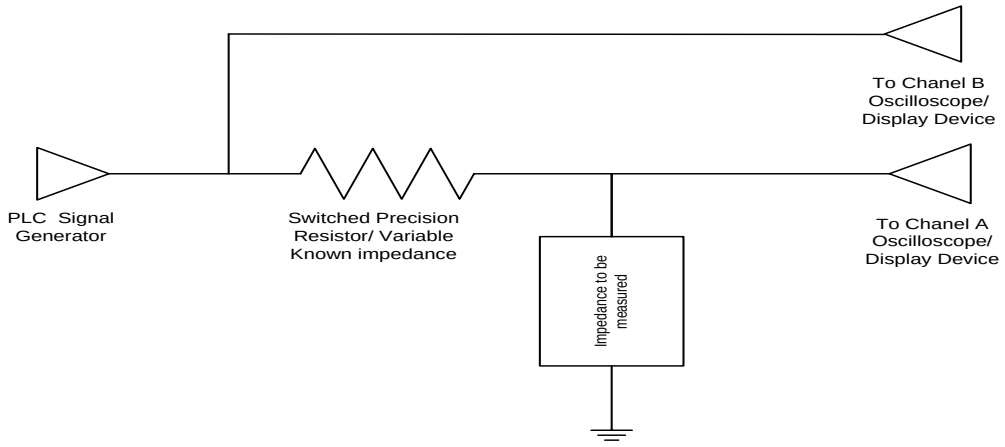

Fig 5.5: Experimental set-up for transformer port impedance measurements [35]

Kikkert [35, 74] developed some equations for the transformer model presented in Fig. 5.4. The equations associated with the optimization of magnitude and phase of the impedance of Port-1 are given below. Similar to Eqs. (5.2) and (5.3), the transformer model of Fig. 5.4 requires error optimization equations for each pair of the transformer ports. The simulated impedance versus frequency characteristic of the transformer model is shown in Fig 5.6 and 5.7.

$$\text{(Magnitude) } EP_1Z_{11}\,M = \frac{M_eP_1Z_{11}M - M_OP_1Z_{11}M}{M_eP_1Z_{11}M - M_OP_1Z_{11}M + 30} \qquad (5.2)$$

$$(\text{Phase})\ EP_1Z_{11}\ P = M_eP_1Z_{11}P - M_OP_1Z_{11}P \qquad (5.3)$$

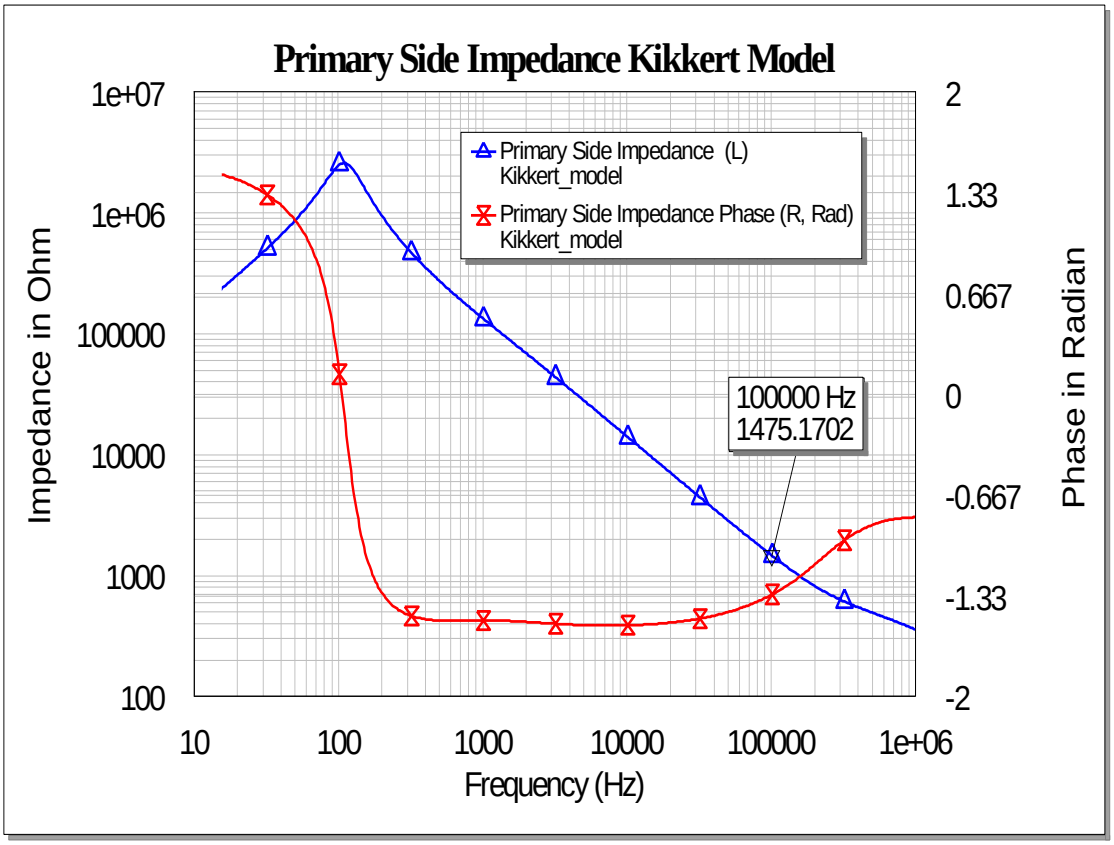

Fig 5.6: Primary side impedance of the SWER transformer (Kikkert's Model [35])

Other researchers determined similar impedance characteristics for high frequency transformer models [65, 117, 118]. All these models require complex mathematical models and sophisticated repetitive experimental procedures for the justification. The shortcomings of these contemporary models can be summarized as follows:

- To justify transformer model, many R, L, C components have been used, but there is no definite procedure to identify these components to integrate them. This makes the technique confusing to be justified as a global or unique model.
- To measure impedance values, this method requires a sophisticated experimental setup and repetitive measurements to be carried out for each of the port combinations and frequency components.

- The need for complex mathematical equations for each port to minimize the error between modelled and measured values.
- Software based optimization of many R, L and C components is required to finalize the model.

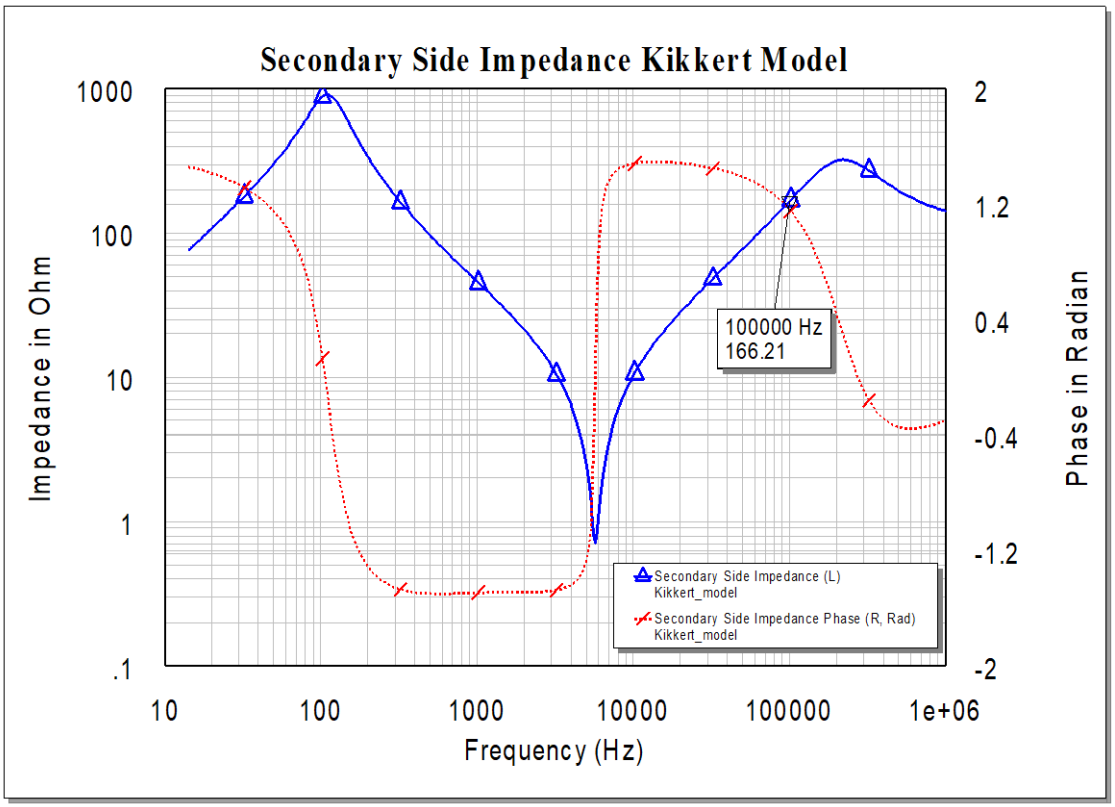

Fig 5.7: Secondary side impedance of the SWER transformer (Kikkert's Model [35])

5.3 Details of SWER Distribution and Isolations Transformers

To demonstrate the performance of the method, real-time ETEL SWER isolation and distribution transformers have been used in this study. These transformers are currently in use in a rural Victorian SWER network. However, internal port combination configuration and circuitry of transformer could be different which could be found from company specified data sheet. Fig 5.8 shows the theoretical network configuration of SWER isolation and distribution transformer, studied in this work. The specifications of the transformers are given in Table 16.

Conceptual configuration of SWER isolation and SWER distribution transformer:

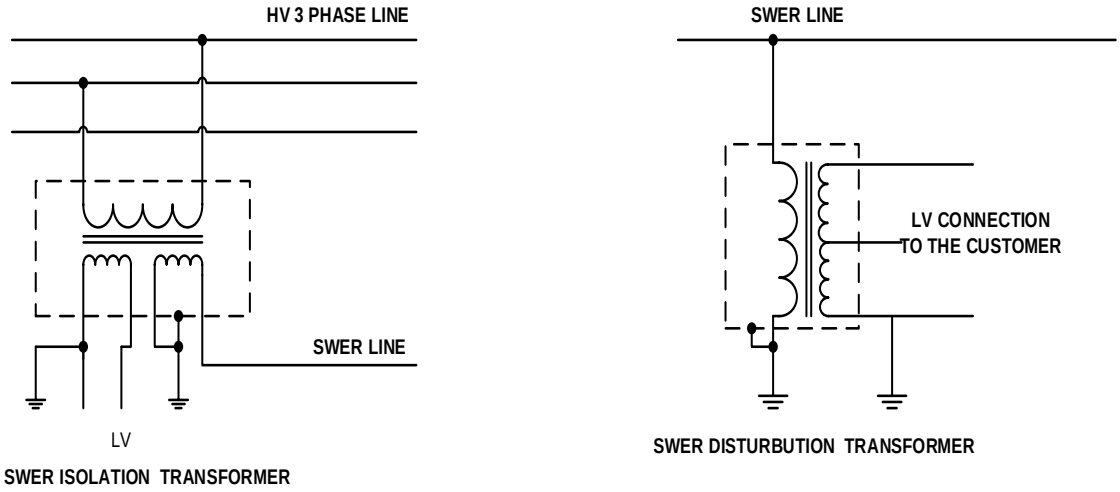

Fig 5.8 SWER isolation/distribution transformers network connection configuration

Table 16 : Transformer specifications

Item	**SWER Distribution Transformer**	**SWER Isolation Transformer**
Ratings	10 KVA, 20 kVA, 25 kVA	100 kVA
Voltage	12700 V/480 V or 240 V	22000 V/12700 V/480 V/240 V
Frequency	50 Hz	50 Hz
Tapping	Only one taping might be given	Tapings provided according to the required output voltage
Cooling and tank type	Oil immersed free breathing outdoor types	Oil immersed free breathing outdoor types
Bushing	One HV bushing for 12.7 kV and two LV bushings for 480 V and 240 V the voltage level.	Two HV bushing for 22 kV and two LV bushings for 480 V and 240 V the voltage level.
Maximum load current	8 A	8 A

5.4 ETEL SWER Impedance Measurements

In the previous section, a conventional high frequency winding impedance measurement technique has been discussed. In this subsection, a simplified VNA-based impedance measurement procedure will be explained and used for the impedance measurements of a SWER transformer. The method will be demonstrated on a 25 kVA ETEL SWER distribution transformer and the impedance of the primary and secondary windings will be measured in the 10 kHz to 200 kHz frequency range. Fig 5.9 (a) shows the schematic view of the transformer's port configuration and 5.9 (b) demonstrates the detailed VNA schematic configuration (for impedance measurements) with port identification.

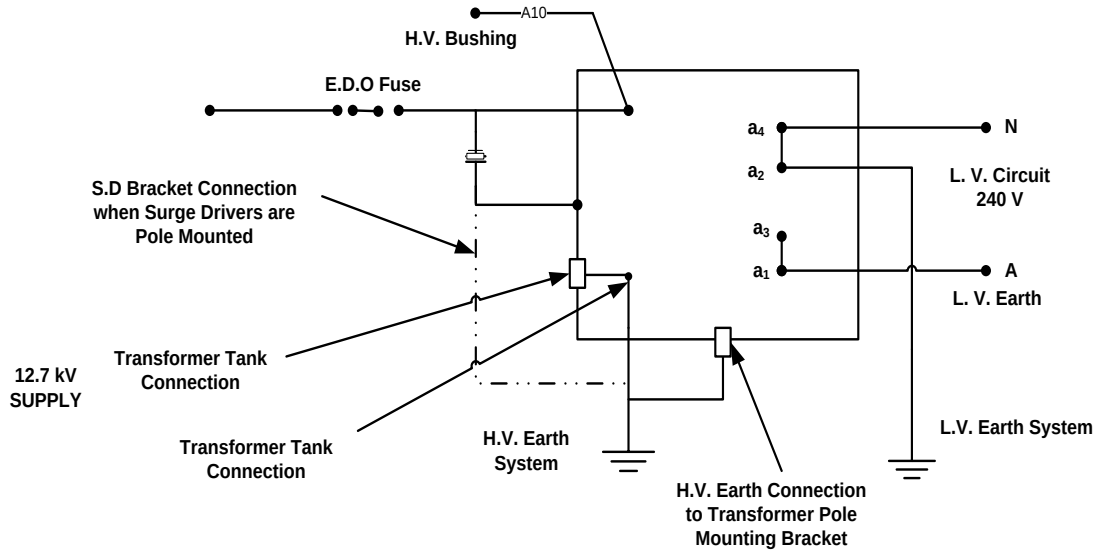

Fig 5.9(a): ETEL 25 kVA SWER distribution transformer port combination

After identifying the primary and secondary windings from the datasheet specified connection diagram of Fig 5.9 (a), the terminals a4 to a1 were determined to be associated with the low voltage or secondary side of the transformer. A10 and HV earth are transformer windings on the high voltage or primary side of the transformer. To measure the impedance of the SWER transformer windings, the Bode 100 Vector Network Analyser (VNA) has been used. A few connectors have been developed by OMICRON Electronics to measure port impedance of the device under test using Bode-100. These include the one port reflection, impedance adopter 3-port technique, shunt thru, shunt thru with series resistance, voltage-current gain etc. Among the above methods, the 1-port based method suits best for

impedance ranges from 0.5 Ω to 10 kΩ. From the literature, it was determined that the impedance of a transformer winding would normally be in this range, and therefore the 1-port method has been adopted in this thesis. The manufacturer provided physical configuration and schematic arrangement to measure the winding impedance of the ETEL 25 kVA SWER is shown in Fig 5.9 (b) and 5.9 (c), where the output port of the VNA has been connected with the HV bushing terminals or with the positive terminal of the primary winding and the negative terminal grounded through HV earth. This procedure has been repeated to measure the impedance of the secondary winding as well across the Active (A) and Neutral (N) terminals.

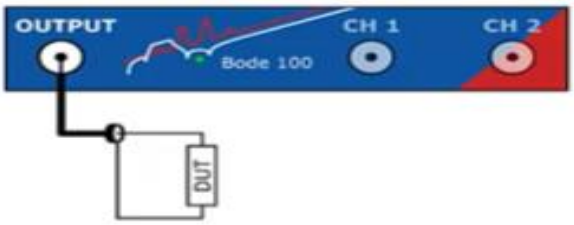

Fig 5.9 (b): Bode-100 VNA based 1-port impedance measurement schematic

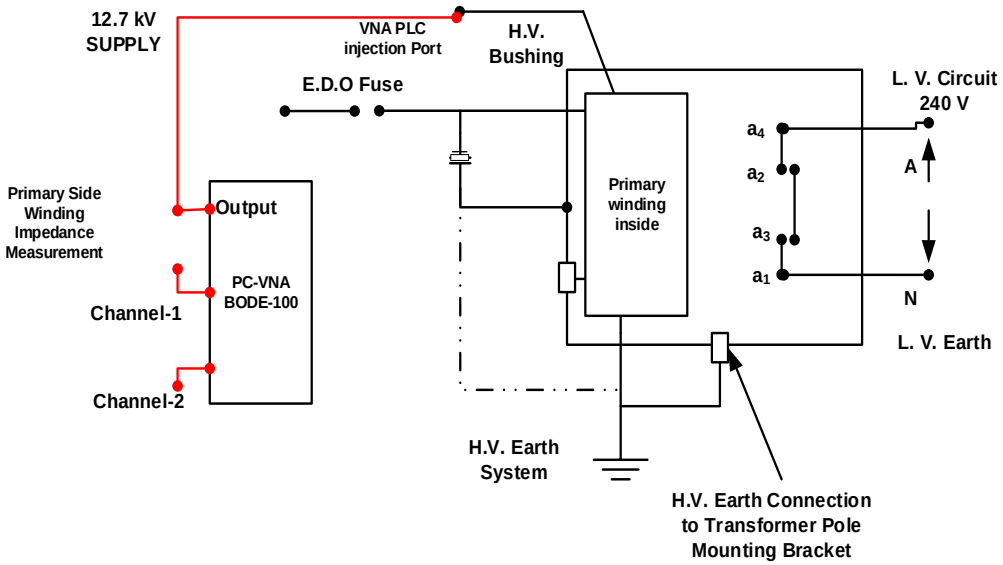

Fig 5.9 (c): Impedance Measurement Procedure of the SWER Distribution Transformer

In this impedance measurement procedure, it was determined that for the ETEL 25 kVA SWER distribution transformer, the high voltage winding impedance is around ~1.5 kΩ at

the 100 kHz centre frequency and the impedance value of the low voltage side winding is around 56.7 Ω at 100 kHz. It can be seen that the HV winding impedance decreases with frequency, but the LV winding impedance has a fluctuating nature. LV winding impedance is at its highest value (around 3 kΩ) at 500 kHz.

An interesting observation has been noticed on the impact of loading conditions of the opposite winding of the transformer. It has been determined impact of loading of the opposite winding is minimal on the impedance of each respective side. The experimental winding impedance measurement under the nominal conditions for both the HV and LV windings (using the Microwave Office platform) is shown in Fig. 5.10.

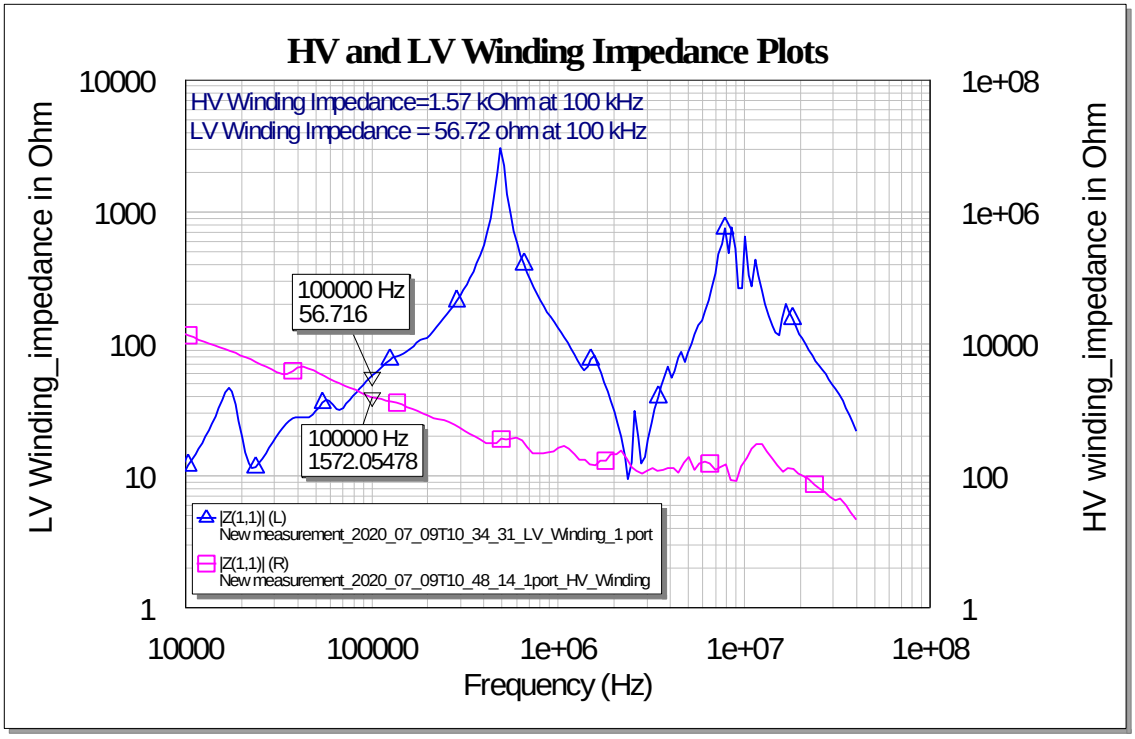

Fig 5.10: Measured impedance of the ETEL 25 kVA SWER distribution transformer

As a final conclusive statement, it must be noted that the overall comparative studies on the previous researches [105, 106, 109] on high frequency impedance modelling of transformers also shows similar trends. But those methods were a lot more complicated in terms of mathematical evaluation and experimental validation. Therefore, this method can be applicable and handy for any future high frequency transformer application research.

5.5 Proposed S-Parameter Based Transformer Models

Due to complexity and challenging nature of previous models, this thesis proposes a new method to model a transformer based on a methodology that involved taking Touchstone file (containing s-parameter measurements) of the same under specific load conditions, which can be used directly in PLC based complex network modelling. One of the benefits is avoidance of the use of complex lumped components. This approach also does not require complex mathematical equations and there is no need to measure or optimise impedance of each port separately, which significantly reduces the effort required towards transformer and network modelling. Accuracy is however the most important outcome of modelling a SWER transformer using s-parameter (Touchstone-file) measurements. This modelling and its integration into an end-to-end network model will be further validated in Chapter 6. The key steps in undertaking measurements for an accurate model are given below:

- Identify the voltage levels and loading conditions at the primary and secondary of the transformer;
- Impedance of the SWER line is considered as 270 Ω for transformer related analysis, though 260-Ω was closest to the estimated SWER line impedance, due to hardware design purpose (hints: 50 Ω **(fixed port impedance)** + **220 Ω (widely available)**) total 270 Ω is selected.
- Measure the s-parameter data from the transformer at three different primary and secondary loading conditions using a Vector Network Analyzer (VNA)
- Undertake the s-parameter measurements for the Medium Voltage (MV) to Low Voltage (LV) path and for the Low Voltage (LV) to Medium Voltage (MV) path.
- Use the measured Touchstone-files as sub-blocks in the Microwave Office platform for fine segment-by-segment modelling.

In the following sub-sections, the proposed method has been used to model SWER transformer and isolation transformer. Fig 5.11 shows the schematic arrangements of various load specified PLC injection models to acquire the s-parameter data. Specifically, Fig 5.11(a) -5.11 (c) represents the schematic for 12.7 kV to 240 V injection. On the other hand, Fig 5.11(d) is showing the 240 V to 12.7 kV injection pattern.

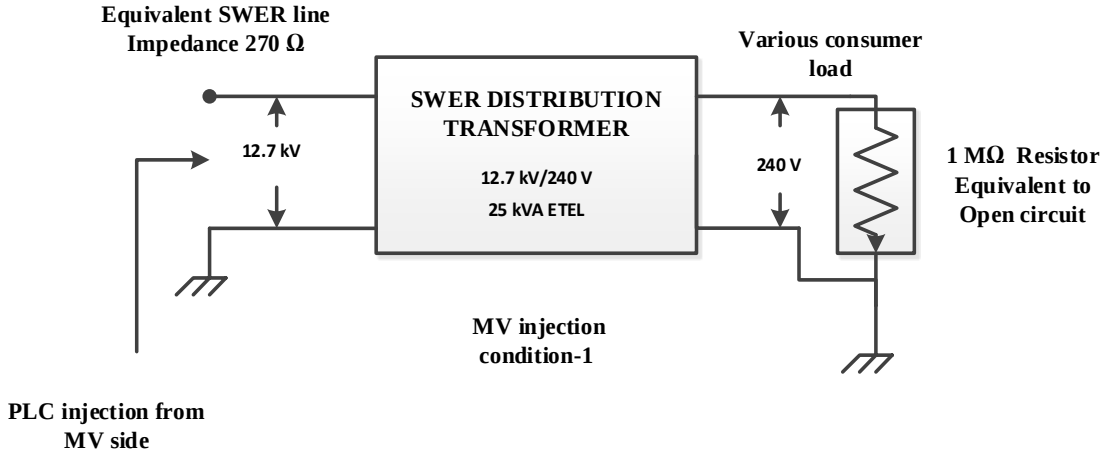

Fig 5.11(a): Schematic arrangement of the SWER transformer s-parameter extraction model (MV to LV injection; 1 MΩ load on LV side)

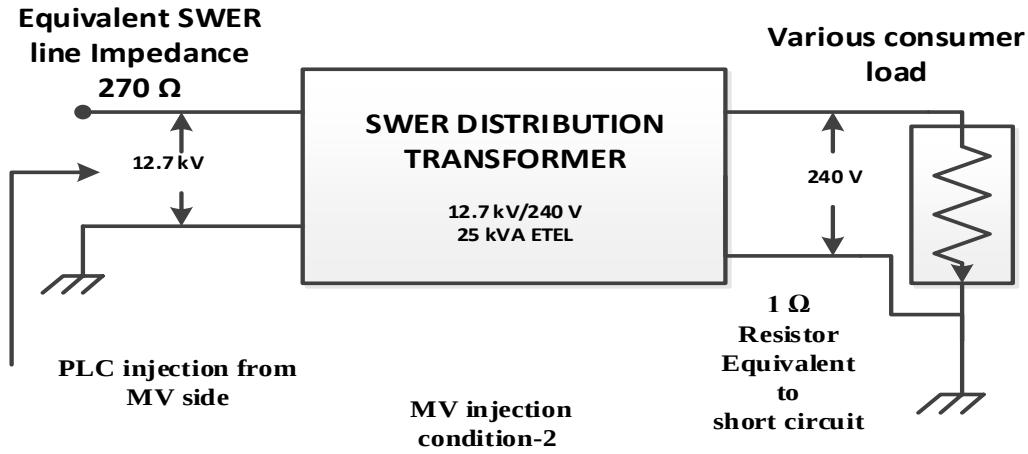

Fig 5.11(b): Schematic arrangement of the SWER transformer s-parameter extraction model (MV to LV injection; 1 Ω load on the LV side)

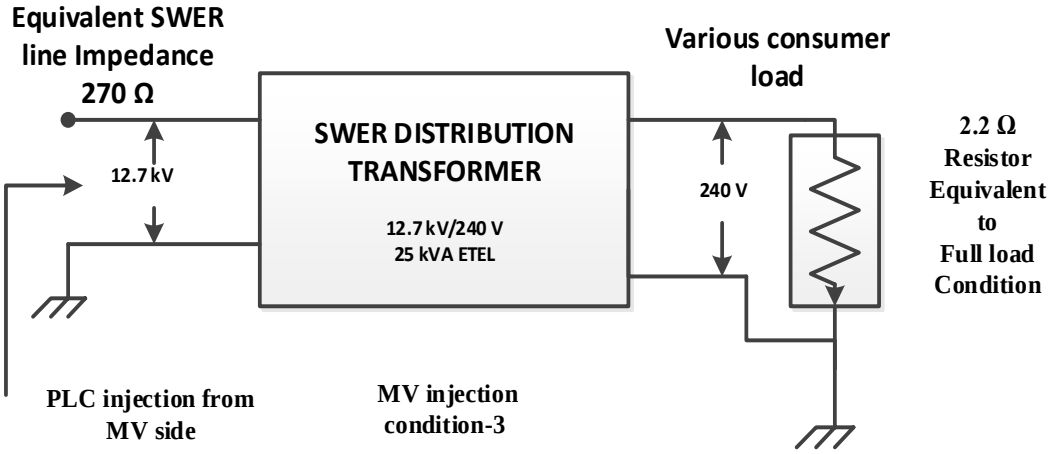

Fig 5.11(c): Schematic arrangement of the SWER transformer s-parameter extraction model (MV to LV injection; 2.2 Ω load on the LV side)

The only LV to MV injection loading condition 50 Ω to 270 Ω:

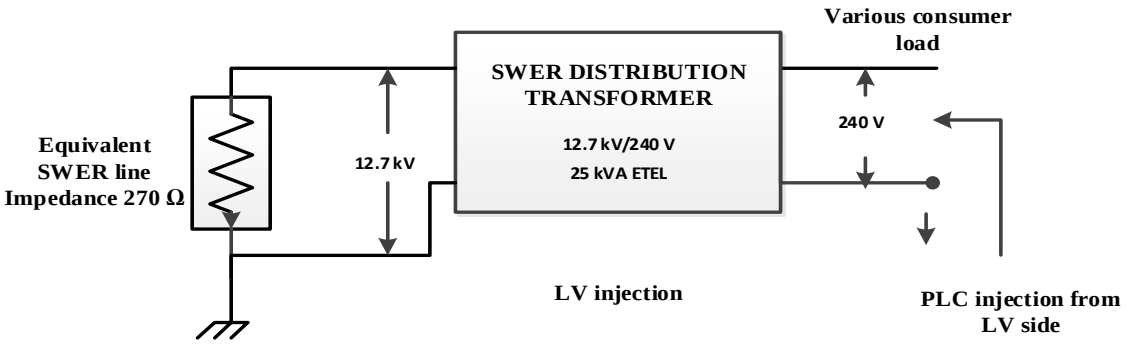

Fig 5.11(d): Schematic arrangement of the SWER transformer S-parameter extraction model (LV injection 50 Ω / MV side 270 Ω load)

Mathematical explanation of the transformer loading conditions can be explained with the typical apparent power equation, which is given in Eqs. (5.2).

$$\text{Transformer rating in kVA, } S = I^2 \times R \qquad (5.2)$$

Using Eqs (5.2) for an open circuit equivalent or 1 MΩ load connected to 25 kVA SWER transformer, load current is found as follows:

$I_{OC} = \sqrt{\frac{S}{R}} = \sqrt{\frac{25\times10^3}{10^6}} = 0.158$ (Amps), which is as low as an open circuit condition.

Similarly, for a short circuit equivalent or when 1 Ω ohm connected to the load side of transformer, the current is found as follows:

$I_{SC} = \sqrt{\frac{S}{R}} = \sqrt{\frac{25\times10^3}{1}} = 158.11$ Amps (high current as to be considered as the short circuit current scenario)

Finally, to represent the full load conditions or a 2.2 Ω load connected to secondary, the secondary winding load current of the transformer is found as follows:

$I_{FL} = \sqrt{\frac{S}{R}} = \sqrt{\frac{25\times10^3}{2.2}} = I_{FL} = 104.2$ Amps, which is very close to the rated full load current of (~106 Amps)

In the following sections, considering the above three loading conditions, s-parameter analysis of primary to secondary (MV to LV) path is undertaken and presented.

5.6.1 SWER Transformer Primary to Secondary Modelling

Fig. 5.12 and 5.13 show the schematic and experimental set-up in acquiring the touchstone file (s-parameter file) for the 25 kVA ETEL SWER TR's MV to LV path. The VNA output port was connected to the MV primary port of the SWER TR through a 270-Ω resistor. To enable 270- Ω impedance, a 220-Ω resistor was connected in series with the 50-Ω output impedance of Channel 1 of the VNA. Three distinct transformers models were developed to take into consideration the different secondary loading conditions. These include the 270-Ω MV_a to 1-Ω LV_a model, 270-Ω MVa to 2.2-Ω LVa and the 270-Ω MV_a to 1-MΩ LV_a models.

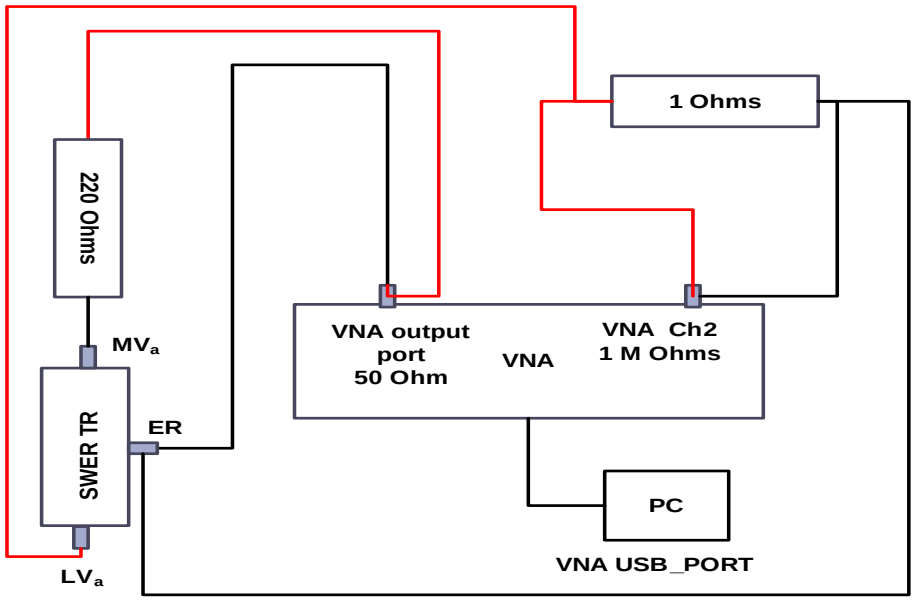

Fig 5.12 Schematic arrangement for Touchstone file acquisition (MV to LV) injection

The 1-Ω LV_a model considers a short circuit scenario on the secondary winding. The 2.2-Ω LVa model shows the full load condition, and finally the 1-MΩ LV_a model is representative of an open circuit on the secondary. In measuring the touchstone file (s-parameter file) for the 270 Ω MV_a to 1-Ω LV_a model, Channel 2 had a 1-Ω resistor in parallel with the 1M-Ω input impedance of Channel 2 giving an equivalent impedance of 1-Ω. Similarly, in measuring the touchstone file for the 270 Ω MV_a to 2.2-Ω LV_a model, Channel

2 had a 2.2-Ω resistor in parallel with the 1M-Ω input impedance of Channel 2 giving an equivalent impedance of 2.2-Ω. In developing the open-circuit model, the secondary port was connected in series to the Channel 2 activating the 1-MΩ port impedance. Photos of detail hardware setup of the SWER TR S21/S11-test also attached on Appendix G.

The purpose of undertaking of this MV to LV path modelling was to enable this primary to secondary path to be modelled to assess the reflection of PLC signals from the primary of the SWER transformers and the impact of these reflections on the received PLC signal. Consideration of different secondary loading enabled the research to measure reflections as a function of the secondary load situation. The MV to LV path model also enables an assessment of the PLC signal strength at the customer premises.

Fig 5.13: Experimental arrangement for the Touchstone file acquisition

5.6.2 SWER Transformer Secondary to Primary Modelling

This subsection explains the test setup configuration for the s-parameter acquisition procedure of the SWER transformer LV to MV PLC injection path. Fig 5.14 shows the schematic configuration of the experimental procedure to acquire the s-parameter response of the transformers LV to MV path using a PC-based Vector Network Analyser.

With respect to the previous configuration of the MV to LV path, the difference in this arrangement is that the PLC signal has been injected in the LV side winding and response is

being recorded at the MV side winding. The LV to MV path model of the SWER transformer allows us to compute how much signal strength would be attenuated in the injection of the PLC signal.

Therefore, the VNA output port with the 50-ohm termination has been connected with the LV side directly to make an equivalent PLC source input impedance. The HV side has been connected to channel 2 having the 1 MΩ termination in parallel with a 270-ohm resistance, which together represent an equivalent impedance of 270-ohm equivalent to the SWER line impedance. After collecting the s-parameter response of the transformer's LV to MV and MV to LV paths for various loading conditions, these have been integrated as sub-blocks in the larger network modelling given in Chapter 6.

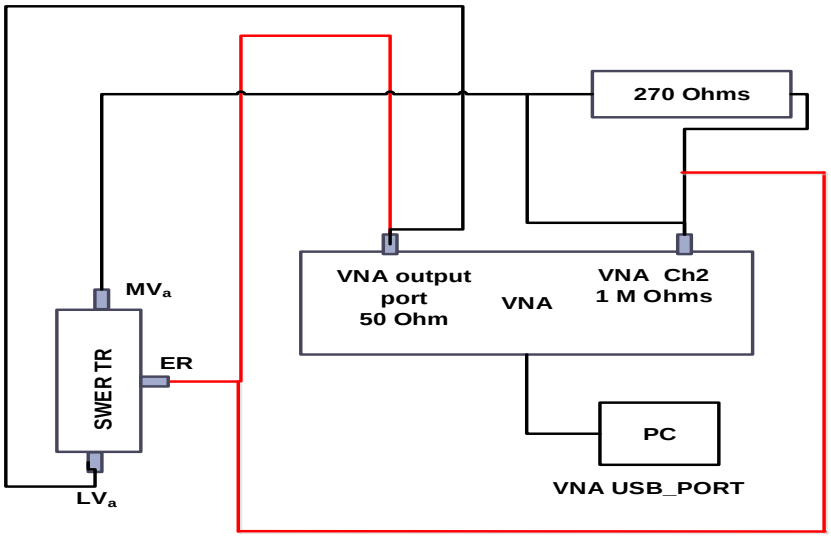

Fig 5.14: Set-up for the SWER TR s-parameter acquisition (LV to MV injection)

5.7 Representation of Transformer Models in Microwave Office

5.7.1 270 Ω MVa – 1 Ω LVa Model (MV to LV)

Fig 5.15 shows the configuration model of the 270-Ω MV_a to 1-Ω LV_a model, where two impedance matching transformers (X_1 and X_2) have been used for the port impedance adjustment in Microwave Office (MWO) modelling software. This is requires as the touchstone sub-block in the MWO platform only functions accurately if the touchstone-block is terminated by 50-Ω impedance on both sides. Therefore, to change the port

impedance from 50 Ω to 270 Ω and to 1 Ω, there was a need to use adjustment transformers with turns-ratio of 0.4303 (X_1) for Port 1 and 7.07106 (X_2) for Port 2. This is needed as the 270-Ω MVa - 1-Ω LVa TR Model is to be used in the fine-detailed segment modelling of a large SWER network where the SWER transformer is connected to the SWER conductor with a characteristic impedance of 270 Ohms and a 240-volts customer loading of 1 Ω.

The touchstone files were measured and recorded with these loading conditions wired into the measurement set-up and hence these uses of these adjustment transformers is only representational allowing the port connections to be accurately displayed while not impacting the frequency response of the Touchstone modelling block.

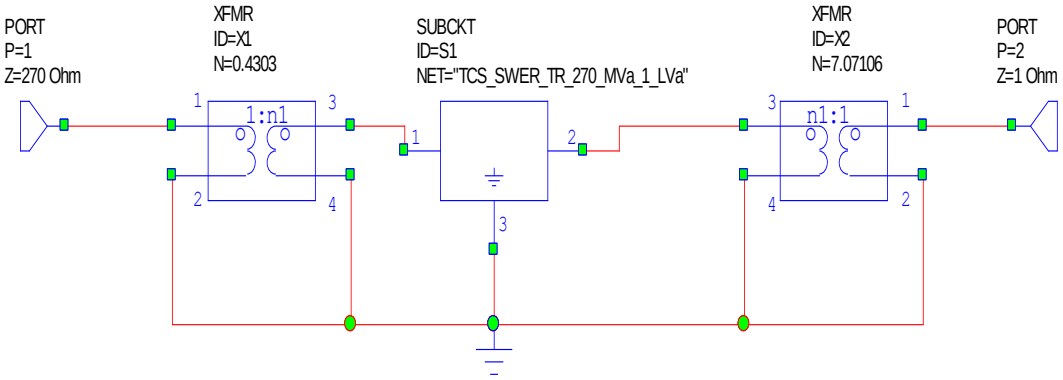

Fig 5.15: 270-Ω MVa - 1-Ω LVa TR Model

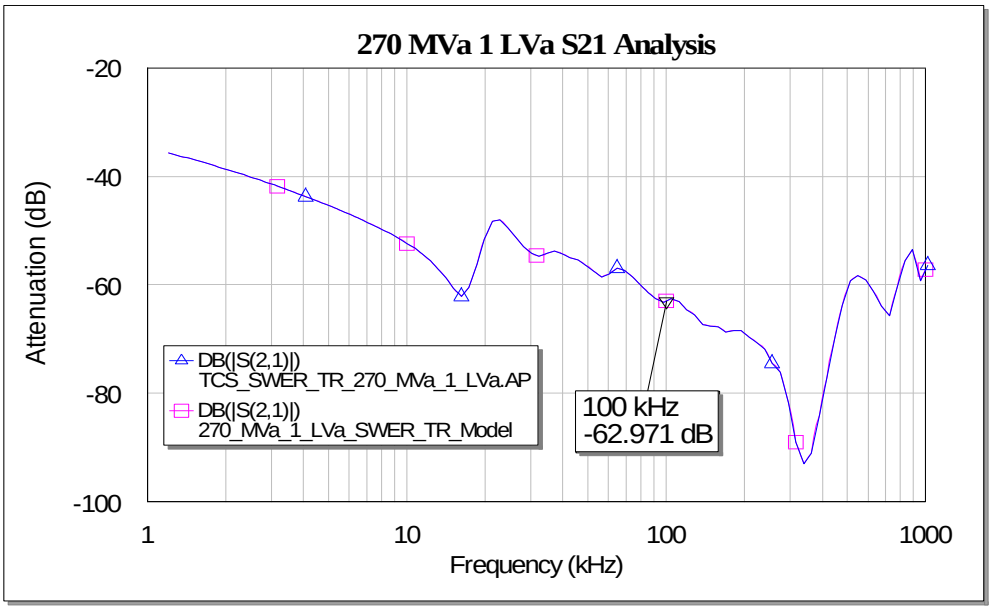

Fig 5.16: 270-Ω MVa/1-Ω LVa Short Circuit Equivalent TR Model S21 Characteristic.

Fig 5.16 shows that the S21 characteristic (or insertion loss) for the SWER transformer's HV to LV path is high at around -63 dB (Transmitted Power Gain = 5×10^{-7} W/W). Hence, almost none of the signal power will be coupled from the primary to secondary and signals injected from the primary winding will not penetrate to the secondary winding. On the other hand, fig 5.17, the S11 characteristics for the transformer HV winding shows very high reflection. At 100 kHz, the reflection is -0.1282 dB (Reflected Power Gain = 0.971 W/W), which implies that around 97% of the injected signal will be reflected.

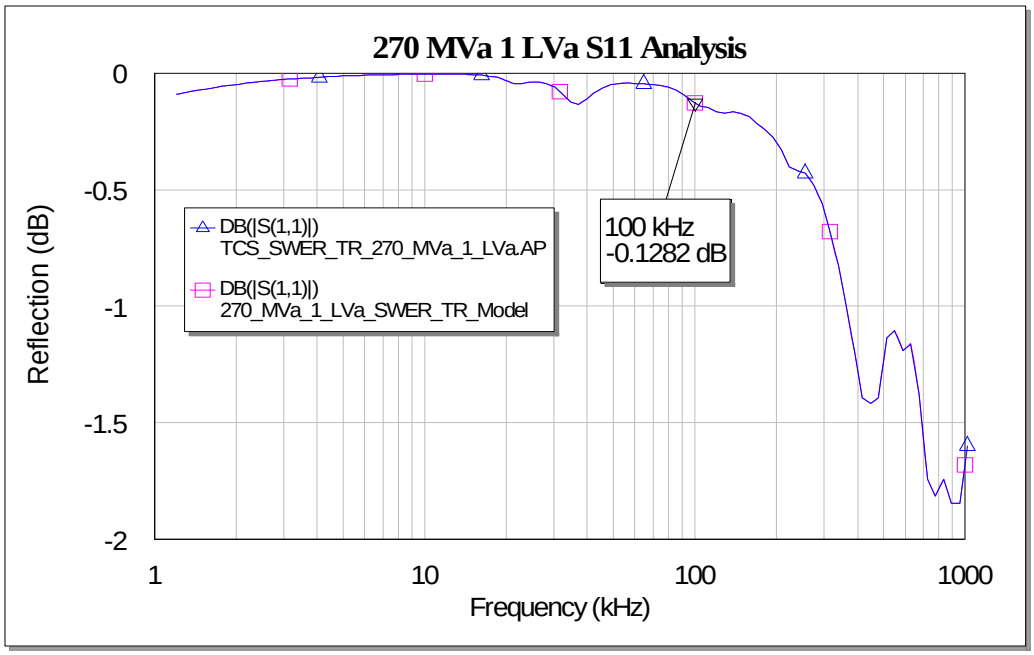

Fig 5.17: 270-Ω MVa - 1-Ω LVa short circuit TR Model S11 Characteristic.

5.7.2 270 Ω MVa – 1 MΩ LVa Open Circuit Model (MV to LV)

Fig 5.18 shows the 270 Ω MVa – 1 MΩ LVa TR model mimicking an open circuit on the secondary. In this combination, one adjustment transformer (X1) is required with a ratio of N=0.4303 for Port 1. The adjustment transformer changes the 50-Ω TCS block port impedance to 270 Ω as required to match the SWER line impedance. The secondary has 1 M-Ω impedance termination in measurement and the allocated 50-Ω port impedance does not alter the response and enables the sub-block to operate correctly as per measurements.

With this open circuited loading, the secondary signal voltage would be higher as there is now decreased attenuation from the HV to LV path as shown by Fig 5.19. The insertion loss is now -36.64 dB (Transmitted Power Gain = 0.000217 W/W) for the open circuited condition, while it was -63 dB (Transmitted Power Gain = 5×10^{-7} W/W) for the prior case.

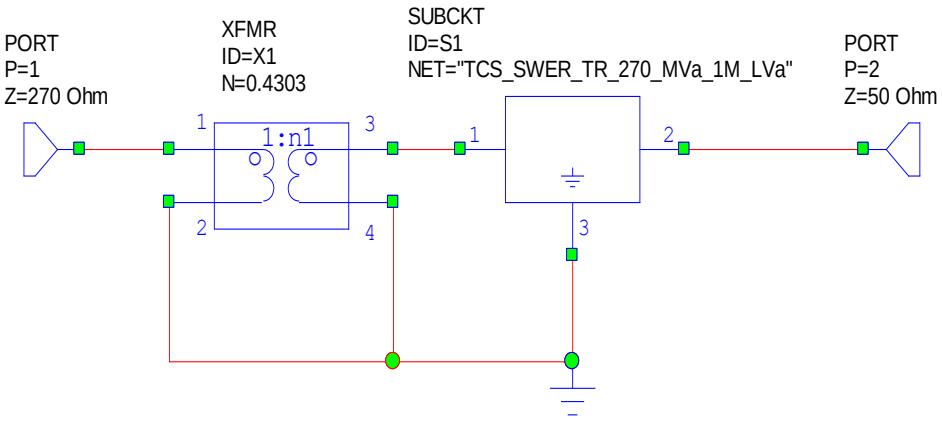

Fig 5.18: 270-Ω MVa - 1-MΩ LVa TR Model.

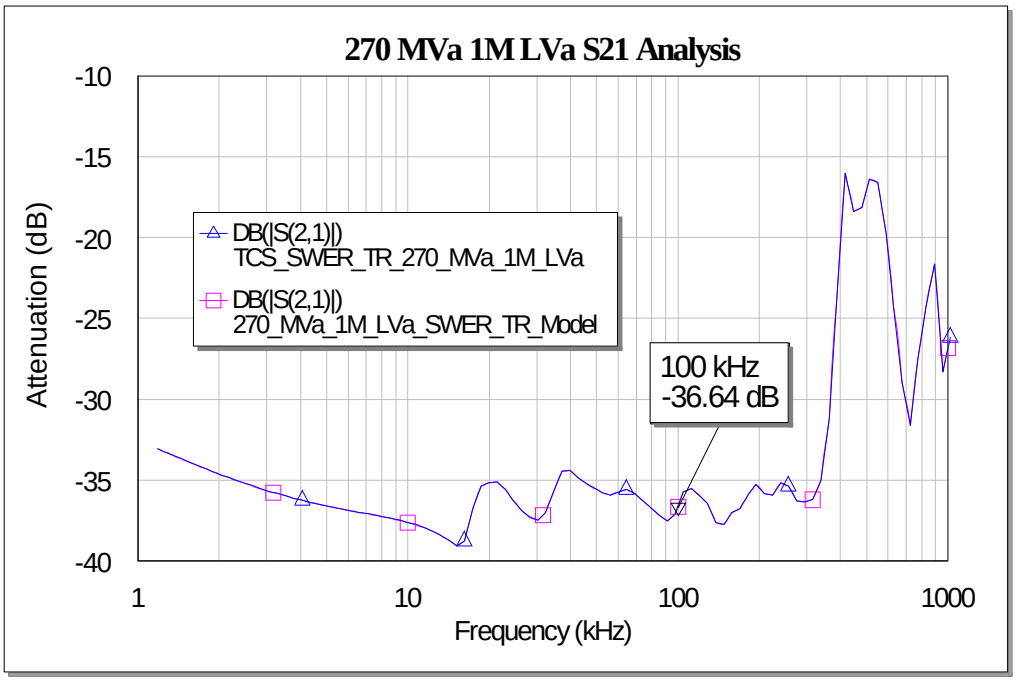

Fig 5.19: S21 Characteristics of 270-Ω MVa - 1-MΩ LVa TR Model.

Signal reflection of -0.1239 dB is shown in Fig 5.20 which is nearly consistent with the previous model, where -0.1282 dB reflection was recorded. This demonstrates that MVa to LVa high-frequency impedance is very high and the termination impedance has significant

impact on the signal insertion loss, but negligible impact on reflection while propagating to through the transformer winding.

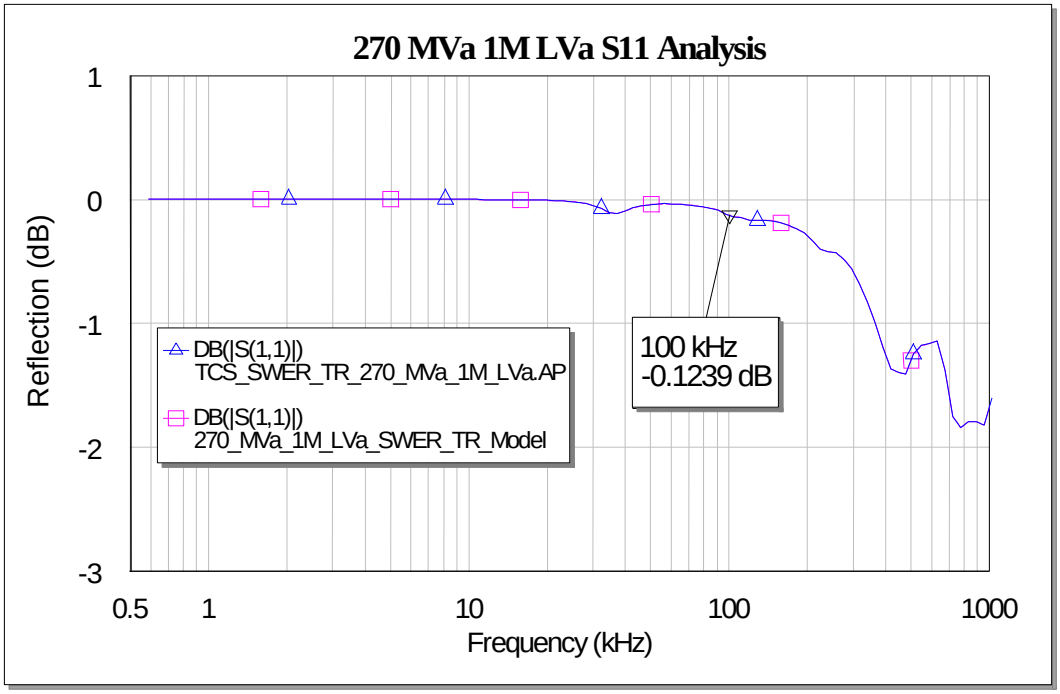

Fig 5.20: 270-Ω MVa-1-MΩ LVa Best-Case TR Model S11 Characteristic.

5.7.3 270 Ω MVa – 2.2 Ω LVa -Full Load Model (MV to LV)

The VNA output port was connected to the MVa port of the transformer through a 220-Ω resistor (giving the line impedance of 270-Ω when summed with the VNA output impedance of 50-Ω). The 270-Ω MVa to 2.2-Ω LVa model is presented in Fig. 5.21 mimicking a full load on the 240 Volt secondary. Channel 2 had a 2.2-Ω resistor in parallel with the 1M-Ω port impedance of the VNA modelling a 2.2-Ω heavily loaded secondary.

The S21 and S11 characteristics have been shown in Fig 5.22 and Fig 5.23. With this full load condition, the insertion loss is high at around -56 dB at 100 kHz and close to open circuit condition which exhibited -63 dB loss for PLC signal while measuring from the low voltage side. The blue coloured trace of the Fig 5.22 shows the S21 characteristic of the simulated transformer model, where the pink-coloured trace shows the S21 characteristic from the actual field measurements, as shown, both traces are aligned. Fig 5.23 shows the S11 or the reflection characteristic coefficient of the 270 Ω MVa -2.2 Ω LVa TR model.

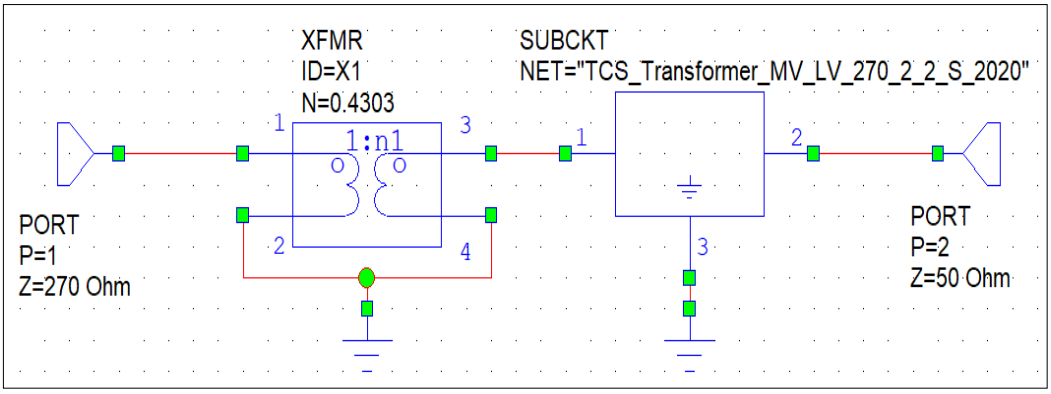

Fig 5.21: 270-Ω MVa – 2.2-Ω LVa TR Model

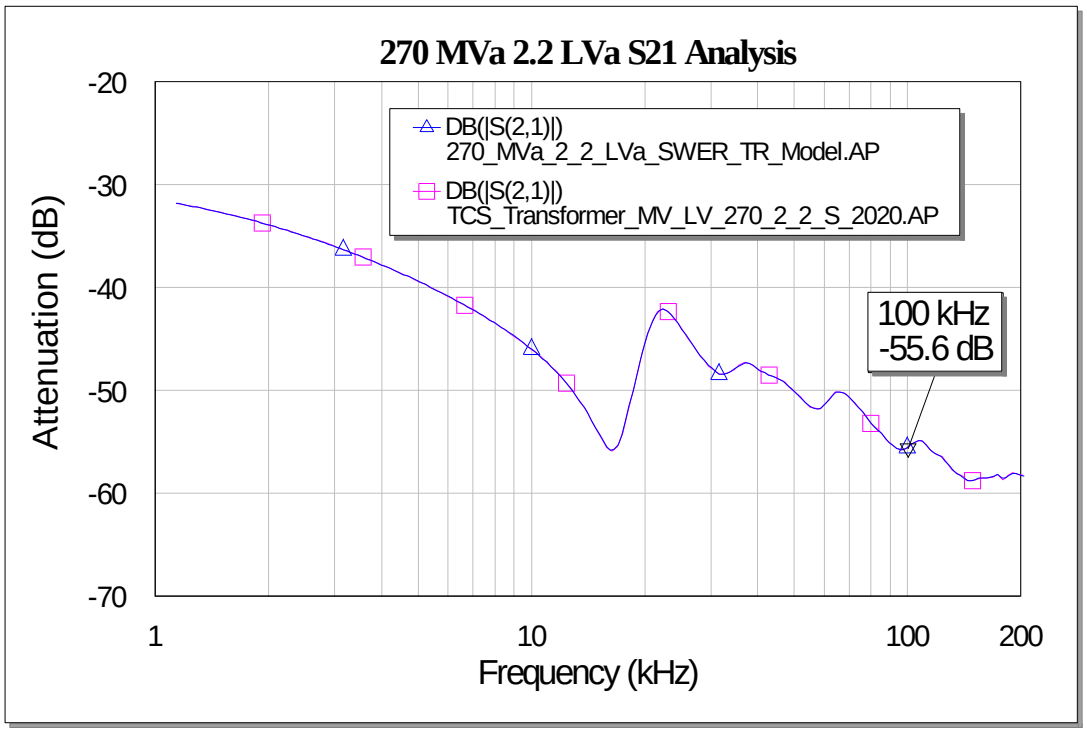

Fig 5.22: S21 Characteristics of 270-Ω MVa -2.2-Ω LVa or full load TR Model.

The curve of Fig 5.23 illustrates -0.152 dB reflection of the PLC signals while penetrating through the transformer in the MV to LV direction at full load conditions. Comparative analysis of the S21 characteristic observes that for the loading conditions, such as the full load and short circuit conditions, the attenuation is quite similar from -55 dB to -62 dB. But for the open circuited condition (higher load, 1-MΩ), PLC signal would experience lower

attenuation at around -36 dB. For a 0 dB signal power on the primary, -36 dB of signal power is received at the secondary. In contrast, comparative analysis of the S11 shows that the reflection loss for the full-load condition (S11 = -0.152 dB; 0.966 W/W) is higher than the other two cases, where the reflection was measured as approximately -0.12 dB (0.973 W/W).

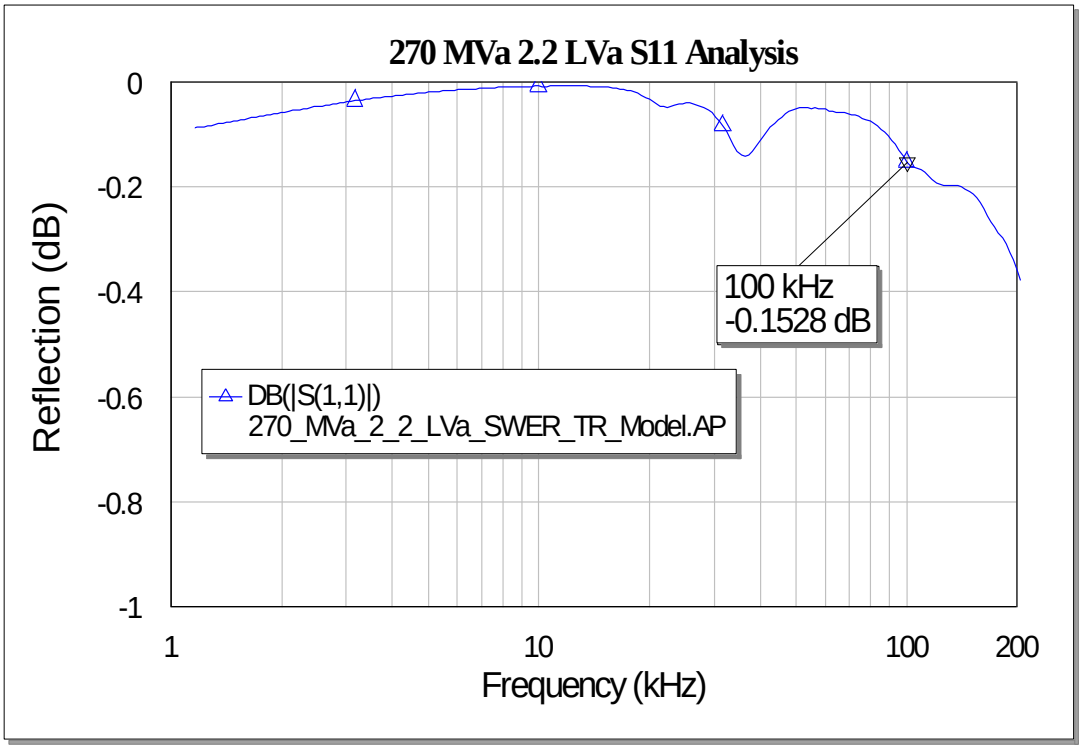

Fig 5.23: 270-Ω MVa-2.2-Ω LVa -Full load TR Model S11 Characteristic.

5.7.4 50 Ω LVa to 270 Ω MVa Model (LV to MV)

This section describes the 50 Ω to 270 Ω nominal LV to MV transformer model. Similar to the previous model, this configuration requires only one adjustment transformer (X2) for Port 2 with a ratio of N=2.225. The adjustment transformer changes the 50 Ω TCS block port impedance to 270 Ω required to represent a SWER line impedance. On the other hand, the low voltage (LV) side has been connected to the 50 Ω port which is considered as the PLC source's output port impedance. The customized configuration of the LV to MV path transformer model in the Microwave Office platform is represented in Fig. 5.24

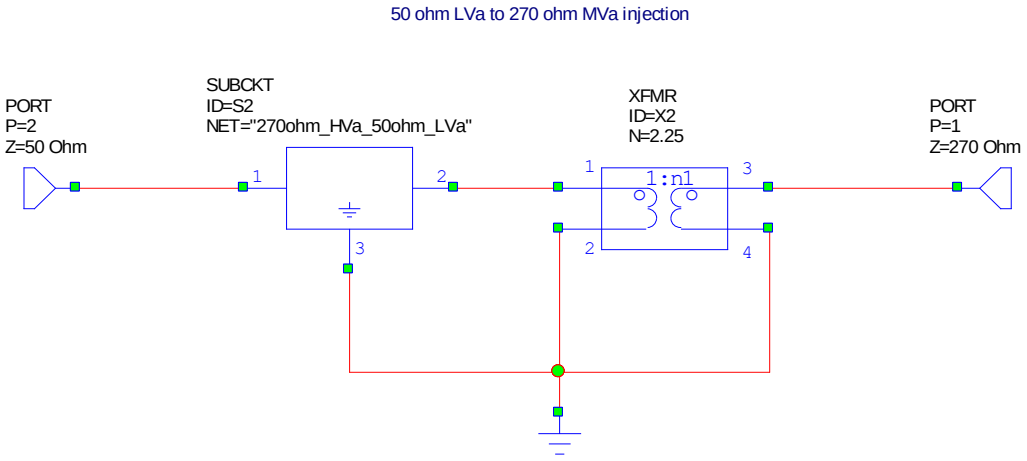

Fig 5.24: 50-Ω LVa - 270-Ω MVa SWER TR Model.

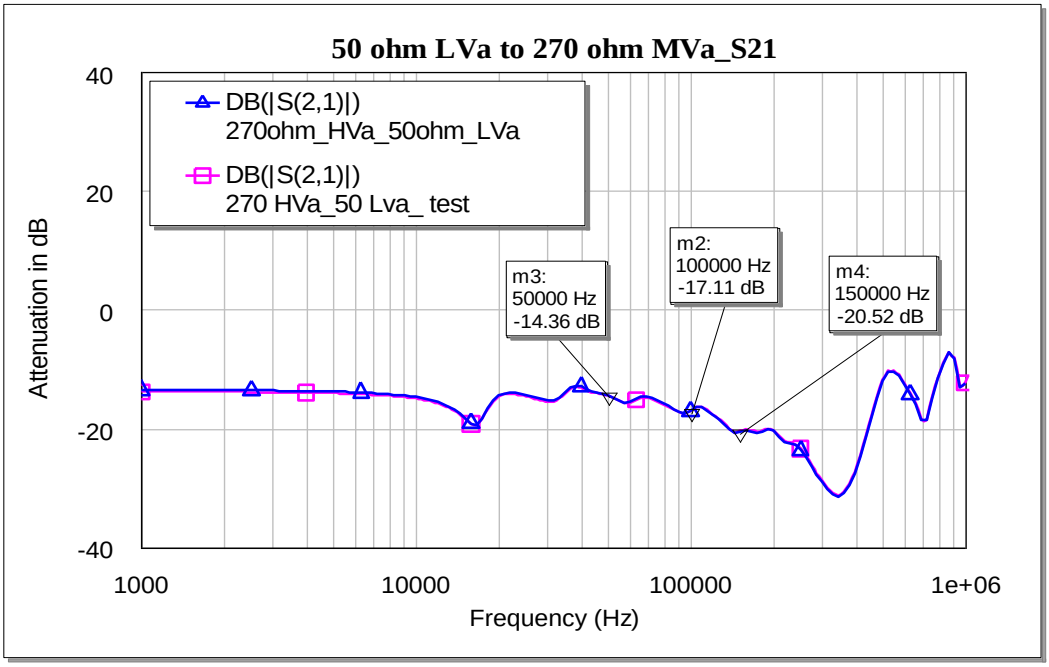

Fig 5.25: S21 characteristics of the 50 Ω LVa – 270 Ω MVa TR Model.

The S21 curve of the above LV to MV injection path circuit configuration is shown in Fig 5.25. From this curve, it can be observed that if the PLC signal is injected from the low voltage side (secondary), the signal strength at the primary winding (MV side) will be quite high compared to the MV to LV configuration. At a frequency of 50 kHz, the attenuation is -14.36 dB, and at 100 kHz, the attenuation was determined to be about -17.11 dB. The 150

kHz attenuation is -20.52 dB after this range. After 150 kHz, the signals experienced higher attenuation by the LV to MV injection path.

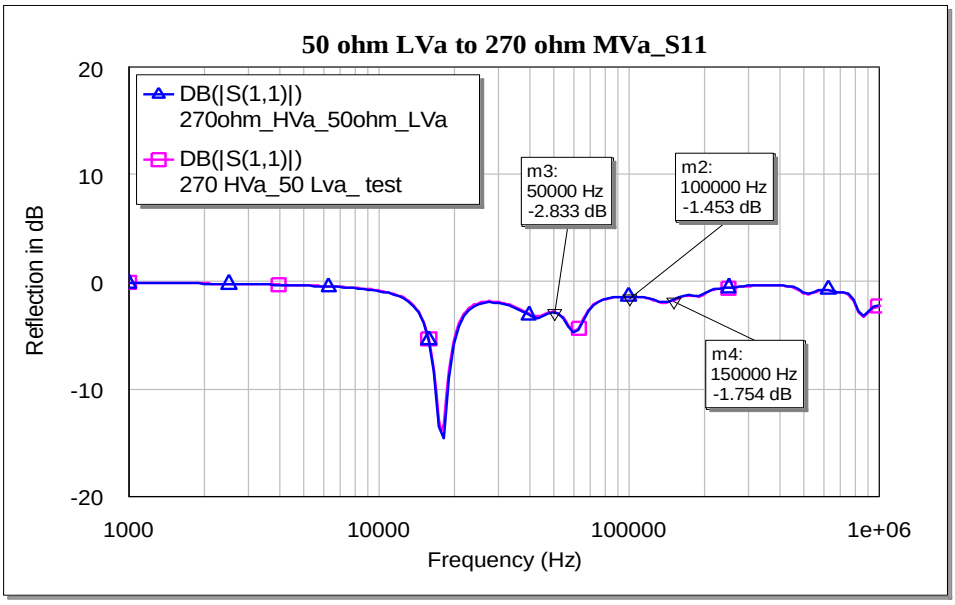

Fig 5.26: S11 Characteristics of the 50 Ω LVa – 270 Ω MVa TR Model

On the other hand, the reflection characteristics (S11) of Fig 5.26 shows that this 50 Ω LVa -270 Ω MVa path model generates a downward spike at a frequency of around 20 kHz and the reflection varies between -2.83 to -1.75 dB for the 50 kHz to 150 kHz range. On the other hand, the reflection for the MV to LV path were higher (-0.12 dB). Due to the high reflection and abnormalities at the lower frequency band, despite having a lower insertion loss, PLC signal injection through the LV side seems more challenging and a tougher choice.

5.8 SWER Transformer Model Simulations in Microwave Office

5.8.1 PLC propagation test on the winding of SWER TR Models

In this section, system level PLC propagation tests have been carried out for the SWER TR windings at the two different load conditions, developed earlier. PLC or HF signal of 100 kHz and magnitude of around 1-V has been injected at the MV primary for both TR models. The magnitude of the HF signal at the LV secondary winding has been measured to determine the impact of secondary loading on the actual PLC signal strengths passing

through the transformers. Fig 5.27 shows the system configuration of the simulation study in the MWO and Fig 5.28 shows the amplitude of the input PLC signal.

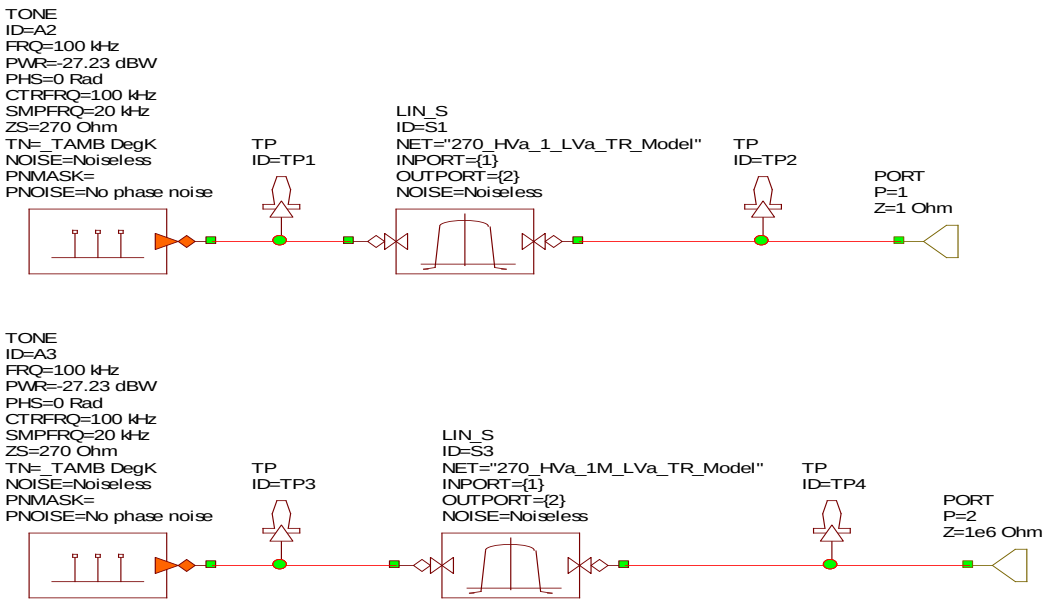

Fig 5.27: SWER TR System Level Simulation.

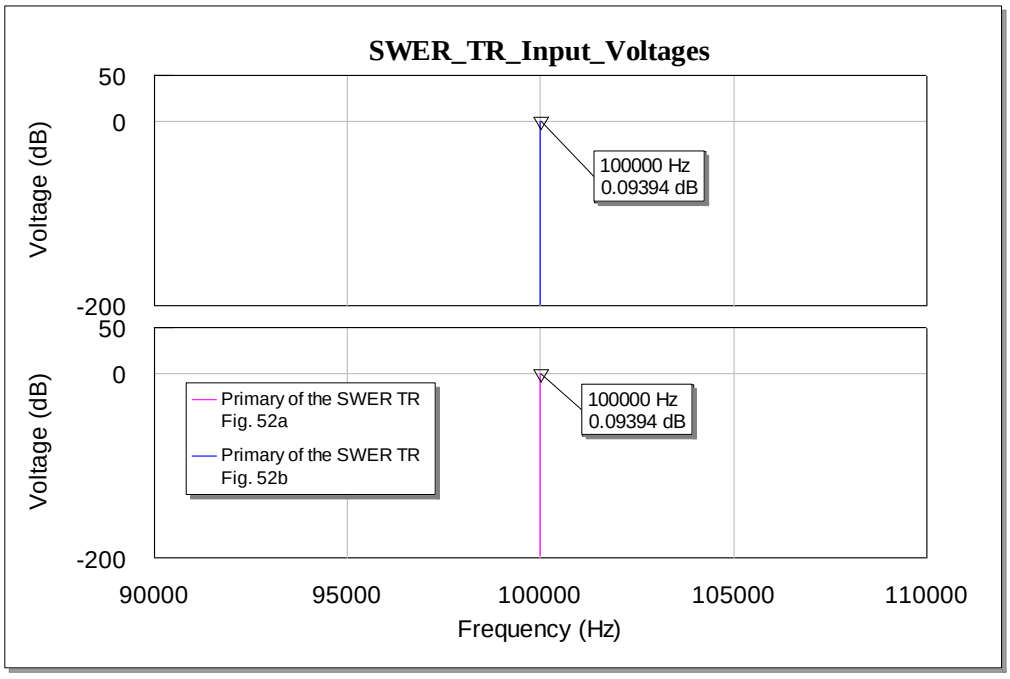

Fig 5.28: SWER TR System Level Simulation: Input Signal at MV Terminal.

Fig 5.29 shows the measured output or HF signals at the LV winding of the SWER TR for both termination options. As shown in both cases, the magnitude HF signal is higher at

around -43 dB HF at the secondary of the 1M-Ohm terminated TR and worst with a -59 dB magnitude at the secondary when terminated with 1-Ω load on the TR.

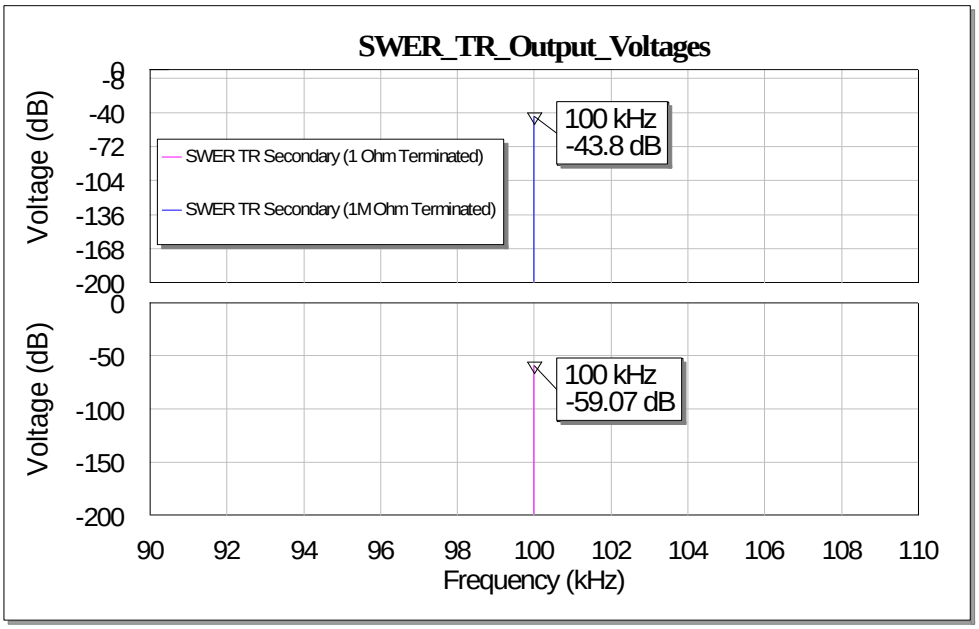

Fig 5.29: SWER TR System Level Simulation: Output Signal at LV Terminal.

PLC signal represents a very low amplitude such as 0.0011 V and 0.0070 V. Therefore, regardless of the secondary loading, the PLC signal penetrating from the MV line to the customer through the SWER transformer will be very low. Due to this low amplitude of PLC signal on the customer end, other home appliances and communication system device will not require any filter circuit or other peripherals.

Herewith, because of negligible amplitude of PLC signals, radiation from the signals will also be very low which will not be able to affect the other communication around the household such as-Wi-Fi signals, or other Microwave communication facilities such as mobile communication or ADSL communication application. For example, the ADSL application input voltage is 2 V [119], which is significantly higher than PLC signal amplitude, so the radiation impact of PLC signals on ADSL communications will be negligible. All the above positive findings show the potential of this technique to implement in power line fault detection.

5.9 Isolation Transformer Modelling

Fig 5.30 shows schematic arrangement and Fig 5.31 shows the experimental set-up in acquiring the Touchstone file for the Isolation (ISO) TR. As shown, the output port of the VNA was connected to the SWER winding of the ISO TR through a 270-Ω resistor.

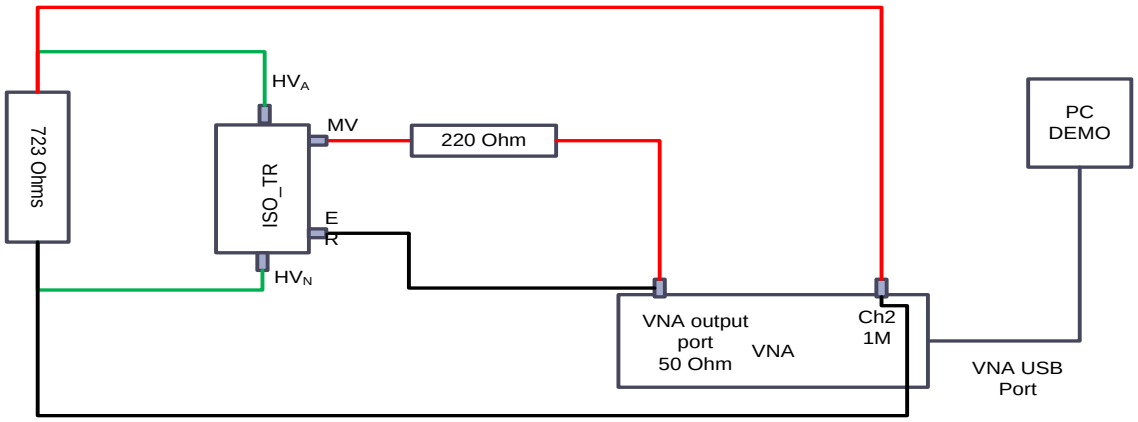

Fig 5.30: Isolation transformer s-parameters acquisition set-up schematic

Fig 5.31: SWER isolation transformer data acquisition set-up

Channel 2 has a 723-Ω resistor (calculated characteristic impedance of the high voltage three phase conductor) in parallel with the 1M-Ω port impedance. In circuit configuration, the PLC signal was injected to the high voltage active (HVA) of the SWER ISO TR, which is connected to the VNA output port and response recorded at the high voltage negative (HVN) terminal, which connected to the Channel 2 of VNA. These tests were undertaken at

the Zinfra switchyard using an ETEL 100-kVA transformer. Extended photographs on SWER ISO test has been added on Appendix H.

Fig 5.32 shows the MWO configuration of the ISO TR model, in this model two adjustment transformer such as -X1 with turns ratio (N=0.4303) and other X2 with turns ratio (N=0.263) have been used to match the impedance conditions.

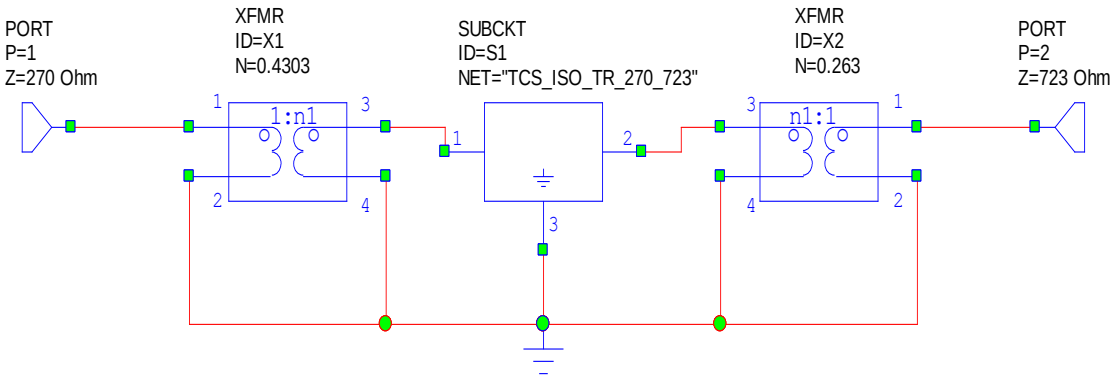

Fig 5.32: Microwave base isolation TR Model

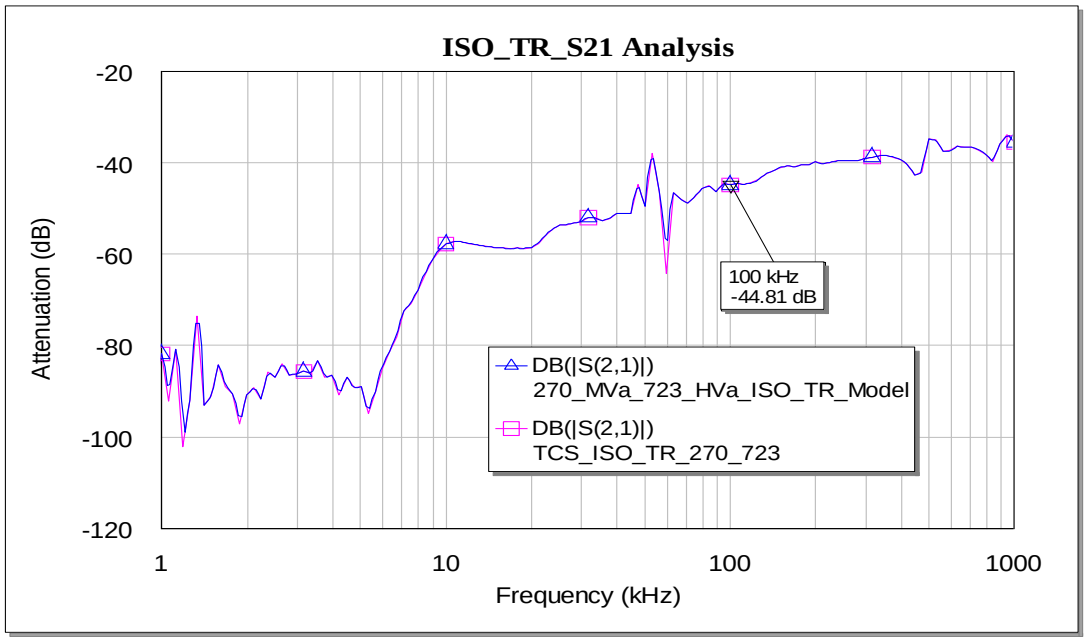

Fig 5.33: ISO TR Model S21 Characteristic

Fig 5.33 and Fig 5.34 shows the S21 and S11 characteristics of the ISO TR. The results demonstrate very high reflection from the SWER terminal of the Isolation transformer and

very low penetration of signals into the HV winding. For example, the value of the S21 coefficient insertion attenuation at 100 kHz is -44.81 dB (Transmitted Power gain = 0.000033 W/W), which means that for a 0 dB signal power at the SWER side of the isolation transformer, the power level of the signal at the HV end would be -44.81 dB. The value of the S11 coefficient at 100 kHz is nearly zero (~0.003111) signifying that all injected signal in the primary side will be reflected.

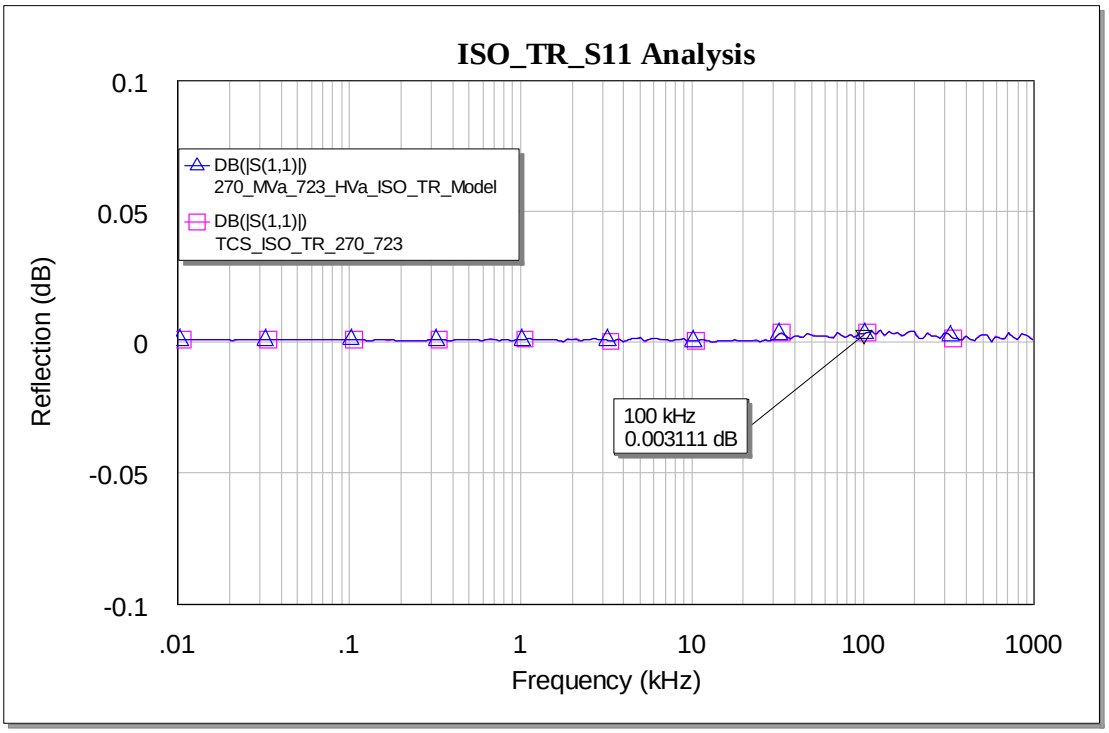

Fig 5.34: ISO TR Model S11 Characteristic

5.9.1 PLC propagation test on the winding of ISO TR Models

Following the system level simulation for SWER transformer, similar system level PLC propagation test has been carried out for the isolation transformer. This simulation reveals the fact that PLC penetration through the windings of the ISO transformer is very low. For example, an injection of 100 kHz signal with an amplitude of around 1-V at the low voltage SWER ISO transformer's terminal, produces a -63 dB penetrating 100 kHz signal measured at the HV side of the SWER ISO transformer, signifying very low propagation of HF signals through the ISO TR.

Fig 5.35 shows the system level simulation the isolation transformer for a PLC propagation test system in the AWR (Microwave Office) platform.

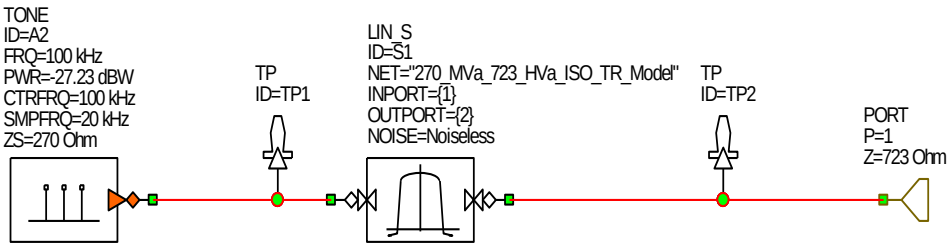

Fig 5.35: ISO TR System Level Simulation.

5.10 Conclusion

Transformers are the most important parts of an electricity distribution network. These are also the most critical candidates to affect the PLC signals while propagating through the power system network. Considering these facts, this chapter has focused on the modelling and characterisation of the transformer at the PLC frequency ranges. This includes a SWER distribution transformer and a SWER isolation transformer. In the following chapter, these proposed transformer model will be integrated into an end-to-end complete SWER network model, where the objective would be to compare the predicted subcarrier tone strengths against measured tone strengths in an OFDM transmission.

Few key novel contributions to research methodology have been made throughout this chapter such as the introduction of a simplified high frequency winding impedance measurement technique and s-parameter measurements of the transformer MV to LV and LV to MV path reflection and transmission characteristics as a means of modelling the high-frequency behaviour of these paths at PLC frequencies for further analysis. The results obtained from this method has been compared with some well-established conventional methods, which justify the accuracy of the proposed method. The proposed impedance measurement technique can also be used for any other transformer impedance measurement. Results show that a SWER transformer's primary winding high-frequency impedance is

around ~1.5 kΩ at the 100 kHz centre frequency while the high-frequency impedance value of the low voltage secondary winding is around 56.7 Ω at 100 kHz.

A novel s-parameter based load-terminated transformer modelling technique has been explained and experimentally applied to both a 25-kVA SWER distribution and a 100-kVA isolation transformer. Important characteristics such as the impact of secondary loading, signal attenuation (S21) and reflection (S11) parameters have been evaluated. A system level PLC injection simulation-test has also been demonstrated to compare the input and output voltage levels, while propagating the PLC signals through the transformers.

A key finding was that regardless of the secondary loading, the PLC signal penetrating from the MV line to the customer through the SWER transformer will be very low while there would be high reflections back onto the SWER from the transformer. Losses at the customer premises are therefore expected to be low. For the LV to MV path, moderate signal attention and reflections were observed making SWER transformers a potential PLC signal injection medium satisfied that a good matching network is developed and used.

Chapter 6

Evaluation of SWER Channel for PLC Propagation

6.1 Introduction

This chapter is the last contributory sections of the thesis, most significant findings with regards to the analysis and modelling of the channel have been summarized in this chapter. One of the key focus of this work is to model and evaluate the High Frequency (HF) Communication channel of a designated SWER network for powerline communication-based protection scheme applications with the Microwave Office platform. The PLC channel modelling has been demonstrated with simulations performed to predict the PLC subcarrier strengths at the receiver end and has been compared with field measurements. High Frequency (HF) modelling of the entire network has enabled simulation of the overhead network to predict PLC signal tone strengths for the de-energised and grid connected network scenarios.

During field tests, PLC signals were injected to the isolated SWER network as well as to the energized SWER network connected to the 22-kV Medium Voltage (MV) multiphase grid through the isolating transformer. Comparison of the test measurements against model predictions has been used in justifying the accuracy of the developed channel model. System level simulations enabled a comparison between actual measured Orthogonal Frequency-Division Multiplexing (OFDM) subcarrier tone voltages in the 50-150 kHz frequency band and those predicted by the modelling. Likewise, the test, in simulation both the scenarios - energized and de-energized have been presented as well. The first scenario explored the HV de-energised case study network when LC-coupling capacitor injection was practiced with an injection sequence matching that applied in field tests. The second scenario investigated the HV-connected (live) network also coupled via the similar LC-coupling capacitor-based circuit. The modelling sought to compare model predicted PLC tone voltages with those measured in the field tests. Comparative accuracy analysis and various case studies such as expansion of the network size, analysis of the loading effect on the secondary loading of the

transformer, pole heights have been demonstrated in this chapter. Some of the critical observations of these case studies can be summarized as follows: network expansion (the distance between the transmitter and receiver) has a significant impact on the received PLC signal strength, but secondary loading of the customer end SWER transformers and the pole height above ground has negligible impact on the PLC propagation.

This chapter also focusses on the discussion of the various fault scenarios in the case study of SWER network. Emphasis has been given to classify different types of High Impedance Fault (HIF) models. Two main HIF fault models such as the arc-resistance and the diode-based models have been explored. Impact of the HIFs on the s-parameter characteristics and the spectrum of PLC signal propagation over the designated SWER network has been represented as another novel contribution in this chapter. In addition to HIFs, open circuit and short circuit scenarios have been created in the network to show impact of these cases on the PLC signal transmission. The workflow of this chapter is shown in Fig 6.1.

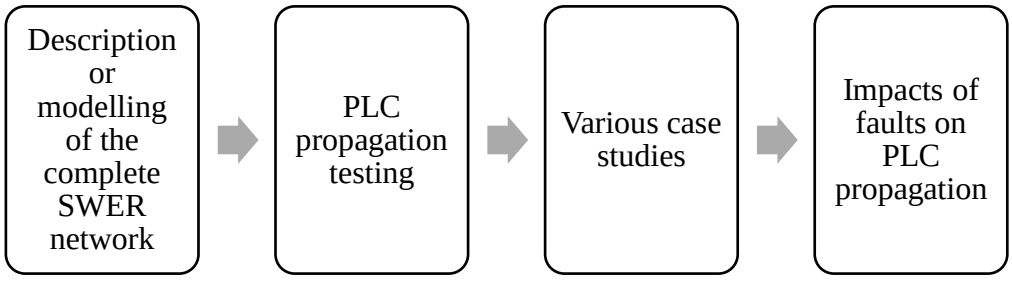

Fig 6.1: Flow chart of this chapter

6.2 Designated SWER network details

The PLC propagation test zone was part of a larger SWER network. The fig 6.2 shows the network schematic diagram of the 12.7 kV RMS Myers Road SWER network in Balnarring. Balnarring is a Victorian town on the south eastern Mornington Peninsula with a large selection of wineries and vineyards located in the rural inland sections. There are 28 customers all supplied through this relatively small SWER network, which has a total network length of 10.2 km. The network consists of many segments. The length of the

segments varies from 1 m to 500 m. Table 17 shows the exact distance of each segment of the network.

Table 17 : Myers Road Network Lengths

Start Point	**End Point**	**Distance (m)**		**Start Point**	**Endpoint**	**Distance(m)**
Pole 1 (Receiver)	Pole 2 ACR	22.357		Pole 19	Pole 22	180.527
Pole 2 (ACR)	Pole 3	331.271		Pole 23	Pole 24	125.202
Pole 3	Pole 3-1	118.325		Pole 23	Pole 23-1	193.21
Pole 3	Pole 4	87.151		Pole 23-1	Pole 23-2	191.8829
Pole 4	Pole 5	165.727		Pole 23-2	Pole 23-3	240.279
Pole 5	Pole 6	195.639		Pole 23-3	Pole 23-3-1	162.646
Pole 5	Pole 11	283.867				
Pole 6	Pole 7	214.219		Pole 23-3	Pole 23-3-2	279.031
Pole 7	Pole HB	66.789		Pole 24	Pole 25	128.611
Pole 7	Pole 8	381.345		Pole 25	Pole 25-1	166.329
Pole 8	Pole 9	221.703		Pole 25-1	Pole 25-2	533.843
Pole 9	Pole 10	250.037		Pole 26	Pole 27	181.277
Pole 8	Pole 8-1	221.703		Pole 27	Pole 28	120.739
Pole 8	Pole 8-2	179.129		Pole 28	Pole 28-1	136.979
Pole 8	Pole 8-3	104.675		Pole 28	Pole 29	172.812
Pole 11	Pole 12	285.857		Pole 29	Pole 30	81.703
Pole 12	Pole 13	424.662		Pole 30	Pole 30-1	129.935
Pole 13	Pole 14	140.206		Pole 30	Pole 30-2-1	115.865
Pole 14	Pole 15	381.1		Pole 30-2-1	Pole 30-2-2	115.851
Pole 15	Pole 16	189.945		Pole 30-2-2	Pole 30-2-3	131.858
Pole 16	Pole 17	350.401		Pole 30	Pole 31	219.506
Pole 16	Pole 23	153.552				
Pole 17	Pole 18	204.524		Pole 31	Pole 32	291.2
Pole 18	Pole 19	196.521				
Pole 19	Pole 20	167.882				
Pole 19	Pole 21	307.384				
Total length (m)	10194.626 m			Distance between TX and RX	3613.361	m
Total length (km)	10.194 km			Distance between TX and RX	3.613	km

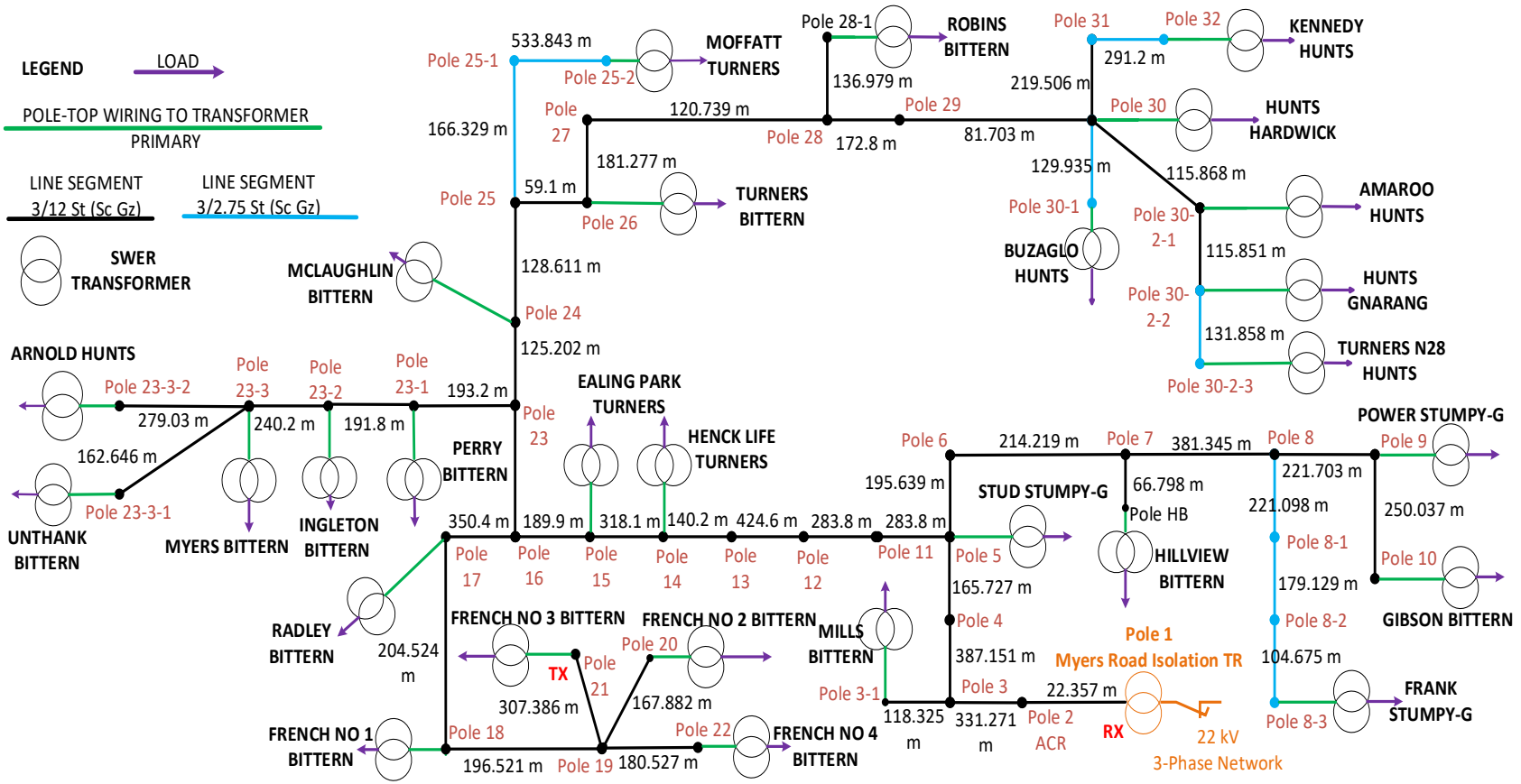

Fig 6.2: Myers Road SWER network in Balnarring.

The direct distance between the transmitter and receiver points is approximately 3.6 km. The transmitter set-up was connected at the 'French No: 3 Bittern' SWER TR pole (Pole 21) as shown in Fig. 6.2. A coupling capacitor was previously mounted on the pole enabling the injection of HF signals directly onto the 12.7 kV conductor through the capacitor. The DAQ system is also capacitively coupled to the network. It is located at the isolation transformer pole (Pole 1), where the SWER network is coupled to the 3-phase network. Pole 1 is the starting point of the SWER network, where the SWER connects to multi-phase 22-kV grid. The Visio based network diagram and AWR network diagram have also been attached in Appendix A and B.

The receiver side data logging was undertaken at the Myers Road network Pole #1, where an Isolation Transformer (ISO TR) isolates the SWER grid from earth, changing the grid voltage from 22 kV to the SWER voltage (12.7 kV). Fig 6.3 shows the Myers SWER network Isolation Transformer point, ACR, and the test site itself (Receiver site). The Automatic Circuit Recloser (ACR) is located on Pole # 2 approximately 22 meters away from the pole where the test set up was located. The data logging test equipment was located in an enclosure placed 3 meters high on Pole #1. Fig. 6.3 shows the view of the receiver end test site and Table 6.1 lists all the network segment lengths.

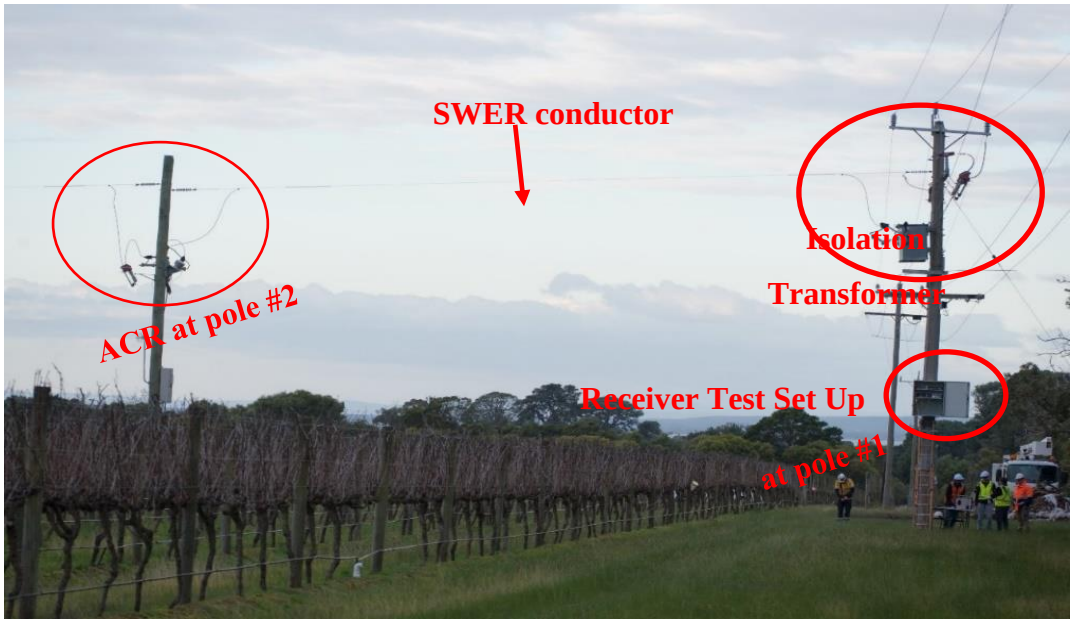

Fig 6.3: Myers Road SWER ISO and ACR (Receiver End)

6.3 PLC transmitter System

The transmitter set-up on the test site is shown in Fig 6.4. The pole is located next to a farmhouse and an enclosure was previously erected 3 meters high on the pole enabling the placement of all relevant injection hardware. A Coupling Capacitor (CC) was previously mounted on the pole enabling the injection of HF signals directly onto the 12.7 kV conductor through the coupling capacitor.

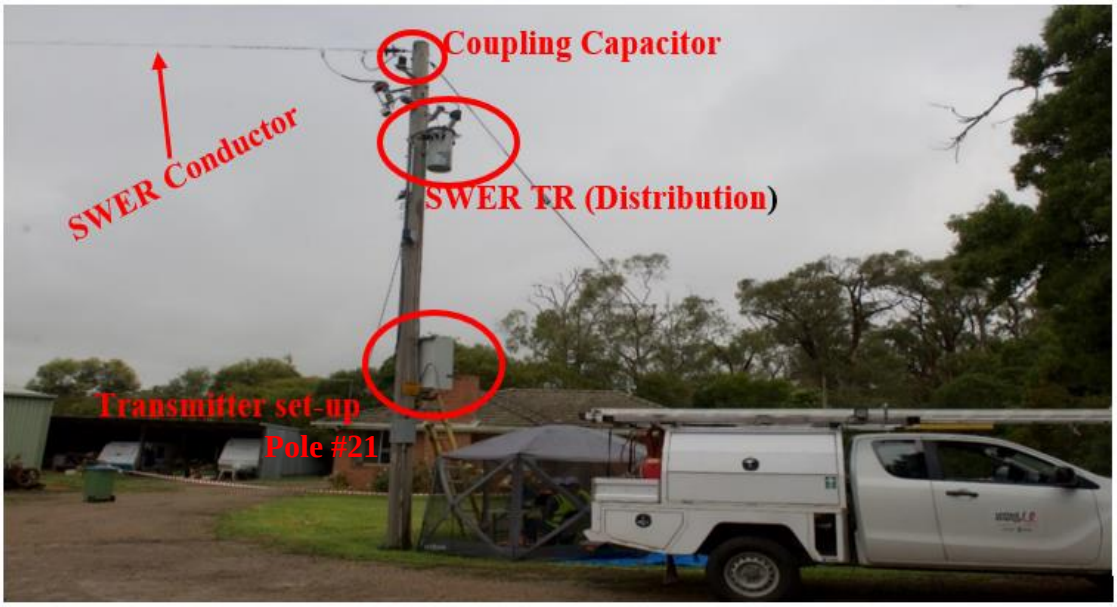

Fig 6.4: Test site transmission Point.

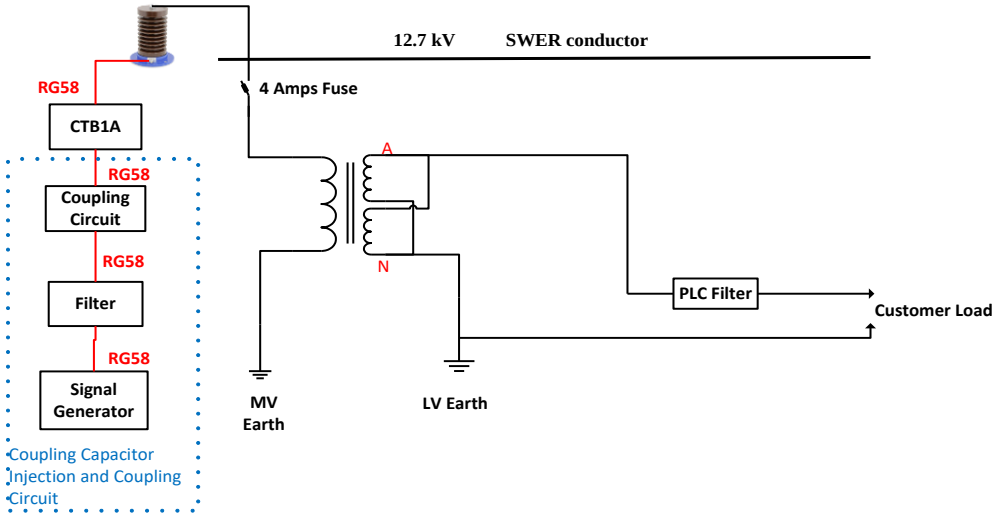

Fig 6.5: Injection Set-Up at French No: 3 Bittern SWER TR.

Fig 6.5 shows the configuration and connection of CC based injection options within the transmitter enclosure. Key elements of the coupling capacitor injection concept included the MCC 124 1.1 nF coupling capacitor, CTB1A, the L-C impedance matching coupling circuit, a low-pass filter, and finally an Arbitrary Signal Generator (ASG). The CTB1A [120] is a commercial coupler termination box is necessary for providing the protective ground for the coupler's BNC signal cable required to work with HV capacitor and the ASG was used to generate the multi-carrier test waveform for measuring the frequency response of the channel.

6.4 PLC Receiver system

Fig 6.6 shows the receiver end Data Acquisition (DAQ) system. The system includes the Omicron CC, 11-metre coaxial, Power Diagnostic Systems CTB1A termination box, the Capacitive Voltage Divider, and the Stanford Research Systems pre-amplifier. The Capacitor Voltage Divider (CVD) is the important element of the receiver data accusation system. It follows the voltage divider rules to proportionately divide the input voltage at its output based on the values of capacitive components, irrespective of the input signal frequency. In this test set-up PLC signal has been injected to the 12.7 kV SWER line whereas data accusation system components like digitiser, filter, pre-amplifier those are operated with low voltage, therefore the CVD reduced the high voltage input to low voltage output for those equipment to operate. The voltage division depends on the value of the capacitive components. The theoretical concept of CVD and extended photos on signal capture arrangement has been added on Appendix I and J.

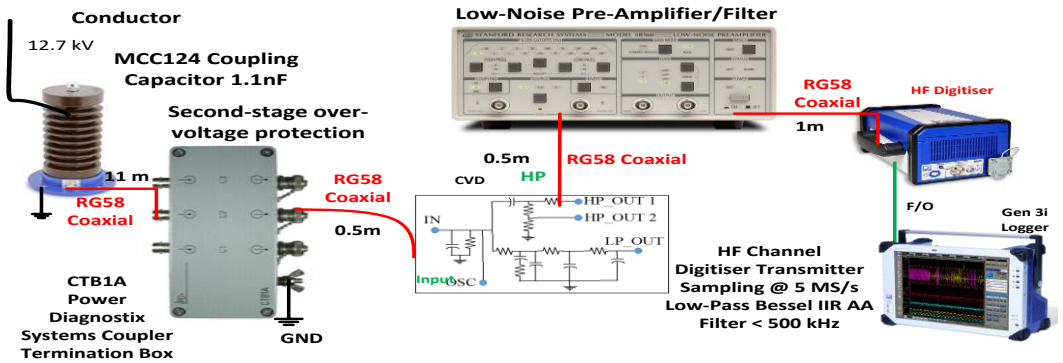

Fig 6.6: Receiving End DAQ System.

Stanford Systems pre-amplifier is a commercial filter integrated amplifier provides passband filtering between 10 kHz and 1 MHz. To analyse the captured PLC signals, some other peripherals such as a digitizer and the Gen3i data logger were sued. Both pieces of equipment helped to record and later visualize the captured signal. The CVD provides High Pass filtering and reduces the voltage levels with either a 110:1 (HP/10) or an alternative 11:1 (HP) setting. During these tests, the s-parameter of the following receiver end measurement circuit was acquired using the HP setting. Design of the CVD and the following measurement system is out of the scope of this thesis and was undertaken as part of the overarching project. The internal circuit schematic of the CVD is shown in Fig 6.7.

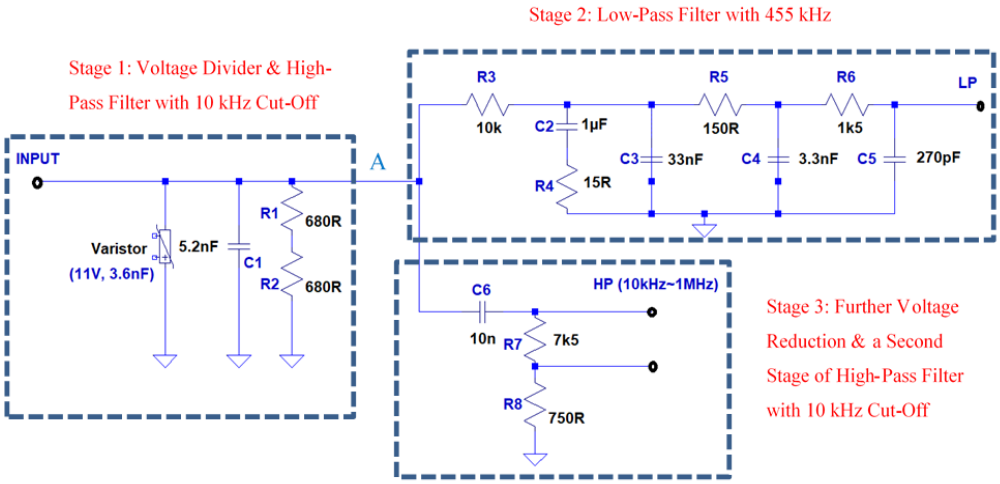

Fig 6.7: Schematic diagram of the CVD.

6.5 Propagation Test: Transmission and Reception of PLC Signals

This section presents system studies to comprehend the developed models and evaluate the performance of the injection method, and parameters affecting signal strengths. The developed Myers Road SWER model has been simulated for both isolated and 22 kV grid connected conditions. The impact of network size, conductor height, and SWER TR loading have been assessed. For the high frequency network model and propagation testing, the L-C matching CC based coupling circuit was used for the PLC injection. The details of the coupling circuit were explained earlier in Chapter 2. Similarly, the lossy line model and SWER transformer model were described in Chapters 4 and 5 respectively.

The complete case study Myers Road SWER network has been modelled in Microwave Office as shown in Fig 6.9. It includes (i) the aerial line models based on the lossy segment line model, and (ii) the SWER transformers based on the MVa-to-LVa path s-parameter measurements. Two different scenarios including the de-energised and energised (grid connected) will be considered, and the SWER conductor height has been taken as 6.7 meters. For analysis two different transformer secondary loading conditions including the 270 Ω MVa-1 MΩ LVa and 270 Ω MVa-1 Ω LVa SWER TR cases will be considered.

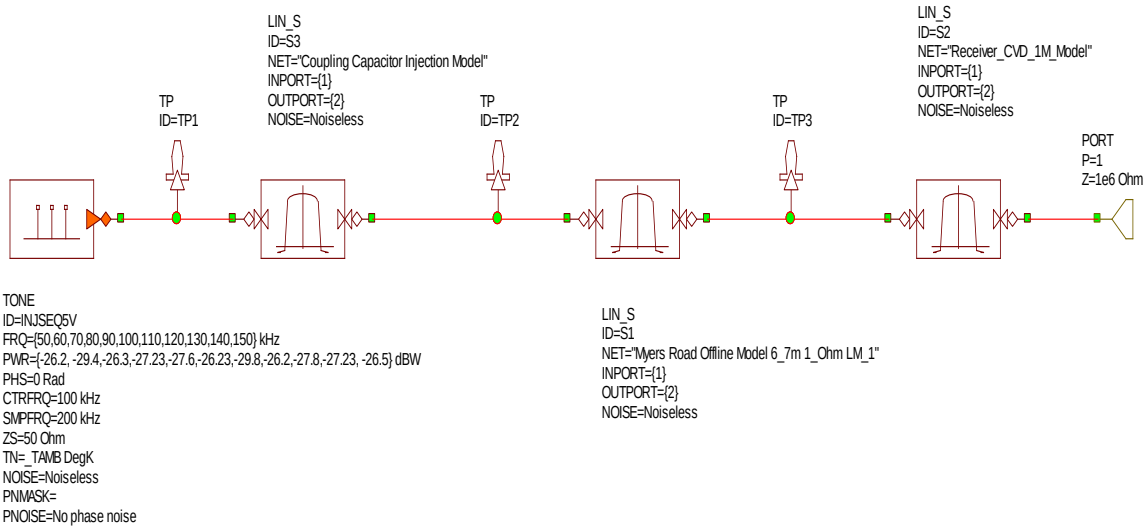

Fig 6.8: Myers Road System Level Simulation.

Fig. 6.8 shows the 'system' modelling of the end-to-end network with all components including the multi-tone source, capacitive coupling, conductors, and receiver-end measurement system. The s-parameter based measurements (integrated as two-port sub-blocks) are specific to the injection and DAQ circuits built by the authors as well as the utilised SWER transformer type. The system model consists of the following components:

- A tone generator replicating the OFDM subcarriers and frequency band of the injected tones.
- The coupling-capacitor injection circuit sub-block for the frequency-dependent behaviour of the injection circuit based on the s-parameter measurements.
- Receiver-end measurement system sub-block for the frequency-dependent behaviour of the receiver end circuit based on the s-parameter measurements.

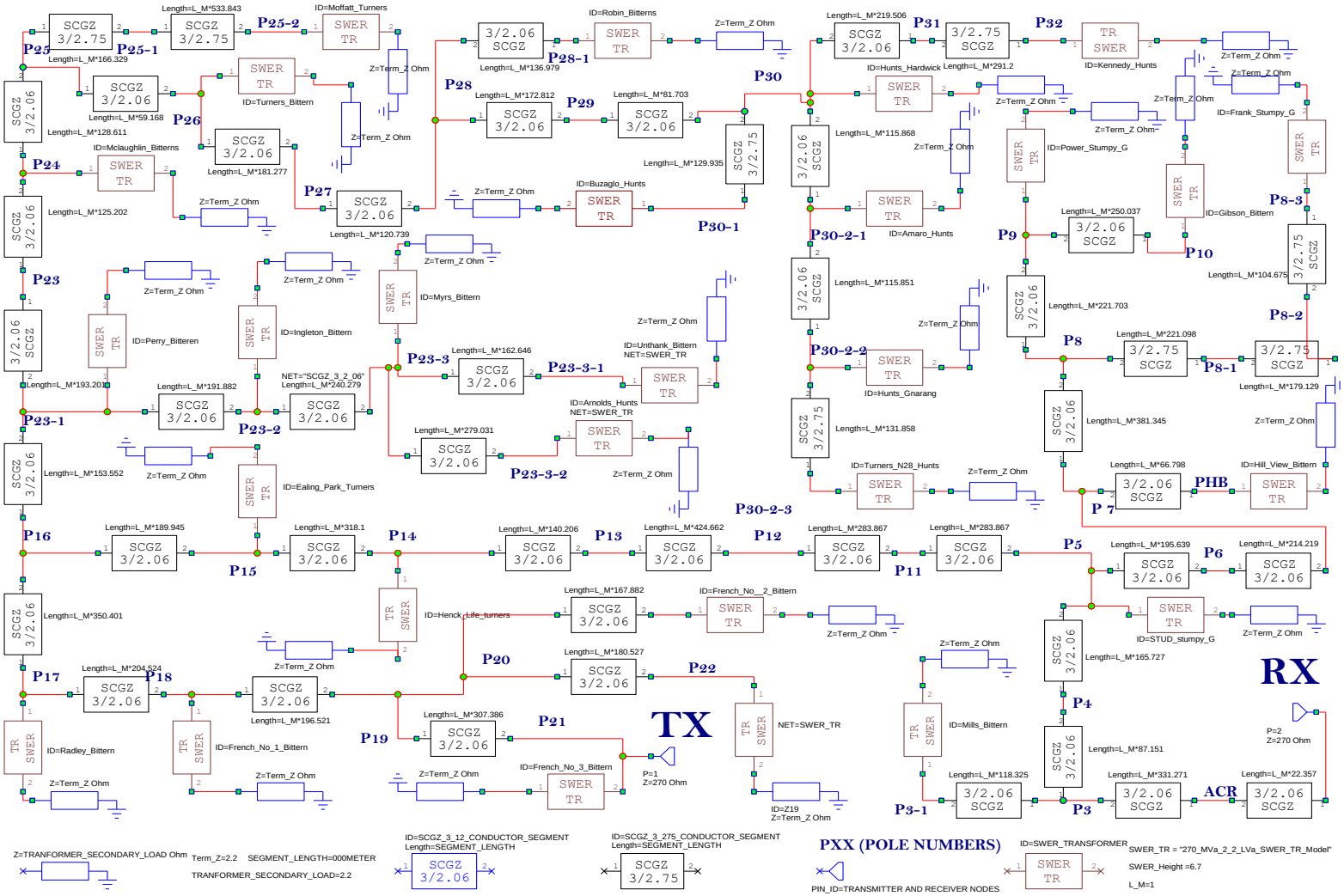

Fig 6.9: Complete Myer Road SWER network model in the Microwave office

6.5.1 Propagation Tests on the Isolated SWER Network

Table 18 shows the summary of the simulation parameters. For, the field PLC propagation testing, the amplitude of the injected OFDM signal was selected as 5 V RMS, which was supplied from the ASG. In simulation, to get the equivalent 5 V RMS input, a discrete tone generator from the Microwave Office suit was used. The input signal generated from the microwave tone generator is shown in Fig 6.10.

Table 18 : System Simulation Parameters 1

Simulation Parameters	Value
Injection Method	Coupling Capacitor
Configuration/SWER TR Type	Isolated/270 MVa 1 LVa
SWER Network Height	6.7 meters
ASG Setting	5 V RMS
Matching Field Test	OfflineSignalCon004.pnrf

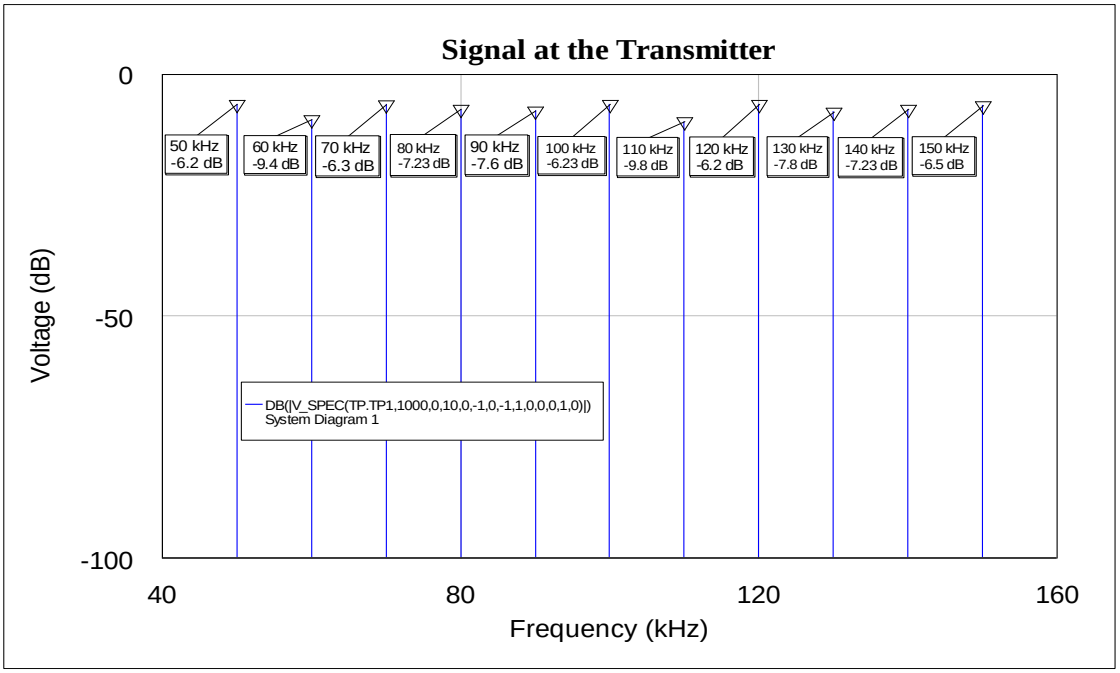

Fig 6.10: Simulated input PLC signal from the MWO tone generator

Fig 6.11 shows the spectral analysis of the HF signal received and recorded during the de-energised network actual measurements taken on the 7th of August 2018. Fig 6.12 shows the predicted signal strengths at Port 1 for the injection sequence of the Fig 6.10.

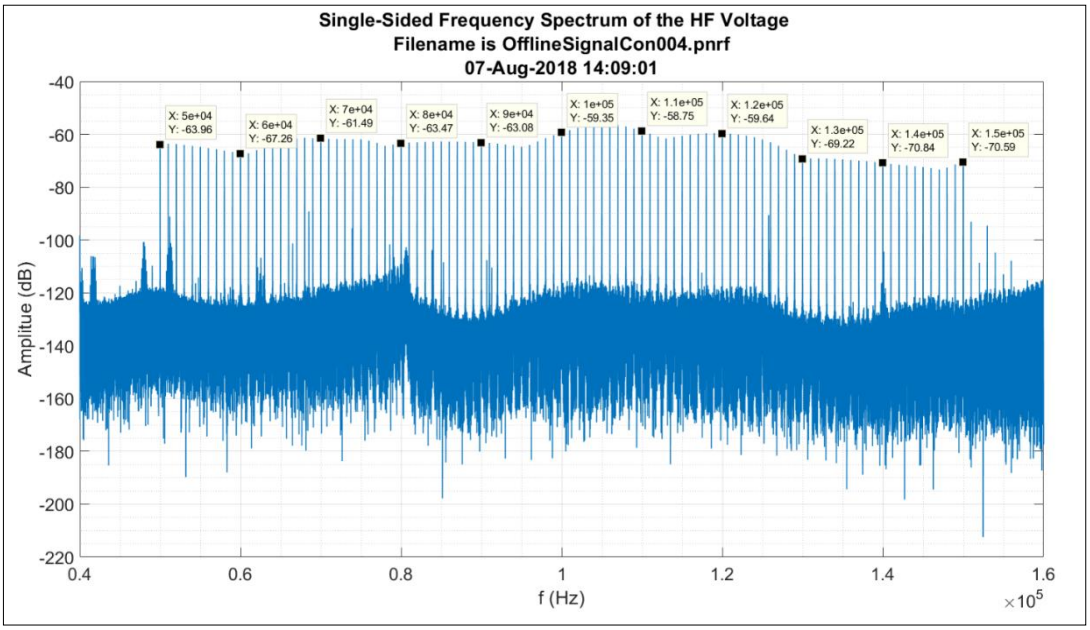

Fig 6.11: Received PLC signal spectrum from the real test on isolated SWER network.

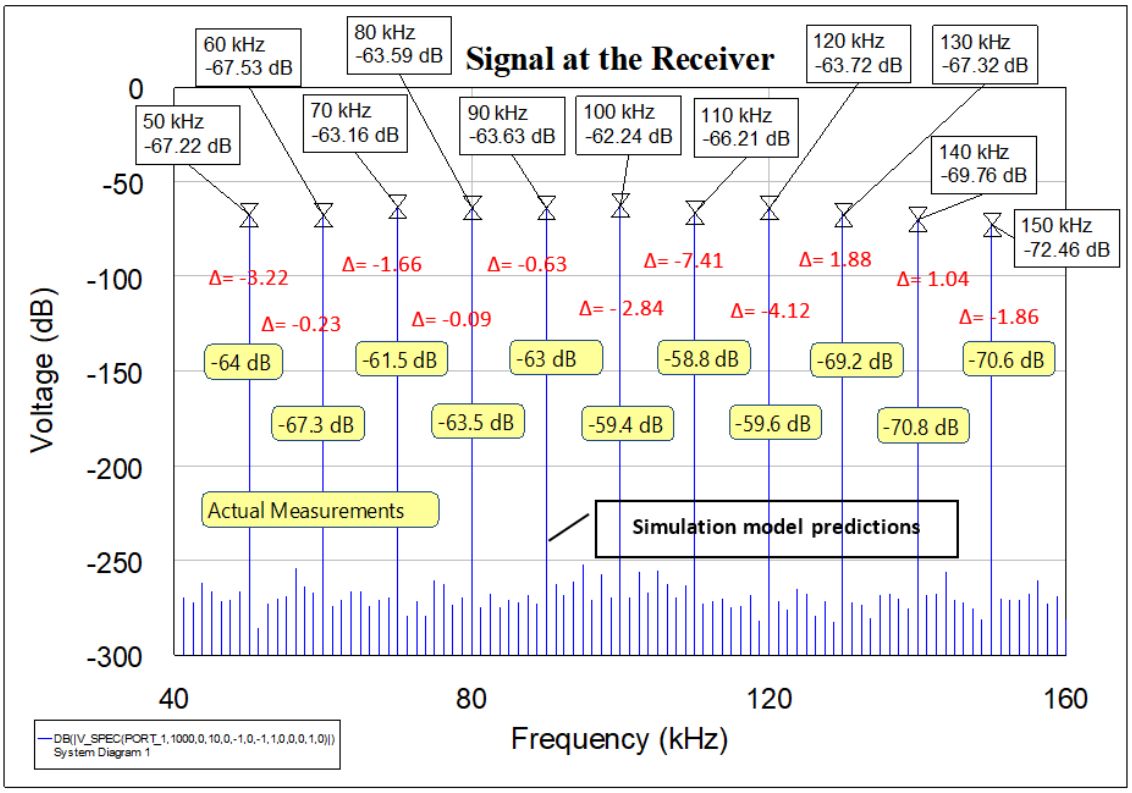

Fig 6.12: Model Prediction for the Isolated Network and Measurements (CC Injection).

Fig 6.12 also displays the error (Δ) calculations on the plot. Following the graphs, in Table 19, with respect to frequency, attenuation for the simulated circuit, measured network, and deviation between these two have been included.

Table 19 : Deviations in signal attenuation predicted and measured signal

Frequency Components (kHz)	Predicted Signal Attenuation in (dB)	Measured Signal Attenuation in (dB)	Deviations in (dB)
50	-67.22	-64	-3.22
60	-67.53	-67.31	-0.23
70	-63.61	-61.5	-1.66
80	-63.59	-63.5	-0.09
90	-63.63	-63	-0.63
100	-62.624	-59.4	-2.84
110	-66.21	-58.8	-7.41
120	-63.72	-59.6	-4.12
130	-67.32	-69.2	-1.88
140	-69.76	-70.8	-1.04
150	-72.46	-70.6	-1.86

From the curve and table it can be stated that, the developed model is quite accurate and computed signal strengths compare well with actual measurements. The measured signal is slightly larger than the predicted signal (at most carrier frequencies) with a mean difference of 2.27 dB, and standard deviation (σ) of 2.12 dB. Error sources would include un-modelled changes in the ground constants and power line clearances caused by line sag, terrain variations and agricultural usage over the test area

6.5.2 Propagation Test on energized SWER network

The network simulation model was then reconfigured to include the isolation transformer model, put back into service at Port 1, for the energised line. The injection sequence matches the injection sequence applied from the ASG during the energised network field tests enabling a direct comparison. PLC propagation testing on the energised case study SWER network was carried out on the 14th December 2018. The received signal spectral analysis is shown in Fig. 6.13 with the simulation predicted tone strengths shown in Fig. 6.14.

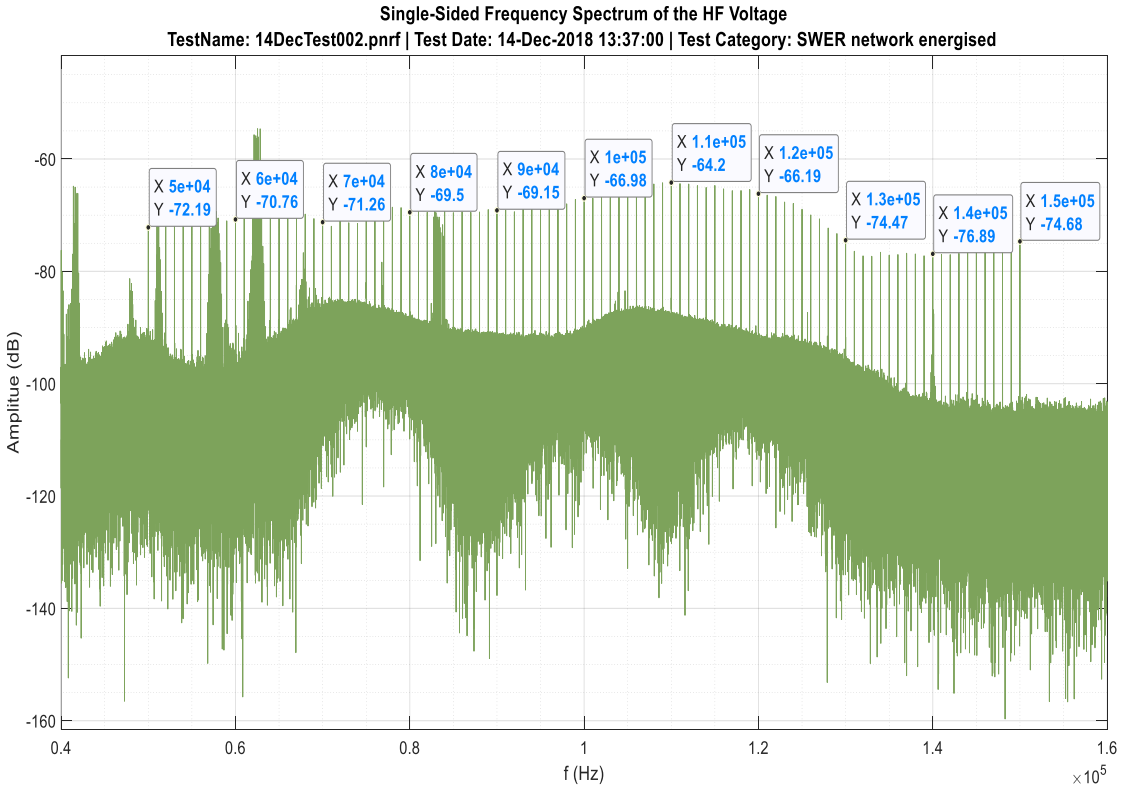

Fig 6.13: Received PLC signal spectrum for the energized SWER network field test.

Assessment of the predicted tone strengths against the measured strengths shows relative accuracy. For most tones, the error is in the 2-3 dB range, whilst for few other carrier frequencies (e.g. 100 kHz, 120 kHz, and 150 kHz) up to 6-7 dB error can be observed. The mean error is now 3.10 dB and σ is 2.10 dB. The error is higher, compared to the offline model. This was expected due to the impedance change caused by the isolation transformer and the fact that all modelling was based on non-energised transformer models. Despite increased error, results still confirm that an accurate narrowband model has been achieved.

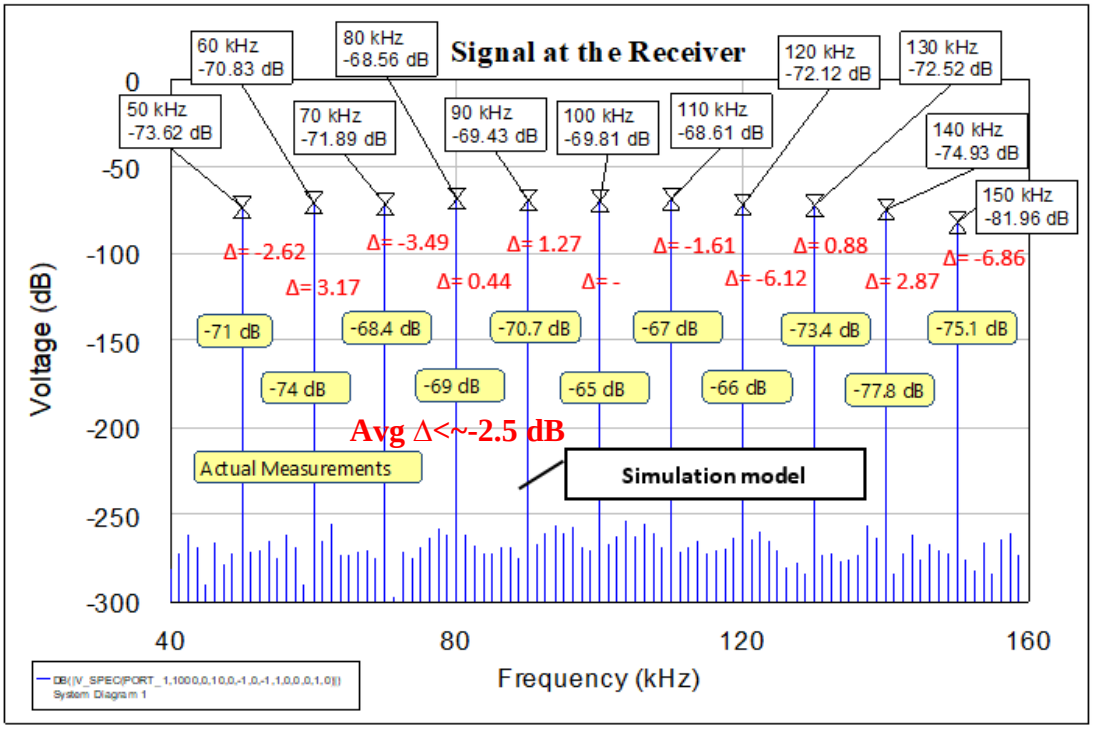

Fig 6.14: Simulated received PLC signal spectrum for energized SWER network

6.6 Case Studies on the Isolated SWER network

This section analyses the correlation of the PLC signal strength against certain parameters such as the conductor height, network size, and the SWER transformer secondary loading. Case studies have been carried out on the isolated network to assess the performance of the PLC signal propagation.

6.6.1 Case Study-I: Impact of Conductor height

The design criteria are minimum height of 6.7 meters, with an average pole height of around 10 m. Regulations allow utilities to go down to about 5.7 meters; therefore, a sensitivity analysis has been undertaken to compare received signal strengths at the two minimum heights. This includes simulating the network model of the Fig 6.8 by setting the SWER conductor height parameter as 5.7 meters. As shown in Fig 6.15, the height of the conductor above the ground does not make a significant impact on the signal strength.

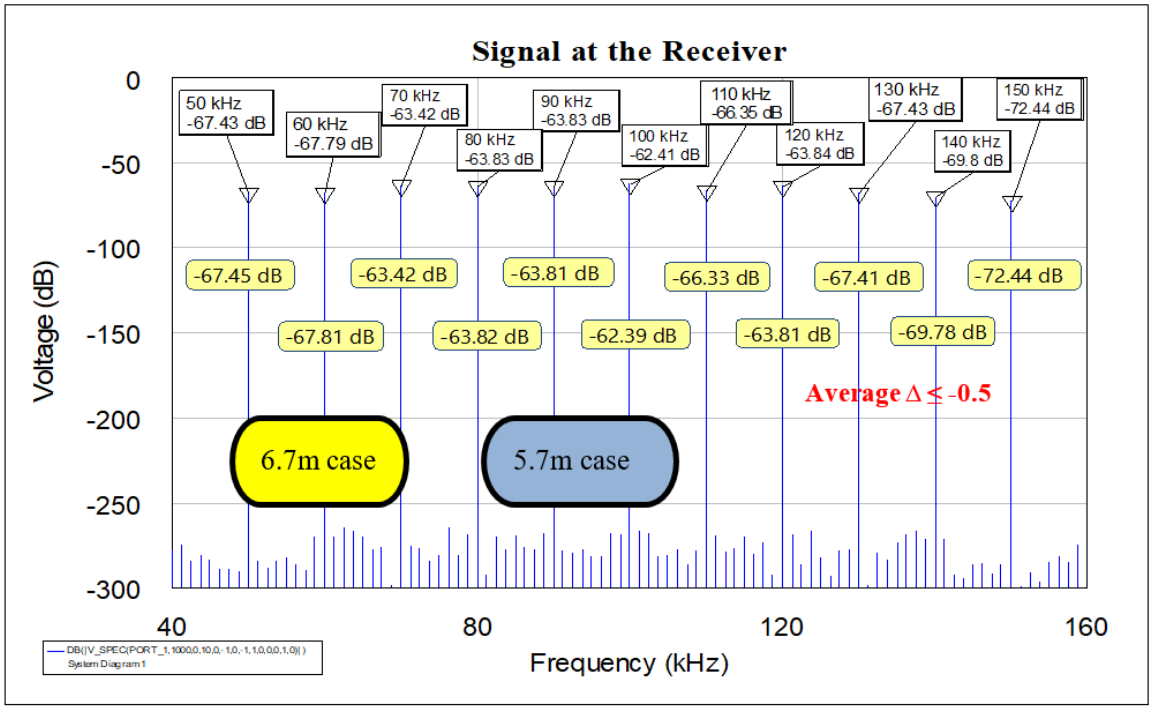

Fig 6.15: Simulation of the Myers Road Network (5.7 meters).

6.6.2 Case Study-II: Impact of Network Size

This section reviews the impact of network size on the signal strengths at the receiver. In undertaking this simulation, the designated SWER network of has been simulated with different segment length multipliers. Table 20 summarises simulation parameters showing the length of the simulated network and the distance between the transmitter and receiver.

The injection method is the coupling capacitor-based injection and the injection sequence is as per that shown in the Fig 6.9. Fig 6.16 shows the case when all segment lengths of the default Myers Road SWER network is multiplied by a factor of two. As shown in Fig 6. 16, signal strengths get weaker when the network size is increased. This is more noticeably at

higher frequencies. For example, at 50 kHz, the change is only -3.15 dB, but at 150 kHz, deviation increases to -28 dB; significantly larger compared to 50 kHz. Hence, the higher frequency tones are clearly more impacted by an increase in network size.

Table 20 : System Simulation Parameters 2

Simulation Parameters	Value
Injection Method	Coupling Capacitor
Configuration/SWER TR Type	Isolated/270 MVa 1 LVa
SWER Network Height	6.7 meters
ASG Setting	5 V RMS
Original Myers Road Network Size	10.2 km network; 3.6 km between RX and TX
Network Scaled by Two	20.4 km network; 7.2 km between RX and TX
Network Scaled by Three	30.6 km network; 10.8 km between RX and TX

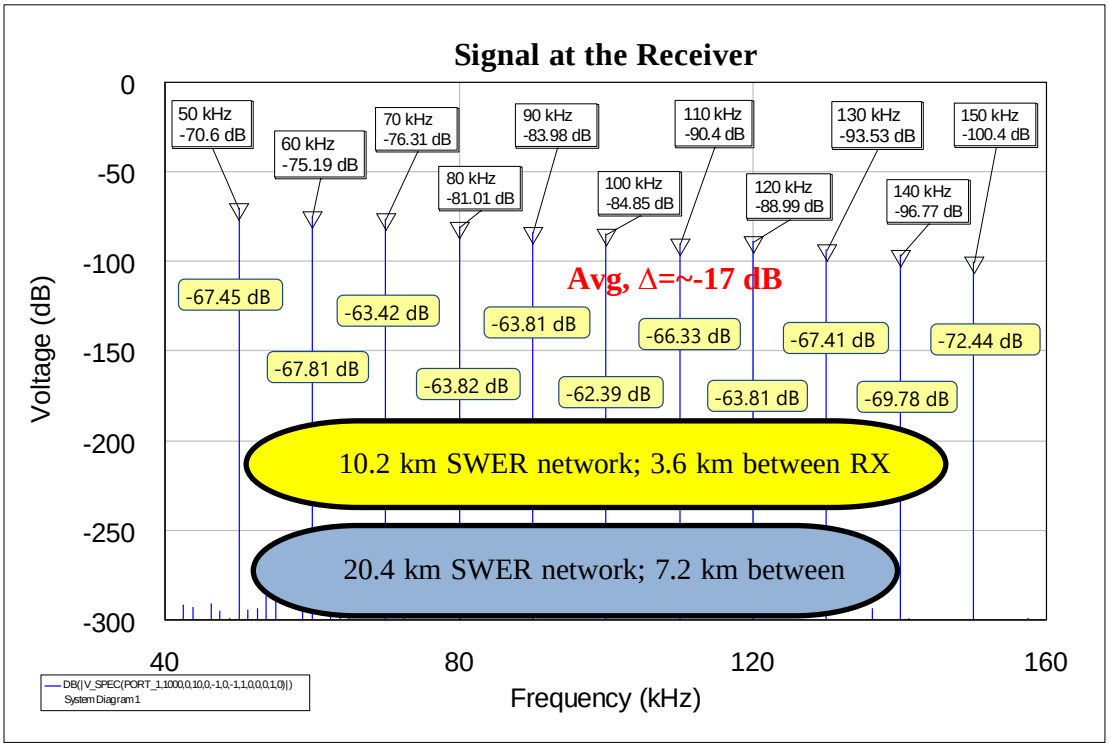

Fig 6.16: Simulation of the Myers Road Network (Size × 2).

Similarly, Fig 6.17 provides a comparison between the default Myers Road SWER network case and the same network enlarged by a factor of three. The markers show the predicted

signal strengths at the receiver for the enlarged network case. The yellow coloured notes show the signal strengths that were computed for the original network. The results clearly demonstrate that higher frequency carrier tones would suffer more from attenuation in a potentially larger network. For example, at 50 kHz, the change is -17.42 dB whereas at 150 kHz, the change is -48.96 dB. Therefore, in larger networks, a transmission bandwidth in the lower frequency band of the CENELEC standards can be considered, though it can also add some noise at this lower band PLC propagation

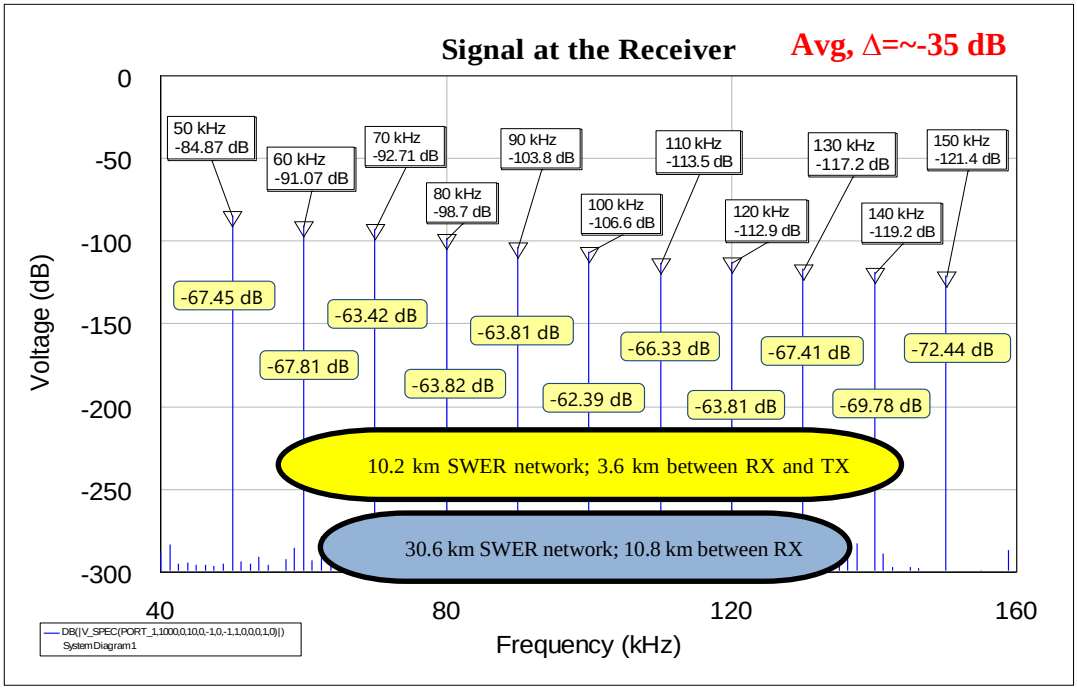

Fig 6.17: Simulation of the Myers Road Network (Size × 3).

6.6.3 Case Study-III: Impact of TR Loading

This section simulates the designated SWER network for the 270 Ω MVa-to-1 MΩ LVa SWER TR case. Table 21 shows the summary of the simulation parameters. The injection method is the coupling capacitor-based injection and the input sequence follows the similar pattern shown in Fig 6.10.

The received signal with different SWER transformer loading condition as shown in Fig 6.18 conceals that, the SWER transformer loading has no major impact on the signal strengths. The notes of yellow background show the signal strengths expected at the receiver when all SWER transformers are terminated by a 1-Ω load at the LV secondary. The markers show signal strengths expected at the receiver when the model is changed in such a way that

the 270 MVa-to-1M LVa SWER TR model is used. As shown, there is no noticeable variation between the two cases.

Table 21 : System Simulation Parameters 3

Simulation Parameters	**Value**
Injection Method	Coupling Capacitor
Configuration/SWER TR Type	Isolated/270 MVa-to-1M LVa
SWER Network Height	6.7 meters
ASG Setting	5 V RMS

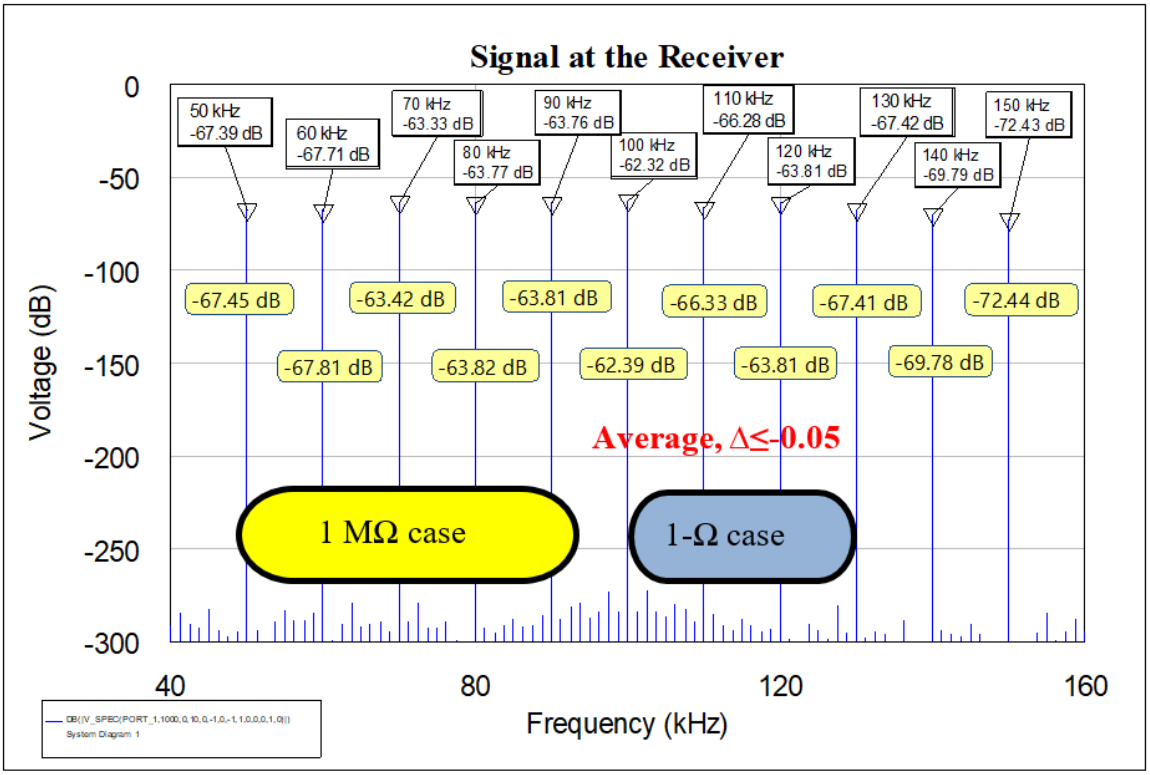

Fig 6.18: Isolated Myers Road Network Simulation (270 MVa -1M LVa TR) case.

6.7 Discussion of the above Results

All High-Frequency (HF) models, developed in this study, included offline models derived from HF Touchstone data (s-parameter recordings) recorded by a Vector Network Analyser (VNA) when the components under test (SWER distribution transformer, and

SWER isolation transformer) were de-energised. The PLC signal strength for the isolated SWER network is higher than the energised SWER network. This implies the fact that in energised SWER network, PLC signal penetrates through the isolation transformer. However, the close match between the predicted and measured signal subcarrier strengths for both the energised (online) and de-energised (offline) cases (as shown in the Fig 6.12 and Fig 6.14) evidences accurate modelling. Conclusions drawn from the analysis of the isolated Myers Road AWR model can be summarised as follows:

- In the energised SWER network, a line trap could be used on the HV side before the isolation transformer to block PLC signal transmission into the 22-kV multiphase grid and to keep the signal strength higher within the SWER network. This will also block noise from the grid improving any correlation functions at the receiver.
- Signal strength predictions by the AWR model are within 2-3 dB of the actual recorded measurements from the 7th of August 2018 test for the isolated (de-energised) SWER network tests. Similar deviation, from the field tests results on the 14th of December 2018, in the order of 2-3 dB has been observed in the signal strengths by the AWR model predictions for the energised network.
- The transformer loading and conductor height above ground have negligible impact on the attenuation of the HF signals. The SWER transformer loading was seen not to have a major impact on attenuation and hence it does not impact the accuracy of the model compared to real world measurements.
- The network size impacts signal strengths more noticeably at higher frequencies. For example, when the Myers Road SWER network size was grown by a factor of two, there was only -3.15 dB change at the 50 kHz subcarrier tone and a -27.96 dB change at 150 kHz subcarrier tone. For the Myers Road SWER network, when its size was grown by a factor of three, the change was -17.42 dB at the 50 kHz subcarrier and -48.96 dB at the 150 kHz subcarrier.
- Along with the above an important point to be mentioned, this research has been mainly focused to analysis the feasibility of the PLC technology to be used for fault detection in a SWER network. Therefore, data communication was not a concern at this stage. Hence, phase analysis of the signal has not been included in this work. But, in future that could be a definite matter of interest.

6.8 Various Faults of SWER line

The construction of SWER line is not like the conventional power transmission line. SWER line consists of a single line that runs through hundreds of kilometres through forests and the countryside. Therefore, the faults in SWER line are different in nature. The faults in SWER line can be mainly classified into the following three types such as a line to ground high impedance faults, low impedance short circuit faults, conductor breakage and open circuit fault. This section presents modelling of HIFs, low fault impedance short circuit faults, and open circuit situations in the Microwave Office platform to be embedded into the case study network to study their impacts on the PLC transmission with regards to the spectrum of the received signal and forward complex transmission coefficient (S_{21}).

6.8.1 Short Circuit Faults and Open Circuit Faults

SWER line runs through forests with abundant vegetation with high tension on the conductor. Generally, a line to ground fault on the SWER transmission line could occur when the conductor drops to the ground or contacts the tree branches or vegetation. The line to ground fault can be a line to ground HIF or a low impedance short circuit fault. Such types of failures may occur in power system due to many reasons such as high-speed winds, falling branches off a tree, lightning, and etc. In the cases of open circuit fault, a conductor may break due to the contact of falling tree branches disconnecting the source and load ends, but it fails to make contact with any low-impedance or high-impedance surface.

6.8.2 High Impedance Faults

A High Impedance Fault (HIF) is one of the most frequent faults that occur in the SWER line. It occurs when there is vegetation contact to the conductor, and the conductor breaks contacting a high impedance surface on the ground. A high impedance ground fault may occur when the energized phase conductor makes an unwanted contact with surfaces of low conductance such as the road surface, sidewalk, lawn or tree branch. HIFs represent one of the most difficult problems for fault detection in the power transmission and distribution networks. In the context of a power network, HIFs are short circuits between energized parts of the power system that are hard to detect using traditional protection relays since these faults draw very low currents and they are hard to be differentiated from potential load increases.

Fig 6.19: Fire creates due to HIF on trees [121]

The most common physical mark of the HIF is the way that it frequently generates electric arcs, which lead to fire ignition on the vegetation. This kind of faults can be called as high impedance arcing fault. The arc starts once the value of the voltage of the conductor touching the surface or vegetation surpasses a voltage limit, known as break down voltage. Therefore, the arc extinction occurs once the voltage moves down to the break down voltage. In each cycle, the HIF results in at least two arc re-ignitions and two arc extinctions. In addition to the low current magnitude and accompanied arc, a HIF results in several physical and electrical characteristics such as intermittence of the arc, asymmetry in the current waveform, randomness and non-linearity in current magnitude, extreme low and high frequency components in the current and voltage waveforms etc.[122-124]. Fig 6.19 shows a fire scene after the occurrence of a HIF.

6.8.3 Conventional Power Line Protection Schemes and HIF Challenges

Conventional protection schemes like-over current, directional over current, distance protection, line current differential protection etc. are currently being popularly used in power line protection schemes. Few communications signal-based pilot protection scheme like Directional Comparison-based Blocking (DCB) and the Permissive Overreaching Trip

(POTT) type protection techniques are being used in pilot basis in some places [125, 126]. The DCB protection method uses the directional relays in different terminals of the network and adopts PLC equipment to transmit signals to the protection zone. In short, if there is a fault occurring in the reach of forward direction of the relay, the signal will trip the relay. On the other hand, if the faults occur in the range of reverse protection relay, it will protect the zone by sending a trip signal. The reverse terminal PLC device will also send a blocking signal to the forward direction relay and controls the trip of the network [126] . The above traditional protections schemes can detect all the symmetrical and asymmetrical line faults by considering the difference between voltage and current of various phases. The fault current of HIF is very low and therefore it is difficult to detect these faults through conventional protection devices such as distance or overcurrent relays. Besides, in cases when transmission network contains a variety of connected nonlinear loads, the detection of such a fault is even more challenging, because HIF currents and nonlinear load currents may have similar RMS values. Hence, it is becoming very difficult for the conventional devices to make a distinction between HIF current and rated current of nonlinear loads to detect these faults.

The nature of HIFs is complex. For example, when the conductor first strikes the high impedance surface, arcing will develop. Often the strike will not be clean, and many strikes occur simultaneously, which will cause multiple arcs. Even when the conductor and object has physically settled, the contact between the two is often not adequate to pass electricity without some arcing between them. The arcing identifies itself as a high frequency voltage spike or RF transient that can be potentially detected down the line. This depends upon the magnitude before intrinsic characteristics of the line to filter it out. The poor connection between the conductor and grounded surface gives rise to an intermittent conduction scenario adding to the earth fault signature. Many methods have been trialled to cover all possible scenarios of HIF [49, 51, 52]. However, due to the variant nature of HIFs and load profiles, these faults are difficult to detect effectively by the common detection techniques.

The main concern of HIF detection is the detection of arc over the power line, because arching is a consequence of HIFs. The detection of the arcing itself could present an opportunity to detect HIFs and protect against bushfire ignition. There are three main approaches for detecting arcing. These include frequency domain methods, where periodic

Fourier transforms are applied to current and voltage signals and compared to known arcing spectral signatures [121, 127-129].

Table 22: Different HIF detection methods with associated shortcomings

Selection Criteria		HIF techniques	Short comings
Measurement		Current measurement	Current transformers are used to measure the line current. The informative part of the HIF current would be lost before reaching the processor which makes this technique less efficient.
		Voltage measurement	The current magnitude of HIF is very low which creates negligible voltage drop, which may not be detectable by voltage measurement technique.
		Current and voltage measurement	This technique requires other facilities like GIS and other remote sensors which makes this economically less viable.
		Magnetic field intensity	This method provides more reliable results but still not feasible in terms of complexity and excessive cost.
Analyzing Domain		Time domain	This technique considers an infinite frequency window while analyzing. It results in the loss of critical frequency domain information, decreases their ability in accurately extracting the HIF signature.
		Frequency domain	Narrow high frequency transient is a challenge to use frequency domain in HIF detection.
		Hybrid domain	Hybrid domain methods require high computational capability compared to the other domains.
Classifier		Simple threshold	The complicated nature of the HIF often necessitates more complex classifiers which is out of the scope of simple threshold method.
		Threshold and counter	This method requires bigger memory and it cannot identify the volatile HIFs.
		Artificial neural	Observations in each layer and huge number of iterations diminish the objectivity of the ANN based
		Other classifiers	Beyond the above other classifier such as fuzzy, Neuro fuzzy etc. are higher state of productivity in identifying the HIF. But the complexity and requirements high computational resource are main

Time domain methods, which compare certain aspects of voltage and current waveforms to known arcing waveform signatures, are also widely utilised. Non-conventional methods such as wavelet analysis, are growing in popularity, where time and frequency domains are plotted against each other and compared against known arcing signatures. Therefore, the main theme of power line protection scheme is the efficient detection of HIFs signature. Unfortunately, these similar signatures also appear when various types of loads are present on the line. Modern power electronics devices such as inverters and motor controllers can

exhibit similar signature to certain HIFs. As a result, most of the techniques are being proved inefficient in detection of critical HIFs of power line. A comprehensive summary on HIFs detection techniques published by different authors [121, 123, 127, 130] have been included in Table 22, which also includes the shortcomings of all the methods.

6.8.4 Arc Resistance and High Impedance Fault Models

The occurrence of a HIF is closely associated with an arc, which is a biproduct of the faults. HIFs naturally initiates arc and in most of the cases, bush fires may start because of the undetected arc persisting on the power line. To characterize the HIFs, a lot of researchers [131-133] used arc resistance models. The characteristics of the arc resistance is dynamic, so it varies with parameters such as the fault current, arc length and the circumstance of the fault scenario. The researcher Andrade [131] , has summarized some of the well-established equations for the arc resistance, which are given below:

$$R_{A1} = \frac{28707.35 \times L}{I^{1.4}} \tag{6.1}$$

$$R_{A2} = \frac{1804.46 \times L}{I} \tag{6.2}$$

$$R_{A3} = (\left(\frac{950}{I} + \frac{5000}{I^2}\right) \times L \tag{6.3}$$

$$R_{A4} = \frac{G \times L}{I} \tag{6.4}$$

$$R_{A4} = (\left(\frac{855.30}{I} + \frac{4501.58}{I^2}\right) \times L \tag{6.5}$$

$$R_{A5} = \frac{1443.57 \times L}{I} \tag{6.6}$$

For all the equations R_A stands for the arc resistance, L is for the arc length and I is the fault current. To establish these equations, researchers such as Warrington [134, 135] and Terzija [136, 137] did extensive experimental works considering different voltage levels, various fault situations, diverse weather conditions, and circumstances.

Considering the dynamic characteristics of the arc resistance, several researchers [138-140] have developed HIFs models to use when analysing network performances. These models consist of various diodes, DC sources, and multiple resistor combinations and are

able to exhibit the equivalent dynamic HIF resistance. Some research works [141, 142] have reviewed various HIFs models. Amongst those, few well-established models are shown in Fig 6.20. Any of these given circuit models can be used to represent HIFs in network simulation.

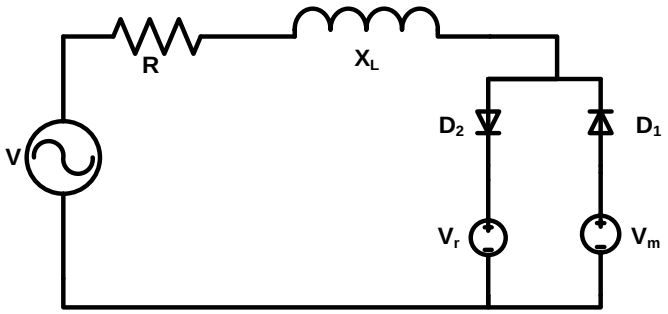

Fig 6.20 (a)

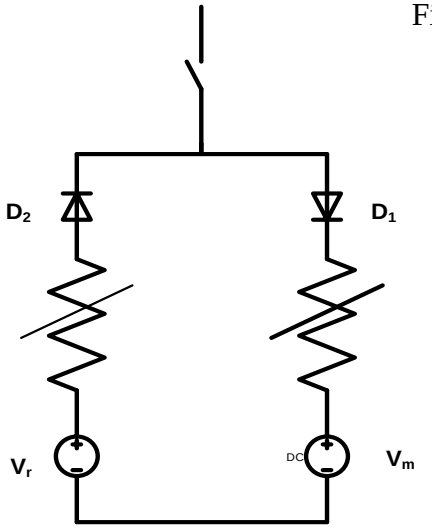

Fig 6.20 (b)

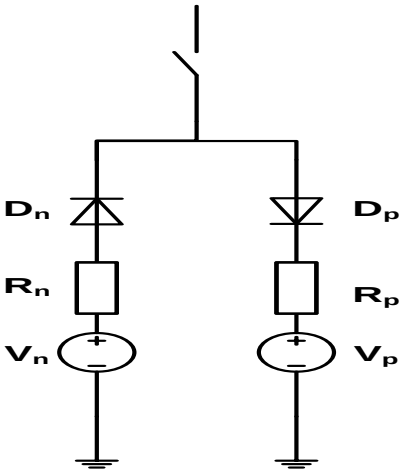

Fig 6.20 (c)

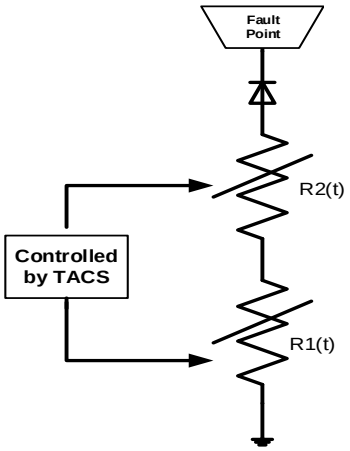

Fig 6.20 (d)

Fig. 6.20: Various HIFs models [141]

It has been mentioned that, the impedance characteristics of HIFs is dynamic and nonlinear which depends on the arc-length and extinction time. All of the above diode-based models intend to represent this dynamic character of the HIF resistance [49, 143]. Models of Fig 6.20(a) to Fig 6.20(c) are purely based on diode configurations, where DC voltage sources like V_n, V_p, V_r, V_m are used to replicate the arcing voltages responsible to initiate the faults. The resistances on the models (R_n and R_p) are used to build the arc resistance between the fault contact and vegetation, or other high impedance surface. Fig 6.20(d) represents a TACS algorithm-based HIF fault model, which basically senses the fault current and voltage and use this algorithm to generate random fault resistances R1 and R2 as shown in Fig 6.20(d). The dynamic changes in the DC voltage generates a randomly varying fault impedance magnitude, which in turns create the HIFs fault signatures in the network.

6.9 Impacts of Faults on PLC Propagation

To observe the impact of the HIFs on the SWER network, an arc model developed by Warrington [134] and an diode based fault model developed by Emmanuel [140] have been re-build in the Microwave Office platform. Both circuits modelled using the Microwave Office platform are shown in Fig 6.21. To analyse the network performance, the developed fault models have been applied to the case study SWER network in subsequent section.

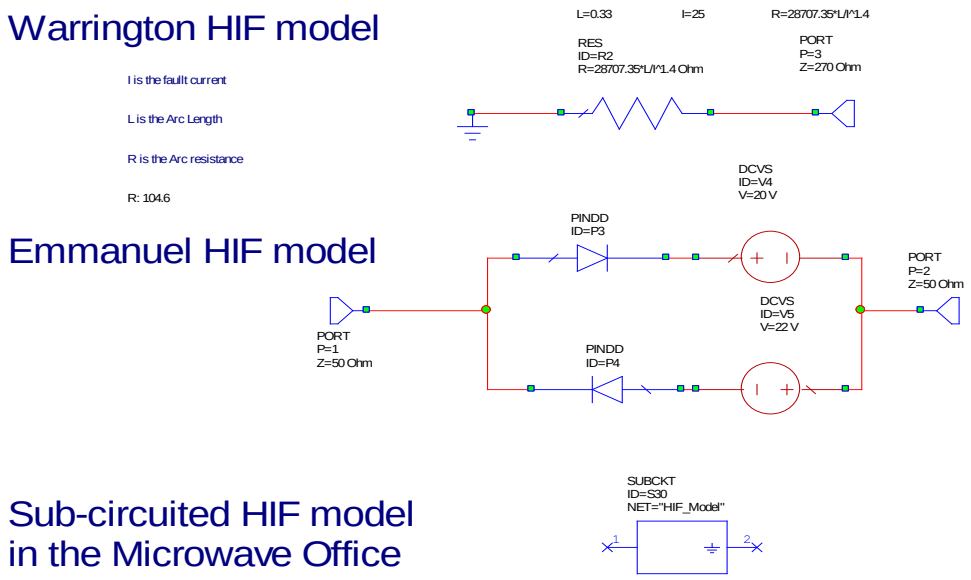

Fig. 6.21: Various HIF Models in the Microwave Office

For the analysis, the Myers Road SWER network has been replicated and the Warrington Arc HIF model [134] has been applied between the Poles 13 and 14 of the network. Fig 6.22 shows the Microwave Office replica of the Myers Road SWER network with the high impedance fault incidence. In simulation of the arc fault model, fault current has been chosen as 25 Amps and the arc length has been chosen as 0.33 m. HIF resistance was determined as 100.4 Ω. Similar parameters were also referred in following research [131, 144]. Herewith, a list HIFs resistance and fault current are shown in Table 23.

Table 23 : High impedance fault currents and resistance [144]

	Fault Currents	HIF Resistance
Reinforced Concrete	35 to 80 A	90 to 200
Wet Grass	20 to 50	150 to 360
Dry Grass	10 to 25	290 to 720
Wet Sand	5 to 15	480 to 1,500

In this network configuration, the line model, transformer model, transmitter-coupling arrangement, receiver-coupling arrangement have been used as per the individual models previously developed and discussed in the previous chapters. The network has also been tested with diode-based fault model and similar performance has been observed.

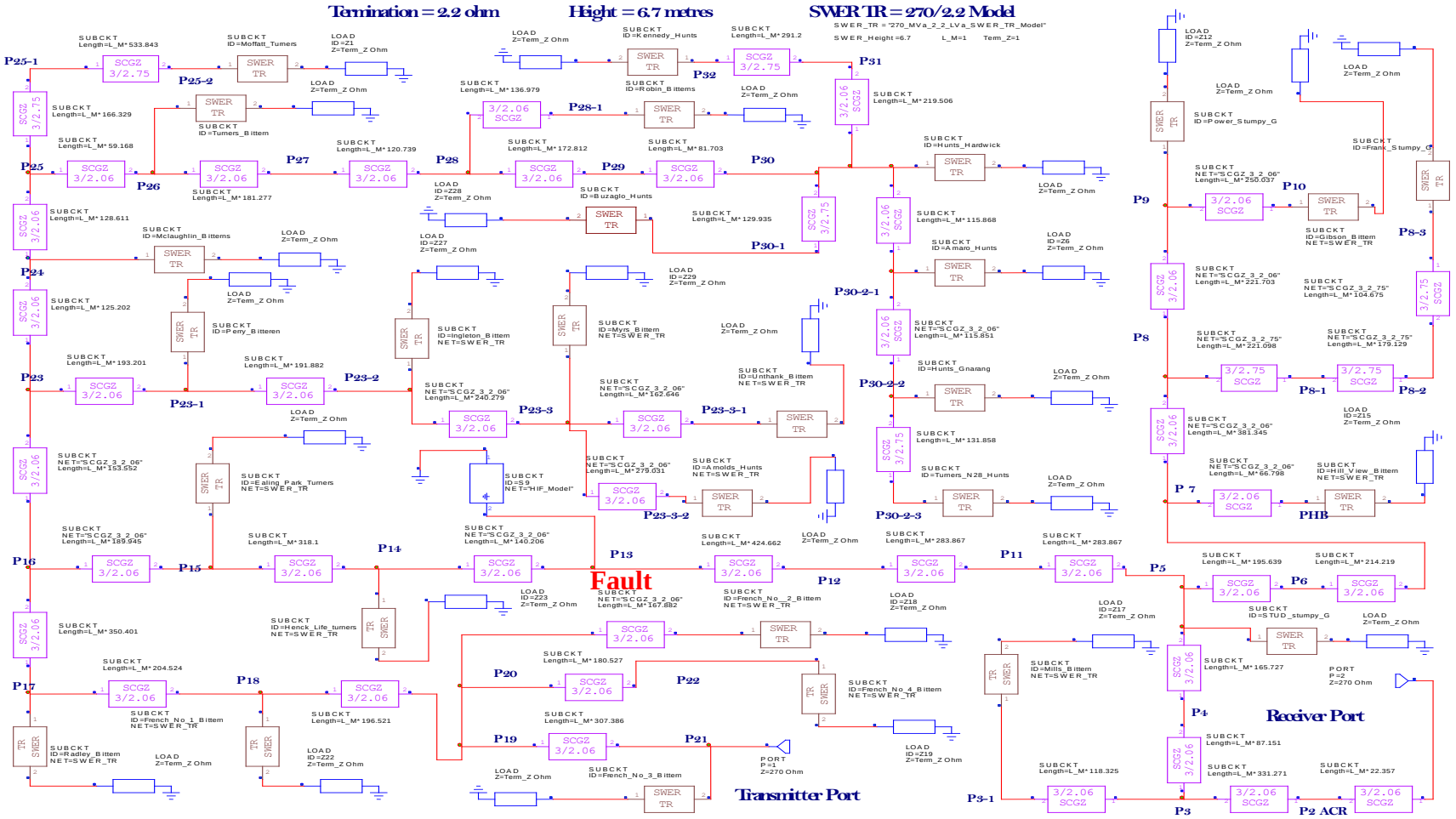

Fig 6.22: Myers Road SWER Network Model with Various Faults

6.9.1 Impacts HIFs on PLC propagation

In this subsection, the impact of HIFs on network has been observed in terms of the forward transmission characteristic as well as the PLC signal tone strength comparison. Fig 6.23 shows the S21 (attenuation graph) for the two network configurations with and without the HIF, where the fault current has been taken 25 amperes. The curve without HIFs represents an attenuation of -24 dB to -29 dB in the 50 kHz to 150 kHz PLC signal transmission range. On the other hand, the S21 curve with the HIF shows a much larger attenuation of -48 dB to -50 dB in the same range of PLC signal. The difference between the two attenuation levels is approximately -20 dB in terms of S-parameter comparison. This shows that when a HIF occurs on the network, it will draw the high-frequency signals resulting in the potential loss of the OFDM signal at the receiver due to a poor signal-to-noise ratio. Such a loss of the OFDM signal can potentially indicate the occurrence of a fault and this information used to trigger the operation of the circuit breaker.

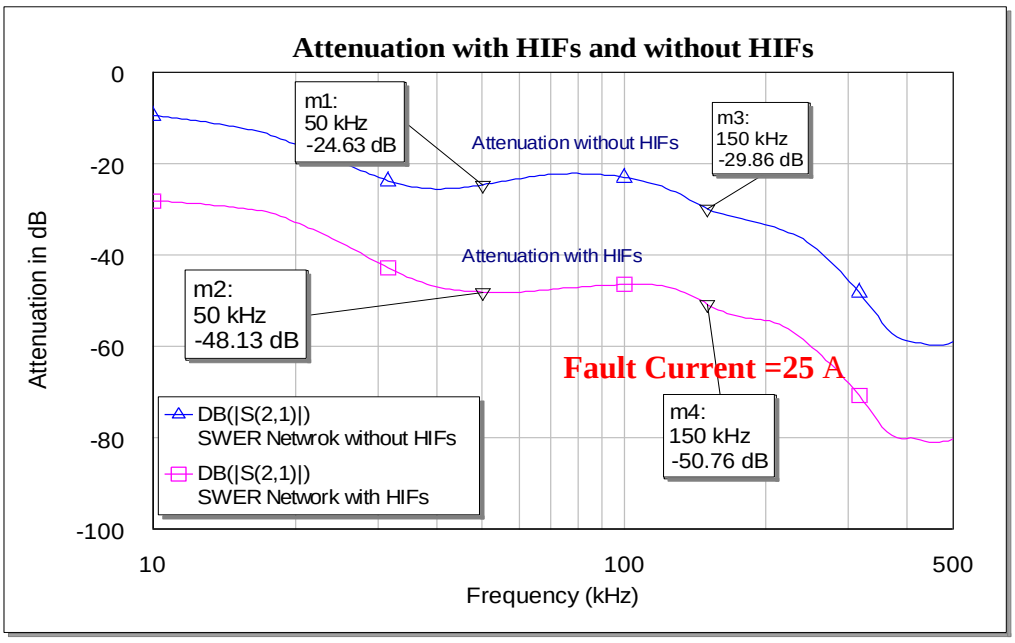

Fig. 6.23: S21 curve of Myer Road SWER network with and without a HIF

From these two attenuation values with average PLC input reference voltage (V_{in}), the received output voltage (V_o) can also be estimated using Eq. (6.8)

$$L_v = 20\log_{10}\frac{V_{in}}{V_o}\,dB \qquad (6.8)$$

Table 24 shows the receiver end comparison of the received signal strength with and without HIFs. The values of output voltage reveal the fact that, for a 5 V PLC signal input voltage, output voltage at the receiver end will be very low (0.15 V) in a network penetrated by a HIFs. In a healthy network, the received signal strength would also be double. This abnormality in the signal voltage level at the receiver end will give hints about the existence of the HIF in the network. A similar outcome has been observed with system level simulation in case of a PLC signal strength comparison, which compare the PLC signal tone strength with and without the fault scenario. Fig 6.24 shows that due to effect of the HIF, the deviation in the tone strengths is more than -20 dB. Therefore, while analysing the received signal spectrum, such a sudden loss in signal strength can be linked to a HIF occurrence.

Table 24: Received PLC signals voltage comparison with HIFs and without HIFs

Cicuit Configuaration	Insertion Loss Value	Transmission Voltage)	Received Signal Voltage
With HIFs	-25 dB	5 V	=~0.15 V
Without HIFs	-50 dB	5 V	0.3 V

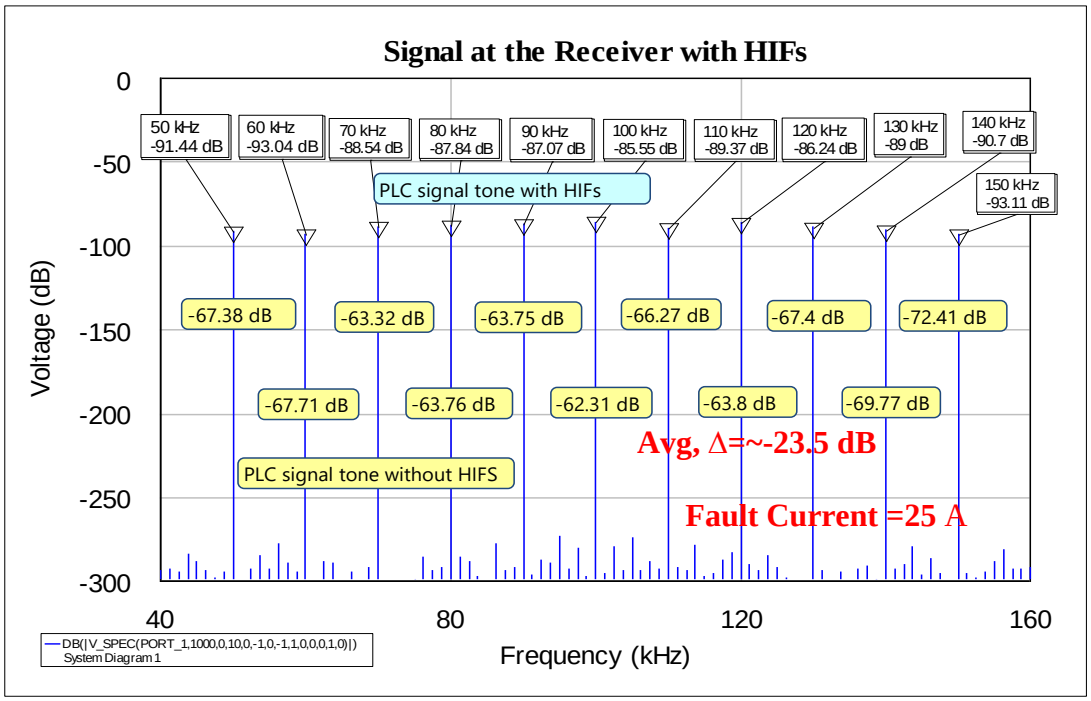

Fig. 6.24: PLC signal tone with HIFs and without HIFs

Though the reference referred to a higher arc or HIFs current, in some cases, the fault current likely to be very low, for this reason another HIFs spectrum analysis has been done with a lower fault current, which has been considered as 2 amperes. The spectrum has been shown in fig 6.25.

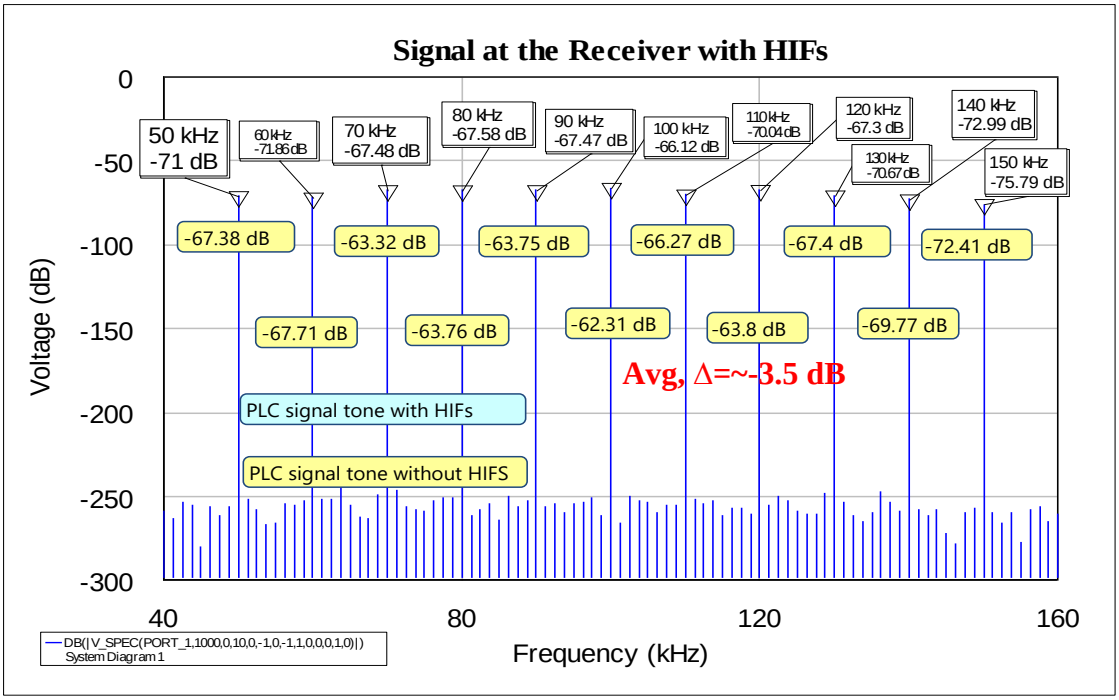

Fig. 6.25: PLC signal tone with HIFs and without HIFs

The new spectrum analysis shows the reduction in fault current, significantly reduce the deviation between a faulty signal and normal signal. In current situation, the deviation is -3.5 dB, whereas previously the deviation was more than -20 dB. However, still the sensitivity between a signal with faults and without faults is enough to discover the HIFs signature from the signal spectrum.

In this HIFs, case analysis, the PLC signal is considered to be propagating continuously and the fault is considered to be of persisting nature. For example, a dry tree branch making contact with a conductor, which will divert the PLC signal to the ground, which will reduce the strength of the received PLC signal.

Therefore, by differentiating the level signal strength, any kind of disturbance in the SWER line like change in load or HIFs can be identified. Table 25 shows the deviation in signal strength due to a worst-case loading condition and two different HIFs impacts.

Table 25: Attenuation measurement for loading and HIFs impact

Frequency Components (kHz)	Signal Attenuation for worst case loading (1 Ω) of SWER line (dB)	Signal Attenuation with HIFs, Fault current 25 A (dB)	Signal Attenuation with HIFs, Fault Current 3.5 A
50	-67.39	-91.38	-71
60	-67.71	-93.04	71.85
70	-63.33	-88.54	-67.48
80	-63.77	-87.84	-67.58
90	-63.76	-87.07	-67.47
100	-62.32	-85.55	-66.12
110	-66.28	-89.37	-70.04
120	-63.81	-86.24	-67.3
130	-67.42	-89.7	-70.67
140	-69.79	-90.7	-72.99
150	-72.43	-93.11	-75.79

The values in the above table show that the impact of loading on SWER line is marginal which has already been discussed in the previous section. But, in case of HIFs higher fault current contributes to the higher attenuation. For example in the 25-A case, the average deviation from the nominal signal is around 23 dB, whereas for the 3.5-A fault, the average deviation goes down to 4 dB. Therefore, from the level of attenuation it can be easily differentiated what kind of disturbance has happened in the network.

6.9.2 Impact of Open Circuit and Low-Impedance Short Circuit Faults

In the case of an open circuit fault or short circuit fault, the PLC signal will not reach to the receiver end. If the conductor breaks, then the PLC signal cannot be transmitted over to the receiver end. Alternatively, if a conductor makes contact with low impedance surface, the PLC signal will flow to the ground rather than to the receiver end. Both incidents have been analysed using the designated SWER network AWR model between Pole #13 and Pole

#14. Fig. 6.26 shows the network section with the fault. Similar attenuation analysis has been performed between the transmitter and receiver end forward transmission characteristic. The measured S-parameter curve is shown in Fig 6.27 which points to complete loss of the signal.

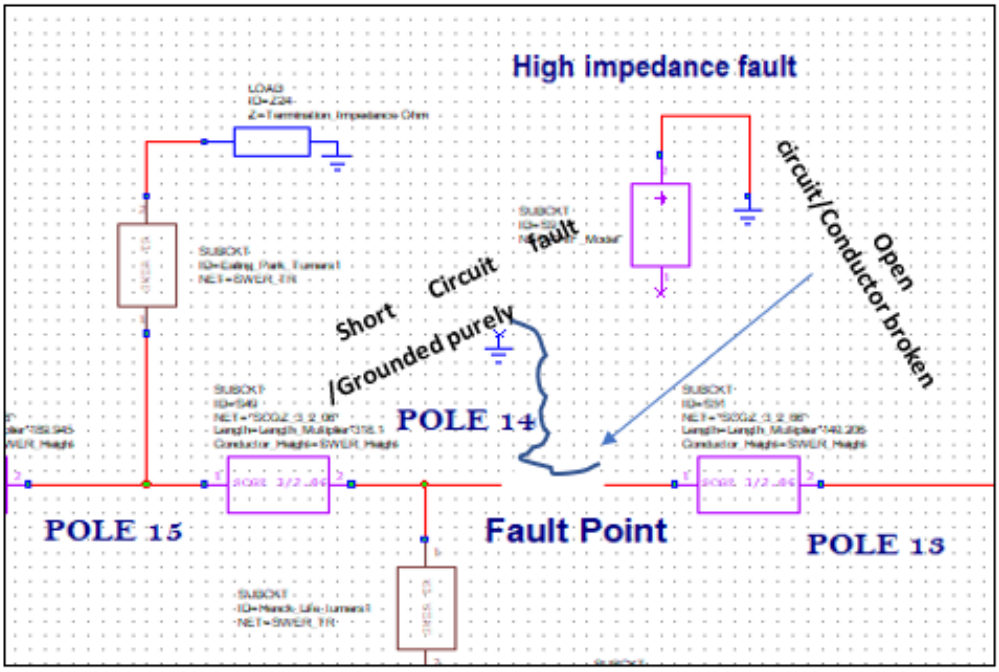

Fig 6.26: Faulted Point of the Myer Road SWER Network

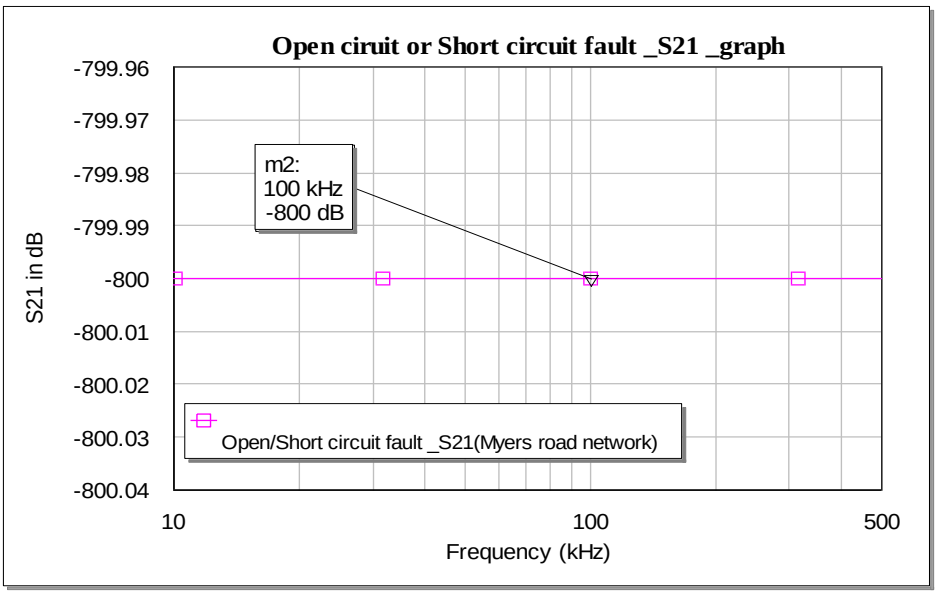

Fig 6.27: Insertion loss curve of open circuit/short circuited SWER network

6.10 Conclusion

This chapter has presented HF modelling of a SWER distribution network as the communication channel for potential PLC applications. Narrowband modelling of an exemplary SWER network was the main highlights. HF modelling of overhead conductors, SWER transformers, a capacitive coupling circuit, and the receiver end measurement system has been presented with the objective of incorporating all these distinct models into an end-to-end system simulation model. All the essential network elements such as transformer design, SWER line model, coupling circuit has been adopted from the design described in the previous chapters. HF modelling of an entire network has enabled simulation of the overhead network to predict PLC signal tone strengths for a number of cases including the de-energised and grid connected network scenarios. Results show high accuracy between the actual measurements and model predicted signal strengths with a mean error rate of 2.27 dB and 3.10 dB across the frequency band for the de-energised and grid connected cases respectively. Some significant case studies have been carried out in this chapter, for example on impact of conductor height, impact of different loading conditions, impact of overall network size and various faults on the PLC propagation test have been analysed.

The findings of the case studies can be summarized as follows. PLC propagation has been tested with two different standard pole height such as with 5.7 m and 6.7-meter, negligible impact was found with the change of conductor height. To observe the impact of the transformer loading on the PLC propagation, two extreme loading conditions of the SWER distribution transformer have been tested including the 1 Ω and 1 MΩ cases. Secondary loading had very low impact on the signal propagation. In the case of network size, network size and the direct distance between the transmitter and receiver had significant impact on the PLC propagation. For example, the attenuation of the received signal for the designated SWER network of 10.2 km long was found around -67.45 dB. With a two-fold increment on the network size, attenuation increases to -70.6 dB and with a three-fold increment, it becomes -84.87 dB for a 50 kHz frequency component. The deviation keeps increasing with higher frequency components like 100 kHz, 150 kHz etc. This chapter also includes a brief modelling study on various faults of the SWER line such as the short circuit, open circuit and high impedance faults. Emphasis has been given on HIFs, various HIF models have been studied and impacts of these faults on PLC propagation over the SWER network observed.

Chapter 7

Conclusion and Future Work

7.1 Conclusion

The originality and significance of the various aspects of the research outlined in this thesis has been demonstrated by discussions and analysis provided in different chapters. This starts with an updated survey which includes the internal description of some of the major technical components of PLC systems such as various line traps, line tuner, drain coils, coupling capacitor etc. Critical implementation challenges such as the frequency-based impedance measurement, appropriate frequency band selection process, and coupling circuit design have been addressed. Along with the challenges, other important factors such as attenuation and the impact of network noise have been highlighted in the literature survey. The findings addresses issues that are currently under major investigation from the network community. The survey also provides some good directions for future research from an industrial perspective.

Followed by the survey section, an off-the-self novel L-C impedance matching coupling circuit has been designed, tailor built, and described in this thesis to inject PLC signals through a commercial HV capacitor to the SWER line. The coupling circuit has been described with specific circuit design and experimental validation. Results have been represented in terms of attenuation and reflection characteristics on the specific PLC signal band. The coupling circuit could be used for any kind of high voltage PLC applications, therefore the design offers a starting point for the future PLC based IoT research or any other application area such as broadband ADSL.

In the SWER line modelling section, three different types of SWER conductors have been modelled using an analytical approach considering all the necessary parameters such as the conductor size, pole height, skin depth, soil conductivity etc. The line model has been built in the Microwave Office platform and various analysis has been presented with respect to attenuation and reflection characteristics of the conductors. Few significant observations

have been developed based on the relationship of attenuation with frequency and length. For example, at a constant frequency, it has been determined that the longer is length of the SWER conductor, the higher is the attenuation. At a constant SWER conductor length, the higher frequency carriers experienced higher attenuation. Besides, with an increase in length, the attenuation of a SWER conductor changes at a higher rate with respect to the change of frequency. All the other conductors also follow the similar mathematical relation with length-based frequency dependent attenuation. These finding can be used as a benchmark in future extension or up-grades of a SWER network.

In this thesis, a novel hardware-in-loop high frequency transformer modelling technique has been developed which employs the use of measured s-parameter data to replicate the frequency response of a SWER transformer with respect to various loading conditions of the transformers primary and secondary windings. Along with the transformer model, a simplified VNA based impedance measurement technique has also been described. Impedance measurement and s-parameter transformer modelling methods can be used for addressing future HF transformer research questions on winding fault detection, saturation parasitic element value finding etc.

In the final chapter of this thesis, an end-to-end network model has been presented which is simulated and findings compared with results from field injection tests. The thesis provides the sophisticated PLC-transmitter side and receiver Data Acquision configurations. The propagation tests were carried out in on-line and off-line modes. The minimal error of few dBs between the test and simulated results justify the accuracy of network model. After the justification of this accuracy of the network model, various case studies on the impact of network size, impact of pole height, impact of transformer loading on PLC signal strength have been analyzed considering largely the attenuation of the PLC signal. Based on the undertaken case studies, some significant observations have been noted such as the pole height and transformer loading having minimal impact on the PLC propagation over a SWER network. On the other hand, the network size was determined to have a significant impact on PLC propagation as perhaps expected. For example, a two-time expansion of the network size was seen to increase signal attenuation by 20 dB.

Along with the above chapter by chapter findings, some important points can also be included about this research. For modulation in this work, OFDM is the utilised technique. Other techniques can be applied, but commercial installation of this setup does not require any proprietary standards because the designated frequency is in the well-established CENELEC band, which is dedicated to various power line applications. About PLC coupling technology, the HV-capacitor based injection is still the best choice due to the availability of the capacitors, but some other options like the medium voltage earth side injections, transformer's low voltage side injections can be a matter interest in future.

This work has focused on all the intended set objectives presented sequentially in each chapter. The discussion in all chapters was enriched with literary contents, technical analysis, mathematical modelling, and experimental validations. Along with literary contents and technical explanation, all significant contributions and critical observations have been highlighted in each chapter. This work also provides some good directions for future research and have its own merit from various industrial perspective. Thus, the work has potential and could have long-term reference value.

7.2 Future work

The works undertaken shade light on various significant technical aspects of PLC based system applications with a lot of scope for future research. Though the research is based on the specialized Australian SWER distribution network context, it has global appeal as SWER networks are popularly used all over the world in different parts of the world. These include African countries such as South Africa, Uganda, Kenya, South Asian nations like India, Nepal, Bangladesh, and South American countries such as Brazil, Chili, and some parts of the USA. In the presented survey, the identification of the critical challenges such as the importance for frequency selection, issues related to the coupling circuit design, noise encounters with measurements, digital transmission techniques have been highlighted. These are all different dimensions of future work that require further attention to.

Along with the literary findings, this thesis also highlights major observations in each one of the chapters. For example, in Chapter 3, the consideration is on the development of a HV-coupling capacitor matching circuit. Besides presenting design and development using off-

the self-components, the work presented also revealed knowledge gaps. Future work could focus on the development of a coupling circuit avoiding the HV-capacitor, which would reduce the cost of the coupling circuit significantly. This could be carried out in future works because an innovation of this nature would be ground breaking and could advance the uptake of PLC applications in communication signal based IoT applications like remote load controlling, and plug in electric vehicle energy management.

The methods of SWER line modelling could be a benchmark for future frequency-based power line modelling applications. This work had presented some mathematical analytical analysis of the SWER conductor behavior; for example its frequency-dependent attenuation characteristic. These findings will be helpful for future research in extending, developing and modelling SWER networks of any size. The developed models could also be useful towards future load modelling and energy management of SWER networks.

The works done in the field of SWER transformer modelling is also very significant for any future work. The simplified impedance measurement method could be applied for any transformer winding impedance measurements. The development of the touchstone file based SWER transformer modelling with respect to various loading conditions is also very significant in driving future high frequency transformer research. This method would help researchers in avoiding the high configuration CAD software based complex models to find out the parasitic element and frequency response analysis for a transformer. Along with this specific finding, the proposed ideas could be adopted for any kind of lab-based MRI and power line integrated electromagnetic research.

Presented network PLC propagation tests and related case studies are some of the most significant aspects of this research and offer the best potential for future expansion. The test results have justified the real-time applicability of the developed models on the successful transmission and reception of the PLC signal with a predicted strength over the network. This has validated the undertaken modelling and its feasibility in being used as a foundation to assess power system communication channels for any sort of PLC-based application.

This work has also discussed the various faults that could occur on the SWER network. A well-established HIF fault model has been developed and applied to the Microwave Office based SWER network model. The impact of a HIF occurring on the network has also been

visualized by studying the simulated spectrum analysis. The spectral analysis has shown that the PLC signal strength gets reduced, when faults occur, a significant amount that can be identified as an abnormal situation. Herewith, other conventional fault situations such as the open circuit and short circuit faults are also clearly noticeable from the signal behavior and strength. Experts are struggling to find conclusive solutions to the problems associated with HIFs on power distribution networks. The findings of this research could possibly open a window for considering PLC systems in their potential application for fault detection in multi-wire networks as well; a clear motivate for future research in this field.

References

[1] M. S. Nirere, "Design of a Single Wire Earth Return (Swer) Power Distribution System and Improvement of Its Voltage Profile Using Capacitors," JKUAT-PAUSTI, 2018.

[2] J. W. Mitchell, "Power line failures and catastrophic wildfires under extreme weather conditions," *Engineering Failure Analysis,* vol. 35, pp. 726-735, 2013.

[3] A. Burns and B. Eltham, "'Catastrophic Failure'Theories and Disaster Journalism: Evaluating Media Explanations of the Black Saturday Bushfires," *Media International Australia,* vol. 137, no. 1, pp. 90-99, 2010.

[4] B. Stewart, "Design and operation of high voltage R and D test facility for bushfire mitigation technologies," *Chemeca 2016: Chemical Engineering-Regeneration, Recovery and Reinvention,* p. 1007, 2016.

[5] D. Coldham, A. Czerwinski, and T. Marxsen, "Probability of bushfire ignition from electric arc faults," *HRL Technology Pty Ltd., Melbourne, VIC., Australia, Tech. Rep. HRL/2010/195,* 2011.

[6] I. P. Da Silva, P. Mugisha, P. Simonis, and G. Turyahikayo, "The use of single wire earth return (SWER) as a potential solution to reduce the cost of rural electrification in Uganda," 2015: Domestic use of energy conference.

[7] A. Mannan, D. Saxena, and M. Banday, "A Study on Power Line Communication," *International Journal of Scientific and Research Publications,* vol. 4, no. 7, 2014.

[8] S. Mudriievskyi, "Power Line Communications: State of the art in research, development and application," *AEU-International Journal of Electronics and Communications,* vol. 68, no. 7, pp. 575-577, 2014.

[9] K. Sharma and L. M. Saini, "Power-line communications for smart grid: Progress, challenges, opportunities and status," *Renewable and Sustainable Energy Reviews,* vol. 67, pp. 704-751, 2017.

[10] H. Peng, Z. Kan, D. Zhao, J. Han, J. Lu, and Z. Hu, "Reliability analysis in interdependent smart grid systems," *Physica A: Statistical Mechanics and its Applications,* vol. 500, pp. 50-59, 2018.

[11] A. B. Batiller, E. F. I. Bugayong, A. A. Caisip, N. P. Coligado, C. A. C. Padilla, and M. A. A. Pedrasa, "Prepaid metering system for isolated microgrids," in *Innovative Smart Grid Technologies-Asia (ISGT-Asia), 2016 IEEE*, 2016, pp. 529-534: IEEE.

[12] S. C. Pereira, A. S. Caporali, and I. R. Casella, "Power line communication technology in industrial networks," in *Power Line Communications and its Applications (ISPLC), 2015 International Symposium on*, 2015, pp. 216-221: IEEE.

[13] C. Sridhathan and F. Samsuri, "Application of power line communication in healthcare for ECG and EEG monitoring," in *Proc. Of Int. Conf. on Advances in Power Electronics and Instrumentation Engeneering*, 2013: Citeseer.

[14] M. Yigit, V. C. Gungor, G. Tuna, M. Rangoussi, and E. Fadel, "Power line communication technologies for smart grid applications: a review of advances and challenges," *Computer Networks,* vol. 70, pp. 366-383, 2014.

[15] F. Aalamifar, A. Schlögl, D. Harris, and L. Lampe, "Modelling power line communication using network simulator-3," in *2013 IEEE Global Communications Conference (GLOBECOM)*, 2013, pp. 2969-2974: IEEE.

[16] *GC9200 LV PLC modem user guide, GridComm Ltd, (2015)*. Available: http://www.gridcomm-plc.com/product/product_gc9200.htm

[17] M. P. Sanders and R. E. Ray, "Power line carrier channel & application considerations for transmission line relaying," in *50th Protective Relay Conference, Georgia Tech, May*, 1996.

[18] *MCC 124 Coupling Capacitor Datasheet, OMICRON Electronics Ltd, (2017)*. Available: https://www.omicronenergy.com/en/products/mcc-112117-c124-c210/

[19] *Power Line Carrier Coupling Filter MCD80, ABB coupling devices, (2017)*. Available: http://new.abb.com/network-management/communication-networks/power-line-carrier/mcd80

[20] *Power line Carrier Coupling Equipment, RFL Electronics Ltd, (2009)*. Available: https://www.rflelect.com/images/products/pdfs/RFL_9512_RFLprint_updated.pdf

[21] P. S. Communications, "Summary of an IEEE guide for power-line carrier applications," *IEEE Transactions on Power Apparatus and Systems,* no. 6, pp. 2334-2337, 1980.

[22] *Line traps products, Grid Solutions Ltd, (2015)*. Available: https://www.gegridsolutions.com/HVMV_Equipment/catalog/linetraps.htm

[23] M. Islam Rizu *et al.*, "Performance Evaluation of Power Line Communication Channel and Design Power Line Coupler Circuit for Efficiency Improvement," Bachelor of Science in EEE, Military Institute of Science of Technology, Bangladesh, 2015.

[24] P. L. So and Y. Ma, "Development of a test bed for power line communications," *IEEE Transactions on Consumer Electronics,* vol. 50, no. 4, pp. 1174-1182, 2004.

[25] E. Ancillotti, R. Bruno, and M. Conti, "The role of communication systems in smart grids: Architectures, technical solutions and research challenges," *Computer Communications,* vol. 36, no. 17-18, pp. 1665-1697, 2013.

[26] T. R. Oliveira, A. A. Picorone, S. L. Netto, and M. V. Ribeiro, "Characterization of Brazilian in-home power line channels for data communication," *Electric Power Systems Research,* vol. 150, pp. 188-197, 2017.

[27] T. Whiffen *et al.*, "A concept review of power line communication in building energy management systems for the small to medium sized non-domestic built environment," *Renewable and Sustainable Energy Reviews,* vol. 64, pp. 618-633, 2016.

[28] M. Kuzlu, M. Pipattanasomporn, and S. Rahman, "Communication network requirements for major smart grid applications in HAN, NAN and WAN," *Computer Networks,* vol. 67, pp. 74-88, 2014.

[29] Y. Biao, Y.-h. LÜ, and H.-x. Zhang, "Coexistence of broadband power line communication systems," *The Journal of China Universities of Posts and Telecommunications,* vol. 16, no. 4, pp. 125-128, 2009.

[30] K. Okokpujie, E. Noma-Osaghae, S. John, and P. C. Jumbo, "Automatic home appliance switching using speech recognition software and embedded system," in *2017 international conference on computing networking and informatics (ICCNI)*, 2017, pp. 1-4: IEEE.

[31] R. Krishna, R. Siddhartha, N. Kumar, and G. Jogi, "Broadband over power lines (BPL) for Indian Telecom network," ed, 2014.

[32] S. Zhu, C. J. Kikkert, and N. Ertugrul, "A wide bandwidth, on-line impedance measurement method for power systems, based On PLC techniques," in *2014 IEEE International Symposium on Circuits and Systems (ISCAS)*, 2014, pp. 1167-1170: IEEE.

[33] C. J. Kikkert, "An On-line PLC frequency impedance analyzer," in *Smart Grid Communications (SmartGridComm), 2013 IEEE International Conference on*, 2013, pp. 606-611: IEEE.

[34] C. J. Kikkert, "A PLC frequency model of 3 phase power distribution transformers," in *Smart Grid Communications (SmartGridComm), 2012 IEEE Third International Conference on*, 2012, pp. 205-210: IEEE.

[35] C. J. Kikkert, "Modelling power transformers at power line carrier frequencies," in *EEA Electricity Engineers Association Conference*, Christchurch, NewZealand, 2010, pp. 1-6: Electricity Engineers Association

[36] C. J. Kikkert, "Calculating radiation from power lines for power line communications," in *In MATLAB for Engineers-Applications in Control, Electrical Engineering, IT and Robotics*: InTech, 2011, p. 23.

[37] C. Kikkert and G. Reid, "Radiation and attenuation of Single Wire Earth return power lines at LF frequencies," in *Power Line Communications and Its Applications, 2009. ISPLC 2009. IEEE International Symposium on*, 2009, pp. 68-72: IEEE.

[38] G. D. Reid and C. J. Kikkert, "Radiation from a single wire earth return power line," in *EEEvolution Symposium, Cairns*, 2008, pp. 28-30.

[39] S. Rinaldi, P. Ferrari, A. Flammini, M. Rizzi, E. Sisinni, and A. Vezzoli, "Performance analysis of power line communication in industrial power distribution network," *Computer Standards & Interfaces,* vol. 42, pp. 9-16, 2015.

[40] W. Ding *et al.*, "A hybrid power line and visible light communication system for indoor hospital applications," *Computers in Industry,* vol. 68, pp. 170-178, 2015.

[41] P. Mlynek, J. Misurec, Z. Kolka, J. Slacik, and R. Fujdiak, "Narrowband power line communication for smart metering and street lighting control," *IFAC-PapersOnLine,* vol. 48, no. 4, pp. 215-219, 2015.

[42] E. Ruffato, C. Sakurai, and V. Pereira, "Evaluation of communication components for monitoring small hydroelectric plants," presented at the 22nd International Conference and Exhibition on Electricity Distribution (CIRED 2013), Stockholm, Sweden, 10-13 June, 2013.

[43] E. Rufato, C. Sakurai, V. Pereira, J. Ribeiro, and D. Miguel, "Power line communication for monitoring small electricity generating plant," in *Innovative Smart Grid Technologies Latin America (ISGT LA), 2013 IEEE PES Conference On*, 2013, pp. 1-6: IEEE.

[44] P. Petit, J. P. Sawicki, F. Maufay, M. Aillerie, and J. P. Charles, "Optimization of Power Line Communication system using a resonant HVDC bus in a distributed renewable energy generator," *Energy Procedia,* vol. 74, pp. 555-563, 2015.

[45] A. G. Phadke, W. Peter, D. Lei, and V. Terzija, "Improving the performance of power system protection using wide area monitoring systems," *Journal of Modern Power Systems and Clean Energy,* vol. 4, no. 3, pp. 319-331, 2016.

[46] P. Zhang, F. Li, and N. Bhatt, "Next-generation monitoring, analysis, and control for the future smart control center," *IEEE Transactions on Smart Grid,* vol. 1, no. 2, pp. 186-192, 2010.

[47] L. Lu, J. Zhou, J. Hu, G. Li, and Y. Song, "Embedded Powerline Communication in Large Scale Distribution Automation and Demand Side Management System," in *Mechatronic and Embedded Systems and Applications, Proceedings of the 2nd IEEE/ASME International Conference on*, 2006, pp. 1-6: IEEE.

[48] R. Benato and R. Caldon, "Application of PLC for the control and the protection of future distribution networks," in *Power Line Communications and Its Applications, 2007. ISPLC'07. IEEE International Symposium on*, 2007, pp. 499-504: IEEE.

[49] A. N. Milioudis, G. T. Andreou, and D. P. Labridis, "Detection and location of high impedance faults in multiconductor overhead distribution lines using power line communication devices," *IEEE Transactions on Smart Grid,* vol. 6, no. 2, pp. 894-902, 2015.

[50] A. N. Milioudis, G. T. Andreou, and D. P. Labridis, "Enhanced protection scheme for smart grids using power line communications techniques—Part II: Location of high impedance fault position," *IEEE Transactions on Smart Grid,* vol. 3, no. 4, pp. 1631-1640, 2012.

[51] A. Milioudis, G. Andreou, and D. Labridis, "High impedance fault evaluation using narrowband power line communication techniques," in *PowerTech, 2011 IEEE Trondheim*, 2011, pp. 1-6: IEEE.

[52] A. Milioudis, G. Andreou, and D. Labridis, "High impedance fault detection using power line communication techniques," in *Universities Power Engineering Conference (UPEC), 2010 45th International*, 2010, pp. 1-6: IEEE.

[53] A. N. Milioudis, G. T. Andreou, and D. P. Labridis, "Enhanced protection scheme for smart grids using power line communications techniques—Part I: Detection of high impedance fault occurrence," *IEEE Transactions on Smart Grid,* vol. 3, no. 4, pp. 1621-1630, 2012.

[54] T. Marxsen, "Vegetation Conduction Ignition Test Report–Final," *Marxsen Consulting Pty Ltd., Department of Economic Development Jobs Transport and Resources,* 2015.

[55] M. S. Yousuf, S. Z. Rizvi, and M. El-Shafei, "Power line communications: An overview-Part II," in *Information and Communication Technologies: From Theory to Applications, 2008. ICTTA 2008. 3rd International Conference on*, 2008, pp. 1-6: IEEE.

[56] Y. Kim and J. Kim, "Characteristic impedances in low-voltage distribution systems for power line communication," *Journal of Electrical Engineering & Technology,* vol. 2, no. 1, p. 29, 2007.

[57] Y.-J. Wang and S.-J. Liu, "A Review of Methods for Calculation of Frequency-dependent Impedance of Overhead Power Transmission Lines (Invited Review Paper)," *PROCEEDINGS-NATIONAL SCIENCE COUNCIL REPUBLIC OF CHINA PART A PHYSICAL SCIENCE AND ENGINEERING,* vol. 25, no. 6, pp. 329-338, 2001.

[58] J. R. Carson, "Wave propagation in overhead wires with ground return," *Bell system technical journal,* vol. 5, no. 4, pp. 539-554, 1926.

[59] C. GARY, "Approche complète de la propagation multifilaire en haute fréquence par utilisation des matrices complexes. bulletin de la direction des études et recherches," Technical report, EDF1976.

[60] A. Deri, G. Tevan, A. Semlyen, and A. Castanheira, "The complex ground return plane a simplified model for homogeneous and multi-layer earth return," *IEEE Transactions on Power Apparatus and Systems,* no. 8, pp. 3686-3693, 1981.

[61] I. H. Cavdar and E. Karadeniz, "Measurements of impedance and attenuation at CENELEC bands for power line communications systems," *Sensors,* vol. 8, no. 12, pp. 8027-8036, 2008.

[62] C. J. Kikkert and S. Zhu, "Design improvements of the resistive shunt online impedance analyzer," in *Innovative Smart Grid Technologies-Asia (ISGT-Asia), 2017 IEEE*, 2017, pp. 1-5: IEEE.

[63] S. Zhu, C. J. Kikkert, and N. Ertugrul, "Software for control and calibration of an inductive shunt on-line impedance analyzer," in *Power Line Communications and its Applications (ISPLC), 2015 International Symposium on*, 2015, pp. 53-58: IEEE.

[64] A. M. Tonello, N. A. Letizia, D. Righini, and F. Marcuzzi, "Machine Learning Tips and Tricks for Power Line Communications," *IEEE Access,* 2019.

[65] D. Liang, H. Guo, and T. Zheng, "Impedance Tracking and Estimation using Power Line Communications," in *2019 IEEE International Symposium on Power Line Communications and its Applications (ISPLC)*, 2019, pp. 1-6: IEEE.

[66] D. Liang, H. Guo, and T. Zheng, "Real-Time Impedance Estimation for Power Line Communication," *IEEE Access,* vol. 7, pp. 88107-88115, 2019.

[67] P. A. J. van Rensburg, M. P. Sibanda, and H. C. Ferreira, "Integrated Impedance-Matching Coupler for Smart Building and Other Power-Line Communications Applications," *IEEE Transactions on Power Delivery,* vol. 30, no. 2, pp. 949-956, 2015.

[68] P. A. J. van Rensburg and H. C. Ferreira, "Design and evaluation of a dual impedance-adapting power-line communications coupler," *IEEE Transactions on power Delivery,* vol. 25, no. 2, pp. 667-673, 2010.

[69] P. A. J. van Rensburg and H. C. Ferreira, "Coupler winding ratio selection for effective narrowband power-line communications," *IEEE Transactions on power Delivery,* vol. 23, no. 1, pp. 140-149, 2008.

[70] S. Wei, W. Gao, L. Zhang, and Z. Cao, "High frequency and broadband coupling characteristics of filter circuit based on low voltage power lines," *Procedia Engineering,* vol. 15, pp. 1978-1982, 2011.

[71] M. Rastogi, D. Mitra, and A. Bhattacharya, "A Novel Implementation of Bidirectional Coupling Circuit for Broadband, High-Voltage, Power-Line Communications," in *Communications, 2005 Asia-Pacific Conference on*, 2005, pp. 38-42: IEEE.

[72] O. Bilal, E. Liu, Y. Gao, and T. O. Korhonen, "Design of broadband coupling circuits for power line communication," in *Proc. IS PLC*, 2004.

[73] C. J. Kikkert, "MV to LV transformer PLC bypass coupling networks for a low cost smart grid rollout," in *Innovative Smart Grid Technologies Asia (ISGT), 2011 IEEE PES*, 2011, pp. 1-6: IEEE.

[74] C. J. Kikkert, "Power transformer modelling and MV PLC coupling networks," in *Innovative Smart Grid Technologies Asia (ISGT), 2011 IEEE PES*, 2011, pp. 1-6: IEEE.

[75] C. J. Kikkert, "Effect of couplers and line branches on PLC communication channel response," in *Smart Grid Communications (SmartGridComm), 2011 IEEE International Conference on*, 2011, pp. 309-314: IEEE.

[76] G. Artale *et al.*, "Medium voltage smart grid: Experimental analysis of secondary substation narrow band power line communication," *IEEE Transactions on Instrumentation and Measurement,* vol. 62, no. 9, pp. 2391-2398, 2013.

[77] A. Zeichner and S. Frei, "Immunity of Automotive Power Line Communication Systems," *IEEE Transactions on Electromagnetic Compatibility,* vol. 58, no. 4, pp. 1289-1296, 2016.

[78] T. Specht and R. Cheek, "Carrier-Frequency Characteristics of Power Transformers," *Transactions of the American Institute of Electrical Engineers. Part III: Power Apparatus and Systems,* vol. 71, no. 1, pp. 442-449, 1952.

[79] L. Lampe, A. M. Tonello, and T. G. Swart, *Power Line Communications: Principles, Standards and Applications from multimedia to smart grid*. John Wiley & Sons, 2016.

[80] V. Taylor, M. Faulkner, A. Kalam, and J. Haydon, "Digital simulation of fault location on EHV lines using wideband spread spectrum techniques," *IEE Proceedings-Generation, Transmission and Distribution,* vol. 142, no. 1, pp. 73-80, 1995.

[81] C. JordA, B. Asare-Bediako, G. Vanalme, and W. Kling, "Overview and comparison of leading communication standard technologies for smart home area networks enabling energy management systems," in *2011 46th International Universities' Power Engineering Conference (UPEC)*, 2011, pp. 1-6: VDE.

[82] A. R. Ndjiongue, A. Snyders, H. C. Ferreira, and S. Rimer, "Review of power line communications standards in Africa," in *International Conference on e-Infrastructure and e-Services for Developing Countries*, 2013, pp. 12-21: Springer.

[83] S. Galli and T. Lys, "Next generation narrowband (under 500 kHz) power line communications (PLC) standards," *China Communications,* vol. 12, no. 3, pp. 1-8, 2015.

[84] A. Kosonen, J. Ahola, and A. Pinomaa, "Analysis of channel characteristics for motor cable communication with inductive signal coupling," in *ISPLC2010*, 2010, pp. 72-77: IEEE.

[85] W. Liu, H. Widmer, and P. Raffin, "Broadband PLC access systems and field deployment in European power line networks," *IEEE Communications Magazine,* vol. 41, no. 5, pp. 114-118, 2003.

[86] *HV outdoor capacitor voltage transformers and coupling capacitors Robust design and proven performance, ABB Electrical Equipment, (2013)*. Available: https://library.e.abb.com/public/ed39ca0ece4d14db4825789c003d288a/HV%20Outdoor%20CVT.pdf

[87] B. Martínez, N. Cante, M. Limas, F. Sierra, and J. Becerra, "Design of a T-coupling circuit for PLC on broadband," in *2014 IEEE Colombian Conference on Communications and Computing (COLCOM)*, 2014, pp. 1-6: IEEE.

[88] M. P. Sibanda, P. A. J. van Rensburg, and H. C. Ferreira, "Impedance matching with low-cost, passive components for narrowband PLC," in *2011 IEEE International Symposium on Power Line Communications and Its Applications*, 2011, pp. 335-340: IEEE.

[89] C.-Y. Park, K.-H. Jung, and W.-H. Choi, "Coupling circuitary for impedance adaptation in power line communications using VCGIC," in *2008 IEEE International Symposium on Power Line Communications and Its Applications*, 2008, pp. 293-298: IEEE.

[90] W.-h. Choi and C.-y. Park, "A simple line coupler with adaptive impedance matching for power line communication," in *2007 IEEE International Symposium on Power Line Communications and Its Applications*, 2007, pp. 187-191: IEEE.

[91] J. B. Hagen, *Radio-frequency electronics: circuits and applications*. Cambridge University Press, 2009.

[92] C. Bowick, "RF Circuit Design Howard W. Sams & Co," *Inc., Indianapolis, Indiana,* 1982.

[93] G. Artale, A. Cataliotti, V. Cosentino, S. Guaiana, D. Di Cara, and G. Tinè, "Development of a coupling system for medium voltage power line communication in the CENELEC A frequency band," in *2016 IEEE International Workshop on Applied Measurements for Power Systems (AMPS)*, 2016, pp. 1-6: IEEE.

[94] G. Artale *et al.*, "A new low cost coupling system for power line communication on medium voltage smart grids," *IEEE Transactions on Smart Grid,* vol. 9, no. 4, pp. 3321-3329, 2016.

[95] R. Alaya and R. Attia, "Coupling unit for narrowband power line communications channel measurement," in *2016 24th International Conference on Software, Telecommunications and Computer Networks (SoftCOM)*, 2016, pp. 1-5: IEEE.

[96] R. Karhammar *et al.*, "Sub-saharan africa: Introducing low-cost methods in electricity distribution networks," *Energy Sector Management Assistance Program (ESMAP), Tech. Rep,* vol. 104, no. 06, 2006.

[97] A. Helwig and T. Ahfock, "Extending SWER line capacity," in *2013 Australasian Universities Power Engineering Conference (AUPEC)*, 2013, pp. 1-6: IEEE.

[98] K. Hemapala, M. Dayarathne, and O. G. Swathika, "Optimized cost enabled rural electrification system," in *2017 Moratuwa Engineering Research Conference (MERCon)*, 2017, pp. 351-356: IEEE.

[99] *The State Electrcity Commision of Victoria, "SWER Distribution Manual", (ed, 2009)*

[100] ActewAGL, "Electrical Data Manual," ed, 2007.

[101] L. L. Grigsby, *Electric power generation, transmission, and distribution*, Third ed. CRC press, 2016.

[102] A. Abu-Siada, "High frequency transformer modelling using state space representation for FRA studies," in *2017 IEEE 11th International Symposium on Diagnostics for Electrical Machines, Power Electronics and Drives (SDEMPED)*, 2017, pp. 422-426: IEEE.

[103] X. Zhao, C. Yao, Z. Zhao, and A. Abu-Siada, "Performance evaluation of online transformer internal fault detection based on transient overvoltage signals," *IEEE Transactions on Dielectrics and Electrical Insulation,* vol. 24, no. 6, pp. 3906-3915, 2017.

[104] B. Jurisic, I. Uglesic, A. Xemard, and F. Paladian, "Difficulties in high frequency transformer modeling," *Electric Power Systems Research,* vol. 138, pp. 25-32, 2016.

[105] B. Masood, M. Usman, M. U. Gul, and W. A. Khan, "Measurements and characterization of power transformer and low voltage access network for NB-PLC," *International Journal of Communication Systems,* vol. 30, no. 17, p. e3344, 2017.

[106] R. Lefort, R. Vauzelle, V. Courtecuisse, N. Idir, and A.-M. Poussard, "Influence of the MV/LV Transformer Impedance on the Propagation of the PLC Signal in the Power Grid," *IEEE Transactions on Power Delivery,* vol. 32, no. 3, pp. 1339-1349, 2016.

[107] J. Biernacki and D. Czarkowski, "High frequency transformer modeling," in *ISCAS 2001. The 2001 IEEE International Symposium on Circuits and Systems (Cat. No. 01CH37196)*, 2001, vol. 3, pp. 676-679: IEEE.

[108] T. Tran-Anh, P. Auriol, and T. Tran-Quoc, "High frequency power transformer modeling for power line communication applications," in *2006 IEEE PES Power Systems Conference and Exposition*, 2006, pp. 1069-1074: IEEE.

[109] W. C. Black and N. E. Badr, "High-frequency characterization and modeling of distribution transformers," in *ISPLC2010*, 2010, pp. 18-21: IEEE.

[110] B. Gustavsen, "Wide band modeling of power transformers," *IEEE Transactions on Power Delivery,* vol. 19, no. 1, pp. 414-422, 2004.

[111] M. Heindl, S. Tenbohlen, and R. Wimmer, "Transformer modeling based on standard frequency response measurements," in *International Symposium on High Voltage Engineering, Hannover, Germany*, 2011.

[112] R. Aghmasheh, V. Rashtchi, and E. Rahimpour, "Gray box modeling of power transformer windings for transient studies," *IEEE Transactions on Power Delivery,* vol. 32, no. 5, pp. 2350-2359, 2017.

[113] R. Aghmasheh, V. Rashtchi, and E. Rahimpour, "Gray box modeling of power transformer windings based on design geometry and particle swarm optimization algorithm," *IEEE Transactions on Power Delivery,* vol. 33, no. 5, pp. 2384-2393, 2018.

[114] S. D. Mitchell and J. S. Welsh, "Modeling power transformers to support the interpretation of frequency-response analysis," *IEEE Transactions on power delivery,* vol. 26, no. 4, pp. 2705-2717, 2011.

[115] N. A. Sabiha and M. Lehtonen, "Lightning-induced overvoltages transmitted over distribution transformer with MV spark-gap operation—Part II: mitigation using LV surge arrester," *IEEE transactions on power delivery,* vol. 25, no. 4, pp. 2565-2573, 2010.

[116] N. A. Sabiha and M. Lehtonen, "Lightning-induced overvoltages transmitted over distribution transformer with MV spark-gap operation—Part I: High-frequency transformer model," *IEEE Transactions on power delivery,* vol. 25, no. 4, pp. 2472-2480, 2010.

[117] Z. Zhao, C. Yao, C. Tang, C. Li, F. Yan, and S. Islam, "Diagnosing transformer winding deformation faults based on the analysis of binary image obtained from FRA signature," *IEEE Access,* vol. 7, pp. 40463-40474, 2019.

[118] E. Karadeniz, "Determining of Impedance and Attenuation on Power Line Communication System," MSc Karadeniz Technical University: Trabzon, , Turkey,, 2006.

[119] P. Golden, H. Dedieu, and K. S. Jacobsen, *Implementation and applications of DSL technology*. CRC press, 2007.

[120] *Power Diagnostix Systems GmbH. Coupling Capacitors Product Information: CMseries Accessories:Coupling Devices, Meggar Ltd,(2010)*. Available: https://www.pdix.com/products/pd-accessories/coupling-capacitors.html

[121] A. Ghaderi, H. L. Ginn, and H. A. Mohammadpour, "High impedance fault detection: A review," *Electric Power Systems Research,* vol. 143, pp. 376-388, 2017.

[122] F. Passerini and A. M. Tonello, "Power line fault detection and localization using high frequency impedance measurement," in *Power Line Communications and its Applications (ISPLC), 2017 IEEE International Symposium on*, 2017, pp. 1-5: IEEE.

[123] M. Kavi, Y. Mishra, and D. Vilathgamuwa, "Detection and identification of high impedance faults in single wire earth return distribution networks," in *Power Engineering Conference (AUPEC), 2016 Australasian Universities*, 2016, pp. 1-6: IEEE.

[124] S. Maximov, V. Torres, H. Ruiz, and J. Guardado, "Analytical model for high impedance fault analysis in transmission lines," *Mathematical Problems in Engineering,* vol. 2014, 2014.

[125] J.-A. Jiang, C.-S. Chen, and C.-W. Liu, "A new protection scheme for fault detection, direction discrimination, classification, and location in transmission lines," *IEEE Transactions on power delivery,* vol. 18, no. 1, pp. 34-42, 2003.

[126] Z. P. Campbell, Y. Xue, and R. C. Dixon, "Power Line Carrier Directional Comparison Blocking Misoperation Event Analyses & Avoidance Techniques," in *Proceedings of the 67th Annual Georgia Tech Protective Relaying Conference*, 2013.

[127] F. Passerini and A. M. Tonello, "Power line fault detection and localization using high frequency impedance measurement," in *2017 IEEE International Symposium on Power Line Communications and its Applications (ISPLC)*, 2017, pp. 1-5: IEEE.

[128] P. A. Gulbhile, J. R. Rana, and B. T. Deshmukh, "Overhead line fault detection using GSM technology," in *2017 International Conference on Innovative Mechanisms for Industry Applications (ICIMIA)*, 2017, pp. 46-49: IEEE.

[129] S. N. Ananthan, R. Padmanabhan, R. Meyur, B. Mallikarjuna, M. J. B. Reddy, and D. K. Mohanta, "Real-time fault analysis of transmission lines using wavelet multi-resolution analysis based frequency-domain approach," *IET Science, Measurement & Technology,* vol. 10, no. 7, pp. 693-703, 2016.

[130] M. Jannati and L. Eslami, "Precise modeling of high impedance faults in power distribution system in emtpworks software," *Journal of Electrical Engineering,* 2013.

[131] V. De Andrade and E. Sorrentino, "Typical expected values of the fault resistance in power systems," in *2010 IEEE/PES Transmission and Distribution Conference and Exposition: Latin America (T&D-LA)*, 2010, pp. 602-609: IEEE.

[132] N. Zamanan, J. Sykulski, and A. Al-Othman, "Arcing high impedance fault detection using real coded genetic algorithm," 2007.

[133] N. I. Elkalashy, M. Lehtonen, H. A. Darwish, M. A. Izzularab, and I. T. Abdel-maksoud, "Modeling and experimental verification of high impedance arcing fault in medium voltage networks," *IEEE Transactions on Dielectrics and Electrical Insulation,* vol. 14, no. 2, pp. 375-383, 2007.

[134] A. v. C. Warrington, *Protective Relays: Their Theory and Practice Volume One*. Springer Science & Business Media, 2012.

[135] A. Warrington and C. Van, "Reactance relays negligibly affected by arc impedance," *Electrical World,* vol. 98, no. 12, pp. 502-505, 1931.

[136] V. V. Terzija and H.-J. Koglin, "On the modeling of long arc in still air and arc resistance calculation," *IEEE Transactions on Power Delivery,* vol. 19, no. 3, pp. 1012-1017, 2004.

[137] V. Terzija and H.-J. Koglin, "New dynamic model, laboratory testing and features of long arc in free air," *Electrical Engineering,* vol. 83, no. 4, pp. 193-201, 2001.

[138] N. Zamanan and J. K. Sykulski, "Modelling arcing high impedances faults in relation to the physical processes in the electric arc," *WSEAS Transactions on power systems,* vol. 1, no. 8, pp. 1507-1512, 2006.

[139] N. Elkalashy, M. Lehtonen, H. Darwish, M. Izzularab, and A. Taalab, "Modeling and experimental verification of a high impedance arcing fault in MV networks," in *2006 IEEE PES Power Systems Conference and Exposition*, 2006, pp. 1950-1956: IEEE.

[140] A. Emmanuel, D. Cygansky, S. Shiller, and E. Gulachenski, "High impedance fault on sandy soil in 15 kV distribution feeders: Contribution to the evaluation of the low frequencies spectrum," *IEEE Trans. Power Delivery,* vol. 5, no. 2, pp. 676-686, 1990.

[141] C. Wester, "High impedance fault detection on distribution systems general electric company," 2008.

[142] S. Salona, "High Impedance Fault Modelling on 11Kv Feeder Using Matlab Simulink," *International Journal of Science and Research (IJSR) Volume,* vol. 5, pp. 462-467, 2013.

[143] A. Mahari and H. Seyedi, "High impedance fault protection in transmission lines using a WPT-based algorithm," *International Journal of Electrical Power & Energy Systems,* vol. 67, pp. 537-545, 2015.

[144] D. Hou, "Comparing Fault Resistance Coverage of Different Distribution System Grounding Methods," in *37th Annual Western Protective Relay Conference*, 2010.

Appendix A – Myers Road Network

CONDUCTOR PARAMETERS

Feature	3/2.75 SCGZ	3/12 SCGZ
Resistivity of Steel	1.74×10^{-7} Ω.m	1.74×10^{-7} Ω.m
Soil resistivity	40 Ω.m	40 Ω.m
Relative Permeability	70 H/m	70 H/m
No of Strands	3	3
DC Resistance (Ω/km)	11 Ω/km	11.93 Ω/km
Conductor Diameter in m	5.93×10^{-3} m	5.1×10^{-3} m
Conductor Radius in m	2.965×10^{-3} m	2.55×10^{-3} m
Strand Diameter (m)	2.75×10^{-3} m	2.06×10^{-3} m (12 Gauge)
Strand Radius (m)	1.375×10^{-3} m	1.03×10^{-3} m
Height above ground	6.7 metres	6.7 metres

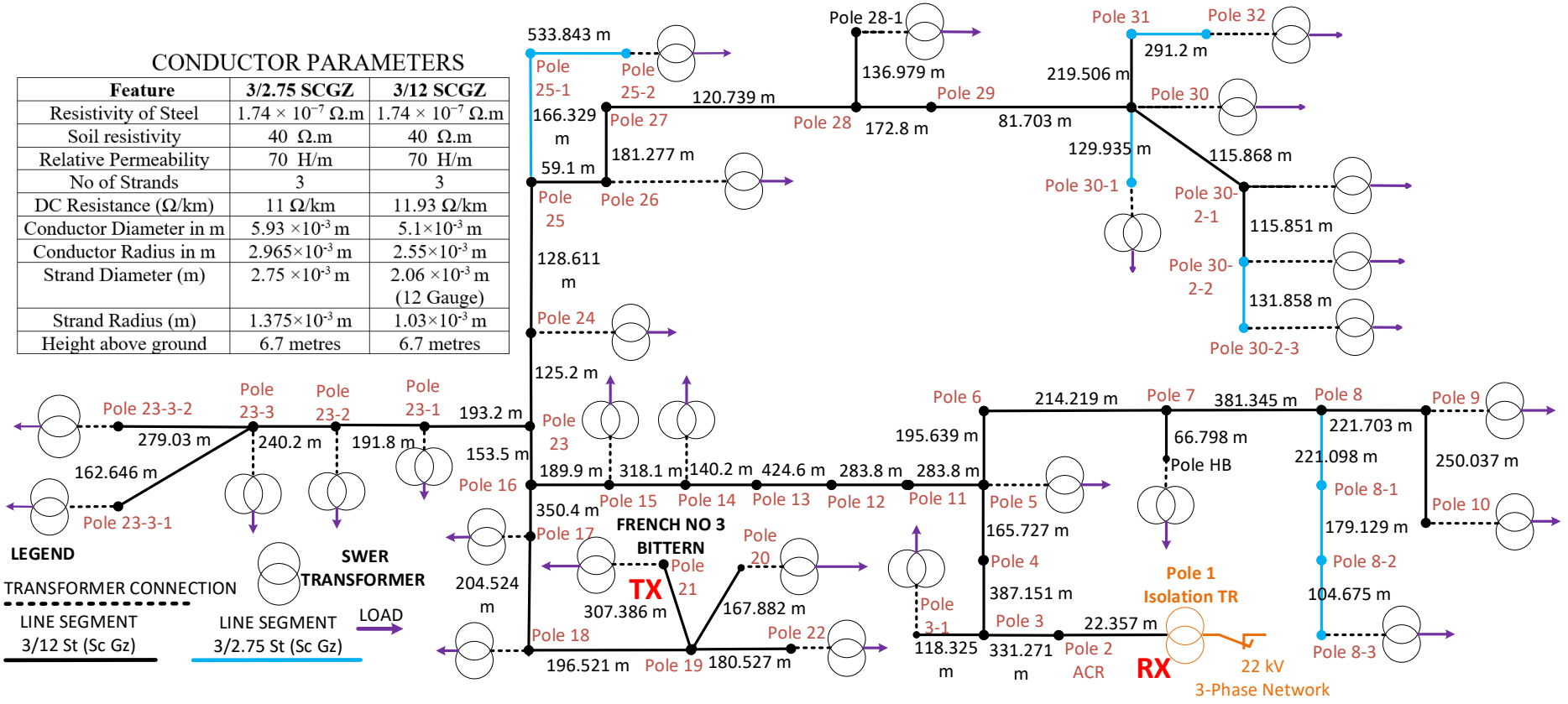

Appendix B – Myers Road Network AWR Model

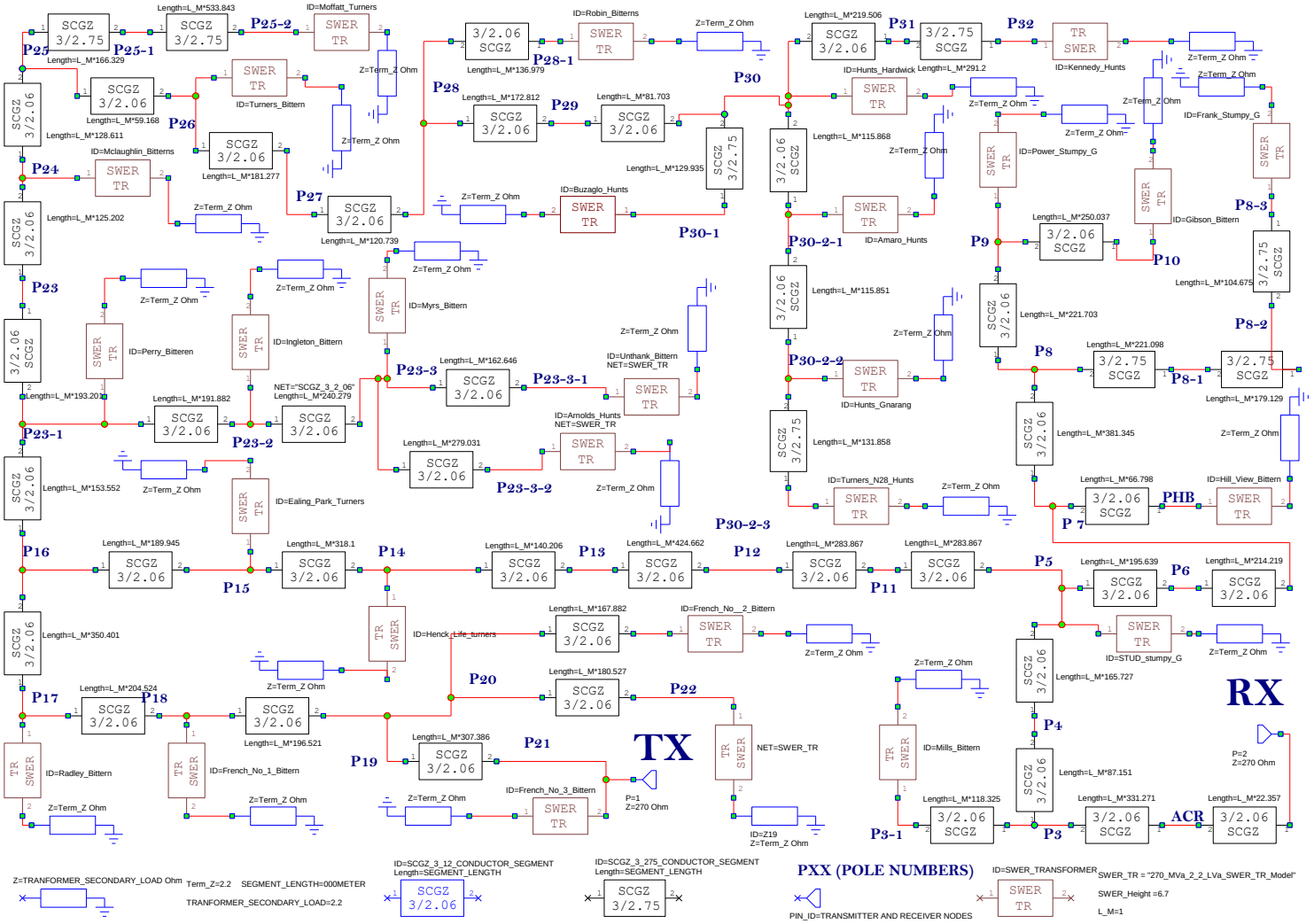

Appendix C – ACSR/GZ Data Sheet

Aluminium Conductors Steel Reinforced (Type ACSR/GZ)

ACSR conductors are a composite, concentrically stranded conductor consisting of a single galvanised steel wire or a stranded galvanized steel central core surrounded with one or more layers of EC grade (alloy 1350) stranded aluminium wires. The combination of the light weight and good conductivity of the aluminium and the high tensile strength of steel in the conductor design make ACSR conductors the most economical solution for overhead high tension transmission lines with an established reputation for dependability under adverse weather conditions.
The illustration below shows typical standard sizes and stranding patterns. The wires in all bare conductors are stranded with each successive layer having an opposite direction of lay, the outermost layer being right-handed.
For installations that require increased corrosion protection ACSR conductors incorporating an aluminium-clad steel central core can be supplied.

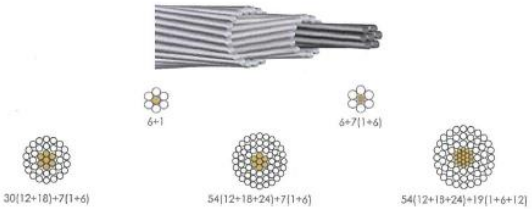

Aluminium conductors, galvanized steel reinforced manufactured to AS 3607 (ACSR). Physical and Mechanical Properties

Conductor code	Stranding and wire diameter No/mm		Nominal Overall diameter	Cross sectional area	Approximate mass	Minimum breaking load	Modulus of elasticity	Coefficient of linear expansion
	Aluminium	Steel	mm	mm²	kg/km	kN	GPa	x10-6/°C
Almond	6/2.50	1/2.5	7.5	34.4	119	10.5	83	19.3
Apricot	6/2.75	1/2.75	8.3	41.6	144	12.6	83	19.3
Apple	6/3.00	1/3.00	9.0	49.5	171	14.9	83	19.3
Banana	6/3.75	1/3.75	11.3	77.3	268	22.7	83	19.3
Cherry	6/4.75	7/1.60	14.3	120	402	33.4	80	19.9
Grape	30/2.50	7/2.50	17.5	182	677	63.5	88	18.4
Lemon	30/3.00	7/3.00	21.0	262	973	90.4	88	18.4
Lychee	30/3.25	7/3.25	22.8	307	1140	105	88	18.4
Lime	30/3.50	7/3.50	24.5	356	1320	122	88	18.4
Mango	54/3.00	7/3.00	27.0	431	1440	119	78	19.9
Orange	54/3.25	7/3.25	29.3	506	1690	137	78	19.9
Olive	54/3.50	7/3.50	31.5	587	1960	159	78	19.9
Pawpaw	54/3.75	19/2.25	33.8	672	2240	178	77	20.0
Quince	3/1.75	4/1.75	5.3	16.8	95	12.7	136	13.9
Raisin	3/2.50	4/2.50	7.5	34.4	195	24.4	136	13.9
Sultana	4/3.00	3/3.00	9.0	49.5	243	28.3	119	15.2
Walnut	4/3.75	3/3.75	11.3	77.3	380	43.9	119	15.2

NAN

Electrical Properties

Conductor code	DC resist at 20°C	AC Resist at 50Hz at 75°C	Inductive reactance to 0.3m at 50Hz	Continuous current carrying capacity - A											
				Rural weathered						Industrial weathered					
				Winter night			Summer noon			Winter night			Summer noon		
	Ω/km	Ω/km	Ω/km	still air	1m/s wind	2m/s wind	still air	1m/s wind	2m/s wind	still air	1m/s wind	2m/s wind	still air	1m/s wind	2m/s wind
Almond	0.975	1.32	0.295	114	195	219	85	172	203	121	195	228	81	166	202
Apricot	0.805	1.07	0.291	126	211	252	97	192	229	135	221	252	90	188	218
Apple	0.677	0.909	0.284	144	235	279	110	210	255	149	249	286	97	214	243
Banana	0.433	0.583	0.272	192	314	365	145	284	336	222	325	371	132	272	318
Cherry	0.271	0.366	0.256	262	415	492	195	369	444	289	441	499	177	368	428
Grape	0.196	0.264	0.241	335	515	605	242	454	539	372	525	628	215	444	528
Lemon	0.136	0.165	0.223	448	686	789	311	593	702	495	705	816	272	571	695
Lychee	0.116	0.143	0.220	490	768	885	349	668	787	559	795	917	302	529	766
Lime	0.100	0.124	0.218	551	838	975	383	711	852	613	874	1018	333	690	828
Mango	0.0758	0.0957	0.213	652	961	1158	445	828	1002	723	1012	1192	394	794	974
Orange	0.0646	0.0815	0.208	736	1058	1293	499	903	1123	806	1123	1328	429	872	1082
Olive	0.0557	0.0706	0.203	811	1172	1448	556	989	1238	896	1235	1475	467	940	1203
Pawpaw	0.0485	0.0617	0.197	896	1275	1559	601	1078	1358	985	1348	1628	512	1018	1325
Quince	3.25	4.35	0.345	52	94	107	40	63	99	57	96	119	42	82	98
Raisin	1.59	2.13	0.326	84	148	171	65	132	159	95	152	177	60	130	154
Sultana	0.897	1.20	0.300	121	209	232	92	180	220	135	211	248	85	177	213
Walnut	0.573	0.771	0.287	160	258	311	123	245	289	177	280	321	113	235	288

Note: Current ratings are based to the following conditions

- Conductor temperature rise above ambient of 40°C
- Ambient air temp. of 35°C for summer noon or 10°C for winter night
- Direct solar radiation intensity of 1000W/m2 for summer noon or zero for winter night
- Diffuse solar radiation intensity of 100W/m2 for summer noon or zero for winter night
- Ground reflectance of 0.2
- Emissivity of 0.5 for rural weathered conductor or 0.85 for industrial weathered weathered conductor
- Solar absorption coefficient of 0.5 for rural weathered conductor or 0.85 for industrial weathered conductor

Cross sections not to scale

Appendix D – GMR Calculation Tables

CALCULATIONS - CONDUCTOR PROPERTIES

Contents - Calculations – Conductor Properties

Below are properties of the conductors that are used in the calculations in this manual.
Stranding Constant
Given in Metal Manufactures Ltd. Publication 5/81-October 1981, "Kembla®, Conductors for Overhead Transmission and Distribution.", Table 6
Resistivity Constant
Given in Metal Manufactures Ltd. Publication 5/81-October 1981, "Kembla®, Conductors for Overhead Transmission and Distribution.", Table 6
K_s – Skin effect ratio – assumed to be 1.015 for all conductors.
K_m – Magnetic Effect Ratio – typically between 1.0 and 1.1. Given by ESAA Publication D(b)5-1988 - "Current Rating of Bare Overhead Line Conductors"., page 11

GMR
Geometric Mean Radius, a function of the dimensions and magnetic properties of the conductor. It is calculated by using the following table:
Let d_s = diameter of 1 strand.

Total Number Of Strands	Nominal Diameter	GMR
3	$(1+ 2/\sqrt{3})d_s$	$0.6779r_c$
7	$3d_s$	$0.7255r_c$
19	$5d_s$	$0.7576r_c$
37	$7d_s$	$0.7681r_c$
61	$9d_s$	$0.7720r_c$

Where r_c = nominal radius = radius of the conductor = nominal diameter / 2.

These coefficients of GMR came from "Electrical Characteristics of Overhead Lines", by S. Butterworth, ERA: Technical Report O/T4, 1954; page 25.

Note that these values do not take into account type of material used in the conductor. This means that there can not be any factor taken into account if the conductor has, say, a steel core.

AS 3851 – 1991 also has a formula for the GMR (given in appendix B).
It is the same, but with different coefficients for the GMR:

Total Number Of Strands	GMR as given by AS 3851 - 1991
3	$0.8411r_c$
7	$0.8255r_c$
19	$0.8723r_c$
37	$0.8800r_c$
61	$0.8878r_c$

NOTE: these values were **NOT** used in the calculation of this manual. It was decided that it is better to keep the values consistent with the values as calculated previously, calculated with the formula from Butterworth.

The impedance and voltage drop values using the 3 formulae for the GMR (Butterworth, Kembla®, Standards) were compared to each other. The worst case between the Kembla® and Butterworth values was a 7.6% rise from the Butterworth, for the Raisin low voltage positive sequence reactance. The worst case between the Standards and Butterworth values was a –3.5% drop from the Butterworth, for the Steel low voltage positive sequence reactance. Conductor specifications are in accordance with Metal Manufactures Ltd. Publication 5/81-October 1981, "Kembla®, Conductors for Overhead Transmission and Distribution."

Top Of This Section

Appendix E – Coupling Capacitor Based Injection Circuit S21/S11 Test Setup

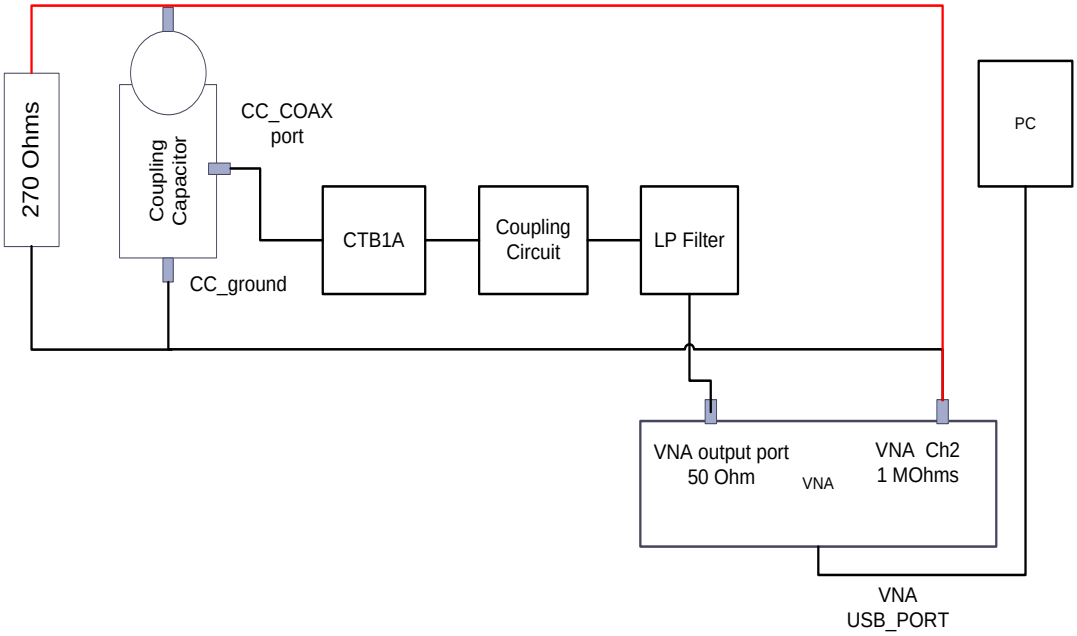

Appendix F – Coupling Capacitor Based Receiver Circuit S21/S11 Test

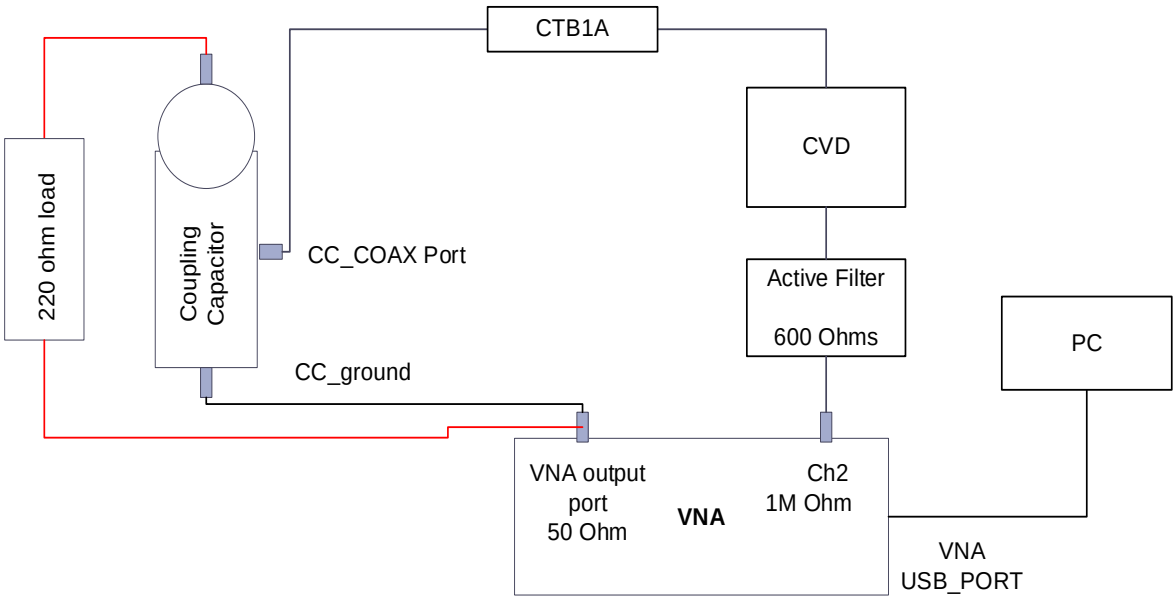

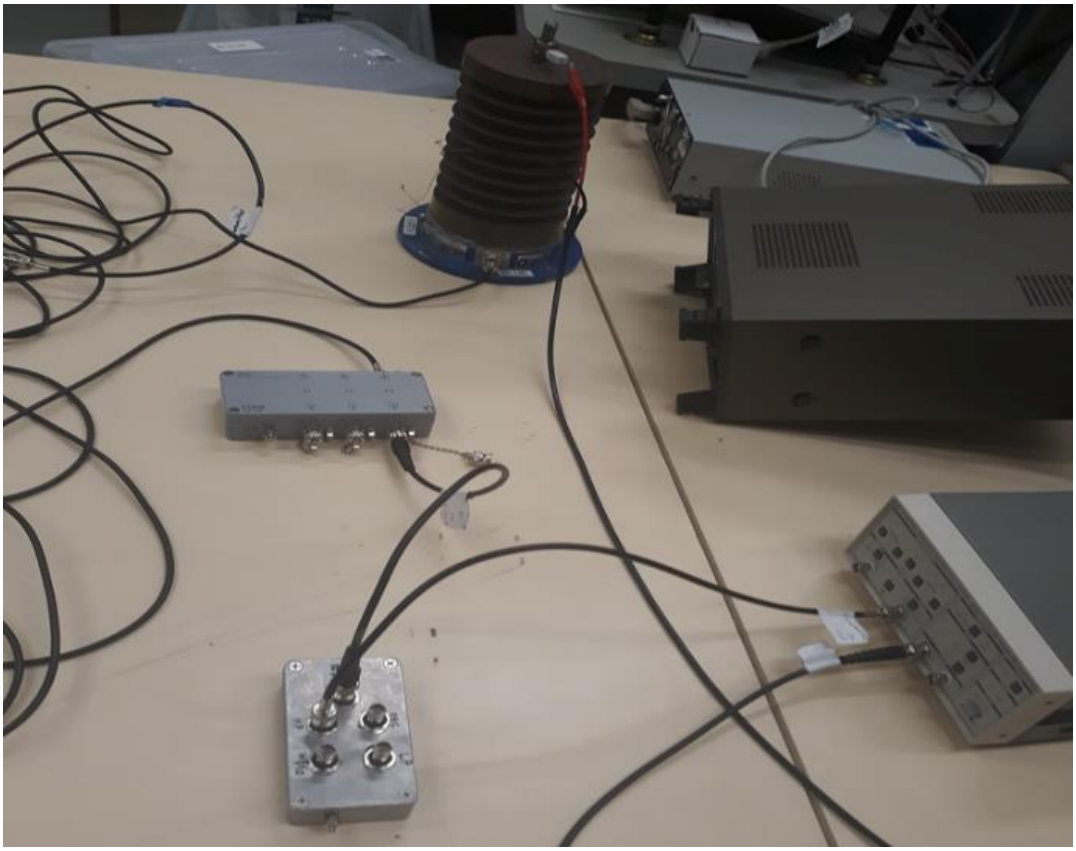

Appendix G – SWER TR S21/S11 Test

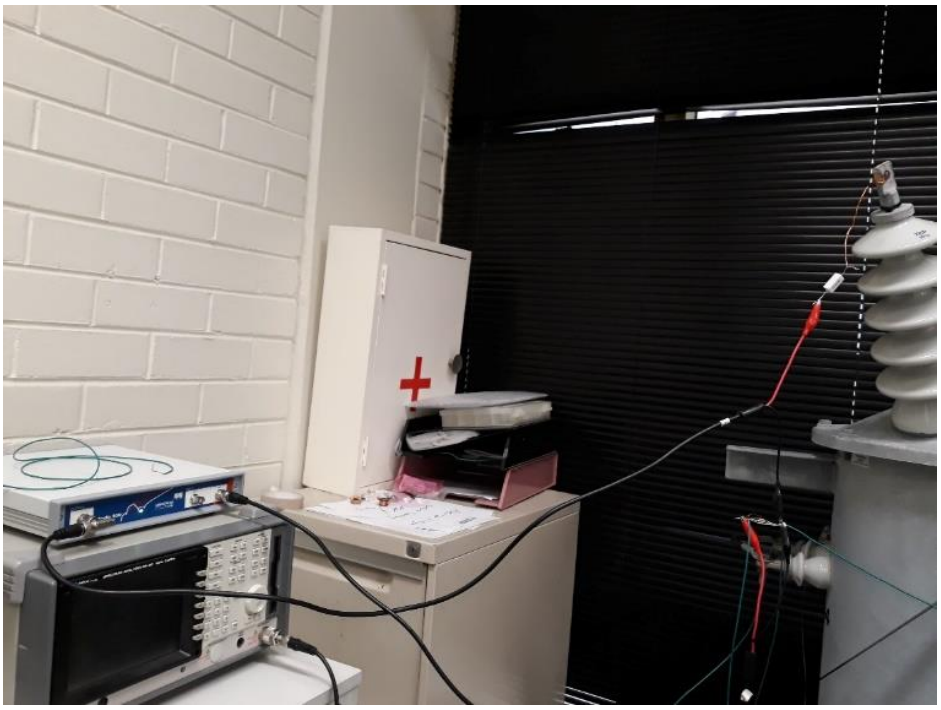

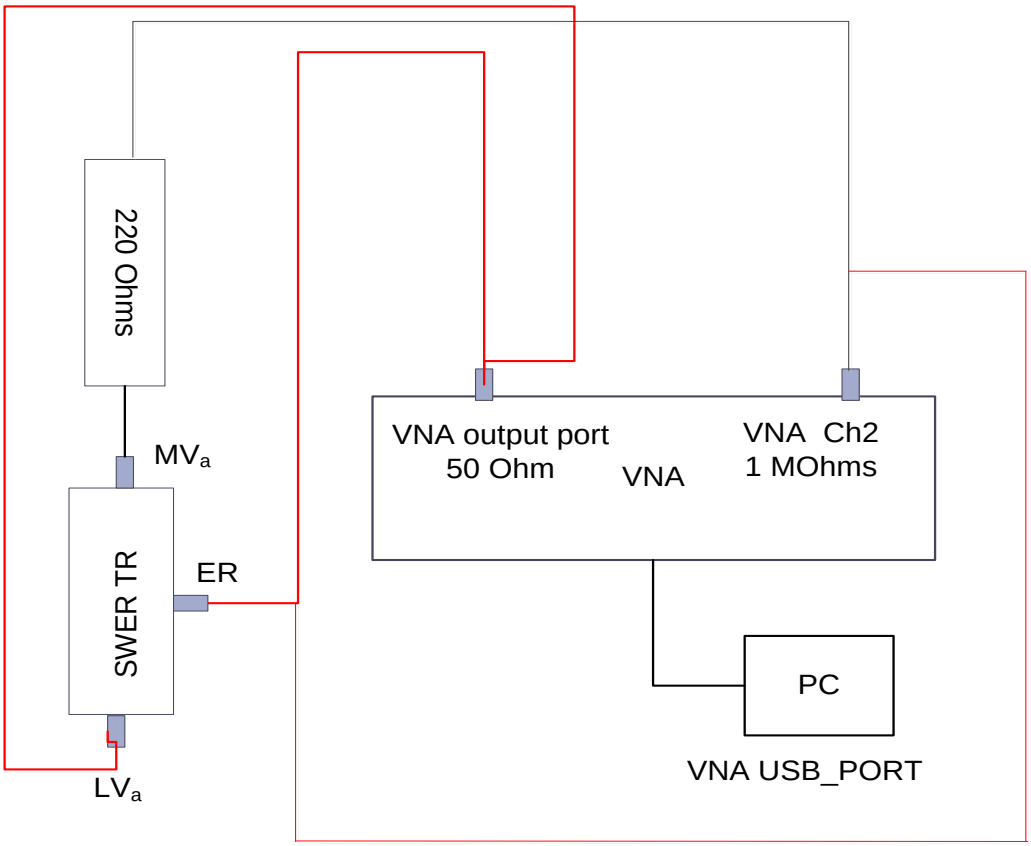

Appendix H – Isolation Transformer S21/S11 Test

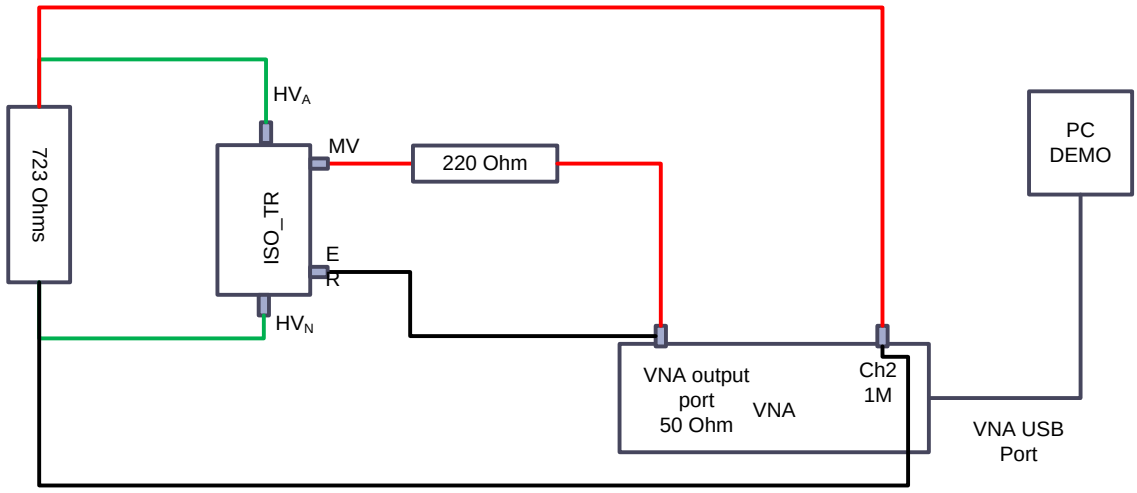

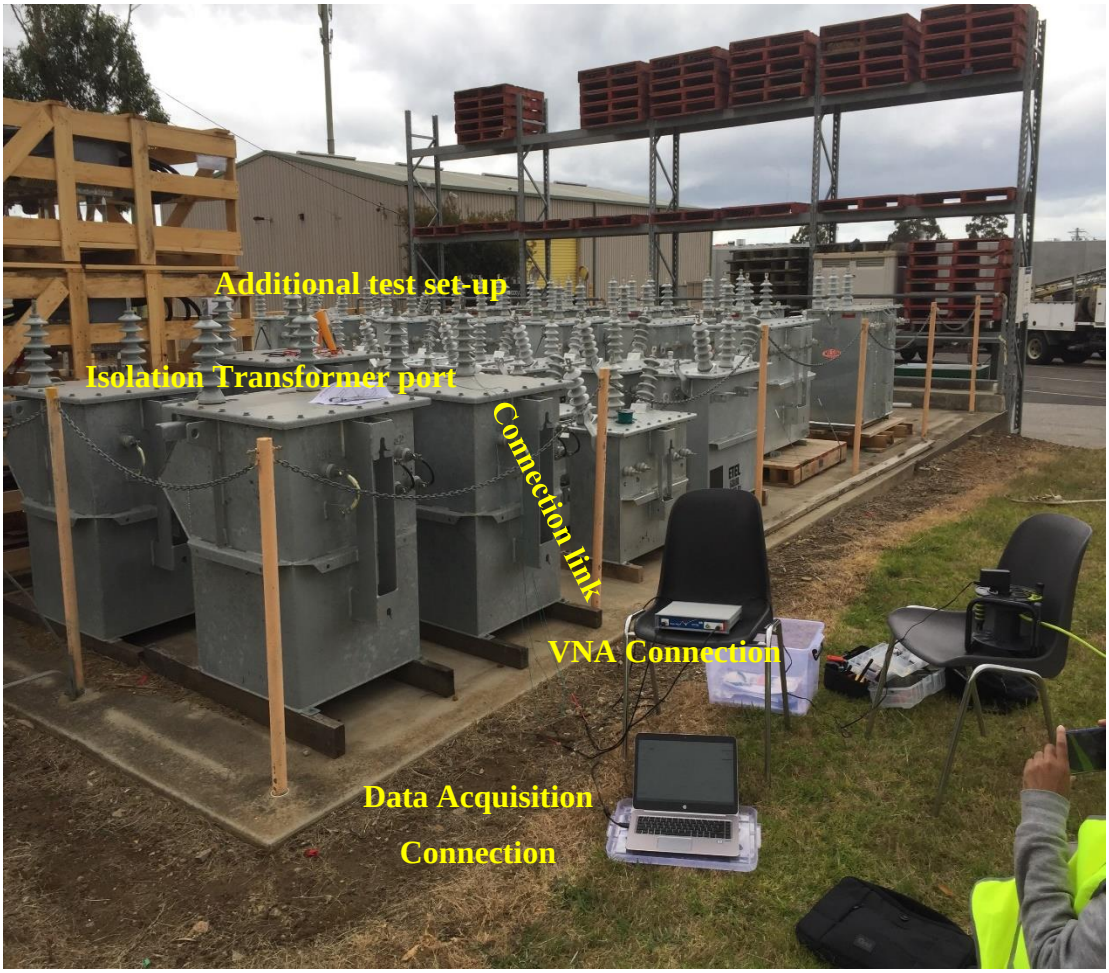

Appendix I – PLC Signal Capture arrangement

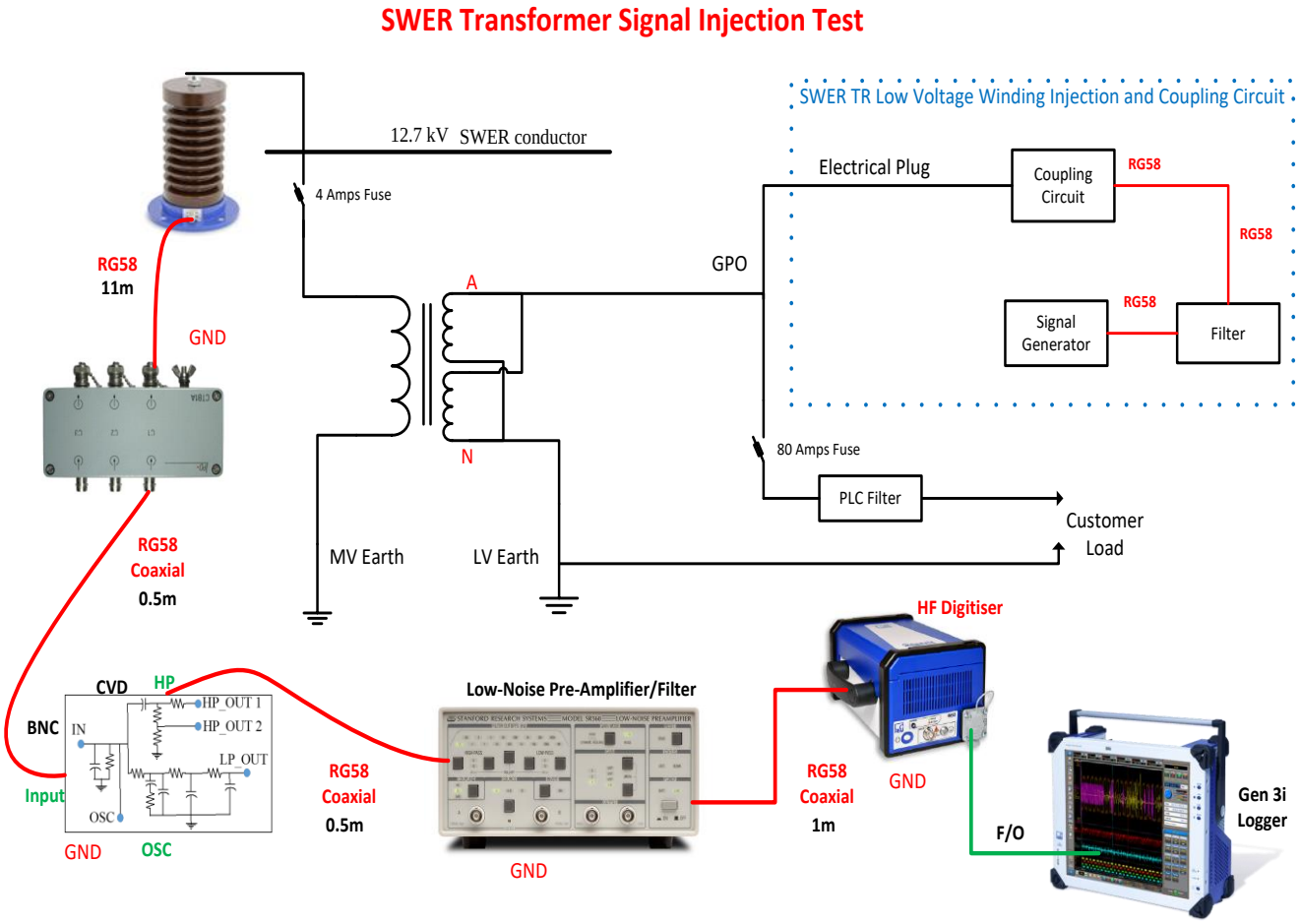

Appendix J– CVD theoretical concept